Metal-Based Drugs

Metal-Containing Proteins, Macrocycles, and Coordination Complexes in Therapeutic Applications and Disease

Guest Editors: Jannie C. Swarts, Michael J. Cook, and Edward N. Baker

Metal-Containing Proteins, Macrocycles, and Coordination Complexes in Therapeutic Applications and Disease

Metal-Containing Proteins, Macrocycles, and Coordination Complexes in Therapeutic Applications and Disease

Guest Editors: Jannie C. Swarts, Michael J. Cook, and Edward N. Baker

Contents

Hindawi Publishing Corporation
Metal-Based Drugs
Volume 2008, Article ID 286363, 2 pages
doi:10.1155/2008/286363

Editorial

Metal-Containing Proteins, Macrocycles, and Coordination Complexes in Therapeutic Applications and Disease

Jannie C. Swarts,[1] Michael J. Cook,[2] and Edward N. Baker[3]

[1] *Department of Chemistry, University of the Free State, Bloemfontein 9300, South Africa*
[2] *School of Chemical Sciences and Pharmacy, University of East Anglia, Norwich NR4 7TJ, UK*
[3] *Centre for Molecular Biodiscovery and School of Biological Sciences, University of Auckland, 3A Symonds Street, Private Bag 92019, Auckland 1142, New Zealand*

Correspondence should be addressed to Jannie C. Swarts, swartsjc.sci@ufs.ac.za

Received 8 January 2008; Accepted 8 January 2008

Treatment of diseases with natural and synthetic materials has been an aspiration of mankind since the dawn of human development. From the use of willow-bark to the marketing of aspirin, a steady move from folk remedies to the use of chemistry and biology to develop new therapies has been observed. In terms of metal-containing drugs, the platinum-containing drug cisplatin has long been the most effective metal-containing anticancer drug on the market.

However, severe side effects of conventional drugs are associated with the inability to distinguish between healthy and cancer cells. Hence, a concerted world-wide effort is in progress to discover and characterise new drugs that may distinguish between healthy and cancer or other diseased cells. New techniques of drug delivery are sought and the use of natural products, proteins, antibodies, and synthetic polymers as drug delivery devices capable of targeting a diseased site is being investigated.

These issues are nicely illustrated by macrocycles such as porphyrins, phthalocyanines, and related systems. Some of these compounds exhibit selective absorption by cancer cells and have the ability to photosensitize formation of singlet oxygen. These attributes have led to the development of alternative cancer treatments known as photodynamic therapy. Sadly, many potentially good new therapeutic agents often never leave the designers' laboratory due to some pharmacological problems associated with its in vivo use. The use of drug delivering devices, including water-soluble synthetic polymeric drug delivery systems, may help overcome many pharmacological drug-related problems, including those of solubility, specificity, and biocompatibility, factors that currently prevent many potentially good therapeutic agents from reaching clinics.

The focus of this special issue is the synthesis, characterisation, physical studies, and application of synthetic metal-containing complexes and natural occurring proteins in serious human diseases such as cancer, diabetes, arthritis, viral disease, malaria, and tuberculosis with special focus on the following:

(a) porphyrins, phthalocyanines, and related complexes in photodynamic cancer therapy;

(b) proteins, enzymes, and synthetic polymeric drug delivery systems in the treatment of cancer and other diseases;

(c) coordination and organometallic compounds in cancer, arthritis, malaria, and viral disease.

Towards these goals, L. Josefsen and R. Boyle describe in their review article the development and application of metal-based photosensitisers, including porphyrins and phthalocyanines, in photodynamic therapy. Four other publications highlight different aspects of porphyrin-based macrocyclic photosensitisers. S. Lee et al. focus on the cellular uptake and toxicity of thiotetra (ethylene glycol) monomethyl ether-functionalized porphyrazines. J.-Y. Liu et al. focus on in vitro photodynamic activity of novel amphiphilic zinc(II) phthalocyanines bearing oxyethylene-rich substituents. E. Antunes and T. Nyokong highlight the syntheses and photophysical properties of tetraazatetrabenzcorrole photosensitizers. Sakamoto et al. present a fundamental study of

zinc bis(1,4-didecylbenzo)-bis(2,3-pyrido)porphyrazine for application in photodynamic therapy of cancer.

Considering polymeric drug delivery systems, South African E. Neuse's excellent review describes the use of synthetic polymers as metal-containing drug delivery vehicles in medicine. M. David Maree et al. provided a fine treatise on why biocompatible synthetic polymeric drug delivery systems are becoming increasing popular as drug delivering devices. They also demonstrate the principles behind these systems in a practical study utilising ferrocene and phthalocyanine derivatives anchored on a water-soluble polymeric drug carrier derived from lysine and aspartic acid. Italians Longo and Vasapollo demonstrated the use of phthalocyanine-based molecularly imprinted polymers as nucleoside receptors. X. Sun et al. report on the identification of proteins related to nickel homeostasis in *Helicobater pylori* by immobilized metal affinity chromatography and two-dimensional gel electrophoresis. P. Nagababu reported DNA-binding and photocleavage studies of cobalt (III) ethylenediamine pyridine complexes.

M. Blackie and K. Chibale's excellent minireview focuses on metallocene antimalarials. The development of new metal-containing chemotherapeutic drugs is highlighted by contributions from M. Hogan et al. in their synthetic and cytotoxic study of new titanocene analogous. S. Mahepal et al. look at the in vitro antitumor activity of novel, mitochondrial-interactive, gold-based lipophilic cations. Sathisha et al. describe bis-isatin thiocarbohydrazone metal complexes and their antitumor activity against Ehrlich Ascites Carcinoma in Swiss albino mice. In conclusion, J. M. Botha and A. Roodt report mechanistic studies on trans-aquatetracyanooxo complexes of Re(V) and Tc(V) and discuss the implications of their results for nuclear medicine.

We hope that this special issue will stimulate new research in all areas of metal-containing drug research and that it will help to focus research efforts of new and experienced researchers on key problems in the exciting field of metal-containing drug research.

Jannie C. Swarts
Michael J. Cook
Edward N. Baker

Hindawi Publishing Corporation
Metal-Based Drugs
Volume 2008, Article ID 276109, 24 pages
doi:10.1155/2008/276109

Review Article

Photodynamic Therapy and the Development of Metal-Based Photosensitisers

Leanne B. Josefsen and Ross W. Boyle

Department of Chemistry, The University of Hull, Kingston-upon-Hull HU6 7RX, UK

Correspondence should be addressed to Ross W. Boyle, r.w.boyle@hull.ac.uk

Received 7 September 2007; Accepted 30 October 2007

Recommended by Michael J. Cook

Photodynamic therapy (PDT) is a treatment modality that has been used in the successful treatment of a number of diseases and disorders, including age-related macular degeneration (AMD), psoriasis, and certain cancers. PDT uses a combination of a selectively localised light-sensitive drug (known as a photosensitiser) and light of an appropriate wavelength. The light-activated form of the drug reacts with molecular oxygen to produce reactive oxygen species (ROS) and radicals; in a biological environment these toxic species can interact with cellular constituents causing biochemical disruption to the cell. If the homeostasis of the cell is altered significantly then the cell enters the process of cell death. The first photosensitiser to gain regulatory approval for clinical PDT was Photofrin. Unfortunately, Photofrin has a number of associated disadvantages, particularly pro-longed patient photosensitivity. To try and overcome these disadvantages second and third generation photosensitisers have been developed and investigated. This Review highlights the key photosensitisers investigated, with particular attention paid to the metallated and non-metallated cyclic tetrapyrrolic derivatives that have been studied *in vitro* and *in vivo*; those which have entered clinical trials; and those that are currently in use in the clinic for PDT.

1. PHOTODYNAMIC THERAPY: BACKGROUND

The use of light in the treatment of disease has been known for many centuries and can be traced back over 4000 years to the ancient Egyptians [1]. The Egyptian people used a combination of the orally ingested Amni Majus plant and sunlight to successfully manage vitiligo: a skin disorder of unknown cause. The active ingredient of this plant (psoralen, Figure 1) is now successfully employed in the worldwide treatment of psoriasis [1–4].

Photodynamic therapy (PDT) is a treatment involving light and a chemical substance (a photosensitiser), used in conjunction with molecular oxygen to elicit cell death. More explicitly, photodynamic therapy is a selective treatment modality for the local destruction of diseased cells and tissue. The selectivity is based on the ability of the photosensitiser to preferentially accumulate in the diseased tissue and efficiently generate singlet oxygen or other highly reactive species such as radicals, which induce target cell death.

The principle of photodynamic therapy is based on a multi-stage process (Figure 2). The first of these stages

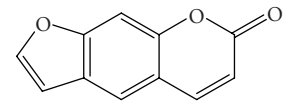

Figure 1: Structure of psoralen.

(Figure 2(a)) sees the administration of a photosensitiser with negligible dark toxicity, either systemically or topically, in the absence of light. When the optimum ratio of photosensitiser in diseased *versus* healthy tissue is achieved, the photosensitiser is (Figure 2(c)) activated by exposure to a carefully regulated dose of light which is shone directly onto the diseased tissue for a specified length of time. The light dose is regulated in order to allow a sufficient amount of energy to be delivered to activate the photosensitiser, but at the same time the dose should be small enough to minimise damage inflicted on neighbouring healthy tissue. It is the activated form of the photosensitiser which evokes a toxic response in the tissue, resulting in cell death. The success of photodynamic therapy lies in the prolonged accumulation of

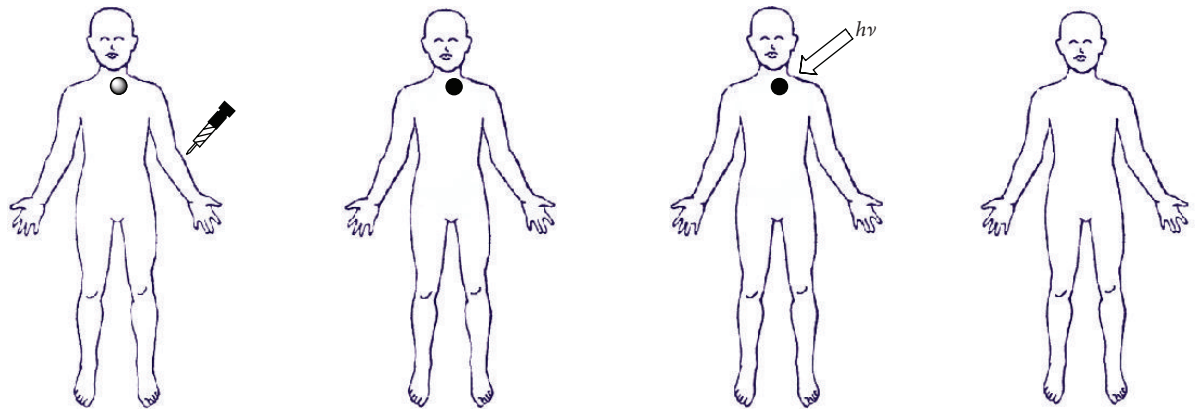

(a) Photosensitiser delivery (b) Selective accumulation in diseased tissue (c) Light irradiation (d) Selective destruction of diseased tissue

Figure 2: Photosensitiser administration.

photosensitiser in diseased tissue, relative to the more rapid clearance from normal tissue cells.

Photodynamic therapy is commonly practiced in the treatment of a number of cancers, including those present in the head and neck, the lungs, bladder, and particular skin cancers [5–16]. It has also been successfully used in the treatment of non-cancerous conditions such as age-related macular degeneration (AMD), psoriasis, atherosclerosis, and has shown some efficacy in anti-viral treatments including herpes [2, 3, 5–7, 9, 17–20].

Photodynamic therapy carries advantages for both the patient and the physician: the need for delicate surgery and lengthy recuperation periods is minimised, along with minimal formation of scar tissue and disfigurement. However, photodynamic therapy is not without its drawbacks: a major limitation is the associated general photosensitisation of skin tissue.

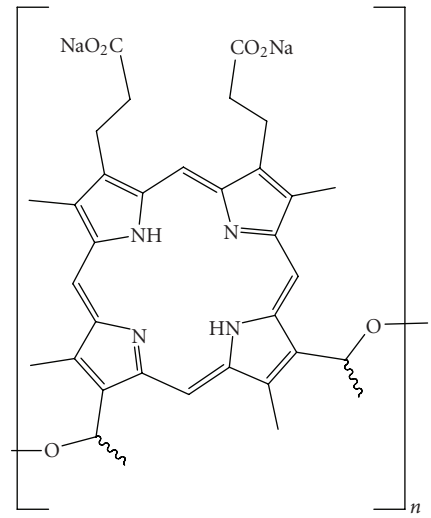

Figure 3: Structure of Photofrin, $n = 1$–9.

2. HISTORY OF PHOTODYNAMIC THERAPY

Reports of contemporary photodynamic therapy came first in the investigations led by Finsen in the late nineteenth century [8]. Finsen successfully demonstrated phototherapy by employing heat-filtered light from a carbon-arc lamp (the "Finsen lamp") in the treatment of a tubercular condition of the skin known as *lupus vulgaris*, for which he won the Nobel Prize in Physiology or Medicine in 1903 [8]. But it was not until the early twentieth century that reports of photodynamic therapy for the treatment of cancer patients (with solid tumours) were made by von Tappeiner's group in Munich [2, 4, 6, 9]. In 1913 another German scientist, Meyer-Betz, described the major stumbling block of photodynamic therapy. After injecting himself with haematoporphyrin (Hp, a photosensitiser), he swiftly experienced a general skin sensitivity upon exposure to sunlight—a problem still persistent with many of todays' photosensitisers [2, 3, 7, 18].

Further studies, investigating the accumulation of haematoporphyrin and the purified haematoporphyrin derivative (HpD) in tumours, culminated in the late 1980s with the photosensitiser Photofrin (Figure 3). A photosensitiser which, after further purification, was first given approval in 1993 by the Canadian health agency for use against bladder cancer and later in Japan, USA and parts of Europe for use against certain cancers of the oesophagus and non-small cell lung cancer [3–9, 17, 18, 21, 22].

Photofrin was far from ideal and carried with it the disadvantages of prolonged patient photosensitivity and a weak long-wavelength absorption (630 nm) [6, 7, 21]. This led to the development of improved (second generation) photosensitisers, including Verteporfin (a benzoporphyrin derivative, also known as Visudyne) and more recently, third generation photosensitisers based around targeting strategies, such as antibody-directed photosensitisers [4, 5, 7, 18, 19, 23–25].

3. CYCLIC TETRAPYRROLIC CHROMOPHORES AND PHOTOSENSITISERS

Cyclic tetrapyrrolic molecules are good examples of fluorophores (see Glossary) and photosensitisers. Photosensitisers are molecules, which, when excited by light energy, can utilise the energy to induce photochemical reactions to

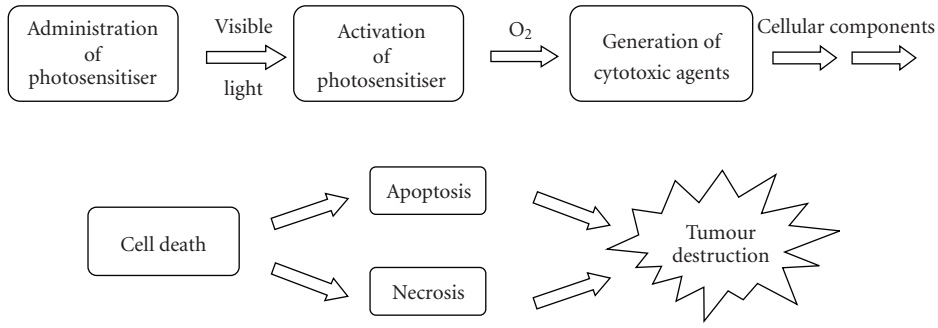

Figure 4: Photosensitiser initiated cell death.

Apoptosis: a form of programmed cell death (often referred to as cell suicide) in response to key physiological cues and intracellular damage. In apoptosis, the orchestrated collapse of a cell is characterised by key morphological and biochemical changes followed by rapid engulfment of cellular remains by neighbouring cells (phagocytosis). These key changes include maintenance of adenosine triphosphate (ATP) levels, caspase activation, membrane blebbing, cell shrinkage, chromatin condensation, DNA fragmentation, and the formation of small intact fragments (apoptotic bodies). Apoptosis can be distinguished from necrotic cell death by the distinct absence of an associated inflammatory response.

Necrosis: an uncontrolled form of cell death. A less ordered process than apoptosis and usually in response to injurious agents such as infection, physical injury, ischemia (deficiency of oxygenated blood), or excessive accumulation of ROS. In contrast to apoptosis, a local inflammatory response is normally observed as a result of cellular debris released directly into surrounding tissue.

Box 1

produce lethal toxic agents. In a cellular environment, these agents (reactive oxygen species (ROS) and radicals) ultimately result in cell death and tissue destruction (Figure 4) [5–9]. Photosensitisers are absorbed into cells all over the body and alone are harmless, that is, in the absence of light, and usually oxygen they have no effect on healthy or abnormal tissue. Ideally, they should be retained by diseased tissue, particularly tumours, for longer periods of time in comparison to healthy tissue; thus it is important to carefully time light exposure and ensure that activation only occurs when the ratio of photosensitiser is greater in diseased tissue than in healthy tissue, thereby minimising unwanted damage to surrounding non-cancerous cells [3, 19].

Photosensitisers also have alternative applications. They have been employed in the sterilisation of blood plasma and water in order to remove blood-borne viruses and microbes and have been considered for agricultural uses, including herbicides and insecticides [5, 9, 26–28].

4. PHOTOCHEMISTRY: PHOTOCHEMICAL PROCESSES

Only when a photosensitiser is in its excited state (^{3}Psen*) can it interact with molecular oxygen ($^3O_2$) and produce radicals and activated oxygen species (ROS), crucial to the Type II mechanism which is thought to predominate in PDT (see below). These species include singlet oxygen ($^1O_2$), hydroxyl radicals ($^{\bullet}$OH), and superoxide (O_2^-) ions and can interact with cellular components including unsaturated lipids; amino acid residues; and nucleic acids. If sufficient oxidative damage ensues, this will result in target-cell death (only within the immediate area of light illumination).

5. PHOTOCHEMICAL MECHANISMS

When a chromophore, such as a cyclic tetrapyrrolic molecule, absorbs a photon of electromagnetic radiation in the form of light energy, an electron is promoted into a higher-energy molecular orbital, elevating the chromophore from the ground state (S_0) into a short-lived, electronically excited state (S_n) composed of a number of vibrational sub-levels (S'_n). The excited chromophore can lose energy by rapidly decaying through these sub-levels *via* internal conversion (IC) to populate the first excited singlet state (S_1), before quickly relaxing back to the ground state (Figure 5).

The decay from the excited singlet state (S_1) to the ground state (S_0) is *via* **fluorescence** ($\mathbf{S_1 \rightarrow S_0}$). Singlet state lifetimes of excited fluorophores are very short ($\tau_{fl.} = 10^{-9}$–10^{-6} seconds) since transitions between the same spin states (S → S or T → T) conserve the spin multiplicity of the electron and, according to the Spin Selection Rules, are therefore considered "allowed" transitions [3, 6, 8]. Alternatively, an excited singlet state electron (S_1) can undergo spin inversion and populate the lower-energy first

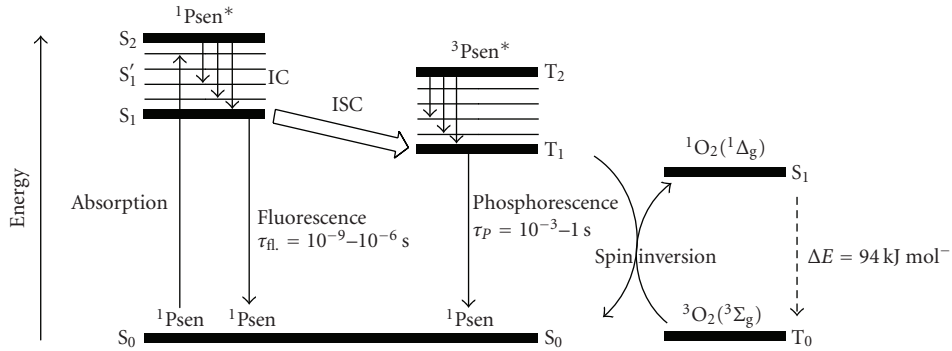

Figure 5: Modified Jablonski energy diagram.

Quantum Yields

Photochemical quantum yields (Φ) are one of the key measurements made in the photochemical techniques described above. According to the Stark-Einstein law:

"every photon absorbed by a species excites only **one** molecule of the species." Later refined to: "one **particle** is excited for each quanta of radiation absorbed" (Second Law of Photochemistry).

The quantum yield can therefore be described as the number of molecules undergoing the process of interest (formation of product or consumption of reactants) for each quantum of radiation energy absorbed (equation 1):

$$\Phi = \frac{\text{number of species undergoing process of interest}}{\text{number of photons absorbed}}$$

Equation 1: Quantum Yields

Quantum yields may also be expressed in terms of the rate of the reaction:

$$\Phi = \frac{\text{rate of chemical process/event}}{\text{intensity of absorbed light}} = \frac{d[x]/dt}{I_{abs}}$$

The quantum yield(s) for a species cannot be greater than unity ($\Phi \leq 1$) unless a secondary reaction or a series of chain reactions are taking place within the sample, in which case the quantum yields are respectively $\Phi \leq 2$ and $\Phi \geq 2$.

Singlet Oxygen Quantum Yields

If the fraction of excited triplet state molecules quenched by molecular oxygen to produce singlet oxygen ($^1\Delta_g$) is represented as S_Δ, the quantum yield of singlet oxygen (Φ_Δ) can be determined (equation 2):

$$\Phi_\Delta = \Phi_T S_\Delta$$

Equation 2: Singlet Oxygen Quantum Yield

Box 2

excited triplet state (T_1) *via* intersystem crossing (ISC); a spin-forbidden process, since the spin of the electron is no longer conserved [29–34]. The excited electron can then undergo a second spin-forbidden inversion and depopulate the excited triplet state (T_1) by decaying back to the ground state (S_0) *via* **phosphorescence** ($\mathbf{T_1 \rightarrow S_0}$) [29–34]. Owing to the spin-forbidden triplet to singlet transition, the lifetime of phosphorescence ($\tau_P = 10^{-3} - 1$ second) is considerably longer than that of fluorescence.

6. PHOTOSENSITISERS AND PHOTOCHEMISTRY

Tetrapyrrolic photosensitisers in the excited singlet state (^{1}Psen*, $S_{>0}$) are relatively efficient at undergoing intersystem crossing and can consequently have a high triplet-state quantum yield, Box 2 (Φ_T 0.62 (tetraphenylporphyrin (TPP), methanol)), 0.83 (etiopurpurin, benzene), 0.71 (tetrasulphonated TPP, D_2O), and 0.47 (tetrasulphonated zinc phthalocyanine, methanol)) [8, 35, 36]. The longer

$$\begin{aligned}
&\text{Psen}^{*} + \text{Subs} \longrightarrow \text{Psen}^{\bullet -} + \text{Subs}^{\bullet +}{}_{\text{oxi}}\\
&\text{Psen}^{\bullet -} + \text{O}_2 \longrightarrow \text{Psen} + \text{O}_2^{\bullet -}\\
&\text{Psen}^{*} + \text{O}_2 \longrightarrow \text{Psen}^{\bullet +} + \text{O}_2^{\bullet -}\\
&2\text{O}_2^{\bullet -} + 2\text{H}^{+} \longrightarrow {}^3\text{O}_2 + \text{H}_2\text{O}_2\\
&\text{O}_2^{\bullet -} + \text{Fe}^{3+} \longrightarrow {}^3\text{O}_2 + \text{Fe}^{2+}\\
&\text{Fe}^{2+} + \text{H}_2\text{O}_2 \longrightarrow \text{Fe}^{3+} + \text{OH}^{\bullet} + \text{OH}^{-}\\
&\text{O}_2^{\bullet -} + \text{OH}^{\bullet} \longrightarrow {}^1\text{O}_2 + \text{OH}^{-}
\end{aligned}$$

Figure 6: Type-I process (i).

$$\begin{aligned}
&\text{Psen}^{*} + \text{R-H} \longrightarrow \text{Psen-H}^{\bullet} + \text{R}^{\bullet}\\
&\text{R}^{\bullet} + \text{O}_2 \longrightarrow \text{RO}_2^{\bullet}\\
&\text{RO}_2^{\bullet} + \text{R-H} \longrightarrow \text{RO}_2\text{H} + \text{R}^{\bullet}
\end{aligned}$$

Figure 7: Type-I process (ii).

$$\begin{aligned}
&{}^3\text{Psen} + {}^3\text{O}_2 \longrightarrow {}^1\text{Psen} + {}^1\text{O}_2\\
&{}^1\text{O}_2 + \text{Subs} \longrightarrow \text{Oxidative damage}
\end{aligned}$$

Figure 8: Type-II process.

lifetime of this species is sufficient to allow the excited triplet state photosensitiser to interact with surrounding biomolecules, including cell membrane constituents [5, 17].

7. PHOTOCHEMICAL REACTIONS

Excited triplet-state photosensitisers can react in two ways defined as Type-I and Type-II processes. Type-I processes can involve the excited singlet or triplet photosensitiser (^{1}Psen*, S_1; ^{3}Psen*, T_1), however due to the short lifetime of the excited singlet state, the photosensitiser can only react if it is intimately associated with a substrate, in both cases the interaction is with readily oxidisable or reducable substrates. Type-II processes involve the direct interaction of the excited triplet photosensitiser (^{3}Psen*, T_1) with molecular oxygen ($^3O_2$, $^3\Sigma_g$) [5–8, 17, 18, 37].

Type-I processes can be divided into two further mechanisms; Type I(i) and Type I(ii). The first of these mechanisms (i) involves the transfer of an electron (oxidation) from a substrate molecule to the excited state photosensitiser (Psen*), generating a photosensitiser radical anion ($\text{Psen}^{\bullet -}$) and a substrate radical cation ($\text{Subs}^{\bullet +}$). The majority of the radicals produced from Type-I(i) reactions react instantaneously with oxygen, generating a complex mixture of oxygen intermediates. For example, the photosensitiser radical anion can react instantaneously with molecular oxygen ($^3O_2$) to generate a superoxide radical anion ($O_2^{\bullet -}$), which can go on to produce the highly reactive hydroxyl radical ($OH^{\bullet}$, Figure 6), initiating a cascade of cytotoxic free radicals; this process is common in the oxidative damage of fatty acids and other lipids [17, 18]. Some of the more common Type-I(i) reactions are shown in Figure 6.

The second Type-I process (ii) involves the transfer of a hydrogen atom (reduction) to the excited state photosensitiser (Psen*). This generates free radicals capable of rapidly reacting with molecular oxygen and creating a complex mixture of reactive oxygen intermediates, including reactive peroxides (Figure 7). Once again, this can trigger a torrent of cytotoxic events, culminating in cell damage and death.

On the other hand, Type-II processes involve the direct interaction of the excited triplet state photosensitiser (^{3}Psen*) with ground state molecular oxygen ($^3O_2$, $^3\Sigma_g$, Figure 8); a spin allowed transition—the excited state photosensitiser and ground state molecular oxygen are of the same spin state (T, Figure 5).

When the excited photosensitiser collides with a molecule of molecular oxygen, a process of triplet-triplet annihilation takes place (^{3}Psen* $\rightarrow {}^1$Psen and $^3O_2 \rightarrow {}^1O_2$). This inverts the spin of one of molecular oxygens ($^3O_2$) outermost antibonding electrons, generating two forms of singlet oxygen ($^1\Delta_g$ and $^1\Sigma_g$, Figure 9), while simultaneously depopulating the photosensitiser's excited triplet state ($T_1 \rightarrow S_0$, Figure 5). The higher-energy singlet oxygen state ($^1\Sigma_g$, 157 kJ mol^{-1} > $^3\Sigma_g$) is very short-lived ($^1\Sigma_g \leq 0.33$ milliseconds (methanol), undetectable in H_2O/D_2O) and rapidly relaxes to the lower-energy excited state ($^1\Delta_g$, 94 kJ mol^{-1} > $^3\Sigma_g$) [36]. It is, therefore, this lower-energy form of singlet oxygen ($^1\Delta_g$) which is implicated in cell injury and cell death [38].

The highly-reactive oxygen species ($^1O_2$) produced *via* the Type-II process act near to their site of generation and within a radius of action of approximately 20 nm, with a typical lifetime of approximately 40 nanoseconds in biological systems [2, 7, 17]. However, it has recently been suggested that (over a 6 microsecond period) singlet oxygen can diffuse up to approximately 300 nm *in vivo* [39–41]. Singlet oxygen can theoretically only interact with proximal molecules and structures within this radius [17]. ROS are known to initiate a large number of reactions with biomolecules, including amino acid residues in proteins, such as tryptophan; unsaturated lipids like cholesterol and nucleic acid bases, particularly guanosine and guanine derivatives (Box 3) with the latter base more susceptible to ROS [2, 5, 8, 17, 36, 42–45]. These interactions cause damage and potential destruction to cellular membranes and enzyme deactivation, culminating in cell death [8].

It is highly probable that in the presence of molecular oxygen, and as a direct result of the photoirradiation of the photosensitiser molecule, both Type-I and II pathways play a pivotal role in disrupting cellular mechanisms and cellular structure. Nevertheless, there is considerable evidence to suggest that the Type-II photo-oxygenation process predominates in the induction of cell damage, a consequence of the interaction between the irradiated photosensitiser and molecular oxygen [2, 5, 8, 18, 43, 46]. It has been suggested, however, that cells *in vivo* are partially protected against the effects of photodynamic therapy by the presence of singlet oxygen scavengers (such as histidine) and that certain skin cells are somewhat resistant to photodynamic therapy in the absence of molecular oxygen; further supporting

Typical Singlet Oxygen Reactions

Singlet molecular oxygen is known to react with systems by attacking electron rich double bonds, in an "*-ene*" type reaction, to form peroxides or hydroperoxides.

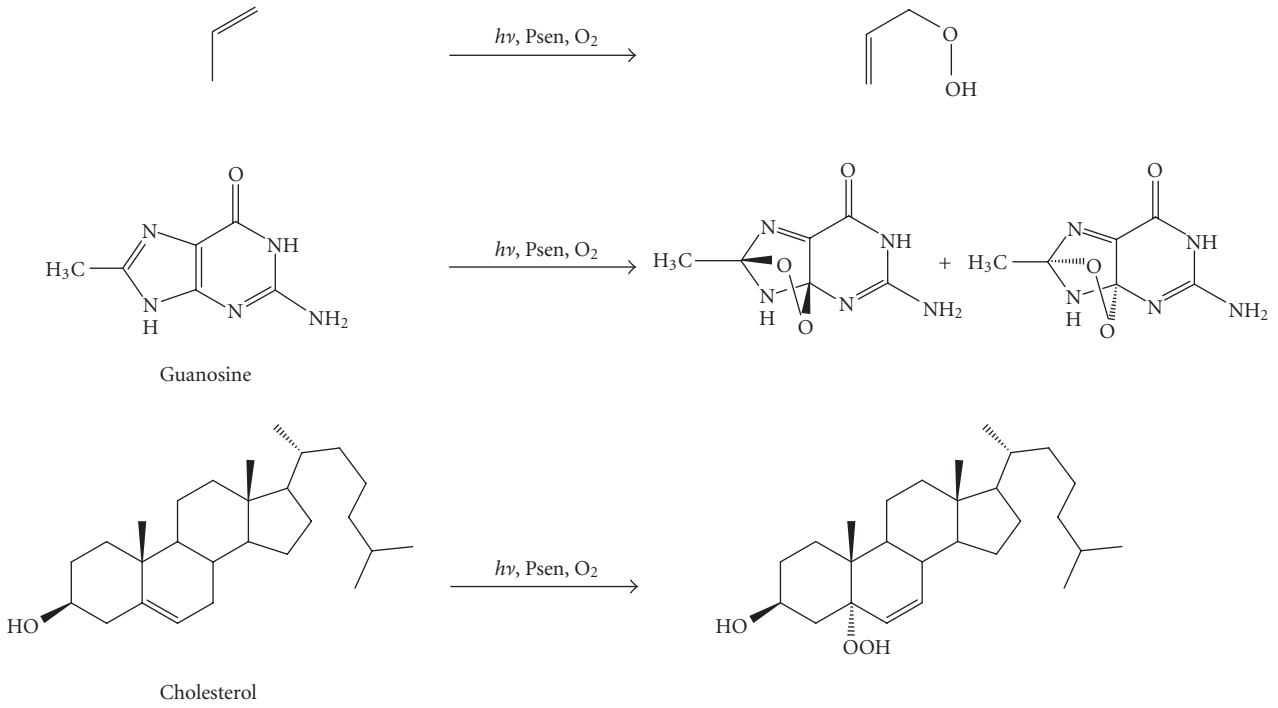

Box 3

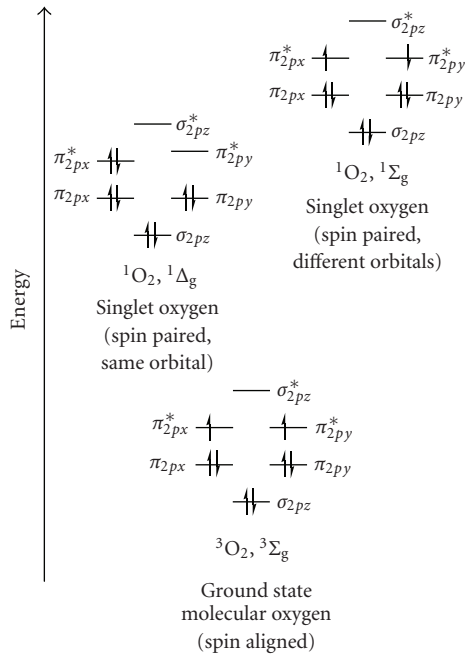

Figure 9: Molecular orbital diagram of oxygen ($^3\Sigma_g$, $^1\Delta_g$, and $^1\Sigma_g$).

the proposal that the Type-II process is at the heart of photoinitiated cell death [17, 43, 47, 48].

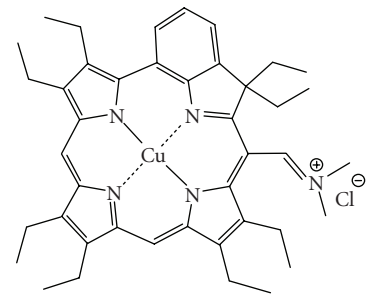

Figure 10: A copper metallated photosensitiser.

The efficiency of Type-II processes is dependent upon the triplet state lifetime τ_T (see Glossary, under luminescence life time) and the triplet quantum yield (Φ_T) of the photosensitiser. Both of these parameters have been implicated in the effectiveness of a photosensitiser in phototherapeutic medicine; further supporting the distinction between Type-I and Type-II mechanisms. However, it is worthy to note that the success of a photosensitiser is not exclusively dependent upon a Type-II process taking place. There are a number of photosensitisers whose excited triplet lifetimes are too short to permit a Type-II process to occur. For example, the copper metallated octaethylbenzochlorin photosensitiser (Figure 10) has a triplet state lifetime of less

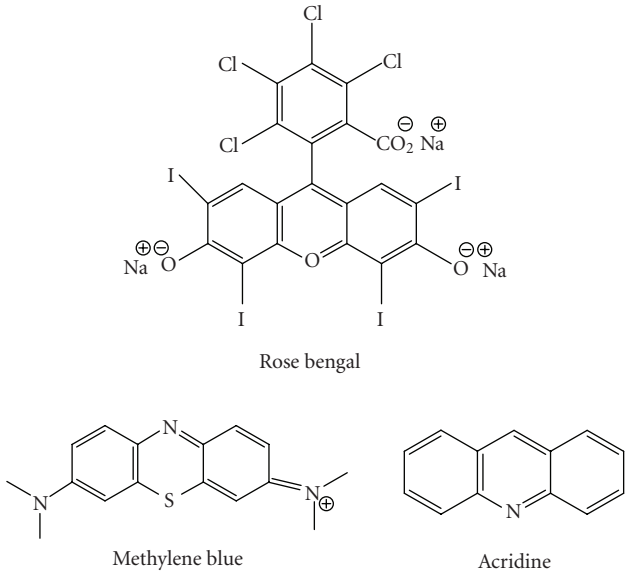

Figure 11: Examples of non-porphyrinic photosensitisers.

than 20 nanoseconds and is still deemed to be an efficient photodynamic agent [13, 43].

8. PHOTOSENSITISERS—IDEAL PHOTOSENSITISERS

Although a number of different photosensitising compounds, such as methylene blue (see Glossary), rose bengal, and acridine (Figure 11), are known to be efficient singlet oxygen generators (and therefore potential photodynamic therapy agents), a large number of photosensitisers are cyclic tetrapyrroles or structural derivatives of this chromophore; in particular porphyrin, chlorin, bacteriochlorin, expanded porphyrin, and phthalocyanine (PCs) derivatives (Figure 12). This is possibly because cyclic tetrapyrrolic derivatives have an inherent similarity to the naturally occurring porphyrins present in living matter—consequently they have little or no toxicity in the absence of light [2, 5, 17, 18, 36, 44, 49].

Porphyrins are a group of naturally occurring and intensely coloured compounds, whose name is drawn from the Greek word *porphura*, the Greek word for purple [50, 51]. These molecules are known to be involved in a number of biologically important roles, including oxygen transport and photosynthesis, and have applications in a number of fields, ranging from fluorescence imaging to medicine [2, 5, 17, 42]. Porphyrins are classified as tetrapyrrolic molecules, with the heart of the skeleton a heterocyclic macrocycle, known as a porphine. The fundamental porphine frame consists of four pyrrolic sub-units linked on opposing sides (α-positions, numbered 1, 4, 6, 9, 11, 14, 16, and 19, Figure 13) through four methine (CH) bridges (5, 10, 15, and 20), known as the *meso*-carbon atoms/positions (Figure 13). The resulting conjugated planar macrocycle may be substituted at the *meso*- and/or β-positions (2, 3, 7, 8, 12, 13, 17, and 18): if the *meso*- and β-hydrogens are substituted with non-hydrogen

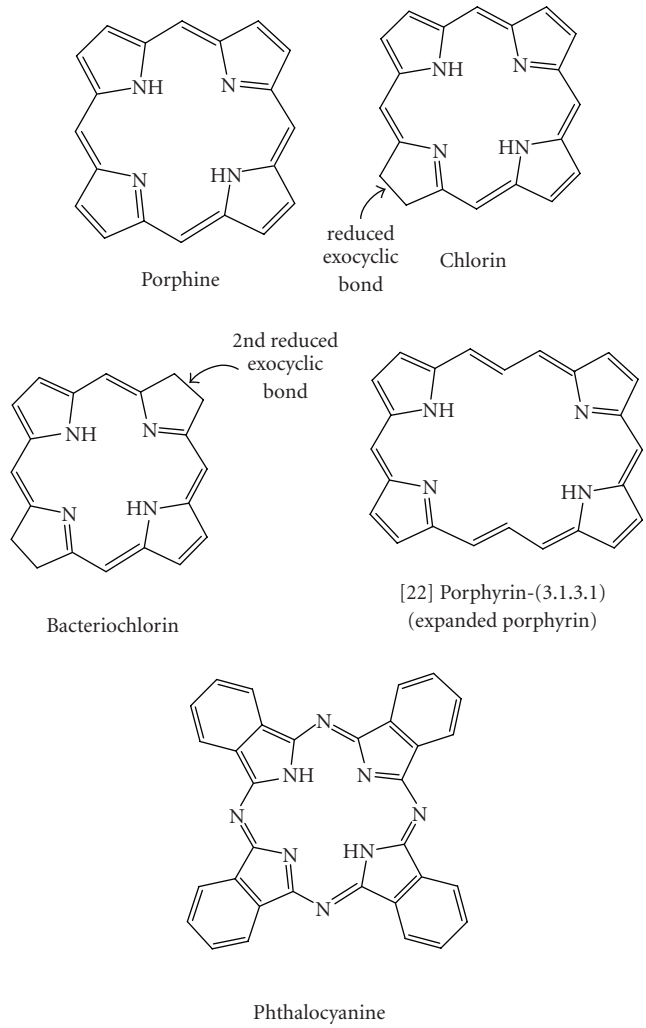

Figure 12: Porphine, chlorine, bacteriochlorin, expanded porphyrin, and phthalocyanine structures.

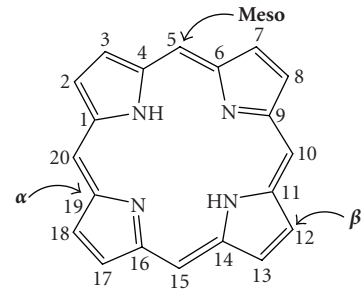

Figure 13: Porphine macrocycle.

atoms or groups, the resulting compounds are known as porphyrins.

The inner two protons of a free-base porphyrin can be removed by strong bases such as alkoxides, forming a dianionic molecule; conversely, the inner two pyrrolenine nitrogens can be protonated with acids such as trifluoroacetic acid affording a dicationic intermediate (Figure 14). The

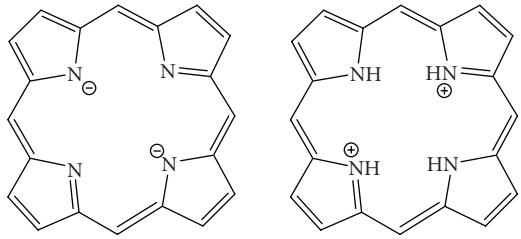

Figure 14: Porphyrin dianionic and dicationic species.

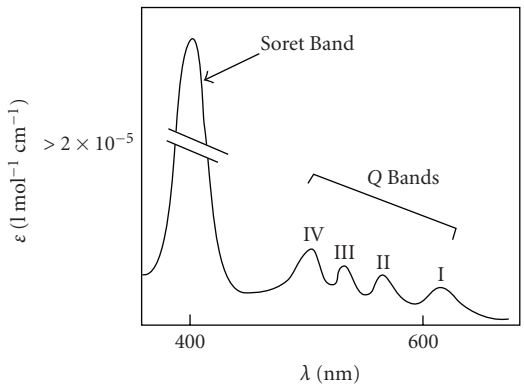

Figure 15: Typical porphyrin absorption spectrum [55, (modified)].

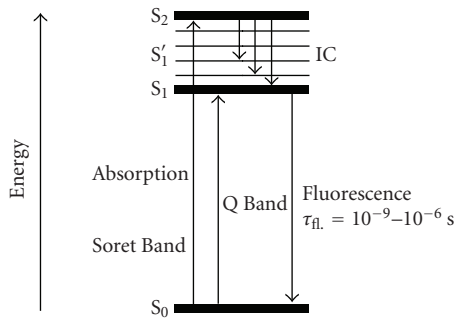

Figure 16: Modified Jablonski energy diagram.

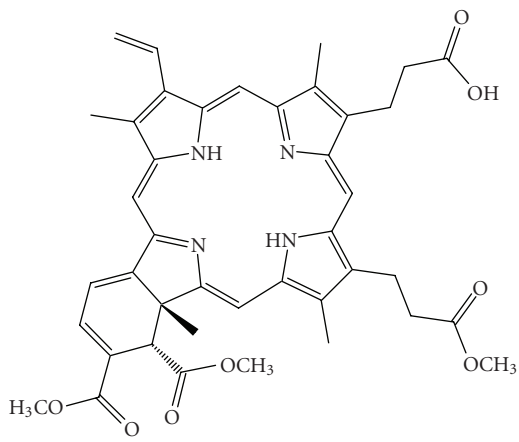

Figure 17: Verteporfin.

tetradentate anionic species can readily form complexes with most metals.

9. PORPHYRIN ABSORPTION SPECTROSCOPY

On account of their highly conjugated skeleton, porphyrins have a characteristic ultra-violet visible (UV-VIS) spectrum (Figure 15). The spectrum typically consists of an intense, narrow absorption band ($\varepsilon > 200\,000\,\text{l mol}^{-1}\text{cm}^{-1}$) at around 400 nm, known as the Soret or B band, followed by four longer wavelength (450–700 nm), weaker absorptions ($\varepsilon > 20\,000\,\text{l mol}^{-1}\text{cm}^{-1}$ (free-base porphyrins)) referred to as the Q bands [6, 17, 50, 53, 54].

The Soret band arises from a **strong** electronic transition from the (porphyrin) ground state to the second excited singlet state ($S_0 \rightarrow S_2$, Figure 16); whereas the Q band is a result of a **weak** transition to the first excited singlet state ($S_0 \rightarrow S_1$). The dissipation of energy *via* internal conversion (IC) is so rapid that fluorescence is only observed from depopulation of the first excited singlet state to the lower-energy ground state ($S_1 \rightarrow S_0$).

10. SECOND-GENERATION PHOTOSENSITISERS

10.1. Ideal photosensitiser properties

The key characteristic of any photodynamic sensitiser is its ability to preferentially accumulate in diseased tissue and, *via* the generation of cytotoxic species, induce a desired biological effect. In particular, a good photodynamic sensitiser should adhere to the following criteria:

(i) have strong absorption with a high extinction coefficient in the red/near infrared region of the electromagnetic spectrum (600–850 nm)—allows deeper tissue penetration by light [5–7, 17, 36, 43],

(ii) be effective generators of singlet oxygen and other ROS,

(iii) have suitable photophysical characteristics: a high-quantum yield of triplet formation ($\Phi_T \geq 0.5$); a high singlet oxygen quantum yield ($\Phi_\Delta \geq 0.5$); a relatively long triplet state lifetime (τ_T, microsecond range); and a high triplet-state energy ($\geq$94 KJ mol^{-1}) [3, 8, 18, 36, 56]. To date the parameters $\Phi_T = 0.83$ and $\Phi_\Delta = 0.65$ (haematoporphyrin); $\Phi_T = 0.83$ and $\Phi_\Delta = 0.72$ (etiopurpurin); and $\Phi_T = 0.96$ and $\Phi_\Delta = 0.82$ (tin etiopurpurin) have been achieved [2, 36],

(iv) have minimum dark toxicity and negligible cytotoxicity in the absence of light,

(v) exhibit greater retention in diseased/target tissue over healthy tissue,

(vi) present rapid clearance from the body,

(vii) be single, well-characterised compounds, with a known and constant composition,

(viii) have a short and high yielding synthetic route (with easy translation into multi-gram scales/reactions),

(ix) have a simple and stable drug formulation,

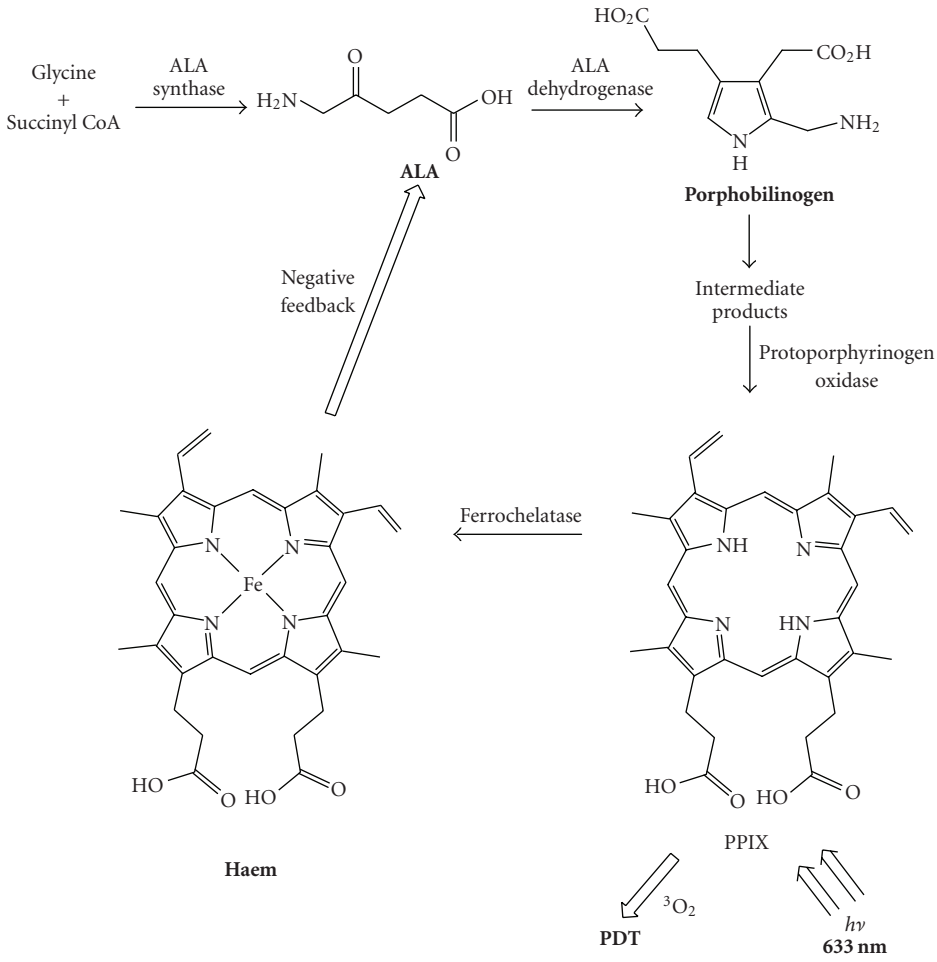

Scheme 1: Simplified haem biosynthesis.

(x) be soluble in biological media, allowing direct intravenous administration and transport to the intended target. Failing this, a hydrophilic delivery system should be sought enabling efficient and effective transportation of the photosensitiser to the target site *via* the bloodstream.

While the major disadvantages associated with the first generation photosensitisers HpD and Photofrin (skin sensitivity and weak absorption at 630 nm) have not prevented the treatment of some cancers and other diseases, they have markedly reduced the successful application of these photosensitisers to a wider field of disease. The development of second generation photosensitisers, designed to minimise the drawbacks of the first generation photosensitisers, was key to the development of photodynamic therapy. A number of new photosensitisers were therefore developed to overcome these short comings.

5-Aminolaevulinic acid

5-Aminolaevulinic acid (ALA) is a prodrug used in the clinic to treat and image a number of superficial cancers and tumours (see Tables 2 and 3) [5–9, 11, 17, 18]. ALA on its own is not a photosensitiser, but a key precursor in the biosynthesis of the naturally occurring porphyrin, haem (Scheme 1).

Haem is synthesised in every energy-producing cell in the body and is a key structural component of haemoglobin, myoglobin, and other haemproteins. The immediate precursor to haem is protoporphyrin IX (PPIX), an effective photosensitiser. Haem itself is not a photosensitiser, due to the coordination of a paramagnetic ion (iron; see Glossary; see also diamagnetic species) in the centre of the macrocycle, causing significant reduction in excited state lifetimes [5–9, 11].

The haem molecule is synthesised from glycine and succinyl coenzyme A (succinyl CoA). The rate-limiting step in the biosynthesis pathway is controlled by a tight (negative) feedback mechanism in which the concentration of haem regulates the production of ALA. However, this controlled feedback can be by-passed by artificially adding excess exogenous ALA to cells. The cells respond by producing PPIX (photosensitiser) at a faster rate than the ferrochelatase enzyme can convert it to haem [5–9, 11, 17, 18].

ALA, marketed as Levulan (DUSA Pharmaceuticals Incorporated, Toronto, Canada), has shown promise in

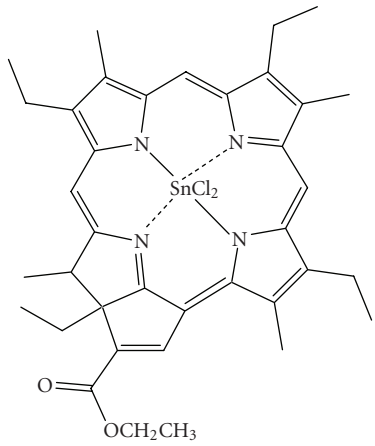

Figure 18: Purlytin.

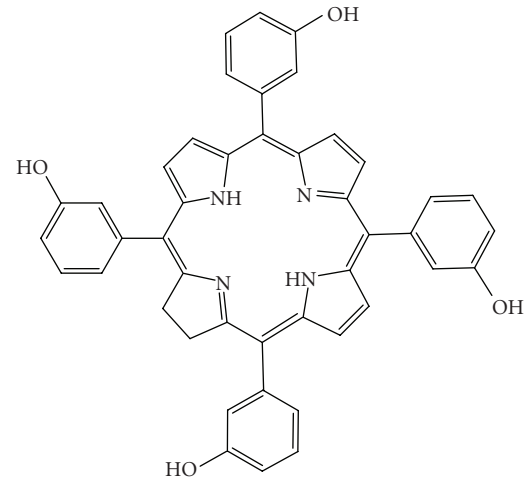

Figure 19: Foscan.

photodynamic therapy (tumours) *via* both intravenous and oral administration, as well as through topical administration in the treatment of malignant and non-malignant dermatological conditions, including psoriasis, Bowen's disease, and Hirsutism (Phase II/III clinical trials, see Glossary) [5–9, 11, 18].

ALA shows a more rapid accumulation in comparison to other intravenously administered sensitisers [5–9, 11]. Typical peak tumour accumulation levels post-administration for PPIX are usually achieved within several hours; compare this with other (intravenously administered) photosensitisers which may take up to 96 hours to reach peak levels and one of the main advantages of ALA can be clearly seen. ALA is also excreted more rapidly from the body (~24 hours) than other photosensitisers, minimising patient photosensitivity [5–8, 11].

In an attempt to overcome the poor bioavailability when ALA is applied topically, esterified ALA derivatives with improved pharmacological properties have been examined [5–8, 11]. A methyl ALA ester (Metvix) is now being marketed by Photocure ASA (Oslo, Norway) as a potential photosensitiser for basal cell carcinoma and other skin lesions [5, 6, 9, 17]. Benzyl (Benvix) and hexyl ester (Hexvix) derivatives are also registered by Photocure ASA for the treatment of gastrointestinal cancers and for the diagnosis of bladder cancer [9].

Verteporfin

The second generation photosensitiser, benzoporphyrin derivative monoacid ring A (BPD-MA, Figure 17) has been developed by QLT Phototherapeutics (Vancouver, Canada) under the trade name Visudyne (Verteporfin, for injection) and, in collaboration with Ciba Vision Corporation (Duluth, GA, USA), has undergone Phase III clinical trials (USA) for the photodynamic treatment of wet age-related macular degeneration (AMD, see Glossary) and cutaneous non-melanoma skin cancer [3, 5–7, 9, 57–59]. Verteporfin is currently marketed by Novartis Pharmaceuticals Corporation (NJ, USA).

The chromophore of BPD-MA has a red-shifted and intensified long-wavelength absorption maxima at approximately 690 nm. Tissue penetration by light at this wavelength is 50% greater than that achieved for Photofrin ($\lambda_{max.}$ = 630 nm) [5, 60].

Verteporfin has further advantages over the first generation sensitiser Photofrin. It is rapidly absorbed by the tumour (optimal tumour-normal tissue ratio 30–150 minutes post-intravenous injection) and is rapidly cleared from the body, minimising patient photosensitivity (1-2 days) [5, 61].

Purlytin

Tin etiopurpurin, a chlorin photosensitiser (Figure 18), is marketed under the trade name Purlytin by Miravant Medical Technologies (Santa Barbara, Calif, USA) [5–9, 62]. Purlytin has also undergone Phase II clinical trials (USA) for cutaneous metastatic breast cancer and Kaposi's sarcoma in patients with AIDS (acquired immunodeficiency syndrome) [3, 7]. Purlytin has been used successfully to treat the non-malignant conditions psoriasis and restenosis [5].

Chlorins (Figure 12) are distinguished from the parent porphyrins by a reduced exocyclic double bond. The result of the reduced bond is a decrease in the symmetry of the conjugated macrocycle, leading to an increased absorption in the long-wavelength portion of the visible region of the electromagnetic spectrum (650–680 nm). More correctly, Purlytin is a purpurin; a degradation product of chlorophyll [8, 9, 12].

Purlytin has a tin atom chelated in its central cavity which causes a red-shift of approximately 20–30 nm (with respect to Photofrin and non-metallated etiopurpurin, $\lambda_{max.}SnEt_2$ = 650 nm) [6, 9, 12]. Purlytin has been reported to localise in skin and produce a photoreaction 7–14 days post-administration [6, 9].

Foscan

Tetra(*m*-hydroxyphenyl)chlorin (*m*THPC, Figure 19) has been developed and entered into clinical trials (USA and Europe) under the trade name Foscan by Scotia

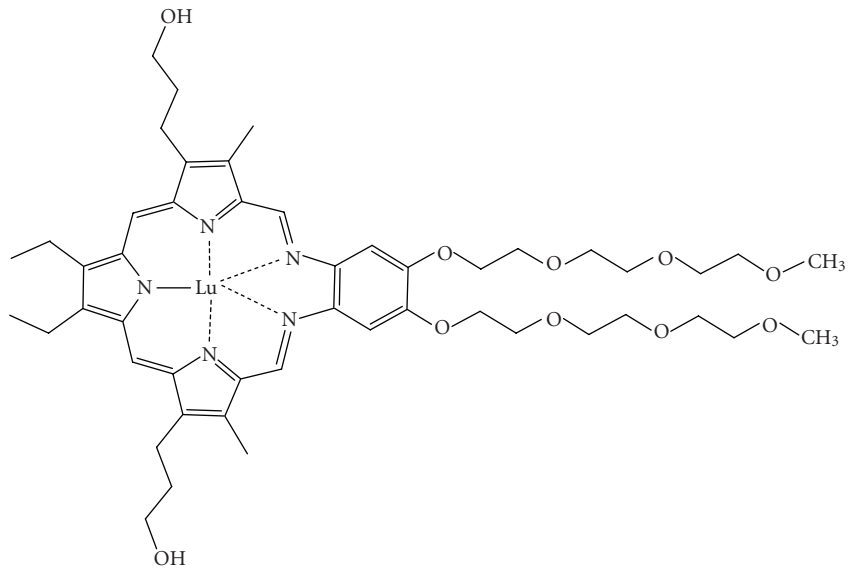

Figure 20: Lutex.

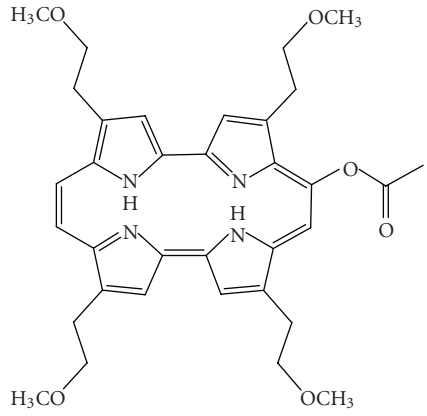

Figure 21: ATMPn.

Pharmaceutics (Guildford, Surrey, UK) and BioLitec Pharma Limited (Dublin, Ireland) [3, 5–9, 11, 18]. Foscan, also known as Temoporfin, has been evaluated as a phototherapeutic agent against head and neck cancers in these trials [5]. It has also been investigated in clinical trials for malignant and non-malignant diseases, including gastric and pancreatic cancers, hyperplasia, field sterilisation after cancer surgery and for the control of antibiotic-resistant bacteria, in the USA, Europe, and the Far East [5, 9, 11].

Foscan has a singlet oxygen quantum yield comparable to other chlorin photosensitisers but the low drug and light doses (approximately 0.1 mg kg^{-1} and as low as 5 J cm^{-2}, resp.) required to achieve photodynamic responses (equivalent to Photofrin, 2–5 mg kg^{-1}, 100–200 J cm^{-2}; therefore Foscan is approximately 100 times more photoactive than Photofrin), potentially make Foscan one of the most potent second generation photosensitisers currently under investigation [5, 7, 9].

Unfortunately, Foscan can render patients photosensitive for up to 20 days after initial illumination [6, 63, 64]. One solution to this problem would be to use lower drug doses.

Lutex

Lutetium texaphyrin, marketed under the trade name Lutex and Lutrin (Pharmacyclics, Calif, USA), is a "texas-sized" porphyrin [5–9, 18, 65, 66]. Texaphyrins (first synthesised in 1987 by Sessler and his group) are expanded porphyrins that have a penta-aza core (Figure 20). The result of this macrocyclic modification is a strong absorption in the 730–770 nm region of the electromagnetic spectrum [9, 12]. This region is particularly important since tissue transparency is optimal in this range. As a result, Lutex-based PDT can (potentially) be carried out more effectively at greater depths and on larger tumours [5, 6].

Lutex has entered Phase II clinical trials (USA) for evaluation against breast cancer and malignant melanomas [6, 67].

A Lutex derivative, Antrin, has also undergone Phase I clinical trials (USA) for the prevention of restenosis (see Glossary) of vessels after cardiac angioplasty by photoinactivating foam cells that accumulate within arteriolar plaques [6, 68]. A second Lutex derivative, Optrin, is in Phase I trials for AMD [5].

Texaphyrins are being developed further by Pharmacyclics as radiosensitisers (Xcytrin, see Glossary) and chemosensitisers (see Glossary) [5]. Xcytrin, a gadolinium texaphyrin (motexafin gadolinium), has been evaluated in Phase III clinical trials against brain metastases and Phase I clinical trials (USA) for primary brain tumours [5].

ATMPn

9-Acetoxy-2,7,12,17-tetrakis-(β-methoxyethyl)-porphycene (Figure 21) has been evaluated by Glaxo Dermatology (GlaxoWellcome, NC, USA) and Cytopharm (Calif, USA)

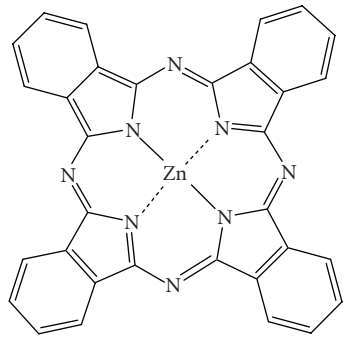

Figure 22: Zinc phthalocyanine CGP55847.

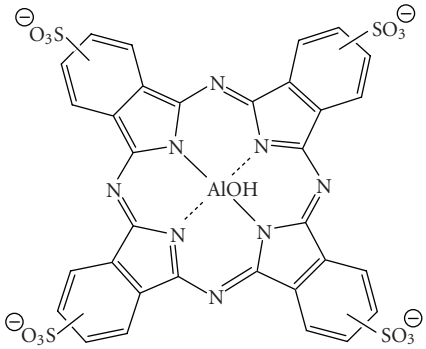

Figure 23: Photosense.

as a photodynamic therapy agent for dermatological applications against psoriasis vulgaris and superficial non-melanoma skin cancer [5, 69–72].

Zinc phthalocyanine CGP55847

A liposomal formulation of zinc phthalocyanine (CGP55847, Figure 22), developed by QLT Phototherapeutics (Vancouver, Canada) and sponsored by Ciba Geigy (Novartis, Basel, Switzerland), has undergone clinical trials (Phase I/II, Switzerland) against squamous cell carcinomas of the upper aerodigestive tract [5, 18, 73, 74]. Phthalocyanines (PCs) (Figure 12) are related to tetra-aza porphyrins. Instead of four bridging carbon atoms at the *meso*-positions, as for the porphyrins, PCs have four nitrogen atoms linking the pyrrolic sub-units together. PCs further differ from porphyrins through the presence of an extended conjugate pathway: a benzene ring is fused to the β-positions of each of the four-pyrrolic sub-units. These benzene rings act to strengthen the absorption of the chromophore at longer wavelengths (with respect to porphyrins). The absorption band of PCs is almost two orders of magnitude stronger than the highest Q band of haematoporphyrin [12]. These favourable characteristics, along with the ability to selectively functionalise their peripheral structure, make PCs favourable photosensitiser candidates [10, 75–78].

A sulphonated aluminium PC derivative (Photosense, Figure 23) has also entered clinical trials (Russian Academy of Medical Sciences, and the surgical clinic of the Moscow Medical Academy, Moscow, Russia) against skin, breast, and

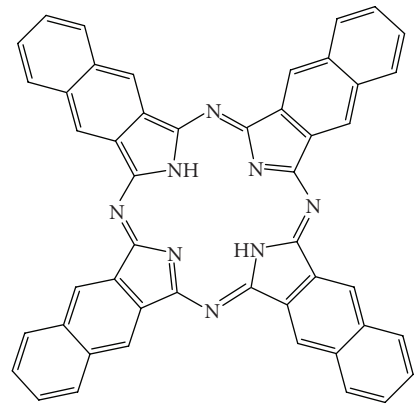

Figure 24: A naphthalocyanine.

lung malignancies and cancer of the gastrointestinal tract [5, 18, 79–81]. Sulphonation significantly increases PC solubility in polar solvents including water, circumventing the need for alternative delivery vehicles [9, 12, 18, 82].

A third PC under investigation is a silicon complex, PC4. This photosensitiser is being examined for the sterilisation of blood components at the New York Blood Centre (VI Technologies Incorporated (Vitex), Melville, NY, USA), against human colon, breast, and ovarian cancers and against glioma [5, 83–89].

A shortcoming of many of the metallo-PCs is their tendency to aggregate in aqueous buffer (pH 7.4), resulting in a decrease, or total loss, of their photochemical activity. This behaviour can be minimised in the presence of detergents [12].

Metallated cationic porphyrazines (PZ), including $PdPZ^+$, $CuPZ^+$, $CdPZ^+$, $MgPZ^+$, $AlPZ^+$, and $GaPZ^+$, have been developed and also tested *in vitro* on V-79 (Chinese hamster lung fibroblast) cells. Results have suggested these photosensitisers are capable of inducing substantial dark toxicity [12].

Naphthalocyanines

Naphthalocyanines (NCs, Figure 24) are an extended PC derivative. They have an additional benzene ring attached to each isoindole sub-unit on the periphery of the PC structure. Subsequently, NCs absorb strongly at even longer wavelengths (approximately 740–780 nm) than PCs (670–780 nm), further increasing the depth NC photosensitisers can be effectively used at. This absorption in the near infrared region makes NCs good candidates for photodynamic treatment of highly pigmented tumours, including melanomas, which present significant problems with respect to transmission of visible light.

However, a number of problems are associated with NC photosensitisers. NCs are generally less stable than their PC relatives: they readily decompose in the presence of light and oxygen; and metallo-NCs, which lack axial ligands, have a tendency to form H-aggregates in solution [12, 90]. These aggregates are photoinactive, thus compromising the photodynamic efficacy of NCs [12]. The main investigations

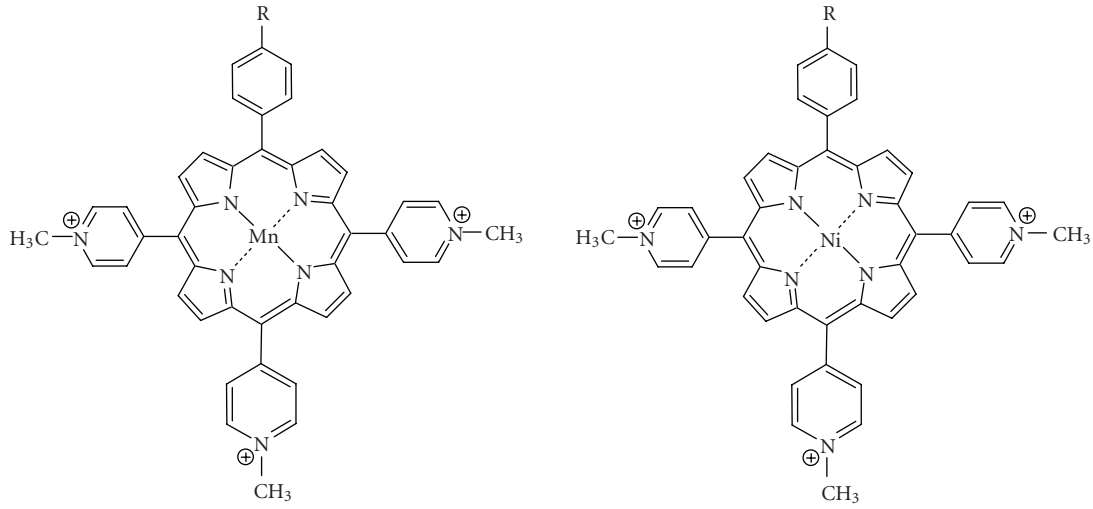

R = $C(CH_3)_3$, NH_2, NO_2 or OH

Figure 25: Water-soluble cationic metallated porphyrins.

into NCs as photodynamic therapy agents have been carried out by Kenney and co-workers, van Lier's group and the Bulgarian Academy of Sciences (Sofia, Bulgaria) (see below).

Functional groups

Altering the peripheral functionality of porphyrin-type chromophores can also have an effect on photodynamic activity.

Diamino platinum porphyrins show high anti-tumour activity, demonstrating the combined effect of the cytotoxicity of the platinum complex and the photodynamic activity of the porphyrin species [12, 91].

Positively charged PC derivatives have also been investigated [12, 64, 76, 77]. Cationic species are believed to selectively localise in the vital sub-cellular organelle, the mitochondrion. Mitochondria are key to the survival of a cell; being the site of oxidative phosphorylation, and hence are potentially important PDT targets.

Zinc and copper cationic derivatives have been investigated. Although, the positively charged zinc complexed PC was found to be less photodynamically active than its neutral counterpart *in vitro* against V-79 cells [12].

Water-soluble cationic porphyrins bearing nitrophenyl, aminophenyl, hydroxyphenyl, and/or pyridiniumyl functional groups exhibit varying cytotoxicity to cancer cells *in vitro*, depending on the nature of the metal ion (Mn, Fe, Zn, Ni), and on the number and type of functional groups [12, 77, 92]. The manganese pyridiniumyl derivative has shown the highest photodynamic activity, while the nickel analogue is photoinactive (Figure 25) [12, 92].

Another metallo-porphyrin complex, the iron chelate, was found to be more photoactive (towards HIV and simian immunodeficiency virus in MT-4 cells) than the manganese complexes; the zinc derivative was found to be photoinactive [12, 93].

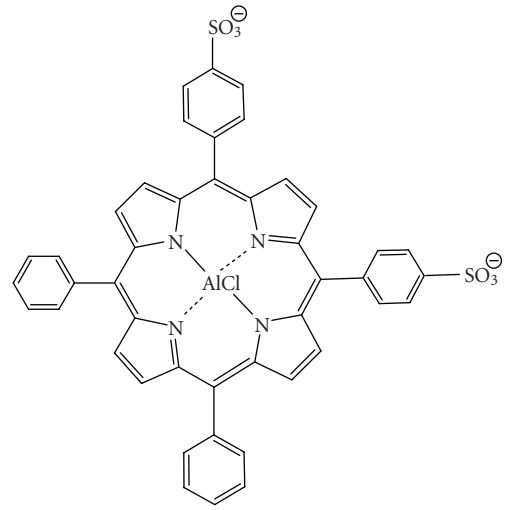

Figure 26: 5,10-Di-(4-sulphonatophenyl)-15,20-diphenylporphyrinato aluminium chloride.

The hydrophilic sulphonated porphyrins and PCs (AlPorphyrin and AlPC) compounds were tested for photodynamic activity [94]. The disulphonated analogues (with adjacent substituted sulphonated groups, Figure 26) exhibited greater photodynamic activity than their di-(symmetrical), mono-, tri- and tetra-sulphonated counterparts; tumour activity increased with increasing degree of sulphonation [8, 78].

11. THIRD-GENERATION PHOTOSENSITISERS

The poor solubility of many photosensitisers in aqueous media, particularly at physiological pH, prevents their intravenous delivery directly into the bloodstream. It would be advantageous therefore, if a delivery model could be

conceived which would allow the transportation of these (otherwise potentially useful) photosensitisers to the site of diseased tissue.

Work has recently focused on designing systems to effect greater selectivity and specificity on the photosensitiser in order to enhance cellular uptake [7, 38]. A number of possible delivery strategies have been suggested, ranging from the use of oil-in-water (o/w) emulsions to liposomes and nanoparticles as potential carrier vehicles [3, 7, 18, 36, 95, 96]. There is concern however, that although the use of these systems may increase the therapeutic effect observed as a result of photodynamic therapy, the carrier system may inadvertently decrease the "observed" singlet oxygen quantum yield (Φ_Δ) of the encapsulated photosensitiser: the singlet oxygen generated by the photosensitiser would have to diffuse out of the carrier system; and since it (singlet oxygen) is believed to have a narrow radius of action, singlet oxygen may not reach the target and elicit its desired effect [18]. It may also be possible that, if the size of the carrier is not sufficiently small or that the carrier system does not fully dissolve in physiological media, the incidence/exciting light may not be appropriately absorbed and light scattering may be significant, thus inadvertently reducing the singlet oxygen yield. An alternative delivery method which would remove this problem is the use of targeting moieties. Typical targeting strategies have included the investigation of photosensitisers directly attached to biologically active molecules such as antibodies [23–25]. These third generation photosensitisers are currently showing promise *(in vitro)* against colorectal tumour cells [24].

Metallation

A wide range of metals have been used to form complexes with photosensitiser macrocycles, with variable photodynamic results. A number of the second generation photosensitisers described earlier contain a chelated central metal ion. The main metals which have been used are transition metals, although a number of photosensitisers co-ordinated to group 13 (Al, $AlPcS_4$) and group 14 (Si, SiNC, and Sn, $SnEt_2$) metals have also been synthesised.

There seems to be no consistent observation as to the potential success of metallated photosensitisers. Indeed, a wide range of photosensitisers are metallated, but the metal ion does not confer definite photoactivity on the photosensitiser. Copper (II), cobalt (II), iron (II), and zinc (II) complexes of Hp are all photoinactive in contrast to metal-free porphyrins [12]. Yet the reverse has been observed for texaphyrin and PC photosensitisers; only the metallo-complexes have demonstrated efficient photosensitisation [12].

The presence and nature of the central metal ion, bound by a number of photosensitisers, strongly influences the photophysical properties of the photosensitiser [12, 64, 77]. Chelation of paramagnetic metals to a PC chromophore appears to shorten triplet lifetimes (down to nanosecond range), generating variations in the triplet quantum yield and triplet lifetime of the photoexcited triplet state of the metallated PC (mPC) [12, 64, 77, 97].

Intersystem crossing (ISC) is an important parameter of photosensitisers. The triplet quantum yield and lifetime of a photosensitiser are directly related to the efficiency of singlet oxygen generation; a key component in the success of a photosensitiser [97].

Certain heavy metals are known to enhance ISC. Generally, diamagnetic metals promote ISC and have a long triplet lifetime [64, 77, 97]. In contrast, paramagnetic species deactivate excited states, reducing the excited-state lifetime and preventing photochemical reactions from taking place [97]. However, there are well-known exceptions to this generalisation, including copper octaethylbenzochlorin [13].

For many of the metallated paramagnetic texaphyrin species, triplet-state lifetimes are down in the nanosecond range [97]. These results are also mirrored by metallated PCs. PCs metallated with diamagnetic ions, such as Zn^{2+}, Al^{3+}, and Ga^{3+}, generally yield photosensitisers with desirable quantum yields and lifetimes (Φ_T 0.56, 0.50 and 0.34 and τ_T 187, 126 and 35 μs, resp.) [12, 97]. The ZnPC photosensitiser ($ZnPcS_4$) has a singlet oxygen quantum yield of 0.70; nearly twice that of most other mPCs (Φ_Δ at least 0.40) [12, 18]. Hence, the latter diamagnetic complexes should be strong candidates for PDT.

Since the heavy metal effect (see Glossary) is known to promote ISC, theoretically, it should be possible to enhance the photophysical properties (Φ_T, Φ_Δ, and τ_T) of any photosensitiser *via* metallation. In practice, this is not the case. Only one metallo-porphyrin photosensitiser (copper octaethylbenzochlorin) has shown photodynamic promise, the remaining efficient porphyrin photosensitisers are metal-free [13]. The reverse of this behaviour is observed for PCs and texaphyrins; only the (diamagnetic) metallated complexes have exhibited potential as photosensitisers [10, 12]. The metal-free analogues have shown no promise as photosensitisers [12].

Expanded metallo-porphyrins

Expanded porphyrins have a larger central binding cavity, increasing the number of potential metals it can accommodate.

Diamagnetic metallo-texaphyrins have shown encouraging photophysical properties; high triplet quantum yields and efficient generation of singlet oxygen [12, 64, 77]. In particular, the zinc and cadmium derivatives have shown triplet quantum yields close to unity [12]. In contrast, the paramagnetic metallo-texaphyrins, Mn-Tex, Sm-Tex, and Eu-Tex, have undetectable triplet quantum yields. This behaviour is parallel with that observed for the corresponding metallo-porphyrins [12].

The cadmium-texaphyrin derivative has shown *in vitro* photodynamic activity against human leukemia cells and Gram positive (*Staphylococcus*) and Gram negative (*Escherichia coli*) bacteria [98–101]. Although follow-up studies have been limited with this photosensitiser due to the toxicity of the complexed cadmium ion.

A zinc-metallated *seco*-porphyrazine (Figure 27) has been developed with a high quantum singlet oxygen yield (Φ_Δ 0.74) [102]. This expanded porphyrin-like

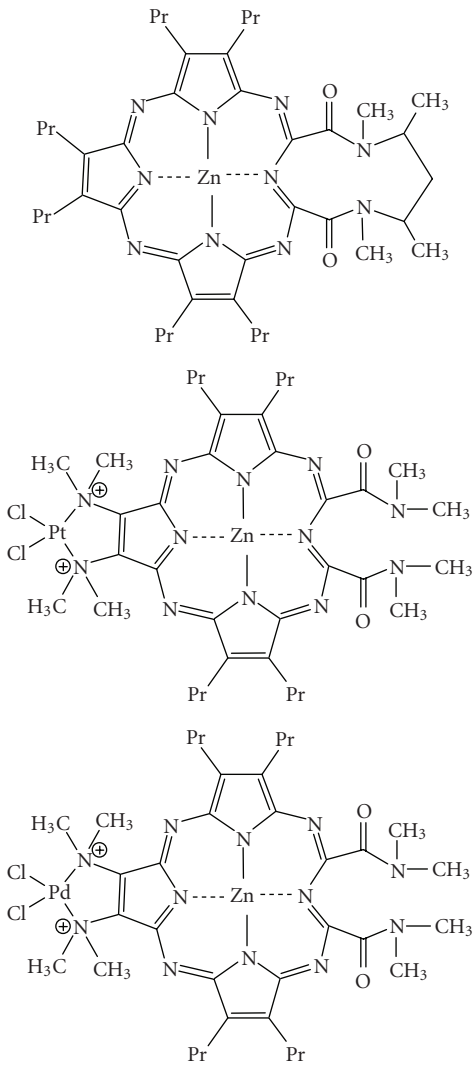

Figure 27: Zinc metallated *seco*-porphyrazine, platinum, and palladium derivatives.

photosensitiser has shown the best singlet oxygen photosensitising ability of any of the reported *seco*-porphyrazines. Platinum and palladium derivatives have also been synthesised with singlet oxygen quantum yields of 0.59 and 0.54, respectively, (Figure 27) [102].

Metallochlorins/bacteriochlorins

The tin (IV) purpurins were found to be more active when compared with analogous zinc (II) purpurins, when evaluated against human cancers [5–7, 9, 18, 103, 104].

Sulphonated benzochlorin derivatives have demonstrated a reduced phototherapeutic response against murine leukemia L1210 cells *in vitro* and transplanted urothelial cell carcinoma in rats, whereas the tin (IV) metallated benzochlorins exhibited an increased photodynamic effect in the same tumour model (Figure 28) [105].

The previously mentioned copper octaethylbenzochlorin (Figure 10) demonstrated an unexpected result. Despite

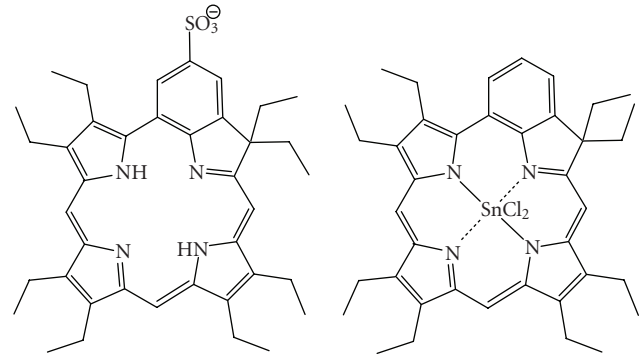

Figure 28: Sulphonated and tin (IV) benzochlorin derivatives.

an undetectable triplet state, it appears to be more *photoactive* towards leukemia cells *in vitro* and a rat bladder tumour model [106–108]. Suggestions for this unusual effect have pointed to interactions between the cationic iminium group and biomolecules [109]. Such interactions may allow electron-transfer reactions to take place *via* the short-lived excited singlet state and lead to the formation of radicals and radical ions. The copper-free derivative exhibited a tumour response with short intervals between drug administration and photodynamic therapy. Increased *in vivo* activity was observed with the zinc benzochlorin analogue [109].

Metallo-phthalocyanines

The photophysical properties of PCs are strongly influenced by the presence and nature of the central metal ion [12, 18, 64, 77]. Co-ordination of transition metal ions gives metallo-complexes with short triplet lifetimes (nanosecond range), resulting in different triplet quantum yields and lifetimes (with respect to the non-metallated analogues) [12]. The diamagnetic metals, such as zinc, aluminium, and gallium, generate metallo-phthalocyanines (MPC) with high triplet quantum yields ($\Phi_T \geq 0.4$) and short lifetimes ($ZnPCS_4$ $\tau_T = 490$ Fs and $AlPCS_4$ $\tau_T = 400$ Fs) and high singlet oxygen quantum yields ($\Phi_\Delta \geq 0.7$) [12, 18, 64, 77, 110]. As a result, ZnPC and AlPC have been evaluated as second generation photosensitisers active against certain tumours [12].

Metallo-naphthocyaninesulfobenzo-porphyrazines (M-NSBP)

Aluminium has been successfully coordinated to M-NSBP (Figure 29). The resulting complex has shown photodynamic activity against EMT-6 tumour-bearing Balb/c mice (disulphonated analogue demonstrated greater photoactivity than the mono-derivative) [111].

Metallo-naphthalocyanines

Wöhrle and co-workers (Bulgaria) have concentrated their investigations on a zinc NC with various amido substituents. They observed the best phototherapeutic response

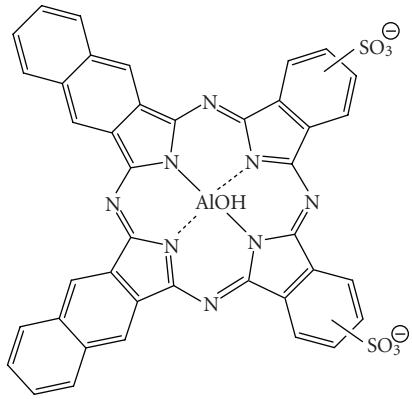

Figure 29: An aluminium naphthalocyaninesulfobenzoporphyrazine.

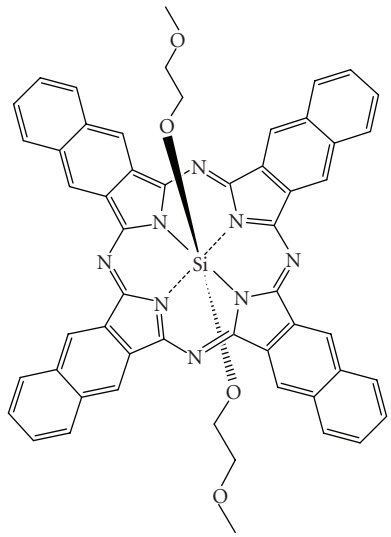

Figure 30: A siloxane naphthalocyanine.

(Lewis lung carcinoma in mice) with a tetrabenzamido analogue [112–114]. Kenney's group in the USA have studied complexes of silicon (IV) NCs (Figure 30) with two axial ligands in anticipation the ligands would minimise aggregation [115]. In particular, they investigated the disubstituted analogues as potential photodynamic agents [116, 117]. Kenney's results suggested that a siloxane NC substituted with two methoxyethyleneglycol ligands is an efficient photosensitiser against Lewis lung carcinoma in mice and that SiNC[OSi(i-Bu)$_2$-n-$C_{18}H_{37}$]$_2$ is effective against Balb/c mice MS-2 fibrosarcoma cells [118, 119]. van Lier and his group in Canada have also extensively investigated siloxane NCs as agents for photodynamic therapy [5, 76]. van Lier's research on these compounds suggests that they are efficacious photosensitisers against EMT-6 tumours in Balb/c mice also [120, 121]. The ability of certain metallo-NC derivatives (AlNc) to generate singlet oxygen is weaker than the analogous (sulphonated) metallo-PCs (AlPC); reportedly 1.6–3 orders of magnitude less [12].

Table 1: Quantum triplet yields of texaphyrin metallated with paramagnetic and diamagnetic lanthanides (data reproduced from [97]).

Paramagnetic MTex	Φ_T		Diamagnetic MTex
Eu-Tex	0.090	0.563	Y-Tex
Gd-Tex	0.156	0.500	In-Tex
Yb-Tex	0.126	0.340	Lu-Tex

It can be seen from the above examples that generalisation(s) between the nature of the parent chromophore; the presence/absence of a central metal ion; and the desirable photophysical properties required for a successful photosensitiser are difficult to make. In the porphyrin systems, the zinc ion appears to hinder the photodynamic activity of the compound; whereas, in the higher/expanded π-systems, dyes chelated with the same metal ion are observed to form complexes with good to high photophysical/photodynamic properties.

In order to try and address these observations, Sessler and his group undertook an extensive study into the metallated texaphyrins, investigating the "influence of large metal cations on the photophysical properties of texaphyrins." They particularly studied "the effect of metal cations on the photophysical properties of coordinating ligands." The group concentrated on the lanthanide (III) metal ions, Y, In, Lu, Cd, Nd, Sm, Eu, Gd, Tb, Dy, Ho, Er, Tm, and Yb [97].

Sessler and co-workers observed that when diamagnetic Lu (III) was complexed to texaphyrin, an effective photosensitiser (Lutex) was generated. When they substituted the paramagnetic Gd (III) ion for the Lu metal, photodynamic activity was lost. As a result, the group investigated a range of diamagnetic and paramagnetic ions [97].

Sessler further reported a correlation between the excited-singlet and triplet state lifetimes and the rate of ISC of the diamagnetic texaphyrin complexes, Y(III), In (III), and Lu (III), and the atomic number of the cation [97].

Paramagnetic metallo-texaphyrins were observed to display rapid ISC. Greater effects on the rates of triplet decay were also observed, and the triplet lifetimes were strongly affected by the choice of metal centre [97]. The diamagnetic ions (Y, In, and Lu) were recorded as having triplet lifetimes ranging from 187, 126, and 35 μs, respectively. Comparable lifetimes for the paramagnetic species (Eu-Tex 6.98 μs, Gd-Tex 1.11, Tb-Tex < 0.2, Dy-Tex 0.44×10^{-3}, Ho-Tex 0.85×10^{-3}, Er-Tex 0.76×10^{-3}, Tm-Tex 0.12×10^{-3}, and Yb-Tex 0.46) were obtained [97].

Sessler and his group were only able to measure the triplet quantum yields for three of the paramagnetic complexes (see Table 1). The results were significantly lower than the diamagnetic metallo-texaphyrins [97].

The data collected from Sessler and co-workers experiments suggests that, in general, singlet oxygen quantum yields closely follow the triplet quantum yields.

Their experimental data leads to the conclusion that various diamagnetic and paramagnetic texaphyrins investigated have independent photophysical behaviour with respect to a complex's magnetism. The diamagnetic complexes were

- **Imaging Agents**

Imaging agents enhance the detection of certain tissues and can be used as tools in diagnostic applications including determining the physiology of the body, in managing disease and locating abnormalities in the body. In particular, certain imaging agents such as the fluorescent tetrapyrrolic-type photosensitisers described in this Review can aid in determining (photosensitiser) localisation and degree of photosensitiser uptake by diseased tissue. The main diagnostic imaging techniques include magnetic resonance imaging (MRI), positron emission tomography (PET), scintigraphy (radionucleotides), ultrasound imaging, CT scans and x-rays. MRI, PET, and scintigraphy are well-suited techniques used in medical applications to demonstrate pathological or physiological alterations in living tissue. Unfortunately, the degree of signal enhancement for diseased *verses* normal tissue is often insufficient and the images formed from these techniques do not adequately show the anatomy or pathology of the desired area. To overcome this problem the images can be enhanced with contrast enhancement agents.

The contrast agents used for MRI imaging are normally paramagnetic complexes, although diamagnetic compounds may also be used. The gadolinium-chelates have shown promise as contrast enhancement agents in pre-clinical trials and clinical use [122]. The gadolinium-enhanced tissue appears brighter on images in comparison to gadolinium-free tissue. Expanded porphyrins are particularly suited to co-ordinating these relatively large cations (Gd ionic radius approximately 1.0 Å, expanded porphyrin ionic radius approximately 2.0 Å) in a stable manner [123, 124]. Forming chelates between a molecule such as an expanded porphyrin and a metal such as gadolinium reduces the toxicity of the free metal ion [122]. The first gadolinium-chelate approved for use as an enhancement agent was Gd-DTPA (gadopentetate dimeglumine, also known as Magnevist [125, 126]. Other chelates such as Gd-DOTA (gadoterate meglumine acid, also known as Dotarem and Gd-Tex have also shown success, with Gd-Tex administered to SMT-F tumour-bearing Balb/c mice [127, 128].

Metallated porphyrins, including manganese (II) tetraarylporphyrins, have also been studied as contrast enhancement agents for MRI [12]. Like the expanded porphyrin example above, metals suited to the technique are generally paramagnetic and include those which are not readily metabolised by the body and which strongly coordinate to the porphyrin macrocycle.

Diamagnetic agents have also shown some success as gastrointestinal imaging agents, while superparamagnetic and ferromagnetic agents have been successful for liver and bowel imaging (Lumirem ($Fe^{2+/3+}$, bowel), also known as GastroMark, and Endrorem ($Fe^{2+/3+}$, liver) [129]. Other paramagnetic agents include LumenHance (Fe^{2+}, bowel) [130, 131].

Radiosensitisers and Radiolabels

A number of the metallated photosensitisers described in the Review are also radiosensitisers (see earlier).

The metallo-photosensitisers have shown further applications as radiolabels. Porphyrins and phthalocyanines exhibit tumour retention in animals, potentially making them candidates as carriers of clinically accepted radioisotopes, such as ^{67}Ga (III). ^{67}Ga (III) coordinated to H_2PCS shows good tumour uptake in C3H mice [12, 132]. They have also been used to image the brain, lymph nodes, melanoma tumours, and as bifunctional chelating agents for antibody labelling. Examples include ^{111}In, ^{64}Cu, ^{67}Cu, ^{99m}Tc (HpD labelled), ^{57}Co-TPP, ^{109}Pd-porphyrins, and ^{54}Mn-HpD. Vanadium has also been attached to a porphyrin and investigated for PET [12].

PET, also a non-invasive diagnostic imaging technique, produces images of the body's basic biochemistry. PET can therefore be useful in observing the body's biochemical changes affected by disease. The imaging agents used in PET contain a radioactive material coupled (labeled) to a compound which is normally present in the body such as water or glucose. The resulting drug (radionucleotide) is administered to the body and physiological images are formed as the body processes the drug. Some of the metals used to label the organic molecules include ^{64}Cu and ^{68}Ga [133, 134]. The latter metal forms a complex which has been used in scans of the meninges—membrane which surrounds the brain and spinal cord [135].

Box 4

Table 2: Summary of a collection of different photosensitiser types and their absorption data.

CLASS OF PHOTOSENSITISER	LONGEST WAVELENGTH ABSORPTION/nm	EXTINCTION COEFFICIENT/ $M^{-1}cm^{-1}$	DRUGS IN CLINICAL TRIAL (Phase I–III)	DRUGS APPROVED FOR PDT (PRECLINICAL AND CLINICAL)
Porphyrins	620–640	3,500	—	Photofrin Levulan Metvix
(Expanded Porphyrins)				
Porphycenes	610–650	50,000		ATMPn
Texaphyrins	730–770	40,000	Lu-Tex Optrin Antrin Xcytrin Benzvix Hexvix	
Chlorins	650–690	40,000	Foscan Puryltin	Visudyne
Bacteriochlorins	730–800	150,000	—	—
Phthalocyanines	680–780	200,000	CGP55847 PC4 Photosense	—
Naphthalocyanines	740–780	250,000	—	—

Table 3: Summary of a range of photosensitisers and their clinical applications.

TRADE NAME	MARKETING COMPANY	PRE-/CLINICAL APPLICATION	COUNTRIES APPROVED IN
Photofrin	QLT Phototherapeutics	Oesophageal, lung, bladder and cervical dysplasia	Canada (1993), The Netherlands (1994), Japan (1994), USA (1995), France (1996), Germany (1997), Finland (1999), UK (1999), Sweden (2000), Italy (2000), Ireland (2000), Poland (2000)
Levulan	DUSA Pharmaceuticals	Actinic keratosis Actinic keratosis and basal-cell carcinoma	USA (1999), Sweden (2001), Europe (2001)
Metvix	Photocure ASA	Actinic keratosis and basal-cellcarcinoma	Sweden (2001), Europe (2001)
Visudyne	QLT Phototherapeutics	Wet-AMD	Europe (2000), USA (2000), Canada (2000),
		Subfoveal choroidal neovascularisation	Europe (2000), USA(2000), Canada (2000)
ATMPn	GlaxoWellcome and Cytopharm	Psorasis and non-melanoma skin cancer	Germany (1997)
Purlytin	Miravant Medical Technologies	Psorasis and restenosis	USA (1998)
Foscan	BioLitec Pharmaceuticals	Head and neck cancers	Europe (2001)

characterised by relatively high fluorescence quantum yields, excited-singlet and triplet lifetimes, and singlet oxygen quantum yields; in distinct contrast to the paramagnetic species investigated [97].

Results suggested that the +2 charged diamagnetic species exhibit a direct relationship between their fluorescence quantum yields, excited state lifetimes, rate of ISC, and the atomic number of the metal ion. The greatest diamagnetic ISC rate was observed for Lu-Tex; a result ascribed to the heavy atom effect. The heavy atom effect also held for the Y-Tex, In-Tex, and Lu-Tex triplet quantum yields and lifetimes. The triplet quantum yields and lifetimes both decreased with increasing atomic number. The singlet oxygen quantum yield correlated with this observation [97].

The photophysical properties displayed by the paramagnetic species were more complex. A simple correlation between the observed data/behaviour and the number of unpaired electrons located on the metal ion could not be made. For example, the ISC rates and the fluorescence lifetimes gradually decreased with increasing atomic number, the Gd-Tex, and Tb-Tex chromophores showed (despite having a larger number of unpaired electrons) slower rates of ISC and longer lifetimes than Ho-Tex or Dy-Tex. Sessler suggested that charge transfer or intermolecular energy transfer is taking place from higher excited states (such as S_2) [97].

12. SUMMARY

A variety of second generation photosensitisers have been developed and evaluated against a range of clinical applications (see Tables 2 and 3). The metallation of a number of these chromophores has generated a variety of photosensitisers with improved photophysical properties. The effectiveness of these metallo-photosensitisers depends largely (but not definitively) on the nature of the coordinated central metal ion. Chromophores chelated to diamagnetic transition metals and lanthanide ions have shown the greatest potential as photodynamic agents, a consequence of the heavy metal effect enhancing the rate of ISC. As a result, a number of these metallated tetrapyrrole-based macrocycles are currently photosensitisers of choice, particularly the zinc (II), aluminium (III), and tin (IV) complexes.

GLOSSARY

1. AMD is the leading cause of blindness in humans over the age of 50. AMD is characterised by a rapid growth of abnormal blood vessels under the central retina causing scarring, and an accelerated loss of visual acuity [58].
2. Chemosensitisers are drugs or chemicals which are used to enhance the therapeutic effects of anti-cancer (chemotherapy) drugs. They make the tumour cells more sensitive to the effects of chemotherapy.
3. Diamagnetic species is a species with no unpaired electrons, that is, all electrons are spin-paired.
4. Fluorophore is generally a molecule capable of absorbing light energy when irradiated at a specific wavelength and emitting energy at longer wavelengths.
5. Heavy atom effect enhances coupling between the excited-singlet (S_1) and excited-triplet (T_1) states. It is the enhancement of a spin-forbidden process by the presence of an atom of high atomic molecular weight. Mechanistically, it responds to a spin-orbit coupling enhancement produced by a heavy atom. Spin-forbidden and spin-allowed processes are highlighted in Section 7.
6. Luminescence lifetime is the average time a molecule spends in an excited state ($S_n > 0$ or $T_n > 0$).
7. Methylene blue is used to sterilize/decontaminate freshly frozen plasma units by inactivating extracellularly enveloped viruses (such as HIV), as well as methaemoglobinaemia [5, 9].
8. Paramagnetic species is a species with one or more unpaired electrons.
9. Phase I clinical trials are used to determine pharmacokinetic properties (metabolism, elimination, and preferred method of administration) and a safe dosage range, and identify any side effects of a new drug. They are performed on a small number of people (20–80).
10. Phase II clinical trials are performed on a larger group of people (100–300). The drug is further evaluated to test its effectiveness and any side effects.
11. Phase III clinical trials: the drugs effectiveness is confirmed and comparisons are made to more commonly used treatment modalities in a range of 1000–3000 people. Potential side effects are monitored.
12. Phase IV clinical trials are post-marketing observations and evaluations.
13. Photochemotherapy is a combination of a chemical substance and light to treat disease.
14. Phototherapy is a term used to describe the treatment of disease by a series of (photo-) chemical processes initiated by light.
15. Radiosensitisers are drugs which boost the effect of radiation therapy (radiotherapy) by making the tumour tissue more vulnerable to the applied radiation. They may be used alone or in conjunction with other drugs.
16. Restenosis is the renarrowing of a coronary artery after angioplasty or stenting.

REFERENCES

[1] M. F. Edelson, "Light-activated drugs," *Scientific American*, vol. 259, pp. 68–75, 1988.

[2] E. D. Sternberg, D. Dolphin, and C. Brückner, "Porphyrin-based photosensitizers for use in photodynamic therapy," *Tetrahedron*, vol. 54, no. 17, pp. 4151–4202, 1998.

[3] R. Bonnett and G. Martinez, "Photobleaching of sensitisers used in photodynamic therapy," *Tetrahedron*, vol. 57, no. 47, pp. 9513–9547, 2001.

[4] R. R. Allison, H. C. Mota, and C. H. Sibata, "Clinical PD/PDT in North America: an historical review," *Photodiagnosis and Photodynamic Therapy*, vol. 1, no. 4, pp. 263–277, 2004.

[5] W. M. Sharman, C. M. Allen, and J. E. van Lier, "Photodynamic therapeutics: basic principles and clinical applications," *Drug Discovery Today*, vol. 4, no. 11, pp. 507–517, 1999.

[6] I. J. MacDonald and T. J. Dougherty, "Basic principles of photodynamic therapy," *Journal of Porphyrins and Phthalocyanines*, vol. 5, no. 2, pp. 105–129, 2001.

[7] T. J. Dougherty, C. J. Gomer, B. W. Henderson, et al., "Photodynamic therapy," *Journal of the National Cancer Institute*, vol. 90, no. 12, pp. 889–905, 1998.

[8] R. Bonnett, "Photosensitizers of the porphyrin and phthalocyanine series for photodynamic therapy," *Chemical Society Reviews*, vol. 24, pp. 19–33, 1995.

[9] M. R. Detty, S. L. Gibson, and S. J. Wagner, "Current clinical and preclinical photosensitizers for use in photodynamic therapy," *Journal of Medicinal Chemistry*, vol. 47, no. 16, pp. 3897–3915, 2004.

[10] L. Kaestner, M. Cesson, K. Kassab, et al., "Zinc octa-n-alkyl phthalocyanines in photodynamic therapy: photophysical properties, accumulation and apoptosis in cell cultures, studies in erythrocytes and topical application to Balb/c mice skin," *Photochemical & Photobiological Sciences*, vol. 2, pp. 660–667, 2003.

[11] S. B. Brown, E. A. Brown, and I. Walker, "The present and future role of photodynamic therapy in cancer treatment," *Lancet Oncology*, vol. 5, no. 8, pp. 497–508, 2004.

[12] H. Ali and J. E. van Lier, "Metal complexes as photo- and radio-sensitizers," *Chemical Reviews*, vol. 99, no. 9, pp. 2379–2450, 1999.

[13] S. H. Selman, J. A. Hampton, A. R. Morgan, et al., "Copper benzochlorin, a novel photosensitizer for photodynamic therapy: effects on a transplantable urothelial tumor," *Photochemistry and Photobiology*, vol. 57, no. 4, pp. 681–685, 1993.

[14] Y. Mir, D. Houde, and J. E. van Lier, "Two-photon absorption of copper tetrasulfophthalocyanine induces phototoxicity towards Jurkat cells *in vitro*," *Photochemical & Photobiological Sciences*, vol. 5, pp. 1024–1030, 2006.

[15] A. Villanueva and G. Jori, "Pharmacokinetic and tumour-photosensitizing properties of the cationic porphyrin *meso*-tetra(4N-methylpyridyl)porphine," *Cancer Letters*, vol. 73, no. 1, pp. 59–64, 1993.

[16] J. L. Sessler, N. A. Tvermoes, J. Davis, et al., "Expanded porphyrins. Synthetic materials with potential medical utility," *Pure and Applied Chemistry*, vol. 71, pp. 2009–2018, 1999.

[17] A. P. Castano, T. N. Demidova, and M. R. Hamblin, "Mechanisms in photodynamic therapy: part one—photosensitizers, photochemistry, and cellular localization," *Photodiagnosis and Photodynamic Therapy*, vol. 1, no. 4, pp. 279–293, 2004.

[18] E. S. Nyman and P. H. Hynninen, "Research advances in the use of tetrapyrrolic photosensitizers for photodynamic therapy," *Journal of Photochemistry and Photobiology B*, vol. 73, no. 1-2, pp. 1–28, 2004.

[19] K. Svanberg, I. Wang, S. Colleen, et al., "Clinical multi-colour fluorescence imaging of malignant tumours-initial experience," *Acta Radiologica*, vol. 39, no. 1, pp. 2–9, 1998.

[20] Z. Smetana, E. Ben-Hur, E. Mendelson, S. Salzberg, P. Wagner, and Z. Malik, "Herpes simplex virus proteins are damaged following photodynamic inactivation with phthalocyanines," *Journal of Photochemistry and Photobiology B*, vol. 44, no. 1, pp. 77–83, 1998.

[21] G. Jori, "Tumour photosensitizers: approaches to enhance the selectivity and efficiency of photodynamic therapy," *Journal of Photochemistry and Photobiology B*, vol. 36, no. 2, pp. 87–93, 1996.

[22] R. Decreau, M. J. Richard, P. Verrando, M. Chanon, and M. Julliard, "Photodynamic activities of silicon phthalocyanines against achromic M6 melanoma cells and healthy human melanocytes and keratinocytes," *Journal of Photochemistry and Photobiology B*, vol. 48, no. 1, pp. 48–56, 1999.

[23] R. Hudson, M. Carcenac, K. Smith, et al., "The development and characterisation of porphyrin isothiocyanate-monoclonal antibody conjugates for photoimmunotherapy," *British Journal of Cancer*, vol. 92, pp. 1442–1449, 2005.

[24] N. Malatesti, K. Smith, H. Savoie, J. Greenman, and R. W. Boyle, "Synthesis and *in vitro* investigation of cationic 5,15-diphenyl porphyrin-monoclonal antibody conjugates as targeted photodynamic sensitisers," *International Journal of Oncology*, vol. 28, pp. 1561–1569, 2006.

[25] C. Staneloudi, K. A. Smith, R. Hudson, et al., "Development and characterization of novel photosensitizer: scFv conjugates for use in photodynamic therapy of cancer," *Immunology*, vol. 120, no. 4, pp. 512–517, 2007.

[26] C. A. Rebeiz, K. N. Reddy, U. B. Nandihalli, and J. Velu, "Tetrapyrrole-dependent photodynamic herbicides," *Photochemistry and Photobiology*, vol. 52, pp. 1099–1117, 1990.

[27] T. BenAmor, M. Tronchin, L. Bortolotto, R. Verdiglione, and G. Jori, "Porphyrins and related compounds as photoactivatable insecticides phototoxic activity of hematoporphyrin towards Ceratitis capitata and Bactrocera oleae," *Photochemistry and Photobiology*, vol. 67, pp. 206–211, 1998.

[28] J. L. Sessler, M. J. Cyr, B. G. Maiya, et al., "Photodynamic inactivation of enveloped viruses using sapphyrin, a 22 pi-electron expanded porphyrin: possible approaches to prophylactic blood purification protocols," in *Photodynamic Therapy: Mechanisms II*, vol. 1203 of *Proceedings of SPIE*, pp. 233–245, Los Angeles, Calif, USA, January 1990.

[29] P. B. Keating, M. F. Hinds, and S. J. Davis, "A singlet oxygen sensor for photodynamic cancer therapy," in *Proceedings of the International Congress on Applications of Lasers and Laser-Optics*, San Diego, Calif, USA, November 1999.

[30] C. E. Wayne and R. P. Wayne, "Photochemical principles," in *Photochemistry*, vol. 39 of *Oxford Chemistry Primers*, chapter 1, pp. 11–12, Oxford Science, Oxford University Press, Oxford, UK, 1996.

[31] C. E. Wayne and R. P. Wayne, "Photophysics," in *Photochemistry*, vol. 39 of *Oxford Chemistry Primers*, chapter 3, p. 41, Oxford Science, Oxford University Press, Oxford, UK, 1996.

[32] C. Schweitzer and R. Schmidt, "Physical mechanisms of generation and deactivation of singlet oxygen," *Chemical Reviews*, vol. 103, no. 5, pp. 1685–1757, 2003.

[33] A. Gilbert and J. Baggott, in *Essentials of Molecular Photochemistry*, chapter 1, pp. 8–9, Blackwell Scientific, Oxford, UK, 1991.

[34] A. Gilbert and J. Baggott, in *Essentials of Molecular Photochemistry*, chapter 4, p. 92, Blackwell Scientific, Oxford, UK, 1991.

[35] I. E. Kochevar and R. W. Redmond, "Photosensitized production of singlet oxygen," *Methods in Enzymology*, vol. 319, pp. 20–28, 2000.

[36] K. Lang, J. Mosinger, and D. M. Wagnerová, "Photophysical properties of porphyrinoid sensitizers non-covalently bound to host molecules; models for photodynamic therapy," *Coordination Chemistry Reviews*, vol. 248, no. 3-4, pp. 321–350, 2004.

[37] J. E. van Lier, "Photosensitization: reaction pathways," in *Photobiological Techniques, Photosensitisation: Reaction Pathways*, D. P. Valenzeno, R. H. Pottier, P. Mathis, and R. H. Douglas, Eds., vol. 216 of *NATO ASI Series, Series A: Life Sciences*, chapter 7, pp. 85–98, Plenum Press, New York, NY, USA, 1991.

[38] F. Wilkinson, W. P. Helman, and A. B. Ross, "Quantum yields for the photosensitized formation of the lowest electronically excited singlet state of molecular oxygen in solution," *Journal of Physical and Chemical Reference Data*, vol. 22, no. 1, pp. 113–262, 1993.

[39] E. Cló, J. W. Snyder, P. R. Ogilby, and K. V. Gothelf, "Control and selectivity of photosensitized singlet oxygen production: challenges in complex biological systems," *ChemBioChem*, vol. 8, no. 5, pp. 475–481, 2007.

[40] J. W. Snyder, E. Skovsen, J. D. C. Lambert, L. Poulsen, and P. R. Ogilby, "Optical detection of singlet oxygen from single cells," *Physical Chemistry Chemical Physics*, vol. 8, no. 37, pp. 4280–4293, 2006.

[41] E. Skovsen, J. W. Snyder, J. D. C. Lambert, and P. R. Ogilby, "Lifetime and diffusion of singlet oxygen in a cell," *Journal of Physical Chemistry B*, vol. 109, no. 18, pp. 8570–8573, 2005.

[42] A. P. Castano, T. N. Demidova, and M. R. Hamblin, "Mechanisms in photodynamic therapy: part two—cellular signaling, cell metabolism and modes of cell death," *Photodiagnosis and Photodynamic Therapy*, vol. 2, no. 1, pp. 1–23, 2005.

[43] M. Oschner, "Photophysical and photobiological processes in the photodynamic therapy of tumours," *Journal of Photochemistry and Photobiology B*, vol. 39, no. 1, pp. 1–18, 1997.

[44] E. Weizman, C. Rothmann, L. Greenbaum, et al., "Mitochondrial localization and photodamage during photodynamic therapy with tetraphenylporphines," *Journal of Photochemistry and Photobiology B*, vol. 59, no. 1–3, pp. 92–102, 2000.

[45] www.chem.ucla.edu/dept/Organic/CSF_Brochure.html, August 2006.

[46] K. L. See, I. J. Forbes, and W. H. Betts, "Oxygen dependency of photocytotoxicity with haematoporphyrin derivative," *Photochemistry and Photobiology*, vol. 39, pp. 631–634, 1984.

[47] L. W. Ma, J. Moan, and K. Berg, "Evaluation of a new photosensitizer, *meso*-tetra-hydroxyphenyl-chlorin, for use in photodynamic therapy. A comparison of its photobiological properties with those of two other photosensitizers," *International Journal of Cancer*, vol. 57, no. 6, pp. 883–888, 1994.

[48] T. Hasan and A. U. Khan, "Phototoxicity of the tetracyclines: photosensitized emission of singlet delta dioxygen," *Proceedings of the National Academy of Sciences of the United States of America*, vol. 83, no. 13, pp. 4604–4606, 1986.

[49] J. Morgan and A. R. Oseroff, "Mitochondria-based photodynamic anti-cancer therapy," *Advanced Drug Delivery Reviews*, vol. 49, no. 1-2, pp. 71–86, 2001.

[50] H. L. Anderson, "Building molecular wires from the colours of life: conjugated porphyrin oligomers," *Chemical Communications*, pp. 2323–2330, 1999.

[51] L. R. Milgrom, "What porphyrins are and what they do," in *The Colours of Life: An Introduction to the Chemistry of Porphyrins and Related Compounds*, chapter 1, pp. 1 and 16, Oxford University Press, Oxford, UK, 1997.

[52] L. R. Milgrom, "How do they do it? —making oxygen," in *The Colours of Life: An Introduction to the Chemistry of Porphyrins and Related Compounds*, chapter 3, pp. 84–85, Oxford University Press, Oxford, UK, 1997.

[53] A. J. Rest, "Porphyrins and phthalocyanines," in *Light, Chemical Changes and Life*, chapter 2.3, pp. 43–51, OUPC, Milton Keynes, UK, 1982.

[54] C. Rimmington, "Spectral absorption coefficients of some porphyrins in the Soret-band region," *Journal of Biochemistry*, vol. 75, pp. 620–623, 1960.

[55] http://chemgroups.ucdavis.edu/~smith/chime/Porph_Struct/lots_of_files/intro.html, September 2007.

[56] R. Bonnett, P. Charlesworth, B. D. Djelal, S. Foley, D. J. McGarvey, and T. G. Truscott, "Photophysical properties of 5,10,15,20-tetrakis(*m*-hydroxyphenyl)porphyrin (m-THPP), 5,10,15,20-tetrakis(*m*-hydroxyphenyl)chlorin (*m*-THPC) and 5,10,15,20-tetrakis(*m*-hydroxyphenyl)bacteriochlorin (m-THPBC): a comparative study," *Journal of the Chemical Society. Perkin Transactions II*, vol. 2, pp. 325–328, 1999.

[57] A. M. Richter, B. Kelly, J. Chow, et al., "Preliminary studies on a more effective phototoxic agent than hematoporphyrin," *Journal of the National Cancer Institute*, vol. 79, no. 6, pp. 1327–1332, 1987.

[58] H. van den Bergh, M. Sickenberg, and J.-P. Ballini, *International Photodynamic Therapy*, vol. 1, pp. 2–5, 1998.

[59] J. G. Levy, C. A. Jones, and L. A. Pilson, "The preclinical and clinical development and potential application of benzoporphyrin derivative," *International Photodynamic Therapy*, vol. 1, pp. 3–5, 1994.

[60] B. M. Aveline, T. Hasan, and R. W. Redmond, "The effects of aggregation, protein binding and cellular incorporation on the photophysical properties of benzoporphyrin derivative monoacid ring A (BPDMA)," *Journal of Photochemistry and Photobiology B*, vol. 30, no. 2-3, pp. 161–169, 1995.

[61] G. I. Stables and D. V. Ash, "Photodynamic therapy," *Cancer Treatment Reviews*, vol. 21, no. 4, pp. 311–323, 1995.

[62] A. R. Morgan, G. M. Garbo, R. W. Keck, and S. H. Selman, "New photosensitizers for photodynamic therapy: combined effect of metallopurpurin derivatives and light on transplantable bladder tumors," *Cancer Research*, vol. 48, pp. 194–198, 1988.

[63] A. Kübler, T. Haase, C. Staff, B. Kahle, M. Rheinwald, and J. Mühling, "Photodynamic therapy of primary non-melanomatous skin tumours of the head and neck," *Lasers in Surgery and Medicine*, vol. 25, no. 1, pp. 60–68, 1999.

[64] D. J. Ball, S. R. Wood, D. I. Vernon, J. Griffiths, T. M. A. R. Dubbelman, and S. B. Brown, "The characterisation of three substituted zinc phthalocyanines of differing charge for use in photodynamic therapy. A comparative study of their aggregation and photosensitising ability in relation to *m*-THPC and polyhaematoporphyrin," *Journal of Photochemistry and Photobiology B*, vol. 45, no. 1, pp. 28–35, 1998.

[65] J. L. Sessler, M. R. Johnson, and V. Lynch, "Synthesis and crystal structure of a novel tripyrrane-containing porphyrinogen-like macrocycle," *Journal of Organic Chemistry*, vol. 52, no. 19, pp. 4394–4397, 1987.

[66] J. L. Sessler, G. Hemmi, T. D. Mody, T. Murai, A. Burrell, and S. W. Young, "Texaphyrins: synthesis and applications," *Accounts of Chemical Research*, vol. 27, no. 2, pp. 43–50, 1994.

[67] K. W. Woodburn, Q. Fan, D. Kessel, Y. Luo, and S. W. Young, "Photodynamic therapy of B16F10 murine melanoma with lutetium texaphyrin," *The Journal of Investigative Dermatology*, vol. 110, pp. 746–751, 1998.

[68] K. W. Woodburn, F. Qing, D. Kessel, and S. W. Young, "Photoeradication and imaging of atheromatous plaque with texaphyrins," in *Photodynamic Therapy for Restenosis*,

vol. 2970 of *Lasers in Surgery: Advanced Characterization, Therapeutics, and Systems VII*, pp. 44–50, San Jose, Calif, USA, February 1997.

[69] R.-M. Szeimies, S. Karrer, C. Abels, et al., "9-Acetoxy-2,7,12,17-tetrakis(β-methoxyethyl)-porphycene (ATMPn), a novel photosensitizer for photodynamic therapy: uptake kinetics and intracellular localization," *Journal of Photochemistry and Photobiology B*, vol. 34, no. 1, pp. 67–72, 1996.

[70] S. Kimmel, V. Gottfried, R. Davidi, and C. Averbuj, "*In vivo* uptake and photodynamic activity of porphycenes," in *Photodynamic Therapy of Cancer I*, vol. 2078 of *Proceedings of SPIE*, pp. 205–211, Budapest, Hungary, August 1993.

[71] A. Aicher, K. Miller, E. D. Reich, and R. E. Hautmann, "Photosensitization of human bladder carcinoma cells *in vitro* by 9-acetoxy-tetra-n-proylporphycence (ATPPn) bound to liposomes from soya phosphatidylcholine," *Optical Engineering*, vol. 32, no. 2, pp. 342–346, 1993.

[72] S. Karrer, C. Abels, R.-M. Szeimies, et al., "Topical application of a first porphycene dye for photodynamic therapy—penetration studies in human perilesional skin and basal cell carcinoma," *Archives of Dermatological Research*, vol. 289, no. 3, pp. 132–137, 1997.

[73] M. Oschner, "Light scattering of human skin: a comparison between zinc(II)-phthalocyanine and photofrin II®," *Journal of Photochemistry and Photobiology B*, vol. 32, no. 1-2, pp. 3–9, 1996.

[74] K. Schieweck, H.-G. Capraro, U. Isele, et al., "CGP 55 847, liposome-delivered zinc(II)-phthalocyanine as a phototherapeutic agent for tumors," in *Photodynamic Therapy of Cancer I*, vol. 2078 of *Proceedings of SPIE*, pp. 107–118, Budapest, Hungary, August 1993.

[75] M. J. Cook, "Properties of some alkyl substituted phthalocyanines and related macrocycles," *The Chemical Record*, vol. 2, no. 4, pp. 225–236, 2002.

[76] C. Fabris, M. Soncin, G. Miotto, et al., "Zn(II)-phthalocyanines as phototherapeutic agents for cutaneous diseases. Photosensitization of fibroblasts and keratinocytes," *Journal of Photochemistry and Photobiology B*, vol. 83, no. 1, pp. 48–54, 2006.

[77] V. Mantareva, V. Kussovski, I. Angelov, et al., "Photodynamic activity of water-soluble phthalocyanine zinc(II) complexes against pathogenic microorganisms," *Bioorganic & Medicinal Chemistry*, vol. 15, no. 14, pp. 4829–4835, 2007.

[78] N. Cauchon, M. Nader, G. Bkaily, J. E. van Lier, and D. Hunting, "Photodynamic activity of substituted zinc trisulfophthalocyanines: role of plasma membrane damage," *Photochemistry and Photobiology*, vol. 82, no. 6, pp. 1712–1720, 2006.

[79] A. S. Sobolev and E. F. Stranadko, *International Photodynamic Therapy*, vol. 1, pp. 2–3, 1997.

[80] V. V. Sokolov, V. I. Chissov, E. V. Filonenko, et al., "First clinical results with a new drug for PDT," in *Photodynamic Therapy of Cancer II*, vol. 2325 of *Proceedings of SPIE*, pp. 364–366, Lille, France, September 1994.

[81] N. N. Zharkova, D. N. Kozlov, V. V. Smirnov, et al., "Fluorescence observations of patients in the course of photodynamic therapy of cancer with the photosensitizer PHOTOSENS," in *Photodynamic Therapy of Cancer II*, vol. 2325 of *Proceedings of SPIE*, pp. 400–403, Lille, France, September 1995.

[82] D. Phillips, "The photochemistry of sensitizers for photodynamic therapy," *Pure and Applied Chemistry*, vol. 67, pp. 117–126, 1995.

[83] N. L. Oleinick, A. R. Antunez, M. E. Clay, B. D. Rihter, and M. E. Kenney, "New phthalocyanine photosensitizers for photodynamic therapy," *Photochemistry and Photobiology*, vol. 57, no. 2, pp. 242–247, 1993.

[84] C. M. Whitacre, D. K. Feyes, T. Satoh, et al., "Photodynamic therapy with the phthalocyanine photosensitizer PC4 of SW480 human colon cancer xenografts in athymic mice," *Clinical Cancer Research*, vol. 6, pp. 2021–2027, 2000.

[85] P.-C. Lo, S. C. H. Leung, E. Y. M. Chan, W.-P. Fong, W.-H. Ko, and D. N. P. Ng, "Photodynamic effects of a novel series of silicon(IV) phthalocyanines against human colon adenocarcinoma cells," *Photodiagnosis and Photodynamic Therapy*, vol. 4, no. 2, pp. 117–123, 2007.

[86] S. I. A. Zaidi, R. Agarwal, G. Eichler, B. D. Rihter, M. E. Kenney, and H. Mukhtar, "Photodynamic effects of new silicon phthalocyanines – *in vitro* studies utilising rat hepatic microsomes and human erythrocyte-ghosts as model membrane sources," *Journal of Photochemistry and Photobiology B*, vol. 58, pp. 204–210, 1993.

[87] V. C. Colussi, D. K. Feyes, J. W. Mulvihill, et al., "Phthalocyanine 4 (PC4) photodynamic therapy of human OVCAR-3 tumour xenografts," *Photochemistry and Photobiology*, vol. 69, pp. 236–241, 1999.

[88] C. M. Whitacre, T. H. Satoh, L.-Y. Xue, N. H. Gordon, and N. L. Oleinick, "Photodynamic therapy of human breast cancer xenografts lacking caspase-3," *Cancer Letters*, vol. 179, no. 1, pp. 43–49, 2002.

[89] J. E. George, Y. Ahmad, D. Varghai, et al., "PC4 photodynamic therapy of U87-derived human glioma in the nude rat," *Lasers in Surgery and Medicine*, vol. 36, no. 5, pp. 383–389, 2005.

[90] M. L. Kaplan, A. J. Lovinger, W. D. Reents Jr., and P. H. Schmidt, "The preparation, spectral properties, and x-ray structural features of 2,3-naphthalocyanines," *Molecular Crystals and Liquid Crystals*, vol. 112, no. 1, pp. 345–368, 1984.

[91] H. Brunner, H. Obermeier, and R.-M. Szeimies, "Platin(II)-komplexe mit porphyrinliganden: synthese und synergismen bei der photodynamischen tumor therapie," *Chemische Berichte*, vol. 128, no. 2, pp. 173–181, 1995.

[92] L. Ding, C. Casas, G. Etemad-Moghadam, B. Meunier, and S. Cros, "Synthesis of water-soluble, cationic functionalised metalloporphyrins having a cytotoxic activity," *New Journal of Chemistry*, vol. 14, pp. 421–431, 1990.

[93] L. Ding, J. Balzarini, D. Schols, B. Meunier, and E. B. De Clercq, "Anti-human immunodeficiency virus effects of cationic metalloporphyrin-ellipticine complexes," *Biochemical Pharmacology*, vol. 44, no. 8, pp. 1675–1679, 1992.

[94] D. Wöhrle, A. Hirth, T. Bogdahn-Rai, G. Schnurpfeil, and M. Shopova, "Photodynamic therapy of cancer: second and third generations of photosensitizers," *Russian Chemical Bulletin*, vol. 47, no. 5, pp. 807–816, 1998.

[95] M. G. Alvarez, N. B. R. Vittar, F. Principe, et al., "Pharmacokinetic and phototherapeutic studies of monocationic methoxyphenylporphyrin derivative," *Photodiagnosis and Photodynamic Therapy*, vol. 1, no. 4, pp. 335–344, 2004.

[96] L. Collins-Gold, N. Feichtinger, and T. Wärnheim, "Are lipid emulsions the drug delivery solution?" *Modern Drug Discovery*, vol. 3, no. 3, pp. 44–46, 2000.

[97] D. M. Guldi, T. D. Mody, N. N. Gerasimchuk, D. Magda, and J. L. Sessler, "Influence of large metal cations on the photophysical properties of texaphyrin, a rigid aromatic

chromophore," *Journal of the American Chemical Society*, vol. 122, no. 34, pp. 8289–8298, 2000.

[98] A. Harriman, B. G. Maiya, T. Murai, G. Hemmi, J. L. Sessler, and T. E. Mallouk, "Metallotexaphyrins: a new family of photosensitisers for efficient generation of singlet oxygen," *Journal of the Chemical Society. Chemical Communications*, vol. 5, pp. 314–316, 1989.

[99] J. L. Sessler, G. Hemmi, B. G. Maiya, et al., "Tripyrroledimethine-derived (texaphyrin-type) macrocycles: potential photosensitizers which absorb in the far-red spectral region," in *Optical Methods for Tumor Treatment and Early Diagnosis: Mechanisms and Techniques*, vol. 1426 of *Proceedings of SPIE*, pp. 318–329, Los Angeles, Calif, USA, January 1991.

[100] B. Ehrenberg, Z. Malik, Y. Nitzan, et al., "The binding and photosensitization effects of tetrabenzoporphyrins and texaphyrin in bacterial cells," *Lasers in Medical Science*, vol. 8, no. 3, pp. 197–203, 1993.

[101] B. Ehrenberg, L. Roitman, A. Lavi, Y. Nitzan, Z. Malik, and J. L. Sessler, "Spectroscopic studies of photosensitization in solutions and in cells," in *Photodynamic Therapy of Cancer II*, vol. 2325 of *Proceedings of SPIE*, pp. 68–79, Lille, France, September 1995.

[102] A. Garrido-Montalban, S. M. Baum, A. G. M. Barrett, and B. M. Hoffman, "Studies on *seco*-porphyrazines: a case study on serendipity," *Dalton Transactions*, vol. 11, pp. 2093–2102, 2003.

[103] G. M. Garbo, "Purpurins and benzochlorins as sensitizers for photodynamic therapy," *Journal of Photochemistry and Photobiology B*, vol. 34, no. 2-3, pp. 109–116, 1996.

[104] N. J. Razum, A. B. Snyder, and D. R. Doiron, "SnET2: clinical update," in *Optical Methods for Tumor Treatment and Detection: Mechanisms and Techniques in Photodynamic Therapy V*, vol. 2675 of *Proceedings of SPIE*, pp. 43–46, San Jose, Calif, USA, January 1996.

[105] D. Kessel and A. R. Morgan, "Photosensitization with etiobenzochlorins and octaethylbenzochlorins," *Photochemistry and Photobiology*, vol. 58, no. 4, pp. 521–526, 1993.

[106] S. H. Selman, J. A. Hampton, A. R. Morgan, R. W. Keck, A. D. Balkany, and D. Skalkos, "Copper benzochlorin, a novel photosensitiser for photodynamic therapy – effects on a transplantable urothelial tumour," *Photochemistry and Photobiology*, vol. 57, pp. 681–685, 1993.

[107] J. A. Hampton, D. Skalkos, P. M. Taylor, and S. H. Selman, "Iminium salt of copper benzochlorin (CDS1), a novel photosensitizer for photodynamic therapy: mechanism of cell killing," *Photochemistry and Photobiology*, vol. 58, no. 1, pp. 100–105, 1993.

[108] D. Skalkos, J. A. Hampton, R. W. Keck, M. Wagoner, and S. H. Selman, "Iminium salt benzochlorins: structure-activity relationship studies," *Photochemistry and Photobiology*, vol. 59, no. 2, pp. 175–181, 1994.

[109] G. M. Garbo, V. H. Fingar, T. J. Weiman, et al., "*In vivo* and *in vitro* photodynamic studies with benzochlorin iminium salts delivered by a lipid emulsion," *Photochemistry and Photobiology*, vol. 68, no. 4, pp. 561–568, 1998.

[110] E. Reddi, G. LoCastro, R. Biolo, and G. Jori, "Pharmacokinetic studies with zinc(II)-phthalocyanine in tumour-bearing mice," *British Journal of Cancer*, vol. 56, no. 5, pp. 597–600, 1987.

[111] P. Margaron, R. Langlois, J. E. van Lier, and S. J. Gaspard, "Photodynamic properties of naphthosulfobenzoporphyrazines, novel asymmetric, amphiphilic phthalocyanine derivatives," *Photochemistry and Photobiology*, vol. 14, pp. 187–199, 1992.

[112] D. Wöhrle, M. Shopova, S. Müller, et al., "Liposome-delivered Zn(II)-2,3-naphthalocyanines as potential sensitizers for PDT: synthesis, photochemical, pharmacokinetic, and phototherapeutic studies," *Journal of Photochemistry and Photobiology B*, vol. 21, no. 2-3, pp. 155–165, 1993.

[113] M. Shopova, D. Wöhrle, N. Stoichkova, et al., "Hydrophobic Zn(II)-naphthalocyanines as photodynamic therapy agents for Lewis-lung carcinoma," *Journal of Photochemistry and Photobiology B, Biology*, vol. 23, pp. 35–42, 1994.

[114] S. Müller, V. N. Mantareva, N. Stoichkova, et al., "Tetraamido-substituted 2,3-napthalocyanine zinc(II) complexes as phototherapeutic agents: Synthesis, comparative photochemical and photobiological studies," *Journal of Photochemistry and Photobiology B*, vol. 35, pp. 167–174, 1996.

[115] B. L. Wheeler, G. Nagasubramanian, A. J. Bard, L. A. Schechtman, D. R. Dininny, and M. E. Kenney, "A silicon phthalocyanine and a silicon naphthalocyanine: synthesis, electrochemistry, and electrogenerated chemiluminescence," *Journal of the American Chemical Society*, vol. 106, no. 24, pp. 7404–7410, 1984.

[116] M. M. Zuk, B. D. Rihter, M. E. Kenney, M. A. J. Rodgers, and M. Kreimer-Birnbaum, "Pharmacokinetic and tissue distribution studies of the photosensitizer bis(di-isobutyl octadecylsiloxy)silicon 2,3-naphthalocyanine (isobosinc) in normal and tumor-bearing rats," *Photochemistry and Photobiology*, vol. 59, no. 1, pp. 66–72, 1994.

[117] M. M. Zuk, B. D. Rihter, M. E. Kenney, M. A. J. Rodgers, and M. Kreimer-Birnbaum, "Effect of delivery system on the pharmacokinetics and tissue distribution of bis(di-isobutyl octadecylsiloxy)silicon 2,3-naphthalocyanine (isobosinc), a photosensitizer for tumor therapy," *Photochemistry and Photobiology*, vol. 63, no. 1, pp. 132–140, 1996.

[118] V. Cuomo, G. Jori, B. Rihter, M. E. Kenney, and M. A. J. Rodgers, "Liposome-delivered Si(IV)-naphthalocyanine as a photodynamic sensitiser for experimental tumours: pharmacokinetic and phototherapeutic studies," *British Journal of Cancer*, vol. 62, no. 6, pp. 966–970, 1990.

[119] V. N. Mantareva, M. Shopova, G. Spassova, et al., "Si(IV)-methoxyethylene-glycol-naphthalocyanine: synthesis and pharmacokinetic and photosensitizing properties in different tumour models," *Journal of Photochemistry and Photobiology B*, vol. 40, no. 3, pp. 258–262, 1997.

[120] N. Brasseur, T.-L. Nguyen, R. Langlois, et al., "Synthesis and photodynamic activities of silicon 2,3-naphthalocyanine derivatives," *Journal of Medicinal Chemistry*, vol. 37, no. 3, pp. 415–420, 1994.

[121] N. Brasseur, R. Ouellet, K. Lewis, W. R. Potter, and J. E. van Lier, "Photodynamic activities and skin photosensitivity of the bis(dimethylthexylsiloxy)silicon 2,3-naphthalocyanine in mice," *Photochemistry and Photobiology*, vol. 62, no. 6, pp. 1058–1065, 1995.

[122] K. N. Raymond and V. C. Pierre, "Next generation, high relaxivity gadolinium MRI agents," *Bioconjugate Chemistry*, vol. 16, no. 1, pp. 3–8, 2005.

[123] J. L. Sessler and A. K. Burrell, "Expanded porphyrins," *Topics in Current Chemistry*, vol. 161, pp. 177–273, 1992.

[124] R. A. Sheldon, in *Metalloporphyrins in Catalytic Oxidations*, R. A. Sheldon, Ed., chapter 1, p. 4, Marcel Dekker, New York, NY, USA.

[125] H. C. Schmidt, M. T. McNamara, R. C. Brasch, and C. B. Higgins, "Assessment of severity of experimental pulmonary

edema with magnetic resonance imaging. Effect of relaxation enhancement by Gd-DTPA," *Investigative Radiology*, vol. 20, no. 7, pp. 687–692, 1985.

[126] W. L. Curati, M. Graif, D. P. Kingsley, H. P. Niendorf, and I. R. Young, "Acoustic neuromas: Gd-DTPA enhancement in MR imaging," *Radiology*, vol. 158, pp. 447–451, 1986.

[127] M. Magerstädt, O. A. Gansow, M. W. Brechbiel, et al., "Gd(DOTA): an alternative to Gd(DTPA) as a T[1,2] relaxation agent for NMR imaging or spectroscopy," *Magnetic Resonance in Medicine*, vol. 3, no. 5, pp. 808–812, 1986.

[128] J. L. Sessler, T. D. Mody, G. W. Hemmi, V. Lynch, S. W. Young, and R. A Miller, "Gadolinium(III) texaphyrin: a novel MRI contrast agent," *Journal of the American Chemical Society*, vol. 115, no. 22, pp. 10368–10369, 1993.

[129] Y.-X. J. Wang, S. M. Hussain, and G. P. Krestin, "Superparamagnetic iron oxide contrast agents: physicochemical characteristics and applications in MR imaging," *European Radiology*, vol. 11, no. 11, pp. 2319–2331, 2001.

[130] W. C. Small, D. DeSimone-Macchi, J. R. Parker, et al., "A multi-site phase III study of the safety and efficacy of a new manganese chloride-based gastrointestinal contrast agent for MRI of the abdomen and pelvis," *Journal of Magnetic Resonance Imaging*, vol. 10, no. 1, pp. 15–24, 1999.

[131] D. D. Schwert, J. A. Davies, and N. Richardson, "Non-gadolinium-based MRI contrast agents," *Topics in Current Chemistry*, vol. 221, pp. 165–199, 2002.

[132] J. Rousseau, R. W. Boyle, A. H. MacLennan, T. G. Truscott, and J. E. van Lier, "Biodistribution and tumor uptake of [Ga-67] chlorogallium-tetraoctadecyloxy phthalocyanine and its sulfonation products in tumor bearing C-3H mice," *Nuclear Medicine and Biology*, vol. 18, no. 7, pp. 777–782, 1991.

[133] W. Cai, K. Chen, K. A. Mohamedali, et al., "PET of vascular endothelial growth factor receptor expression," *The Journal of Nuclear Medicine*, vol. 47, no. 12, pp. 2048–2056, 2006.

[134] J. Schuhmacher, H. W. Zhang, J. Doll, et al., "GRP receptor-targeted PET of a rat pancreas carcinoma xenograft in nude mice with a ^{68}Ga-labeled bombesin(6-14) analog," *Journal of Nuclear Medicine*, vol. 46, no. 4, pp. 691–699, 2005.

[135] M. Henze, A. Dimitrakopoulou-Strauss, S. Milker-Zabel, et al., "Characterization of ^{68}Ga-DOTA-D-Phe1-Tyr3-octreotide kinetics in patients with meningiomas," *Journal of Nuclear Medicine*, vol. 46, no. 5, pp. 763–769, 2005.

Hindawi Publishing Corporation
Metal-Based Drugs
Volume 2008, Article ID 391418, 13 pages
doi:10.1155/2008/391418

Research Article

Synthesis and Biological Analysis of Thiotetra(ethylene glycol) monomethyl Ether-Functionalized Porphyrazines: Cellular Uptake and Toxicity Studies

Sangwan Lee,[1] Benjamin J. Vesper,[2,3] Hong Zong,[1] Neal D. Hammer,[2,3] Kim M. Elseth,[2,3] Anthony G. M. Barrett,[4] Brian M. Hoffman,[1] and James A. Radosevich[2,3]

[1] *Department of Chemistry, Northwestern University, 2145 Sheridan Road, Evanston, IL 60208, USA*
[2] *Center for Molecular Biology of Oral Diseases, College of Dentistry, University of Illinois at Chicago, 801 S. Paulina Street, Chicago, IL 60612, USA*
[3] *Jesse Brown VAMC, 820 South Damen Avenue, Chicago, IL 60612, USA*
[4] *Department of Chemistry, Faculty of Natural Sciences, Imperial College London, Faculty Building, South Kensington Campus, London SW7 2AZ, UK*

Correspondence should be addressed to James A. Radosevich, jrados@uic.edu

Received 29 May 2007; Revised 20 July 2007; Accepted 6 August 2007

Recommended by Michael J. Cook

The porphyrazines (pzs), a class of porphyrin analogues, are being investigated for their potential use as tumor imaging/therapeutic agents. We here examine six peripherally-functionalized M[pz(A_nB_{4-n})] pzs with $n = 4$, 3, or 2 (in a *trans* conformation) and M = H_2 or Zn, where A is an $[S((CH_2)_2O)_4Me]_2$ unit and B is a fused β,β'-diisopropyloxybenzo group. Cell viability/proliferation assays and fluorescence microscopy were carried out in both tumor and normal cells. Dark toxicity studies disclosed that four of the compounds exhibited toxicity in both normal and tumor cells; one was nontoxic in both normal and tumor cells, and one was selectively toxic to normal cells. Additionally, three of the pzs showed enhanced photo-induced toxicity with these effects in some cases being observed at treatment concentrations of up to ten-fold lower than that needed for a response in Photofrin. All six compounds were preferentially absorbed by tumor cells, suggesting that they have potential as in vitro diagnostic agents and as aids in the isolation and purification of aberrant cells from pathological specimens. In particular, two promising diagnostic candidates have been identified as part of this work.

1. INTRODUCTION

Porphyrin antitumor agents have been widely studied in recent years, especially in the area of photodynamic therapy (PDT), where the development of the clinically used porphyrin, haematoporphyrin derivative (HpD, or Photofrin), has garnered significant interest [1, 2]. However, limitations in the design, synthesis, and biological properties of Photofrin have led to the development of many second-generation PDT agents, including a number of porphyrin derivatives [3–9]. One such class of compounds being investigated as an alternative is the porphyrazines (pzs), porphyrin analogues in which the *meso* (CH) groups are replaced by nitrogen atoms linking the pyrrole rings (Scheme 1, Section 3), thereby resulting in compounds with chemical and physical properties distinct from those of the porphyrins [10]. The presence of the *meso*-nitrogen atoms results in the pzs possessing intense long-wavelength absorbance and emission bands, photophysical properties that are intrinsically superior to those of the porphyrins. Furthermore, the porphyrazines are prepared by the templated cyclization of maleonitrile derivatives, while porphyrins are synthesized by the condensation of aldehyde and pyrrole derivatives. This difference allows pzs to be readily prepared with S, N, or O heteroatoms attached to the macrocycle core, while porphyrins cannot. These heteroatom substituents enable the photophysical properties of the pzs to be tuned such that they exhibit optimal near-IR absorbance and emission in the 700–900 nm window, and allow for tuning of their singlet oxygen quantum yields from essentially *off* to *on*—characteristics

which make the pzs attractive candidates for biomedical applications [11–14].

Because of the novelty of these compounds, initial biocompatibility studies involving the pzs have focused upon determining how specific pz structures selectively alter biological functions [15, 16], leading to the establishment of "structure-function rules," which will ultimately be used to predict future biologically active pzs. To this end, we recently reported the biological activity of a suite of three anionic H_2[pz($\mathbf{A}_n\mathbf{B}_{4-n}$)] pzs, in which n = 4, 3, or 2 (*trans*), **A** was an [S-R]$_2$ unit with R = $(CH_2)_3CO_2^-$, and **B** was a fused β,β'-dialkoxybenzo group. These three anionic compounds showed a systematic increase in toxicity as n (and in turn, the number of R groups) was increased, and one pz (n = 2) was found to be selectively toxic to tumor cells. Herein we similarly describe the biocompatibility of a group of M[pz(A_n B_{4-n})] pzs, where M = H_2 or Zn, n = 4, 3, or 2 (*trans*), **A** is an [S-R]$_2$ unit with R = $[(CH_2)_2O]_4Me$, and **B** is again a fused β,β'-dialkoxybenzo group (**5**–**10**, Scheme 1).[1]

As with the aforementioned anionic porphyrazines, the pzs examined here, with thiotriethoxy(ethoxy)methyl groups appended to their periphery, allow us to study the biological effect of a specific functional group. By varying n, we can simultaneously vary the core pz structure and the number of appended R groups, resulting in each compound possessing slightly different chemical and physical properties, thereby impacting the biological effects of each.

This study also marks the first biocompatibility experiments involving metallated pzs. As previously reported, the singlet oxygen quantum yields (Φ_Δ) of the free-base (H_2) pzs increase systematically as n is decreased; the same trend is true for metallated pzs, but the presence of Zn in the pz core increases the value of Φ_Δ approximately five-fold over that of the analogous H_2 pzs [12]. Herein we report the concentration/time-dependent cytotoxicity and phototoxicity measurements, and present confocal fluorescence microscopic visualization, for pzs **5**–**10** in A549 tumor and WI-38 VA13 normal cells.

2. MATERIALS AND METHODS

2.1. Chemical reagents and instrumentation

All chemicals were purchased from Aldrich Chemical Company "Wis, USA" and used as received. Baxter silica gel (60 Å; 230–400 mesh) was used for column chromatography. A Hewlett-Packard HP8452A diode-array spectrophotometer was used to record electronic absorption spectra, and electronic emission spectra were recorded using a Photon Technology International QM2 fluorescence spectrometer. ^{1}H and ^{13}C NMR spectra were obtained using a Varian Inova 500 MHz spectrometer. Electrospray ionization mass spectra (ESI-MS) were recorded using a Finnegan LCQ Advantage mass spectrometer, and matrix-assisted laser desorption ionization-time of flight mass spectra (MALDI-TOF-MS) were recorded using a PE Voyager DE-Pro MALDI-TOF mass spectrometer; α-cyano-4-hydroxycinnamic acid was used as the matrix for MALDI-TOF experiments.

2.2. Porphyrazine synthesis

Disodium 1,2-dicyano-1,2-ethenedithiolate (Na_2MNT) [17] and 1-imino-4,7-bis(1-methylethoxy)-1H-isoindolin-3-amine (diiminoisoindoline, **1**) [11] were prepared as previously reported. During the purification of each pz, distinct bands were observed and pooled together during column chromatography; collected fractions were monitored by UV-visible spectroscopy. Each pz was prepared as a 5 mM working stock solution in dimethyl sulfoxide (DMSO) for use in the tissue culture experiments.

2.3. 2-{2-[2-(2-Methoxyethoxy)ethoxy]ethoxy} ethyl-4-methylbenzenesulfonate (3)

Sodium hydroxide (12 g, 0.3 mol) dissolved in water (55 mL) and tetra(ethylene glycol) monomethyl ether (**2**) (41.7 g, 0.2 mol) in THF (55 mL) were placed in a flask, and the mixture was stirred and cooled in an ice bath. To the mixture was added dropwise p-toluenesulfonyl choride (41.9 g, 0.22 mol) in THF (65 mL) over 30 minutes with continuous stirring and cooling of the mixture below 5°C. The solution was stirred an additional 2 hours at ∼0–5°C, at which time the mixture was poured into ice water (200 mL) and extracted twice with CH_2Cl_2 (200 mL). The combined organic extract was washed twice with water and once with a saturated NaCl solution (brine), and then dried over Na_2SO_4. After evaporation of the solvent, the resulting residue was purified by chromatography on silica gel (4% MeOH in CH_2Cl_2 eluant) to yield the tosylate **3** (63 g, 87%) as a colorless viscous oil: ^{1}H NMR (500 MHz, $CDCl_3$) δ 2.43 (s, 3H, $ArCH_3$), 3.35 (s, 3H, OCH_3), 3.52 (t, 2H, CH_2), 3.50 − 3.60 (m, 10H, CH_2), 3.67 (t, 2H, CH_2), 4.14 (t, 2H, CH_2), 7.33 (d, 2H, ArH), 7.78 (d, 2H, ArH); ^{13}C NMR (125 MHz, $CDCl_3$) 21.8, 59.1, 68.8, 69.4, 70.6, 70.8, 71.2, 71.6, 71.9, 72.2, 128.1, 130.0, 133.1, 145.0; ESI-MS (m/z) calculated for $C_{16}H_{27}O_7S$ $[M + H]^+$ 363.44, found 363.

2.4. bis{2-{2-[2-(2-Methoxyethoxy)ethoxy]ethoxy} ethylthio}maleonitrile (4)

Na_2MNT (7.45 g, 0.04 mol) was treated with two equivalents of **3** (30.45 g, 0.084 mol) in acetone (80 mL) at reflux under a nitrogen atmosphere for 12 hours. The solvent was then removed under reduced pressure, and the resulting residue was purified by chromatography on silica gel (4% MeOH in CH_2Cl_2 eluant) to yield **4** (13.40 g, 64%) as a viscous yellow oil: ^{1}H NMR (500 MHz, $CDCl_3$) δ 3.30 (t, 4H, CH_2), 3.56 (s, 6H, OCH_3), 3.50 (t, 4H, CH_2), 3.53 (t, 4H, CH_2), 3.58 (t, 4H, CH_2), 3.62 ∼ 3.64 (m, 8H, CH_2), 3.65 (t, 4H, CH_2), 3.74 (t, 4H, CH_2); ^{13}C NMR (125 MHz, $CDCl_3$) 21.8, 59.1, 68.8,

[1] To aid the reader, the compounds in this report have been numbered sequentially **1**–**10**. We note, however, that in the Master Compound Log in the lab of B.M.H., the compound numbers are as follows: **5** = **174**; **6** = **175**; **7** = **176**; **8** = **177**; **9** = **178**; **10** = **179**.

69.4, 70.7, 70.8, 71.3, 71.7, 72.0, 73.2, 128.1; ESI-MS (*m/z*) calculated for $C_{22}H_{39}N_2O_8S_2$ $[M + H]^+$ 523.69, found 523.

2.5. 2,3,7,8,12,13,17,18-octakis{2-{2-[2-(2-Methoxyethoxy)ethoxy]ethoxy}ethylthio}-21H,23H-porphyrazine (5)

Mg turnings (0.1 g, 4 mmol) and I_2 (0.01 g, 4×10^{-5} mol) in *n*-PrOH (50 mL) were heated at reflux for 24 hours under N_2 to prepare $Mg(OPr)_2$. $MNT[S(C_2H_4O)_4Me]_2$ (**4**) (5.23 g, 0.01 mol) was added, and the reaction was heated at reflux for 7 hours. The yellow reaction mixture gradually turned green. After 2 hours, the reaction mixture was a deep blue color. Heating and stirring were continued for a total 7 hours after which the solvent was removed under reduced pressure. The resulting residue was dissolved in CH_2Cl_2 (20 mL). TFA (2 mL) was slowly added, and the solution was stirred for 1 hour. After dilution in CH_2Cl_2 (100 mL), the mixture was washed 4 times with a large amount of water to remove any residual TFA, dried over Na_2SO_4, and rotary evaporated. The resulting residue was purified via column chromatography (4% MeOH in CH_2Cl_2 eluant) to produce **5** (628 mg, 12% yield) as a dark blue solid: UV-vis (CH_2Cl_2) λ_{max} (log ε) 360 (4.66), 502 (2.23), 640 (3.10), 710 (3.99) nm; ^{1}H NMR (500 MHz, $CDCl_3$) δ-1.13 (br s, 2H, NH), 3.32 (s, 24H, $-OCH_3$), 3.40 (t, 16H, CH_2), 3.55 ~ 3.59 (m, 64H, CH_2), 3.65 (t, 16H, CH_2), 3.99 (t, 16H, CH_2), 4.28 (t, 16H, CH_2); ^{13}C NMR (125 MHz, $CDCl_3$) 34.76, 59.23, 70.68, 70.72, 70.74, 70.77, 71.11, 72.09, 140.56; MALDI-TOF-MS (*m/z*) calculated for $C_{88}H_{155}N_8O_{32}S_8$ $[M + H]^+$ 2093.72, found 2093.66; calculated for $C_{88}H_{154}N_8NaO_{32}S_8$ $[M + Na]^+$ 2115.71, found 2116.48.

2.6. {2-{2-[2-(2-Methoxyethoxy)ethoxy]ethoxy}ethylthio}porphyrazines 6 and 7

Mg turnings (0.3 g, 12 mmol) and I_2 (0.03 g, 1.2×10^{-4} mol) in *n*-PrOH (150 mL) were heated at reflux for 24 h under N_2 to prepare $Mg(OPr)_2$. $MNT[S(C_2H_4O)_4Me]_2$ (**4**) (5.23 g, 0.01 mol) and diiminoisoindoline (**1**) (5.23 g, 0.02 mol) were added, and the reaction was heated at reflux for 7 hours, during which time the solution went from orange to blue-black. The solvent was removed under reduced pressure, and the residue was dissolved in CH_2Cl_2 (30 mL). TFA (3 mL) was slowly added, and the solution was stirred for 1 hour. After dilution in CH_2Cl_2 (200 mL), the mixture was washed 4 times with a large amount of water to remove any residual TFA, dried over Na_2SO_4, and rotary evaporated. The resulting residue was purified via column chromatography (4% MeOH in CH_2Cl_2 eluant) to yield **6** (260 mg, 4.3%) as a dark blue solid and **7** (477 mg, 6.2%) as a dark green solid, as well as trace amounts of **5**.

2.7. 19,22-bis(1-Methylethoxy)-4,5,9,10,14,15-hexakis{2-{2-[2-(2-methoxyethoxy)ethoxy]-ethoxy}ethylthio}-23H,25H-porphyrazine (6)

UV-vis (CH_2Cl_2) λ_{max} (log ε) 350 (4.61), 658 (3.82), 702 (4.35), 744 (sh) nm; ^{1}H NMR (500 MHz, $CDCl_3$) δ-0.20 (br s, 2H, NH), 2.02 (d, 12H, $-CHMe_3$), 3.69 (s, 18H, OCH_3), 3.76 ~ 3.79 (m, 48H, CH_2), 3.84 ~ 3.87 (m, 24H, CH_2), 4.02 (t, 4H, CH_2), 4.17 (t, 4H, CH_2), 4.19 (t, 4H, CH_2), 4.39 (t, 4H, CH_2), 4.46 (t, 4H, CH_2), 4.51 (t, 4H, CH_2), 5.49 (sept, 2H, $-CHMe_2$), 7.87 (s, 2H, ArH); ^{13}C NMR (125 MHz, $CDCl_3$) 22.3, 22.4, 22.7, 22.9, 29.9, 34.7, 34.8, 34.9, 36.5, 59.2, 70.6, 70.7, 70.8, 71.1, 71.2, 72.1, 72.7, 119.6, 126.5, 138.4, 138.8, 141.9, 150.5; ESI-MS (*m/z*) calculated for $C_{80}H_{133}N_8O_{26}S_6$ $[M + H]^+$ 1815.36, found 1815.70; calculated for $C_{80}H_{132}N_8NaO_{32}S_8$ $[M + Na]^+$ 1837.34, found 1837.76.

2.8. 1,4,13,16-tetrakis(1-Methylethoxy)-8,9,20,21-tetrakis{2-{2-[2-(2-methoxyethoxy)ethoxy]-ethoxy}ethylthio}-25H,27H-dibenzo[b,l]porphyrazine (7)

UV-vis (CH_2Cl_2) λ_{max} (log ε) 342 (4.80), 654 (5.41), 712 (2.20), 796 (4.31) nm; ^{1}H NMR (500 MHz, $CDCl_3$) δ-0.44 (br s, 2H, NH), 2.26 (d, 24H, $CHMe_2$), 3.91 (s, 24H, OCH_3), 3.93 ~ 3.96 (m, 24H, CH_2), 4.08 ~ 4.14 (m, 16H, CH_2) 4.18 (t, 8H, CH_2), 4.24 (t, 8H, CH_2), 4.77 (t, 8H, CH_2), 5.28 (sept, 4H, $CHMe_2$), 7.56 (s, 4H, ArH); ^{13}C NMR (125 MHz, $CDCl_3$) 22.7, 23.0, 35.1, 59.1, 70.6, 70.7, 70.8, 71.0, 71.1, 71.3, 72.0. 72.5, 118.5, 128.3, 138.7, 149.8; ESI-MS (*m/z*) calculated for $C_{72}H_{111}N_8O_{20}S_4$ $[M + H]^+$ 1536.96, found 1536.63; calculated for $C_{72}H_{110}N_8NaO_{20}S_4$ $[M + Na]^+$ 1558.95, found 1558.70.

2.9. Zn porphyrazines 8, 9, and 10

The three metallated pzs were each prepared analogously to zinc pzs previously described [11]. A solution of zinc chloride (20.4 mg, 0.15 mmol) in methanol (10 mL) was added to a solution of metal-free porphyrazine (0.05 mmol) in CH_2Cl_2 (30 mL). The reaction mixture was heated to reflux for 30 minutes or until zinc insertion was completed, as monitored by spectrophotometry. The reaction mixture was diluted with CH_2Cl_2 (60 mL), washed with water to remove excess zinc chloride, dried with Na_2SO_4, and evaporated to dryness under vacuum. The resulting residue was purified by chromatography on silica gel (4% MeOH in CH_2Cl_2 eluant) to yield the desired Zn porphyrazine in quantitative yield.

2.10. 2,3,7,8,12,13,17,18-octakis{2-{2-[2-(2-Methoxyethoxy)ethoxy]ethoxy}ethoxy}ethylthio-porphyrazine zinc(II) (8)

UV-vis (CH_2Cl_2) λ_{max} (log ε) 378 (4.62), 672 (4.67) nm; MALDI- TOF-MS (*m/z*) calculated for $C_{88}H_{153}N_8O_{32}S_8Zn$ $[M + H]^+$ 2157.12, found 2157.32; calculated for $C_{88}H_{152}N_8NaO_{32}S_8Zn$ $[M + Na]^+$ 2179.10, found 2179.24.

2.11. 19,22-bis(1-Methylethoxy)-4,5,9,10,14,15-hexakis{2-{2-[2-(2-methoxyethoxy)ethoxy]-ethoxy}ethylthio}-23H,25H-porphyrazine zinc(II) (9)

UV-vis (CH_2Cl_2) λ_{max} (log ε) 362 (4.60), 618(sh), 676 (4.69), 706(sh) nm; ESI-MS (m/z) calculated for $C_{80}H_{131}N_8O_{26}S_6Zn$ $[M + H]^+$ 1878.73, found 1878.60.

2.12. Zn(II) 1,4,13,16-tetrakis(1-methylethoxy)-8,9,20,21-tetrakis{2-{2-[2-(2-methoxyethoxy)-ethoxy]ethoxy}ethylthio}-25H,27H-dibenzo[b,l]porphyrazine (10)

UV-vis (CH_2Cl_2) λ_{max} (log ε) 352 (4.64), 666 (4.73), 761(4.64) nm; ESI-MS (m/z) calculated for $C_{72}H_{109}N_8O_{20}S_4Zn$ $[M + H]^+$ 1600.34, found 1599.63.

2.13. Cell culture and cell lines

All media and supplements were purchased from Invitrogen "Calif, USA" except where noted. Phosphate-buffered saline (PBS) solution was prepared by adding $Na_2HPO_4 \bullet 7$ H_2O (54.0 g), KH_2PO_4 (5.0 g), KCl (5.0 g), and NaCl (200.0 g) to 25 L of distilled water. A 2.0 g/L solution of 3-[4,5-dimethylthiazol-2-yl]-2,5-diphenyltetrazolium bromide (MTT) in PBS was prepared and sterile filtered (0.2 μm pore size) prior to use in the cytotoxicity assays. Haematoporphyrin derivative (HpD, or Photofrin; QLT Phototherapeutics, Inc. "Vancouver, BC, Canada") was used as a positive control in the phototoxicity assays; concentrations of HpD were calculated using an assigned molecular weight of 600.

The following cell lines were utilized in this study: A549 (human lung adenocarcinoma), WI-38 VA13 (SV40 transfected fibroblast-like human embryonic cell line), five human head and neck squamous cell carcinomas (SCC016, SCC040, SCC056, SCC114, SCC116), and three human breast adenocarcinomas (BT-20, T-47D, and MCF-7). All cell lines were obtained from American Type Culture Collection "Va, USA." The A549 and T-47D cell lines were maintained in RPMI 1640 media supplemented with 10% fetal calf serum heat inactivated at 56°C for 30 minutes, 2 mM L-Glutamine, 100 μg/mL Streptomycin, 100 U/mL Penicillin, and 2.5 mcg/mL Amphotericin B solution. All other cell lines were maintained in minimum essential medium (MEM) with Earle's salts supplemented with 10% fetal calf serum heat inactivated at 56°C for 30 minutes, 2 mM L-Glutamine, 100 μg/mL Streptomycin, 100 U/mL Penicillin, and 2.5 mcg/mL Amphotericin B solution, as well as 100 μM MEM nonessential amino acids and 1 mM Sodium Pyruvate (CellGro, Inc. "Va, USA") in distilled water. Cells were grown at 37°C in a humidified atmosphere containing 5% CO_2.

2.14. Cytotoxicity assays

Cells were seeded (100 μL) into 96-well microtiter plates and grown until they were approximately 70% confluent. The plates were then treated in the dark (to avoid photosensitized killing) with the appropriate concentration of pz or a volume of DMSO equivalent to the volume of compound added at these concentrations. Pz and DMSO solutions were added as 100 μL aliquots to the original media in the well. The subsequent 200 μL of media was thoroughly mixed, after which time 100 μL was removed, resulting in a final volume of 100 μL in each well; final pz/DMSO concentrations ranged from 50–1.56 μM. The media were removed at designated time points (24, 48, 72, 96, or 120 hours), and 100 μL of MTT/PBS solution was added to each well. The plates were then incubated for an additional 5 hours at 5% CO_2 and 37°C. During this time, the tetrazolium ring of the MTT molecules is cleaved by the mitochondrial dehydrogenases of viable cells, resulting in the formation of purple formazan crystals. Following incubation, the supernatant was decanted, and 100 μL of DMSO was added to each well to dissolve any formazan crystals. The absorbance was then read at 540 nm for each well. Each data point represents the average of at least four microtiter wells for each plate, and at least three independent trials were carried out for each experiment. Individual trials were normalized and averaged such that the final reported values represent a minimum of 12 independent values for each reported condition for each cell line.

2.15. Phototoxicity assays

Two identical 96-well plates were seeded with A549 and WI-38 VA13 cells grown to ~70% confluency as described above. The cells were then treated with the desired concentration of pz or HpD and incubated for additional 4 hours. Aluminum foil was then wrapped around the sides and top of the first plate, leaving the bottom of the plate uncovered in order to enable light penetration. The second plate was completely wrapped in aluminum foil to inhibit light from reaching the cells; this plate served as the dark control. The two plates were then placed on top of a standard X-ray illuminator (consisting of four 15 W bulbs, ~3600 total lumens) and exposed to 10 minutes of light. Following the light treatment, the plates were placed back into the incubator for 24 hours, after which time MTT cytotoxicity assays were performed.

2.16. Imaging assays

A549 and WI-38 VA13 cells were plated onto sterilized glass coverslips in 60 × 15 mm dishes and grown at 37°C in a humidified atmosphere containing 5% CO_2. Upon reaching 60–80% confluency, the cells were treated with the desired pz at 25 μM and incubated in the dark under the same conditions for an additional 4 hours. Negative controls were prepared by treating cells with an amount of DMSO equivalent to that of the 25 μM pz sample.

Confocal microscopic images of the red pz emission were obtained at room temperature with a Zeiss 510 LSM confocal microscope. Following the 4-hour incubation period of the cells with the pz, the supernatant was decanted and the cells were washed twice with PBS. The washed coverslips were then inverted onto microscope slides, and the cells were imaged live in PBS. Cells were excited with an argon-ion laser

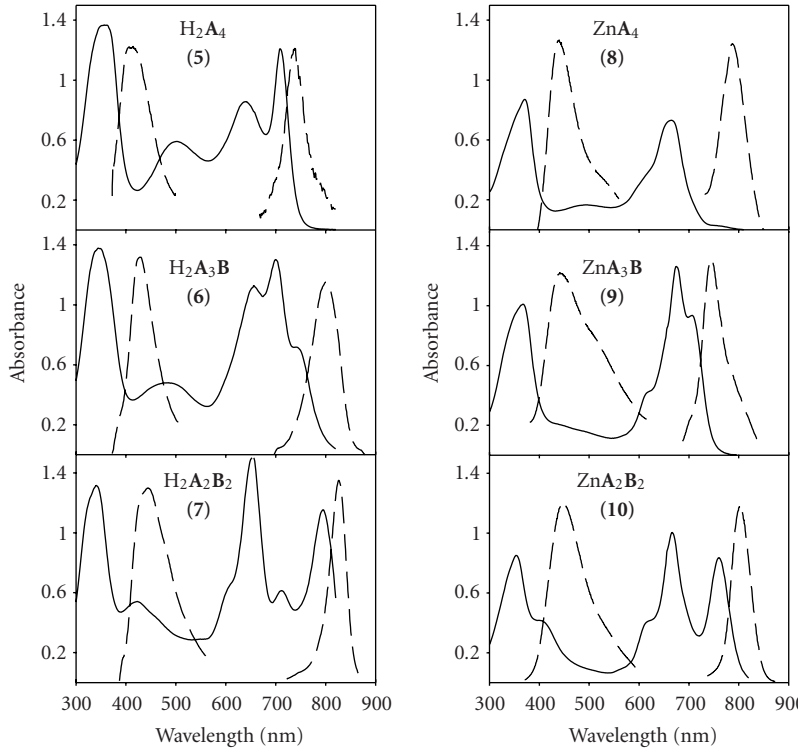

Figure 1: Absorbance (solid lines) and emission (dashed lines) spectra of $H_2[pz(\mathbf{A}_n\mathbf{B}_{4-n})]$ and $Zn[pz(\mathbf{A}_n\mathbf{B}_{4-n})]$ pzs in CH_2Cl_2.

line at 488 nm, and fluorescence was detected with a long-pass 505 nm filter. All images were taken using the same detector gain and amplitude settings.

3. RESULTS AND DISCUSSION

3.1. Pz synthesis and properties

The six compounds examined in this study are of the form $M[pz(\mathbf{A}_n\mathbf{B}_{4-n})]$, where M = H_2 or Zn, **A** is $[S((CH_2)_2O)_4CH_3]_2$, and **B** is a fused 4,7-bis(isopropyloxy)benzo group, with n = 4 (**5**, **8**), n = 3 (**6**, **9**), and the *trans* form of n = 2 (**7**, **10**). Scheme 1 shows the reaction scheme utilized to prepare the pzs.

In order to attach the desired tetra(ethylene glycol) monomethyl ether, $(CH_2CH_2O)_4Me$, functional group onto the periphery of a pz, it was first necessary to prepare 2-{2-[2-(2-methoxyethoxy)ethoxy]ethoxy}ethyl-4-methylbenzenesulfonate (**3**) via tosylation of the commercially available tetra(ethylene glycol) monomethyl ether (**2**). $MNT[S(C_2H_4O)_4Me]_2$ (**4**) was then prepared by treating Na_2MNT with two equivalents of **3** in acetone at reflux for 12 hours.

Magnesium-templated Linstead macrocyclization [18] of $MNT[S(C_2H_4O)_4Me]_2$ (**4**), followed by demetallation in trifluoroacetic acid and purification via column chromatography, led to the formation of the $H_2[pz(\mathbf{A}_4)]$, **5**, in 12% yield. The $H_2[pz(\mathbf{A}_3\mathbf{B})]$ (**6**, 4% yield) and *trans*-$H_2[pz(\mathbf{A}_2\mathbf{B}_2)]$ (**7**, 6% yield) pzs were prepared via a mixed cyclization of $MNT[S(C_2H_4O)_4Me]_2$ (**4**) and 1,3-diiminoisoindoline (**1**), reacted in a 2 : 1 stoichiometric ratio, and followed by demetallation with trifluoroacetic acid. Column chromatography was then used to separate and purify the two compounds. It is noted that the *cis*-$H_2[pz(\mathbf{A}_2\mathbf{B}_2)]$ compound was not produced during this reaction, indicating that under these reaction conditions, the diiminoisoindoline (**1**) reacts preferentially with its cocyclization partner, **4**, resulting in only the *trans* form of the $M[pz(\mathbf{A}_2\mathbf{B}_2)]$. The yield of the *trans*-macrocycle was further improved by the use of 0.38 equivalents of Mg per mole of combined cyclization partners, and by heating the reaction mixture for 7 hours at reflux in *n*-propanol. The corresponding zinc analogues—**8**, **9**, and **10**—were prepared by reacting each of the free-base pzs in a solution of zinc chloride in $CHCl_3$/MeOH at reflux for 30 minutes. All three compounds were obtained in quantitative yield.

Each compound is freely soluble in DMSO. By utilizing different combinations of M (H_2 or Zn) and n (4, 3, or 2, in a *trans* conformation), we can predictably vary the core macrocycle structure, resulting in different optical properties for each of the six pzs. Previous work has shown that the optical properties of the pzs are dependent upon M and n, but independent of R [10, 11, 19, 20]. Figure 1 shows typical spectra obtained in CH_2Cl_2 for the six pzs presented here. All six compounds exhibit an intense B (Soret) band at ~350 nm with high extinctions (~50,000 $M^{-1}cm^{-1}$), but each has a different Q-band region, depending upon M and n. For the free-base pzs, split Q-bands are observed for both

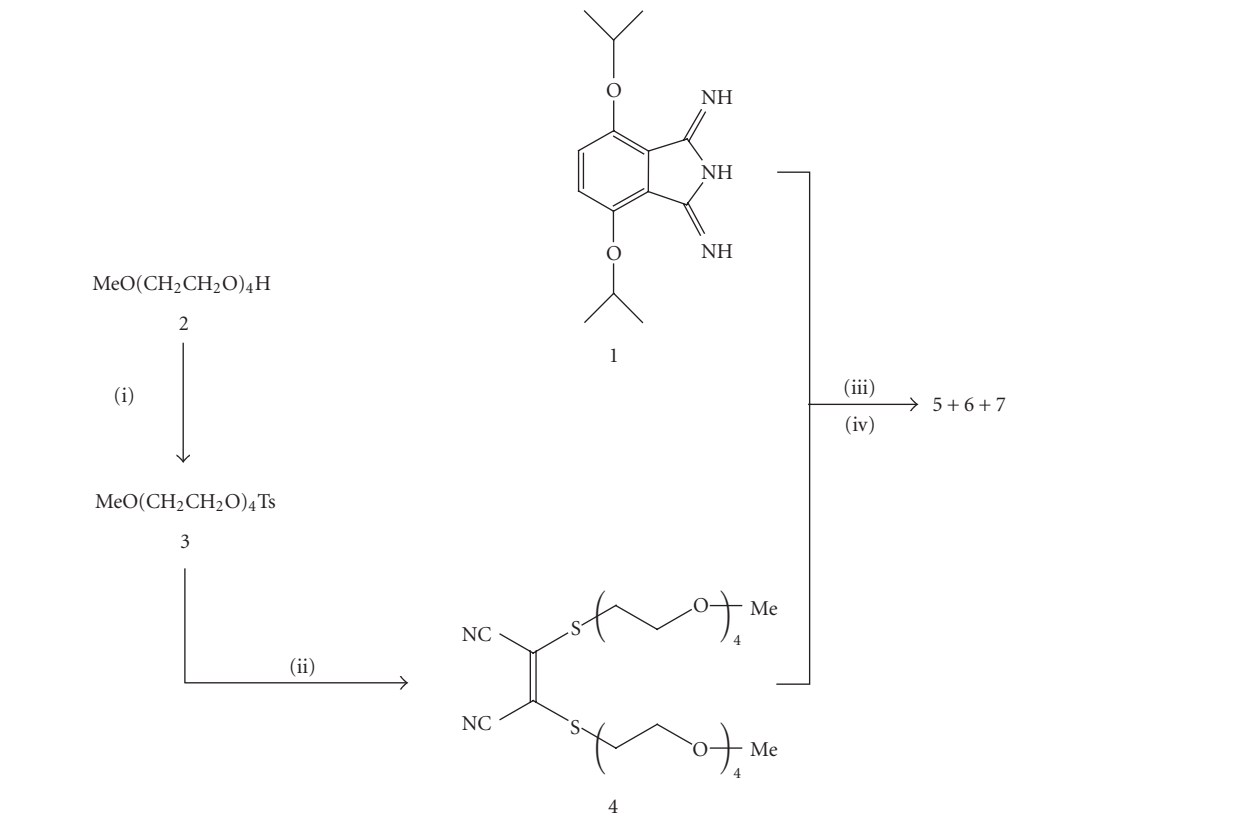

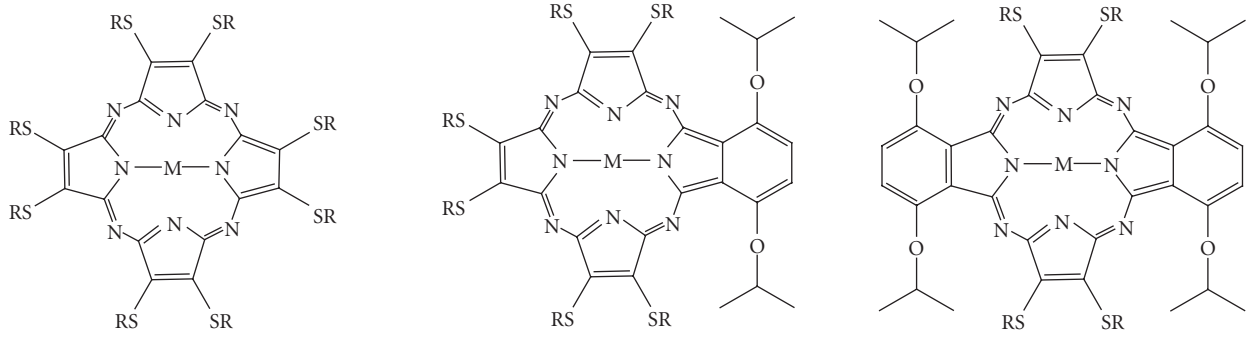

(v) 5 M = 2H → 8 M = Zn

(v) 6 M = 2H → 9 M = Zn

(v) 7 M = 2H → 10 M = Zn

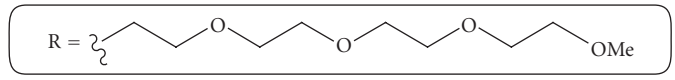

(i) TsCl, NaOH, THF/H_2O, RT, 2 h
(ii) Na_2MNT, acetone at reflux, 12 h
(iii) $Mg(OPr)_2$, n-PrOH at reflux, 7 h
(iv) TFA, CH_2Cl_2, RT, 1 h
(v) $ZnCl_2$, $CHCl_3$/MeOH, at reflux, 0.5 h

Scheme 1: Synthetic route to porphyrazines **5**–**10**.

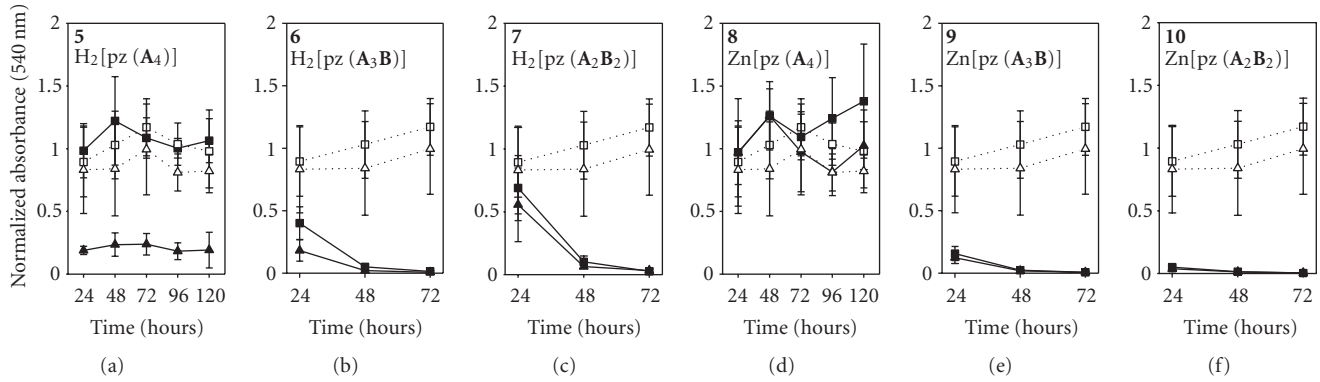

FIGURE 2: MTT time course plot of A549 (□) and WI-38 VA13 (Δ) cells exposed to 50 μM pz. Dotted lines = control (cells + DMSO), solid lines = cells + pz.

n = 3 and n = 2 (*trans*), with H_2[pz(**A**$_3$**B**)] exhibiting a maximum absorption of ~700 nm (ε ~45,000 $M^{-1}cm^{-1}$) and H_2[pz(**A**$_2$**B**$_2$)] having well-defined peaks at ~654 nm and 798 nm (ε ~50,000 $M^{-1}cm^{-1}$ for both), respectively; in contrast, the symmetrical H_2[pz(**A**$_4$)] (n = 4) exhibits only a single Q-band with a maximum absorption at ~712 nm (ε ~35,000 $M^{-1}cm^{-1}$). As expected, similar Q-band patterns are observed in the three Zn[pz(**A**$_n$**B**$_{4-n}$)]pzs, but the peaks are shifted ~30 nm towards the blue. Zn[pz(**A**$_4$)] has a single Q-band absorption at 672 nm (ε ~47,000 $M^{-1}cm^{-1}$); both Zn[pz(**A**$_3$**B**)] and Zn[pz(**A**$_2$**B**$_2$)] have split Q-bands, with the former exhibiting a maximum absorption at 676 nm (ε ~50,000 $M^{-1}cm^{-1}$) and the latter having peaks at 666 nm (ε ~54,000 $M^{-1}cm^{-1}$) and 761 nm (ε ~45,000 $M^{-1}cm^{-1}$), respectively. All six compounds also exhibit dual fluorescence, as shown in Figure 1: for the free-base pzs with n = 4, 3, and 2, short wavelength (uv) fluorescence is observed at λ_{max} = 410, 428, and 440 nm, respectively; and long wavelength (nir) fluorescence occurs at λ_{max} = 737, 800, and 827 nm, respectively; for the Zn pzs with n = 4, 3, and 2, uv emission is observed at λ_{max} = 435, 444, and 440 nm, respectively; and nir emission occurs at λ_{max} = 713, 754, and 795 nm, respectively [10]. Both emissions can be generated with excitation wavelengths to the blue of ~400 nm, while only the nir luminescence is produced upon excitation to the red of ~450 nm. Unlike previously reported pzs in which broadening and aggregation were often observed [15, 16], the uv-visible spectra of **5–10** in DMSO looked nearly identical to the spectra obtained in CH_2Cl_2.

Earlier work with the pzs has also found that the singlet oxygen quantum yields (Φ_Δ) for a series of M[pz(**A**$_n$**B**$_{4-n}$)], where **A** = [S-R]$_2$ and **B** is a fused dialkoxybenzo group, are dramatically affected by both M and n, but are independent of the identity of the R group [12]. For a given M, the quantum yield is found to increase as the value of n is decreased. Therefore, the H_2[pz(**A**$_2$**B**$_2$)], **7**, has the highest quantum yield of the three free-base pzs (Φ_Δ~ 0.130), with **6** (Φ_Δ~ 0.026) and **5** (Φ_Δ~ 0.0074) have markedly lower values. Introducing zinc into the core of the pz results in significantly higher yields than those found in the analogous free-base compounds. Thus the Zn[pz(**A**$_2$**B**$_2$)], **10**, possesses the highest singlet oxygen quantum yield (Φ_Δ~ 0.370) of the six compounds presented in this study, while the quantum yields for **9** (Φ_Δ~ 0.110) and **8** (Φ_Δ~ 0.037) are accordingly lower.

3.2. *Quantitative in vitro effect of porphyrazines*

MTT assays were used to test the proliferation/viability of A549 and WI-38 VA13 cells grown in the presence of compounds **5–10** over a 72-hour time period. Cells were initially treated with a pz concentration of 50 μM, and MTT assays were performed at 24, 48, and 72 hours (Figure 2).

In order to confirm that any toxicity observed was due to the pzs and not the DMSO solvent, control cells were exposed to a volume of DMSO equivalent to the volume of pzs at 50 μM; cells exposed to DMSO exhibited normal growth behavior. Unlike previously reported pzs which exhibited little cellular toxicity after a 24-hour exposure [15, 16], four of the six pzs tested here exhibited marked toxicity to both normal and tumor cells within the first 24 hours upon 50 μM exposure. (We note here that the 50 μM treatment dose was chosen because it corresponds to the approximate amount of HpD typically needed to observe a clinical response in patients undergoing PDT treatments.) Cells grown in the presence of H_2[pz(**A**$_2$**B**$_2$)], **7**, and the M[pz(**A**$_3$**B**)] pzs, **6** (M = H_2) and **9** (M = Zn), showed moderate-to-large decreases in viability after 24 hours, while cells treated with Zn[pz(**A**$_2$**B**$_2$)], **10**, were almost completely killed within the first 24 hours of exposure. An additional 24 hours of exposure to pzs **6**, **7**, and **9** resulted in both normal and tumor cells being nearly completely killed.

The proliferation/viability of cells exposed to the M[(**A**$_4$)] pzs, **5** (M = H_2) and **8** (M = Zn), contrasted sharply to that of the M[pz(**A**$_3$**B**)] and M[pz(**A**$_2$**B**$_2$)] pzs. Compound **8** showed little-to-no toxicity in either cell line over the entire time course of 72 hours, while **5** was found to be selectively toxic to normal cells. Nearly 80% of the WI-38 VA13 normal cells were killed within 24 hours upon exposure to **5**, while no appreciable toxicity was seen for tumor cells exposed to **5** for 72 hours. The nontoxic behavior found with cells exposed to **5** (tumor only) and **8** (both tumor and normal) prompted the study of longer treatment times for these

Table 1: Percent cell viability of various cell lines exposed to 50 μM **5** for 72 hours, relative to DMSO-treated cells.

Cell Line	Cell Line Description	Percent Cell Viability (%)
SCC016	Human tongue squamous cell carcinoma	91.2 ± 19.2%
SCC040	Human tongue squamous cell carcinoma	95.3 ± 23.8%
SCC056	Human tongue squamous cell carcinoma	94.8 ± 20.5%
SCC114	Human floor of mouth squamous cell carcinoma	78.2 ± 17.0%
SCC116	Human alveolar ridge squamous cell carcinoma	102.0 ± 10.2%
BT-20	Human breast adenocarcinoma	118.4 ± 4.5%
MCF-7	Human breast adenocarcinoma	77.7 ± 19.6%
T-47D	Human breast adenocarcinoma	106.4 ± 8.4%
A549	Human pulmonary adenocarcinoma	92.7 ± 23.6%
WI-38 VA13	Human embryonic fibroblast	20.9 ± 23.3%

two compounds. Additional MTT assays were therefore carried out at 96 and 120 hours for both **5** and **8**. However, as shown in Figure 2, these longer exposure times did not result in any additional observed toxicity.

The selective killing of the normal cells upon exposure to **5** prompted us to test this particular compound against other tumor cell lines to determine if the resistance of the A549 cells was consistent across different tumor cell lines and types. Table 1 shows the percent viability of human breast adenocarcinomas (BT-20, T-47D, and MCF-7) and human head and neck squamous cell carcinomas (SCC016, SCC040, SCC056, SCC114, and SCC116) exposed to **5** at 50 μM for 72 hours, relative to DMSO-treated control cells. In general, very little toxicity was observed for any of the eight additional tumor cell lines, as growth rates of the pz-treated cells were similar to the growth rates of the DMSO-treated controls.

3.3. Dose-dependent effects of porphyrazines

As described above, exposure to the M[pz($\mathbf{A_3B}$)] and M[pz($\mathbf{A_2B_2}$)] pzs at concentrations of 50 μM resulted in significant toxicity in both tumor and normal cells (Figure 2). To determine the toxicity limits of each pz, MTT assays were carried out in both A549 tumor and WI-38 VA13 normal cells at varying concentrations (1.56–50 μM) for 72 hours. Figure 3 shows the dose-dependent results as percent cell viability, calculated relative to the viability of the control DMSO-treated cells. (Note that treated cells growing at an equivalent rate to the DMSO control cells would have a 0% change in cell viability; treated cells which grew slower and/or were less viable than the control cells would have a negative percent change in cell viability.)

With the exception of the M[pz($\mathbf{A_4}$)] pzs, the thiotriethoxy(ethoxy)methyl-appended pzs were generally found to exhibit significant toxicity even at lower concentrations. Both of the M[pz($\mathbf{A_2B_2}$)] pzs, **7** and **10**, caused nearly 100% cell killing at treatment concentrations of 12.5 μM and above. Significant toxicity was still observed for both tumor and normal cell lines exposed to 6.25 μM **10**; however, A549 tumor cells exposed to **7** at 6.25 μM showed only very little toxicity (~10% killed), while normal cells exposed to the same concentration resulted in nearly 80% of the cells dying. Slight toxicity was still observed in both normal and tumor cells exposed to the lowest concentration of **10** tested (1.56 μM), while normal and tumor cells exposed to **7** at a treatment concentration of 1.56 μM showed essentially normal growth upon a 72-hour exposure.

While **7** and **10** showed a somewhat similar dose-dependent proliferation/viability behavior, the two M[pz($\mathbf{A_2B_2}$)] pzs, **6** and **9**, differed depending upon the identity of M. The H_2[pz($\mathbf{A_3B}$)], **6**, was found to exhibit a growth behavior very similar to that observed for its H_2[pz($\mathbf{A_2B_2}$)] analogue, **7**. Significant toxicity was found in both tumor and normal cells exposed to **6** at concentrations of 12.5 μM and above for 72 hours; and similar to **7**, the normal cells showed selective toxicity at treatment concentrations of 6.25 μM and below. However, unlike cells exposed to **7**, normal cells treated with **6** at 1.56 μM still exhibited a moderate amount of toxicity (~30% cell death). The Zn[pz($\mathbf{A_3B}$)] analogue, **9**, showed significantly less toxicity at the higher treatment concentrations (25 and 12.5 μM) in both normal and tumor cells than that observed in cells treated with the free-base **6** at the same concentrations. However, slight toxicity (~10–20% cell killing) was still observed for both tumor and normal cells exposed to low concentrations of **9,** whereas A549 tumor cells exposed to **6** at treatment concentrations of 6.25 μM and below exhibited normal growth behavior.

Based upon the 50 μM time-course plots in Figure 2, it was expected that the dose-dependence results of the M[pz($\mathbf{A_4}$)] pzs (Figure 3) would generally show little toxicity. To this end, the free-base **5** exhibited selective toxicity towards WI-38 VA13 cells at concentrations of 25 μM and higher upon a 72-hour exposure; at treatment concentrations of 12.5 μM and below, any toxicity observed in either the tumor or normal cells fell within the experimental error limits for normal growth (i.e., within the error range for a 0% change in cell viability). Both normal and tumor cells exposed to the Zn[pz($\mathbf{A_4}$)] pz, **8**, also exhibited normal growth behavior at all concentrations studied.

3.4. Photosensitizing effects of the porphyrazines

In addition to the dark toxicity studies described above (Figures 2 and 3), light-dependent proliferation/viability studies were employed to determine if the compounds possessed

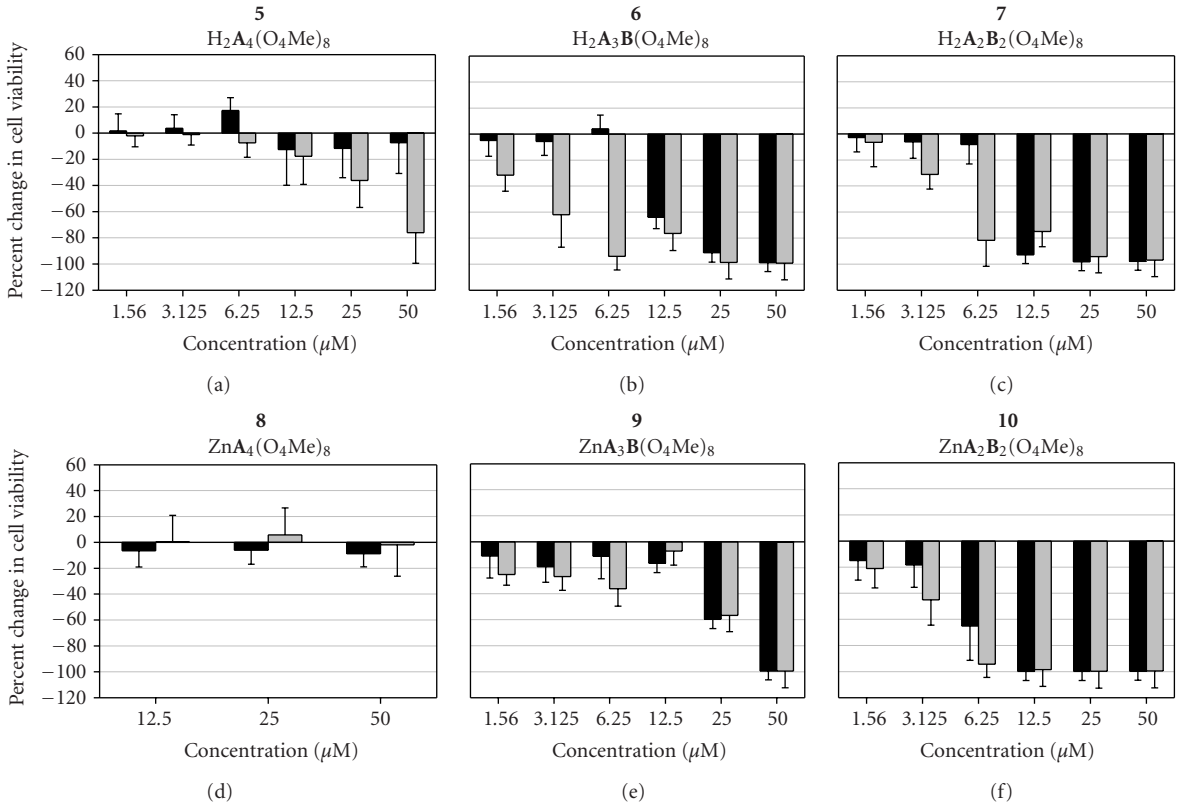

Figure 3: Percent cell viability, relative to DMSO control, of A549 (black bars) and WI-38 VA13 (gray bars) cells after a 72-hour exposure to pzs at varying concentrations. (Note that a 0% change in the percent cell viability correlates to cells which grew at the same rate as the control cells; negative values correlate to cells which grew at rates below those of the control cells.)

additional photosensitizing properties. Due to the high levels of toxicity observed in the MTT dose-dependence studies (Figure 3), a shorter incubation time and a lower treatment concentration were employed for these compounds than used in the biological studies of previously reported pzs [15, 16]. Cell lines were treated with 25 μM of **5–10** and 25 or 50 μM HpD as a reference for 4 hours and were then exposed to white light for a period of 10 minutes. The microtiter plate serving as the dark control was completely wrapped in aluminum foil so that the cells would avoid any light exposure, but would still be exposed to any potential heat being generated by the bulbs of the X-ray illuminator during the 10-minute treatment period. The cells were incubated overnight following the light treatment, and MTT assays were performed after 24 hours. Figure 4 shows data comparing no light treatment versus cells exposed to 10 minutes of white light.

Both untreated (data not shown) and DMSO-treated cells were used as controls; similar results were obtained for both; therefore, Figure 4 shows only the DMSO-treated cells.

As expected, growth of the DMSO-treated cells was not adversely affected by the additional light exposure. However, unlike previously studied pzs [15, 16], three of the compounds reported here—**7**, **9**, and **10**—showed a distinct photosensitizing effect in the A549 tumor cells. It could not be determined if a similar effect occurred in the WI-38 VA13, due to the inherent toxicity of **7**, **9**, and **10** in the normal cells; absorption readings at the 0-minute light-exposure time point were extremely low for these three compounds in the WI-38 VA13 cell line (Figure 4). It is noted that, of the six pzs tested in this study, the three exhibiting the phototoxic effect in A549 cells correspond to the three compounds having the highest singlet oxygen quantum yield (Φ_Δ). Accordingly, the compounds with relatively low Φ_Δ values—**5**, **6**, and **8**—did not show any appreciable phototoxic effect in either cell line, as viability levels remained steady with and without light treatment. Interestingly, no appreciable light effect was observed for either tumor or normal cells exposed to 25 μM HpD (a dose that is two-fold below the typical clinical treatment dose); however, treatment of cells with HpD at the usual clinical dose, 50 μM, results in substantial photoinduced cell death in both A549 and WI-38 VA13 cells, as shown in Figure 4.

Additional dose-dependent phototoxicity studies were carried out for **7**, **9**, and **10** in A549 cells to determine if a light-dependent response could be observed for the pzs below the 25 μM treatment dose employed in Figure 4. Cells were treated with the pzs at concentrations of 25–1.56 μM for 4 hours and then exposed to either 0 or 10 minutes of white light. MTT assays were carried out after an overnight incubation (Figure 5). As expected from the results of Figure 4, Photofrin did not show any light-induced toxicity

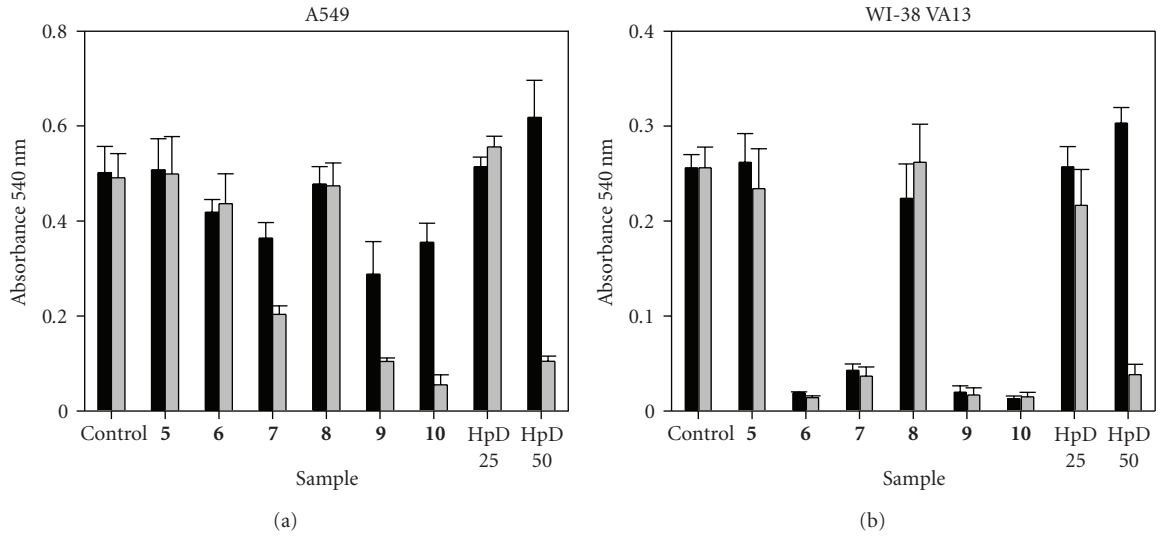

Figure 4: MTT results for A549 (a) and WI-38 VA13 (b) cells exposed to pz (25 μM) or HpD (25 or 50 μM) for 4 hours, followed by white light exposure for 0 (black bars) or 10 (gray bars) minutes. Control cells were treated with an amount of DMSO equivalent to 25 μM pz.

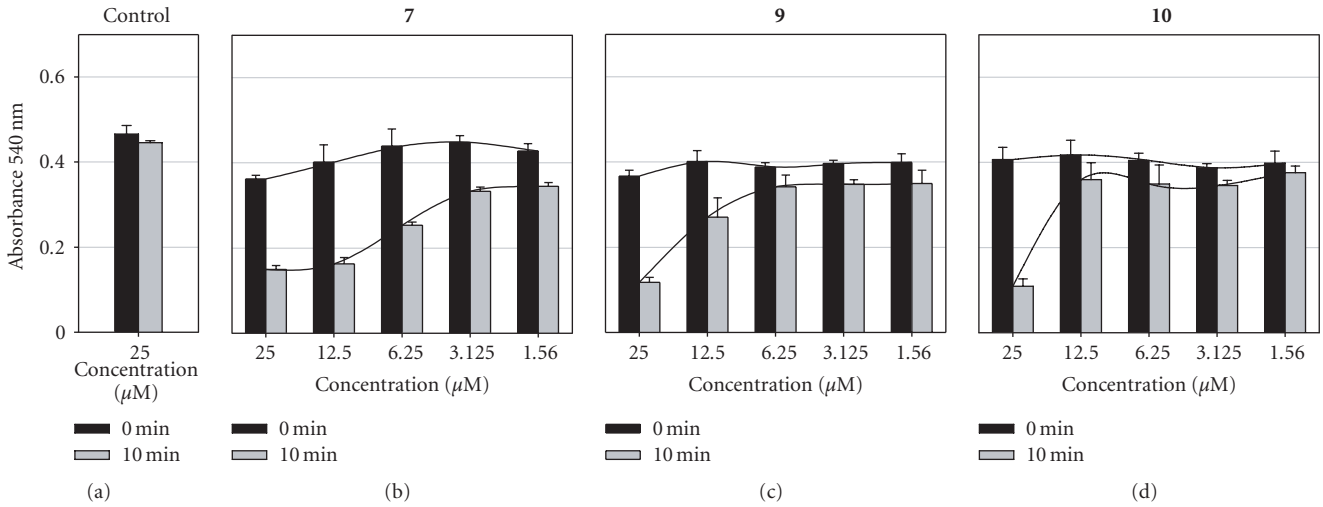

Figure 5: MTT results for A549 cells exposed to varying concentrations of pz or DMSO for 4 hours, followed by white light exposure for 0 (black bars) or 10 (gray bars) minutes. Line graphs are overlaid for clarity.

at treatment concentrations of 25 μM or below (data not shown). However, significant phototoxicity was still observed in A549 cells treated with **7** at concentrations below 25 μM upon a 10-minute white light exposure; a treatment dose of 12.5 μM resulted in additional 60% of the cells being killed when exposed to light, while cells treated with 6.25 μM **7** resulted in approximately 40% cell death, relative to the dark toxicity (i.e., 0 minute white light exposure). Even at the lowest treatment concentration of **7** studied, 1.56 μM, a moderate amount (~15–20% cell death) of toxicity was still observed. In contrast, both pzs **9** and **10** exhibited far less sensitivity than **7**. Moderate phototoxicity (~30% cell death) was observed in A549 cells exposed to **9** at 12.5 μM, but little effect was detected at doses of 6.25 μM and below. Cells treated with **10** did not show any additional phototoxicity at doses below 25 μM.

3.5. Cellular uptake of porphyrazines

Experiments were carried out to assess the cellular uptake and general localization behavior of each of the six pzs. Figure 6 presents the confocal microscopic images of A549 and WI-38 VA13 cells exposed to each compound for 4 hours at 25 μM. Due to the rapid onset of toxicity caused by these compounds, as discussed above, the cells were treated at a lower concentration and for a shorter period of time than the conditions used in previous cellular uptake studies of the pzs [15].

Moderate autofluorescence was observed for the control (DMSO-treated) cells in both tumor and normal samples. All six of the pzs showed enhanced intracellular luminescence in A549 cells upon treatment with compound; each of the six compounds displayed similar fluorescence intensity and

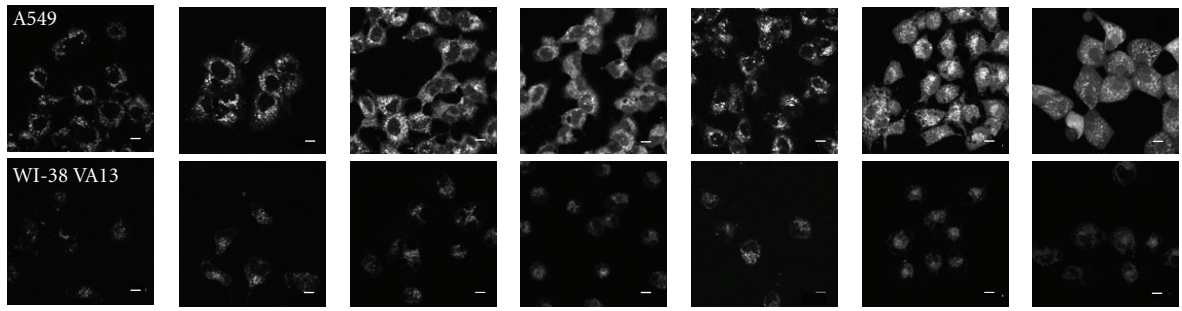

Figure 6: Cellular uptake of pzs using false-white confocal fluorescence microscopy images of A549 (top) and WI-38 VA13 (bottom) cells treated with 25 μM agent: (a) DMSO control, (b) **5**, (c) **6**, (d) **7**, (e) **8**, (f) **9**, (g) **10**. Scale bar = 10 μm.

exhibited uniform staining of the cytoplasm with no uptake by the nucleus. In contrast, WI-38 VA13 cells showed little-to-no measurable increase in fluorescence upon treatment of the cells with the pzs. Significant vacuole formation was also observed in both tumor and normal cells exposed to **6**, **9**, and **10**.

4. CONCLUSIONS

Recent work has sought to study the structure-function relationships of the porphyrazines (pzs) in biological systems, in an effort to develop these compounds for use as therapeutic and diagnostic agents [15, 16]. Herein we continue our structure-function studies of the porphyrazines by examining a series of six new M[pz($\mathbf{A}_n\mathbf{B}_{4-n}$)] porphyrazines, where M = H_2 or Zn, **A** is $[S((CH_2)_2O)_4CH_3]_2$, **B** is a fused 4,7-bis(isopropyloxy)benzo group, and n = 2, 3, or 4 (Scheme 1). The thiotetra(ethylene glycol) monomethyl ether functional group is hydrophilic in nature, while the pz core is hydrophobic; thus for a given M, as the value of n is increased in the series, the resulting compounds progressively become more hydrophilic in character. Furthermore, by introducing zinc into the core of the pzs (**8**–**10**), the solubility of the compound and the singlet oxygen quantum yield are both enhanced, relative to their free-base analogues. The zinc pzs reported here are the first metallated pzs to be tested for their biological behavior. Concentration/time-dependent MTT proliferation/viability assays were carried out, both in the presence and absence of white light, in order to measure the dark and photoinduced toxicity of each pz in normal (WI-38 VA13) and tumor (A549) cell lines, and confocal microscopy was used to determine the cellular uptake and localization of each compound.

The dark toxicity studies of the six pzs revealed a dose-dependent response in which cellular toxicity increased in both normal and tumor cell lines as n was decreased (Figures 2 and 3). With the exception of **8**, all of the pzs were found to be toxic to normal cells at higher concentrations (25 μM and above); and for the M[pz($\mathbf{A}_3\mathbf{B}$)] and M[pz($\mathbf{A}_2\mathbf{B}_2$)] pzs, significant toxicity was also observed in the tumor cells at higher concentrations. In general, for a given concentration, the observed toxicity was found to be greater in the normal cells than in the tumor cells. Furthermore, in the case of the M[pz($\mathbf{A}_3\mathbf{B}$)] and M[pz($\mathbf{A}_2\mathbf{B}_2$)] pzs, for a given n, toxicity was generally found to be higher for the free-base compounds than for the metallated pzs.

A particularly interesting result from the dark toxicity studies is the finding that **5** is selectively toxic to normal cells. As shown in Figure 2 and Table 1, **5** was found to be non-toxic across a number of different tumor cell lines and tumor types (both adenocarcinomas and squamous cell carcinomas), suggesting that this compound might possess multiple uses as a diagnostic agent. First, when attempting to establish a cell line derived from a human tumor (for purposes of preparing a cell line that will grow continuously in the laboratory), it is necessary to selectively remove and purify the tumor cells from the tumor sample removed from the patient, which contains a mixture of normal and cancerous tissue. This procedure is often very difficult and time-consuming; if **5** were added during this process, one could theoretically remove the normal cells more quickly, leading to faster purification of the desired tumor cell line. Second, the results of many patient biopsies are unclear as to whether a particular tissue sample is malignant or benign; in such unclear cases, one could treat the biopsy sample with **5** to verify the malignancy of the tissue.

The photo-induced toxicity studies (Figure 4) found further toxicity in A549 cells exposed to the pzs with higher singlet oxygen quantum yields—**7**, **9**, and **10**. These three compounds are the first members of the M[pz($\mathbf{A}_n\mathbf{B}_{4-n}$)] subclass to exhibit photosensitivity [15, 16]. The result for **7** is particularly interesting, considering that previously studied H_2[pz($\mathbf{A}_2\mathbf{B}_2$)] pzs all contained **A** groups that resulted in aggregation of the compound in aqueous media, thereby suppressing singlet oxygen generation. The result observed here suggests that we have achieved the proper hydrophobic/hydrophilic balance necessary for sufficient solubility in cellular environments, and this enhanced solubility is likely a key contributing factor in the observed photosensitivity of **7** at relatively low doses (Figure 5). Furthermore, the observation that **6** ($\mathbf{H}_2A_3B$) did not exhibit a light-dependent toxicity, while **9** ($\mathbf{Zn}A_3B$) did show a response, suggests that the inherent singlet oxygen quantum yield of the free-base A_3B structure may not be high enough to be applicable in PDT

applications. Likewise, no photo-induced toxicity was observed for the M[pz($\mathbf{A}_4$)] pzs, **5** and **8**, regardless of the identity of M. Therefore, the development of future pzs for PDT applications will focus mainly on members of the A_2B_2 (both free-base and metallated) and metallated A_3B subfamilies. However, while members of the M[pz($\mathbf{A}_4$)] and H_2[pz($\mathbf{A}_3\mathbf{B}$)] pz subfamilies may not provide any additional PDT activity, it is still important to study pzs belonging to these subfamilies in an effort to discover new selectively toxic antitumor agents.

Confocal fluorescence microscopy images revealed that all six of the compounds prepared in this study were preferentially incorporated into the A549 tumor cells and localized in the cytoplasm. The results of the cellular uptake studies further suggest that **8** is a particularly promising imaging agent since it was found to be nontoxic upon exposure to both tumor and normal cells and was selectively taken up by tumor cells. As mentioned above, vacuole formation was observed in both the tumor and normal cells upon exposure to **6**, **9**, and **10**, suggesting that these compounds may be inducing terminal differentiation, a specialized form of apoptosis [21, 22]. Future work will more closely examine the mechanism by which the pzs in this report (**5–7**, **9**, **10**) cause cell death. By determining the role of the pzs in cell destruction, we may be able to slightly alter the structure of the compounds in order to minimize toxicity (while maintaining the proper pz solubility and selective tumor uptake), thus leading to many other potential imaging agents from this class of compounds.

The results of this study are the first steps in the search for useful tumor specific imaging agents and compounds for use in purifying cell lines from clinical samples. If the issue of nonselective toxicity can be overcome, the path to developing porphyrazines as useful antitumor drugs (both traditional and PDT-activated) will be opened up.

ACKNOWLEDGMENTS

This work was supported by the NIH (CA 88850) and by the Illinois Department of Public Health (76280040, 76280042). Its contents are solely the responsibility of the authors and do not necessarily reflect the official views of the NIH or the Illinois Department of Public Health.

REFERENCES

[1] R. K. Pandey and G. Zheng, "Porphyrins as photosensitizers in photodynamic therapy," in *The Porphyrin Handbook*, K. M. Kadish, K. M. Smith, and R. Guilard, Eds., vol. 6, pp. 157–230, Academic Press, San Diego, Calif, USA, 2000.

[2] D. Wöhrle, A. Hirth, T. Bogdahn-Rai, G. Schnurpfeil, and M. Shopova, "Photodynamic therapy of cancer: second and third generations of photosensitizers," *Russian Chemical Bulletin*, vol. 47, no. 5, pp. 807–816, 1998.

[3] T. J. Dougherty, "Photodynamic therapy (PDT) of malignant tumors," *Critical Reviews in Oncology/Hematology*, vol. 2, no. 2, pp. 83–116, 1984.

[4] F. M. Little, C. J. Gomer, S. Hyman, and M. L. J. Apuzzo, "Observations in studies of quantitative kinetics of tritium labelled hematoporphyrin derivatives (H_pD_I and H_pD_{II}) in the normal and neoplastic rat brain model," *Journal of Neuro-Oncology*, vol. 2, no. 4, pp. 361–370, 1984.

[5] R. K. Pandoy, "Synthetic strategies in designing porphyrin-based photosensitizers for photodynamic therapy," in *CRC Handbook of Organic Photochemistry and Photobiology*, W. Horspool and F. Lenci, Eds., pp. 144-1–144-21, CRC Press, Boca Raton, Fla, USA, 2nd edition, 2004.

[6] C. M. Allen, W. M. Sharman, and J. E. Van Lier, "Current status of phthalocyanines in the photodynamic therapy of cancer," *Journal of Porphyrins and Phthalocyanines*, vol. 5, no. 2, pp. 161–169, 2001.

[7] R. K. Chowdhary, I. Shariff, and D. Dolphin, "Drug release characteristics of lipid based benzoporphyrin derivative," *Journal of Pharmacy and Pharmaceutical Sciences*, vol. 6, no. 1, pp. 13–19, 2003.

[8] J. L. Sessler and D. Seidel, "Synthetic expanded porphyrin chemistry," *Angewandte Chemie International Edition*, vol. 42, no. 42, pp. 5134–5175, 2003.

[9] D. Kessel and T. J. Dougherty, "Agents used in photodynamic therapy," *Reviews in Contemporary Pharmacotherapy*, vol. 10, no. 1, pp. 19–24, 1999.

[10] S. L. J. Michel, B. M. Hoffman, S. M. Baum, and A. G. M. Barrett, "Peripherally functionalized porphyrazines: novel metallomacrocycles with broad, untapped potential," in *Progress in Inorganic Chemistry*, vol. 50, pp. 473–590, John Wiley & Sons, New York, NY, USA, 2001.

[11] S. Lee, A. J. P. White, D. J. Williams, A. G. M. Barrett, and B. M. Hoffman, "Synthesis of near-IR absorbing/emitting porphyrazine derivatives with tunable solubility," *Journal of Organic Chemistry*, vol. 66, no. 2, pp. 461–465, 2001.

[12] S. Lee, R. Stackow, C. S. Foote, A. G. M. Barrett, and B. M. Hoffman, "Tuning the singlet oxygen quantum yield of near-IR-absorbing porphyrazines," *Photochemistry and Photobiology*, vol. 77, no. 1, pp. 18–21, 2003.

[13] E. G. Sakellariou, A. G. Montalban, H. G. Meunier, et al., "Peripherally metalated secoporphyrazines: a new generation of photoactive pigments," *Inorganic Chemistry*, vol. 41, no. 8, pp. 2182–2187, 2002.

[14] E. G. Sakellariou, A. G. Montalban, S. L. Beall, et al., "Novel peripherally functionalized seco-porphyrazines: synthesis, characterization and spectroscopic evaluation," *Tetrahedron*, vol. 59, no. 46, pp. 9083–9090, 2003.

[15] N. D. Hammer, S. Lee, B. J. Vesper, et al., "Charge dependence of cellular uptake and selective antitumor activity of porphyrazines," *Journal of Medicinal Chemistry*, vol. 48, no. 26, pp. 8125–8133, 2005.

[16] B. J. Vesper, S. Lee, N. D. Hammer, et al., "Developing a structure-function relationship for anionic porphyrazines exhibiting selective anti-tumor activity," *Journal of Photochemistry and Photobiology B*, vol. 82, no. 3, pp. 180–186, 2006.

[17] A. Davison, R. H. Holm, R. E. Benson, and W. Mahler, "Metal complexes derived from *cis*-1,2-dicyano-1,2-ethylenedithiolate and bis(trifluoromethyl)-1,2-dithiete," in *Inorganic Syntheses*, vol. 10, pp. 8–26, McGraw-Hill, New York, NY, USA, 1967.

[18] R. P. Linstead and M. J. Whalley, "944. Conjugated macrocycles—part XXII: tetrazaaporphyrin and its metallic derivatives," *Journal of Chemical Society*, pp. 4839–4846, 1952.

[19] T. P. Forsyth, D. B. G. Williams, A. G. Montalban, C. L. Stern, A. G. M. Barrett, and B. M. Hoffman, "A facile and regioselective synthesis of trans-heterofunctionalized porphyrazine derivatives," *Journal of Organic Chemistry*, vol. 63, no. 2, pp. 331–336, 1998.

[20] C. S. Velázquez, G. A. Fox, W. E. Broderick, et al., "Star-porphyrazines: synthetic, structural, and spectral investigation of complexes of the polynucleating porphyrazineoctathiolato ligand," *Journal of the American Chemical Society*, vol. 114, no. 19, pp. 7416–7424, 1992.

[21] Y. Capetanaki, S. Smith, and J. P. Heath, "Overexpression of the vimentin gene in transgenic mice inhibits normal lens cell differentiation," *The Journal of Cell Biology*, vol. 109, no. 4, pp. 1653–1664, 1989.

[22] C. E. Gagna, H.-R. Kuo, E. Florea, et al., "Comparison of apoptosis and terminal differentiation: the mammalian aging process," *Journal of Histochemistry and Cytochemistry*, vol. 49, no. 7, pp. 929–930, 2001.

Hindawi Publishing Corporation
Metal-Based Drugs
Volume 2008, Article ID 284691, 8 pages
doi:10.1155/2008/284691

Research Article

Synthesis, Characterization, and In Vitro Photodynamic Activity of Novel Amphiphilic Zinc(II) Phthalocyanines Bearing Oxyethylene-Rich Substituents

Jian-Yong Liu,[1] Xiong-Jie Jiang,[1] Wing-Ping Fong,[2] and Dennis K. P. Ng[1]

[1] *Department of Chemistry and Center of Novel Functional Molecules, The Chinese University of Hong Kong, Shatin, NT, Hong Kong*
[2] *Department of Biochemistry and Center of Novel Functional Molecules, The Chinese University of Hong Kong, Shatin, NT, Hong Kong*

Correspondence should be addressed to D. K. P. Ng, dkpn@cuhk.edu.hk

Received 27 August 2007; Accepted 13 September 2007

Recommended by Michael J. Cook

Three novel zinc(II) phthalocyanines substituted with one or two 3,4,5-tris(3,6,9-trioxadecoxy)benzoxy group(s) have been prepared and spectroscopically characterized. These compounds are highly soluble and remain nonaggregated in *N*,*N*-dimethylformamide. Upon excitation, they exhibit a relatively weak fluorescence emission and high efficiency to generate singlet oxygen compared with the unsubstituted zinc(II) phthalocyanine. These amphiphilic photosensitizers formulated with Cremophor EL are highly photocytotoxic against HT29 human colon adenocarcinoma and HepG2 human hepatocarcinoma cells. The mono-α-substituted analogue **4** is particularly potent with IC_{50} values as low as 0.02 μM. The higher photodynamic activity of this compound can be attributed to its lower aggregation tendency in the culture media as shown by absorption spectroscopy and higher cellular uptake as suggested by the stronger intracellular fluorescence, resulting in a higher efficiency to generate reactive oxygen species inside the cells.

1. INTRODUCTION

Photodynamic therapy (PDT) has emerged as a promising modality for the treatment of malignant tumors and wet age-related macular degeneration [1–3]. It is a binary therapy that involves the combination of visible light and a photosensitizer. Each component is harmless by itself, but in combination with molecular oxygen, they result in the generation of reactive oxygen species (ROS) causing oxidative cellular and tissue damage. This treatment has several potential advantages including its minimally invasive nature, tolerance of repeated doses, and high specificity that can be achieved through precise application of the light with modern fiber-optic systems and various types of endoscopy [3]. Currently, only a few porphyrin derivatives including porfimer sodium, temoporfin, and verteporfin are clinically approved for systemic administration. These compounds, though giving a positive response in a high percentage of patients, still have various deficiencies that demand a further development of better candidates [4]. Owing to the desirable electronic absorption and photophysical properties, phthalocyanines are one of the most promising classes of candidates for this application [5]. Over the last few years, we have been interested in rational modification of this class of functional dyes with the goal of enhancing their PDT efficiency. Several new series of silicon(IV) and zinc(II) phthalocyanines have been synthesized and evaluated for their photo-physical and biological properties; see [6] and the references. As the amphiphilicity of photosensitizers is believed to have a beneficial effect on their photodynamic activity [7], amphiphilic phthalocyanines have been our targets. In this paper, we report the synthesis, photophysical properties, and in vitro photodynamic activity of three novel zinc(II) phthalocyanines bearing one or two 3,4,5-tris(3,6,9-trioxadecoxy)benzoxy substituent(s). Having three or six triethylene glycol chains on one side of the macrocycle, these compounds are amphiphilic in nature, exhibiting a high in vitro photocytotoxicity.

2. MATERIALS AND METHODS

2.1. General

All the reactions were performed under an atmosphere of nitrogen. Tetrahydrofuran (THF), *n*-pentanol, dichloromethane, and *N*,*N*-dimethylformamide (DMF) were distilled from sodium benzophenone ketyl, sodium, calcium hydride, and barium oxide, respectively. Chromatographic purifications were performed on silica gel (Macherey-Nagel, 70–230 mesh) columns with the indicated eluents. Size exclusion chromatography was carried out on Bio-Rad Bio-Beads S-X1 beads (200–400 mesh). All other solvents and reagents were of reagent grade and used as received. Compounds **1** and **6** were prepared as described [8].

^{1}H and ^{13}C{^{1}H} NMR spectra were recorded on a Bruker DPX 300 spectrometer (^{1}H, 300; ^{13}C, 75.4 MHz) in $CDCl_3$ or DMSO-d_6. Spectra were referenced internally using the residual solvent [^{1}H: $CDCl_3$ (δ 7.26); DMSO-d_6 (δ 2.50)] or solvent [^{13}C: $CDCl_3$ (δ 77.0); DMSO-d_6 (δ 39.7)] resonances relative to $SiMe_4$. Electrospray ionization (ESI) mass spectra were measured on a Thermo Finnigan MAT 95 XL mass spectrometer.

UV-Vis and steady-state fluorescence spectra were taken on a Cary 5G UV-Vis-NIR spectrophotometer and a Hitachi F-4500 spectrofluorometer, respectively. Fluorescence quantum yields (Φ_F) were determined by the equation: $\Phi_{F(sample)} = (F_{sample}/F_{ref})(A_{ref}/A_{sample})(n_{sample}{}^2/n_{ref}{}^2)\Phi_{F(ref)}$ [9], where F, A, and n are the measured fluorescence (area under the emission peak), the absorbance at the excitation position (610 nm), and the refractive index of the solvent, respectively. The unsubstituted zinc(II) phthalocyanine (ZnPc) in DMF was used as the reference [$\Phi_{F(ref)} = 0.28$] [10]. To minimize reabsorption of radiation by the ground-state species, the emission spectra were obtained in very dilute solutions where the absorbance at 610 nm was less than 0.03. Singlet oxygen quantum yields (Φ_Δ) were measured in DMF by the method of chemical quenching of 1,3-diphenylisobenzofuran (DPBF) using ZnPc as reference ($\Phi_\Delta = 0.56$) [11].

2.2. Syntheses

2.2.1. Preparation of 3-[3,4,5-tris(3,6,9-trioxadecoxy)benzoxy]phthalonitrile (2)

To a mixture of 3-nitrophthalonitrile (1.73 g, 10 mmol) and compound **1** (2.97 g, 5 mmol) in DMF (30 mL) was added anhydrous K_2CO_3 (6.90 g, 50 mmol). The resulting mixture was stirred at 80°C for 4 days. The solvent was then evaporated under reduced pressure and the residue was mixed with $CHCl_3$ (60 mL) and water (60 mL). The aqueous layer was separated and extracted with $CHCl_3$ (60 mL × 3). The combined organic layers was dried over anhydrous $MgSO_4$, then evaporated to dryness. The residue was purified by silica-gel column chromatography using $CHCl_3$/MeOH (60 : 1 v/v) as eluent to give compound **2** as a colorless liquid (1.41 g, 39%). ^{1}H NMR: δ 7.61 (vt, J = 8.7 Hz, 1 H, ArH), 7.37 (d, J = 7.5 Hz, 1 H, ArH), 7.25 (d, J = 7.5 Hz, 1 H, ArH), 6.66 (s, 2 H, ArH), 5.17 (s, 2 H, $ArCH_2$), 4.13–4.18 (m, 6 H, CH_2), 3.85 (t, J = 4.8 Hz, 4 H, CH_2), 3.79 (t, J = 5.1 Hz, 2 H, CH_2), 3.70–3.74 (m, 6 H, CH_2), 3.62–3.68 (m, 12 H, CH_2), 3.53–3.57 (m, 6 H, CH_2), 3.37 (two partially overlapping s, 9 H, CH_3); ^{13}C{^{1}H} NMR (DMSO-d_6): δ 160.9, 152.4, 137.7, 136.0, 130.7, 126.2, 119.3, 116.0, 115.6, 113.9, 107.1, 103.6, 72.0, 71.5, 71.2, 70.2, 70.0, 69.9, 69.8, 69.1, 68.5, 58.2 (some of the CH_2 signals are overlapped); MS (ESI): an isotopic cluster peaking at m/z 743 100%, $[M + Na]^+$; HRMS (ESI): m/z calcd for $C_{36}H_{52}N_2NaO_{13}[M + Na]^+$: 743.3362, found 743.3365.

2.2.2. Preparation of 4-[3,4,5-tris(3,6,9-trioxadecoxy)benzoxy]phthalonitrile (3)

According to the above procedure using 4- instead of 3-nitrophthalonitrile as a starting material, compound **3** was obtained as a colorless liquid (1.71 g, 47%). ^{1}H NMR ($CDCl_3$): δ 7.70 (d, J = 8.7 Hz, 1 H, ArH), 7.31 (d, J = 2.4 Hz, 1 H, ArH), 7.22 (dd, J = 2.4, 8.7 Hz, 1 H, ArH), 6.60 (s, 2 H, ArH), 5.02 (s, 2 H, $ArCH_2$), 4.11–4.15 (m, 6 H, CH_2), 3.82 (t, J = 4.8 Hz, 4 H, CH_2), 3.76 (t, J = 5.1 Hz, 2 H, CH_2), 3.68–3.71 (m, 6 H, CH_2), 3.60–3.65 (m, 12 H, CH_2), 3.50–3.53 (m, 6 H, CH_2), 3.34 (s, 9 H, CH_3); ^{13}C{^{1}H} NMR ($CDCl_3$): δ 161.5, 152.9, 138.7, 135.2, 129.7, 120.0, 119.6, 117.3, 115.5, 115.1, 107.5, 107.2, 72.2, 71.8, 71.0, 70.7, 70.6, 70.4, 69.6, 68.9, 58.9 (some of the CH_2 signals are overlapped); MS (ESI): an isotopic cluster peaking at m/z 743 100%, $[M + Na]^+$; HRMS (ESI): m/z calcd for $C_{36}H_{52}N_2NaO_{13}[M + Na]^+$: 743.3362, found 743.3361.

2.2.3. Preparation of phthalocyanine (4)

A mixture of phthalonitrile **2** (0.26 g, 0.36 mmol), unsubstituted phthalonitrile (0.46 g, 3.59 mmol), and $Zn(OAc)_2 \cdot 2H_2O$ (0.22 g, 1.00 mmol) in *n*-pentanol (15 mL) was heated to 100°C, then a small amount of 1,8-diazabicyclo[5.4.0]undec-7-ene (DBU) (0.5 mL) was added. The mixture was stirred at 140–150°C for 24 hours After a brief cooling, the volatiles were removed under reduced pressure. The residue was dissolved in $CHCl_3$ (120 mL), then filtered to remove part of the unsubstituted zinc(II) phthalocyanine formed. The filtrate was collected and evaporated to dryness in vacuo. The residue was purified by silica-gel column chromatography using $CHCl_3/CH_3OH$ (30 : 1 v/v) as eluent, followed by size exclusion chromatography using THF as eluent. The crude product was further purified by recrystallization from a mixture of THF and hexane (0.11 g, 26%). ^{1}H NMR ($CDCl_3$ with a trace amount of pyridine-d_5): δ 9.41–9.46 (m, 5 H, Pc-H$_\alpha$), 9.16 (d, J = 7.5 Hz, 1 H, Pc-H$_\alpha$), 9.13 (d, J = 6.9 Hz, 1 H, Pc-H$_\alpha$), 8.07–8.15 (m, 7 H, Pc-H$_\beta$), 7.69 (d, J = 7.8 Hz, 1 H, Pc-H$_\beta$), 7.30 (s, 2 H, ArH), 5.80 (s, 2 H, $ArCH_2$), 4.31 (t, J = 5.1 Hz, 2 H, CH_2), 4.19 (t, J = 5.1 Hz, 4 H, CH_2), 3.90 (t, J = 5.1 Hz, 2 H, CH_2), 3.78–3.82 (m, 2H, CH_2), 3.66–3.75 (m, 8 H, CH_2), 3.55–3.59 (m, 6 H, CH_2), 3.47–3.51 (m, 8 H, CH_2), 3.38–3.41 (m, 7 H, CH_2 and CH_3), 3.24 (s, 6 H, CH_3); ^{13}C{^{1}H} NMR (DMSO-d_6): δ 155.6, 152.7, 152.6, 152.3, 152.2, 140.3, 138.4, 137.9, 137.7, 137.6, 133.5, 130.6, 129.1, 125.3, 122.5, 122.4, 122.1, 115.3, 114.0, 107.8, 72.3, 71.6, 71.5, 71.0, 70.2, 70.0, 69.9, 69.8, 69.3, 68.8,

58.3, 58.2 (some of the signals are overlapped); MS (ESI): an isotopic cluster peaking at *m*/z 1191 100%, $[M + Na]^+$; HRMS (ESI): *m/z* calcd for $C_{60}H_{64}N_8NaO_{13}Zn$ $[M + Na]^+$: 1191.3777, found 1191.3783.

2.2.4. Preparation of phthalocyanine (5)

According to the above procedure, phthalonitrile **3** (0.26 g, 0.36 mmol) was treated with unsubstituted phthalonitrile (0.46 g, 3.59 mmol) and $Zn(OAc)_2 \cdot 2H_2O$ (0.22 g, 1.00 mmol) to give phthalocyanine **5** as a blue solid (0.09 g, 21%). ^{1}H NMR ($CDCl_3$ with a trace amount of pyridine-d_5): δ 9.20–9.35 (m, 6 H, Pc-H$_\alpha$), 9.05 (d, J = 7.8 Hz, 1 H, Pc-H$_\alpha$), 8.66 (s, 1 H, Pc-H$_\alpha$), 8.06–8.12 (m, 6 H, Pc-H$_\beta$), 7.62 (d, J = 8.4 Hz, 1 H, Pc-H$_\beta$), 6.99 (s, 2 H, ArH), 5.46 (s, 2 H, $ArCH_2$), 4.33 (t, J = 4.8 Hz, 4 H, CH_2), 4.24 (t, J = 5.1 Hz, 2 H, CH_2), 3.94 (t, J = 4.8 Hz, 4 H, CH_2), 3.86 (t, J = 4.8 Hz, 2 H, CH_2), 3.76–3.80 (m, 6 H, CH_2), 3.62–3.71 (m, 12 H, CH_2), 3.53–3.57 (m, 6 H, CH_2), 3.38 (s, 3 H, CH_3), 3.36 (s, 6 H, CH_3); ^{13}C{^{1}H} NMR (DMSO-d_6): δ 159.9, 152.6, 152.4, 152.3, 152.2, 152.0, 151.7, 151.6, 139.5, 137.8, 137.5, 132.7, 130.7, 129.0, 128.9, 123.0, 122.2, 117.8, 107.2, 105.6, 72.1, 71.5, 70.3, 70.1, 70.0, 69.9, 69.4, 68.8, 58.3, 55.1 (some of the signals are overlapped); MS (ESI): an isotopic cluster peaking at *m*/z 1191 95%, $[M + Na]^+$; HRMS (ESI): *m/z* calcd for $C_{60}H_{64}N_8NaO_{13}Zn$ $[M + Na]^+$: 1191.3777, found 1191.3771.

2.2.5. Preparation of 3,6-bis[3,4,5-tris(3,6,9-trioxadecoxy)benzoxy]phthalonitrile (7)

A mixture of compound **6** (2.06 g, 3.36 mmol), 2,3-dicyanohydroquinone (0.27 g, 1.69 mmol), and K_2CO_3 (1.17 g, 8.47 mmol) in DMF (10 mL) was stirred at 100°C for 24 hours The volatiles were then removed under reduced pressure. The residue was mixed with water (50 mL) and the mixture was extracted with $CHCl_3$ (50 mL × 3). The combined organic extracts was dried over anhydrous $MgSO_4$ and evaporated under reduced pressure. The residue was then purified by silica-gel column chromatography using $CHCl_3$/MeOH (20:1 v/v) as eluent to give the product as a pale yellow transparent liquid (1.95 g, 88%).^{1}H NMR ($CDCl_3$): δ 7.13 (s, 2 H, ArH), 6.64 (s, 4 H, ArH), 5.07 (s, 4 H, $ArCH_2$), 4.12–4.17 (m, 12 H, CH_2), 3.84 (t, J = 4.8 Hz, 8 H, CH_2), 3.78 (t, J = 5.1 Hz, 4 H, CH_2), 3.71–3.74 (m, 12 H, CH_2), 3.62–3.67 (m, 24 H, CH_2), 3.52–3.57 (m, 12 H, CH_2), 3.37 (two partially overlapping s, 18 H, CH_3); ^{13}C{^{1}H} NMR ($CDCl_3$): δ 154.7, 152.8, 138.2, 130.3, 119.4, 112.9, 106.4, 105.7, 72.2, 71.7, 71.6, 70.6, 70.5, 70.3, 69.5, 68.7, 58.8 (some of the CH_2 signals are overlapped); MS (ESI): an isotopic cluster peaking at *m*/z 1336 100%, $[M + Na]^+$; HRMS (ESI): *m/z* calcd for $C_{64}H_{100}N_2NaO_{26}$ $[M + Na]^+$: 1335.6457, found 1335.6462.

2.2.6. Preparation of phthalocyanine (8)

According to the procedure described for **4**, phthalonitrile **7** (0.50 g, 0.38 mmol) was treated with unsubstituted phthalonitrile (0.49 g, 3.82 mmol) and $Zn(OAc)_2 \cdot 2H_2O$ (0.23 g, 1.05 mmol) to give phthalocyanine **8** as a blue-green oil (54 mg, 8%). ^{1}H NMR ($CDCl_3$): δ 9.43–9.47 (m, 4 H, Pc-H$_\alpha$), 9.20 (d, J = 7.5 Hz, 2 H, Pc-H$_\alpha$), 8.03–8.15 (m, 6 H, Pc-H$_\beta$), 7.68 (s, 2 H, Pc-H$_\beta$), 7.37 (s, 4 H, ArH), 5.90 (s, 4 H, $ArCH_2$), 4.05 (t, J = 5.1 Hz, 4 H, CH_2), 3.80 (t, J = 5.1 Hz, 8 H, CH_2), 3.70 (t, J = 5.1 Hz, 4 H, CH_2), 3.61–3.65 (m, 4 H, CH_2), 3.55–3.58 (m, 8 H, CH_2), 3.44–3.48 (m, 12 H, CH_2), 3.34–3.37 (m, 12 H, CH_2), 3.30 (s, 6 H, CH_3), 3.18–3.21 (m, 8 H, CH_2), 3.12 (s, 12 H, CH_2), 2.90 (s, 12 H, CH_3); ^{13}C{^{1}H} NMR ($CDCl_3$): 153.6, 153.4, 153.3, 152.5, 152.2, 150.2, 138.6, 138.3, 138.1, 137.5, 133.6, 129.0, 128.8, 128.6, 128.5, 122.6, 122.3, 122.1, 116.5, 107.0, 72.3, 72.2, 71.8, 71.3, 70.5, 70.4, 69.9, 69.7, 69.2, 68.1, 58.8, 58.4 (some of the CH_2 signals are overlapped); MS (ESI): an isotopic cluster peaking at *m*/z 1784 20%, $[M + Na]^+$; HRMS (ESI): *m/z* calcd for $C_{88}H_{112}N_8NaO_{26}Zn$ $[M + Na]^+$: 1783.6871, found 1783.6862.

2.3. In vitro studies

2.3.1. Cell lines and culture conditions

The HT29 human colorectal carcinoma cells (from ATCC, no. HTB-38) were maintained in Dulbecco's modified Eagle's medium (DMEM) (Invitrogen, cat no. 10313-021) supplemented with fetal calf serum (10%), penicillin-streptomycin (100 units mL^{-1} and 100 $mgmL^{-1}$, resp.), L-glutamine (2 mM), and transferrin (10 $mgmL^{-1}$). The HepG2 human hepatocarcinoma cells (from ATCC, no. HB-8065) were maintained in RPMI medium 1640 (Invitrogen, cat no. 23400-021) supplemented with fetal calf serum (10%) and penicillin-streptomycin (100 units mL^{-1} and 100 $mgmL^{-1}$, resp.). Approximately 3×10^4 (for HT29) or 4×10^4 (for HepG2) cells per well in these media were inoculated in 96-multiwell plates and incubated overnight at 37°C in a humidified 5% CO_2 atmosphere.

2.3.2. Photocytotoxicity assay

Phthalocyanines **4**, **5**, and **8** were first dissolved in DMF to give 1.5 mM solutions, which were diluted to 80 μM with an aqueous solution of Cremophor EL (Sigma, 0.47 g in 100 mL of water). The solutions were filtered with a 0.2 μm filter, then diluted with the culture medium to appropriate concentrations (two-fold dilutions from 8 μM). The cells, after being rinsed with phosphate buffered saline (PBS), were incubated with 100 μL of these phthalocyanine solutions for 2 hours at 37°C under 5% CO_2. The cells were then rinsed again with PBS and refed with 100 μL of the culture medium before being illuminated at ambient temperature. The light source consisted of a 300 W halogen lamp, a water tank for cooling, and a color glass filter (Newport) cut-on 610 nm. The fluence rate ($\lambda > 610$ nm) was 40 mW cm^{-2}. An illumination of 20 minutes led to a total fluence of 48 J cm^{-2}.

Cell viability was determined by means of the colorimetric MTT assay [12]. After illumination, the cells were incubated at 37°C under 5% CO_2 overnight. An MTT (Sigma) solution in PBS (3 $mgmL^{-1}$, 50 μL) was added to each well followed by incubation for 2 hours under the same environment. A solution of sodium dodecyl sulfate (SDS, Sigma)

(10% by weight, 50 μL) was then added to each well. The plate was incubated in an oven at 60°C for 30 minutes, then 80 μL of *iso*-propanol was added to each well. The plate was agitated on a Bio-Rad microplate reader at ambient temperature for 10 sec before the absorbance at 540 nm at each well was taken. The average absorbance of the blank wells, which did not contain the cells, was subtracted from the readings of the other wells. The cell viability was then determined by the equation: % Viability = $[\Sigma(A_i/A_{control} \times 100)]/n$, where A_i is the absorbance of the ith data ($i = 1, 2, \ldots, n$), $A_{control}$ is the average absorbance of the control wells, in which the phthalocyanine was absent, and n (= 4) is the number of the data points.

2.3.3. Fluorescence microscopic studies

For the detection of the intracellular fluorescence intensity of compounds **4**, **5**, and **8**, approximately 1.2×10^5 HT29 cells in the culture medium (2 mL) were seeded on a coverslip (diameter = 25 mm) and incubated overnight at 37°C under 5% CO_2. The medium was removed, then the cells were incubated with 2 mL of an 8 μM phthalocyanine dilution in the medium for 2 h under the same conditions. The cells were then rinsed with PBS and viewed with an Olympus IX 70 inverted microscope. The excitation light source (at 630 nm) was provided by a multiwavelength illuminator (Polychrome IV, TILL Photonics). The emitted fluorescence (>660 nm) was collected using a digital cooled CCD camera (Quantix, Photometrics). Images were digitalized and analyzed using MetaFluor V.4.6 (Universal Imaging).

3. RESULTS AND DISCUSSION

3.1. Molecular design and chemical synthesis

Zinc(II) phthalocyanines are good candidates for PDT application. In addition to their relatively high stability, the closed-shell zinc(II) center imparts desirable photophysical characteristics to the macrocycles [13]. Introduction of substituents at the peripheral positions can also tailor the properties of the macrocycles such as their solubility in biological media, aggregation behavior, and targeting properties. As a result, zinc(II) phthalocyanines have received considerable attention as efficient photosensitizers [5]. We describe herein three novel zinc(II) phthalocyanines (compounds **4**, **5**, and **8**) which contain the bulky and hydrophilic 3,4,5-tris(3,6,9-trioxadecoxy)benzoxy moiety. Having one or two of these substituents, the π-π stacking tendency is reduced and the macrocycles become amphiphilic in nature. These properties should be advantageous for singlet oxygen generation and cellular uptake, by which the photodynamic activity can be enhanced. The relatively rare 1,4-disubstituted phthalocyanine **8** also has a longer Q-band maximum compared with the α- and β-monosubstituted counterparts, which is also an advantage that can increase the light penetration depth [14].

Scheme 1 shows the synthetic route used to prepare the monosubstituted phthalocyanines **4** and **5**. Reaction of benzyl alcohol **1** with 3- or 4-nitrophthalonitrile in the presence of K_2CO_3 in DMF gave the substituted phthalonitrile **2** or **3**, respectively. These compounds then underwent a mixed cyclization with an excess of the unsubstituted phthalonitrile (10 equiv.) in the presence of $Zn(OAc)_2 \cdot 2H_2O$ and DBU in *n*-pentanol to afford the corresponding "3+1" products **4** and **5**. These reactions also produced the unsubstituted ZnPc as a major side-product, which could be separated readily by filtration and chromatography as a result of its lower solubility and slower mobility in the silica gel column. During the chromatographic purification, a trace amount of some other blue products was also separated, but no attempt was made to characterize these minor side-products. Similarly, treatment of 2,3-dicyanohydroquinone with benzyl chloride **6** and K_2CO_3 afforded dinitrile **7**, which was then cyclized with the unsubstituted phthalonitrile in the presence of $Zn(OAc)_2 \cdot 2H_2O$ to give **8** (Scheme 2). All these zinc(II) phthalocyanines were soluble in common organic solvents and possessed high stability, which facilitated the purification by silica-gel column chromatography, size exclusion chromatography, followed by recrystallization.

3.2. Spectroscopic characterization and photophysical properties

All the new compounds were fully characterized with various spectroscopic methods. The NMR signals for the phthalocyanine ring protons of **4**, **5**, and **8** are very distinct in $CDCl_3$ (with a trace amount of pyridine-d_5 for the former two complexes to reduce their aggregation), which provide a useful means for characterization. As shown in Figure 1, the ^{1}H NMR spectrum of the α-substituted phthalocyanine **4** shows a multiplet at δ 9.41–9.46 (5 H) and two doublets at δ 9.16 (1 H) and 9.13 (1 H) for the 7 phthalocyanine α protons. The 8 β protons resonate as a multiplet at δ 8.07–8.15 (7 H) and a doublet at δ 7.69 (1 H). For the β-analogue **5**, a multiplet at δ 9.20–9.35 (6 H), a doublet at δ 9.05 (1 H), and a singlet at δ 8.66 (1 H) are seen for the 8 phthalocyanine α protons, while the signals for the 7 β protons appear as a multiplet at δ 8.06–8.12 (6 H) and a doublet at δ 7.62 (1 H). Phthalocyanine **8** has a C_{2v} symmetry. The doublet at δ 9.20 can be assigned to the two phthalocyanine α ring protons close to the benzoxy groups, while the multiplet at δ 9.43–9.47 is due to the remaining four α protons. The singlet at δ 7.68 can be readily assigned to the two β protons adjacent to the benzoxy groups, while the multiplet at δ 8.03–8.15 is attributed to the remaining six β protons.

The ^{13}C NMR data of these compounds were also in accord with the structures though some of the phthalocyanine ring carbon signals (for **4** and **5**) and the chain CH_2 signals were overlapped. For compound **8**, a total of 20 signals were observed in the aromatic region (δ 107.0–153.6) for the 16 phthalocyanine and 4 benzene ring carbons, which is consistent with the C_{2v} symmetry.

The ESI mass spectra of these phthalocyanines were also recorded. The molecular ion $[M + Na]^+$ isotopic cluster could be detected in all the cases. The isotopic distribution was in good agreement with the corresponding simulated pattern. The identity of these species was also confirmed by accurate mass measurements.

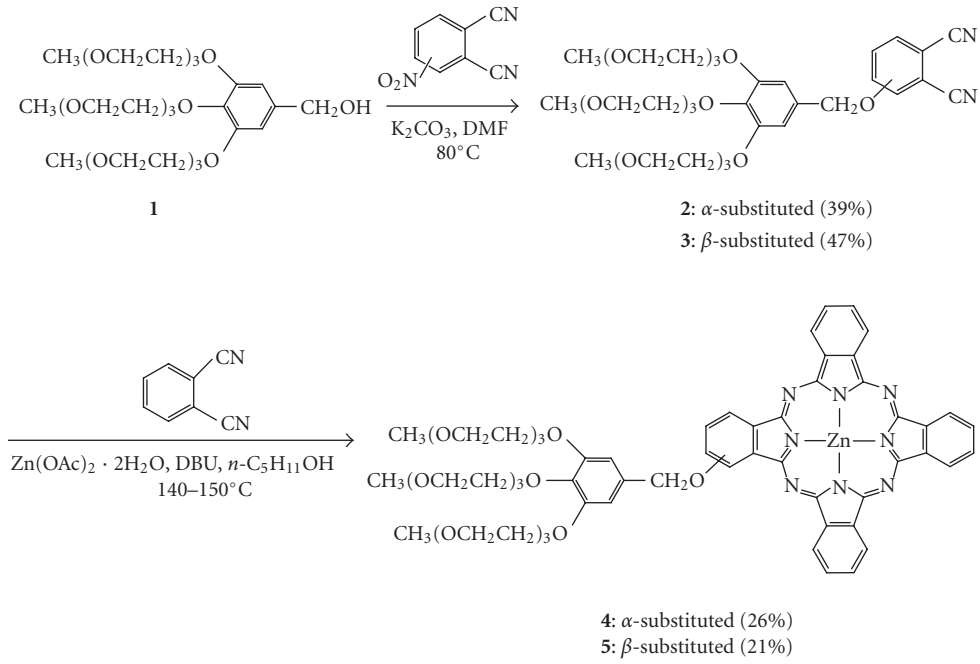

Scheme 1

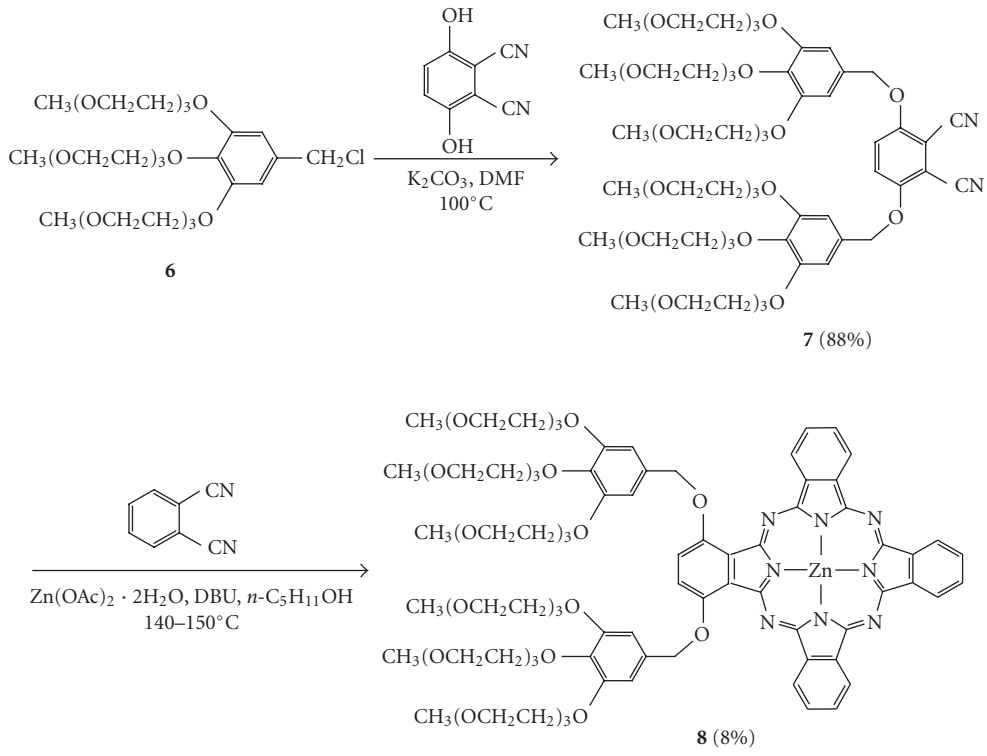

Scheme 2

The electronic absorption and basic photophysical data of phthalocyanines **4**, **5**, and **8** were measured in DMF and are summarized in Table 1. All the three compounds gave very similar UV-Vis spectra, which are typical for nonaggregated phthalocyanines. The spectrum of compound **5**, for example, showed the B-band at 344 nm, a vibronic band at 606 nm, and an intense and sharp Q-band at 672 nm, which strictly followed the Lambert Beer's law (Figure 2). Upon excitation at 610 nm, the compound is emitted at 677 nm with a fluorescence quantum yield of 0.19. Substitution at the α

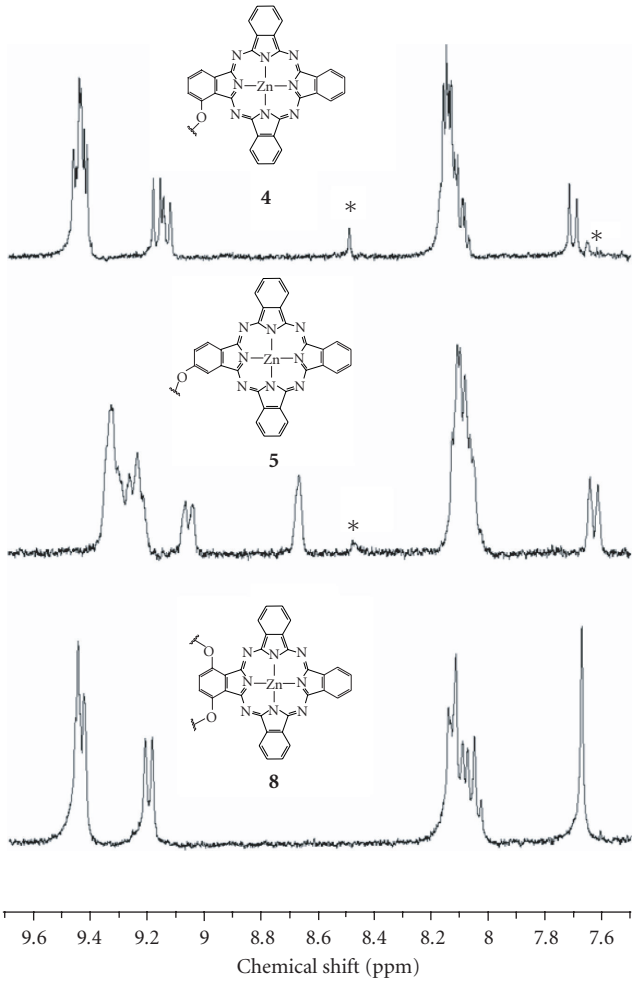

Figure 1: The aromatic region of the ^{1}H NMR spectra of **4**, **5**, and **8** in $CDCl_3$; ∗ indicates the trace amount of pyridine-d_5 added for the former two complexes.

Table 1: Electronic absorption and photophysical data for **4**, **5**, and **8** in DMF.

Compound	λ_{max} (nm) (log ε)	λ_{em} (nm)[a]	Φ_F[b]	Φ_Δ[c]
4	334 (4.69), 611 (4.58), 677 (5.40)	681	0.20	0.60
5	344 (4.79), 606 (4.62), 672 (5.39)	677	0.19	0.62
8	337 (4.73), 621 (4.55), 690 (5.31)	696	0.14	0.84

[a]Excited at 610 nm.
[b]Using unsubstituted zinc(II) phthalocyanine (ZnPc) in DMF as the reference (Φ_F = 0.28).
[c]Using ZnPc as the reference (Φ_Δ = 0.56 in DMF).

position (compound **4**) slightly shifted the Q-band and fluorescence emission to the red by 4-5 nm. Introduction of an additional α-substituent (compound **8**) further shifted the Q-band to 690 nm and the fluorescence emission to 696 nm.

The singlet oxygen quantum yields (Φ_Δ) of these compounds were also determined using 1,3-diphenylisobenzofuran (DPBF) as the scavenger. The concentration of the quencher was monitored spectroscopically at 411 nm along with time, from which the values of Φ_Δ could be determined

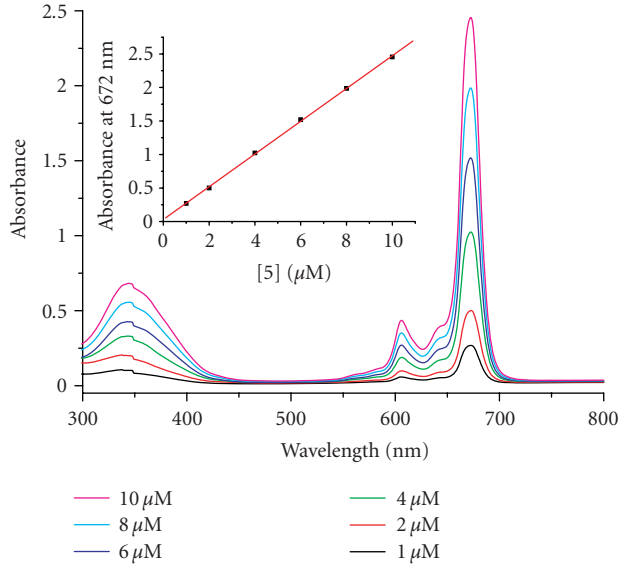

Figure 2: UV-Vis spectra of **5** in DMF. The inset plots the Q-band absorbance versus the concentration of **5**.

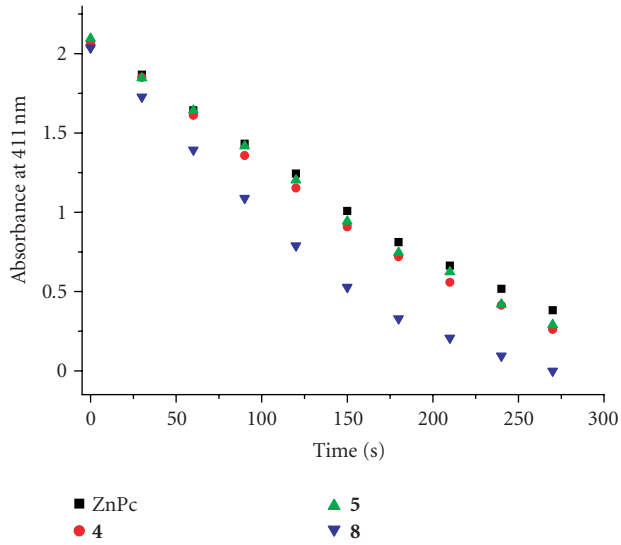

Figure 3: Comparison of the rates of decay of DPBF in DMF, as monitored spectroscopically at 411 nm, using phthalocyanines **4**, **5**, and **8** as the photosensitizers and ZnPc as the reference.

by the method described previously [11]. These data are also summarized in Table 1. Figure 3 compares the rates of decay of DPBF using these compounds and ZnPc as the photosensitizers. It can be seen that all these phthalocyanines are efficient singlet oxygen generators, particularly the 1,4-disubstituted analogue **8**, of which the value of Φ_Δ (0.84) is significantly higher than that of ZnPc (0.56), which was used as the reference.

3.3. *In vitro photodynamic activity*

The in vitro photodynamic activity of photosensitizers **4**, **5**, and **8** in Cremophor EL emulsions was investigated against

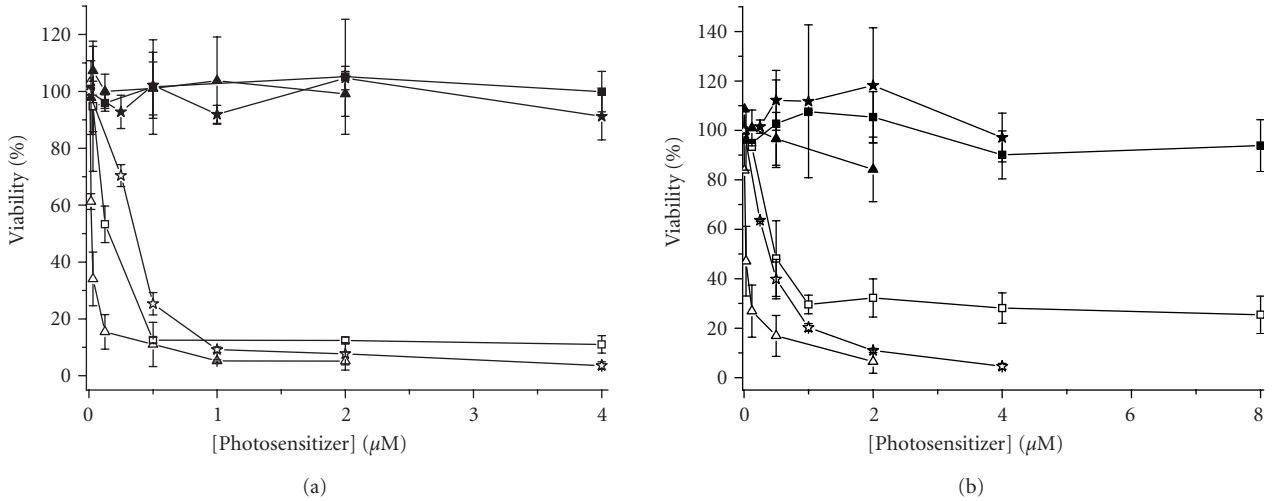

Figure 4: Effects of **4** (triangles), **5** (stars), and **8** (squares) on (a) HT29 and (b) HepG2 in the absence (closed symbols) and presence (open symbols) of light ($\lambda > 610$ nm, 40 mW cm^{-2}, 48 J cm^{-2}). Data are expressed as mean value ± SEM of three independent experiments, each performed in quadruplicate.

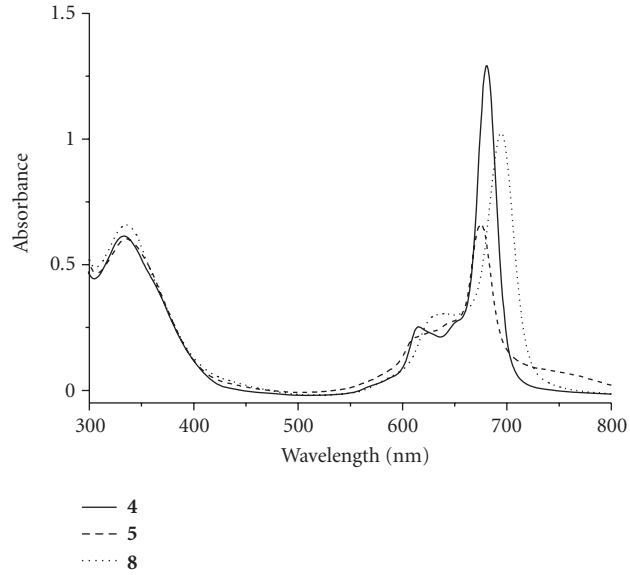

Figure 5: Electronic absorption spectra of **4** (solid line), **5** (dashed line), and **8** (dotted line), formulated with Cremophor EL, in the DMEM culture medium (all at 8 μM).

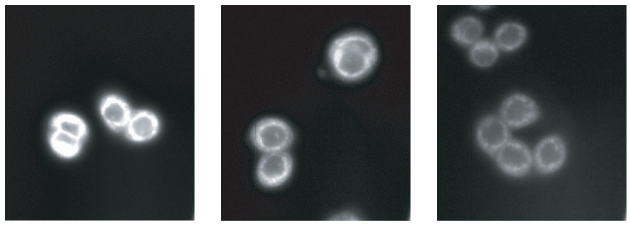

Figure 6: Fluorescence microscopic images of HT29 tumor cells after incubation with (a) **4**, (b) **5**, and (c) **8** at a concentration of 8 μM for 2 hours.

Table 2: Comparison of the IC_{50} values[a] of phthalocyanines **4**, **5**, and **8** against HT29 and HepG2.

Compound	For HT29 (μM)	For HepG2 (μM)
4	0.02	0.03
5	0.36	0.39
8	0.15	0.49

[a]Defined as the dye concentration required to kill 50% of the cells.

two different cell lines, namely, HT29 human colorectal carcinoma and HepG2 human hepatocarcinoma cells. As shown in Figure 4, the three compounds are essentially noncytotoxic in the absence of light, but exhibit a very high photocytotoxicity. The corresponding IC_{50} values are summarized in Table 2. It can be seen that all these compounds are highly potent and the effects on HT29 are greater than those on HepG2. The phthalocyanine **4** is particularly potent with the IC_{50} values down to 0.02 μM. About 1 μM of the dye is sufficient to kill 90% of the cells.

It is worth noting that although phthalocyanine **4** exhibits a relatively lower singlet oxygen quantum yield than the other two analogues in DMF (Table 1), its photocytotoxicity is the highest among the three photosensitizers (Table 2). To account for the results, the absorption spectra of these compounds in the culture media were recorded. As shown in Figure 5, the Q-band for compound **4** in the DMEM medium (for HT29) remains very sharp and intense, while those for **5** and **8** are weaker and broadened. Very similar results were obtained in the RPMI medium (for HepG2). This is a strong indication that compound **4** is significantly less aggregated in these media, which should lead to a higher photosensitizing efficiency.

To further explain the photocytotoxicity results, fluorescence microscopic studies were also carried out to shed light on the cellular uptake of photosensitizers **4**, **5**, and **8**.

After incubation with these compounds (formulated with Cremophor EL) for 2 hours and upon excitation at 630 nm, the HT29 cells showed intracellular fluorescence throughout the cytoplasm as shown in Figure 6, indicating that there was a substantial uptake of the dyes. The qualitative fluorescence intensity follows the order **4** > **5** > **8**, suggesting that the α-substituted phthalocyanine **4** also has the highest uptake among the three photosensitizers. This may also account for the highest photocytotoxicity of this compound.

In conclusion, we have prepared and characterized three novel "3+1" zinc(II) phthalocyanines substituted with one or two 3,4,5-tris(3,6,9-trioxadecoxy)benzoxy group(s). These compounds exhibit a high photocytotoxicity against HT29 and HepG2 cells with IC_{50} values down to 0.02 μM. The mono-α-substituted phthalocyanine **4** is more potent than the other two analogues, which can be partly explained by its lower aggregation tendency in the culture media and higher cellular uptake as shown by absorption spectroscopy and fluorescence microscopy, respectively.

ACKNOWLEDGMENTS

The authors thank Elaine Chan for technical support in the MTT assay and Prof. Wing-Hung Ko for the use of the fluorescence microscope. This work was supported by a grant from the Research Grants Council of the Hong Kong Special Administrative Region, China (Project no. 402103), and a strategic investments scheme administered by The Chinese University of Hong Kong.

REFERENCES

[1] N. Lane, "New light on medicine," *Scientific American*, vol. 288, no. 1, pp. 38–41, 2003.

[2] D. E. J. G. J. Dolmans, D. Fukumura, and R. K. Jain, "Photodynamic therapy for cancer," *Nature Reviews Cancer*, vol. 3, no. 5, pp. 380–387, 2003.

[3] S. B. Brown, E. A. Brown, and I. Walker, "The present and future role of photodynamic therapy in cancer treatment," *The Lancet Oncology*, vol. 5, no. 8, pp. 497–508, 2004.

[4] M. R. Detty, S. L. Gibson, and S. J. Wagner, "Current clinical and preclinical photosensitizers for use in photodynamic therapy," *Journal of Medicinal Chemistry*, vol. 47, no. 16, pp. 3897–3915, 2004.

[5] H. Ali and J. E. van Lier, "Metal complexes as photo- and radiosensitizers," *Chemical Reviews*, vol. 99, no. 9, pp. 2379–2450, 1999.

[6] P.-C. Lo, C. M. H. Chan, J.-Y. Liu, W.-P. Fong, and D. K. P. Ng, "Highly photocytotoxic glucosylated silicon(IV) phthalocyanines. Effects of peripheral chloro substitution on the photophysical and photodynamic properties," *Journal of Medicinal Chemistry*, vol. 50, no. 9, pp. 2100–2107, 2007.

[7] I. J. MacDonald and T. J. Dougherty, "Basic principles of photodynamic therapy," *Journal of Porphyrins and Phthalocyanines*, vol. 5, no. 2, pp. 105–129, 2001.

[8] M. A. Oar, J. M. Serin, W. R. Dichtel, J. M. J. Fréchet, T. Y. Ohulchanskyy, and P. N. Prasad, "Photosensitization of singlet oxygen via two-photon-excited fluorescence resonance energy transfer in a water-soluble dendrimer," *Chemistry of Materials*, vol. 17, no. 9, pp. 2267–2275, 2005.

[9] D. F. Eaton, "Reference materials for fluorescence measurement," *Pure and Applied Chemistry*, vol. 60, no. 7, pp. 1107–1114, 1988.

[10] I. Scalise and E. N. Durantini, "Synthesis, properties, and photodynamic inactivation of *Escherichia coli* using a cationic and a noncharged Zn(II) pyridyloxyphthalocyanine derivatives," *Bioorganic and Medicinal Chemistry*, vol. 13, no. 8, pp. 3037–3045, 2005.

[11] M. D. Maree, N. Kuznetsova, and T. Nyokong, "Silicon octaphenoxyphthalocyanines: photostability and singlet oxygen quantum yields," *Journal of Photochemistry and Photobiology A*, vol. 140, no. 2, pp. 117–125, 2001.

[12] H. Tada, O. Shiho, K.-I. Kuroshima, M. Koyama, and K. Tsukamoto, "An improved colorimetric assay for interleukin 2," *Journal of Immunological Methods*, vol. 93, no. 2, pp. 157–165, 1986.

[13] K. Ishii and N. Kobayashi, "The photophysical properties of phthalocyanines and related compounds," in *The Porphyrin Handbook*, K. M. Kadish, R. M. Smith, and R. Guilard, Eds., vol. 16, pp. 1–42, Academic Press, San Diego, Calif, USA, 2003.

[14] G. Jori, "Far-red-absorbing photosensitizers: their use in the photodynamic therapy of tumours," *Journal of Photochemistry and Photobiology A*, vol. 62, no. 3, pp. 371–378, 1992.

Hindawi Publishing Corporation
Metal-Based Drugs
Volume 2008, Article ID 392090, 7 pages
doi:10.1155/2008/392090

Research Article

Investigation of Zinc bis(1,4-didecylbenzo)-bis(2,3-pyrido) Porphyrazine for Application as Photosensitizer in Photodynamic Therapy of Cancer

Keiichi Sakamoto,[1] Eiko Ohno-Okumura,[1,2] Taku Kato,[1,3] Masaki Watanabe,[1,4] and Michael J. Cook[5]

[1] *Department of Applied Molecular Chemistry, College of Industrial Technology, Nihon University, 1-2-1 Izumi-cho, Narashino-shi, Chiba-ken 275-8575, Japan*
[2] *Research Institute of Chemical Science, Technology and Education, 8-37-1 Narashinodai, Funabashi-shi, Chiba-ken 274-0063, Japan*
[3] *Nissan Chemical Industries, LTD. Electronic Materials Research Laboratories, 722-1 Tsuboi-cho, Funabashi-shi, Chiba-ken 274-8507, Japan*
[4] *U-TEC Corporation, Innovation Technology Development, 21-1 Ohmori-cho, Nara-shi, Nara-ken 630-8131, Japan*
[5] *School of Chemical Sciences and Pharmacy, University of East Anglia, Norwich NR4 7TJ, UK*

Correspondence should be addressed to Keiichi Sakamoto, k5saka@cit.nihon-u.ac.jp

Received 30 June 2007; Revised 22 October 2007; Accepted 5 December 2007

Recommended by Jannie C. Swarts

The phthalocyanine analogue containing nonperipheral long alkyl-substituted benzenoid rings and pyridine rings, zinc bis(1,4-didecylbenzo)-bis(2,3-pyrido) porphyrazine, was synthesized. Zinc bis(1,4-didecylbenzo)-bis(2,3-pyrido) porphyrazine reacted with dimethyl sulfate and monochloroacetic acid to produce their quaternized products and diethyl sulfate to produce the sulfo-substituted products. All quaternized and sulfo-substituted showed amphiphilic character. Identical peaks in cyclic voltammograms appeared for these products before and after quaternization. During the evaluation of zinc bis(1,4-didecylbenzo)-bis(2,3-pyrido) porphyrazine for its photodynamic therapy of cancer (PDT) efficacy by cancer cell culture, the light exposed dimethyl sulfate quaternized zinc bis(1,4-didecylbenzo)-bis(2,3-pyrido) porphyrazines in IU-002 cells produce cell disruption that can be detected as a decrease in fluorescence.

1. INTRODUCTION

Phthalocyanine derivatives have attracted attention as functional chromophores for applications, especially organic charge carriers in photocopiers, as laser light absorbers in data storage systems, as photoconductors in photovoltaic cells, and in electrochromic displays [1–3]. Moreover, phthalocyanine derivatives can be utilized as sensitizers in photodynamic therapy of cancer (PDT).

Sensitizers for PDT require high photostability, high selectivity to tumors, no dark cytotoxity, strong absorption in the region between 600 and 800 nm where penetration of tissue is good, a long triplet lifetime, and satisfactory photosensitization of singlet oxygen. Phthalocyanine derivatives are known to satisfy the aforementioned conditions [3–8].

We previously synthesized the nonperipherally substituted phthalocyanine derivatives, zinc alkylbenzopyridoporphyrazines, which possessed didecylbenzenoid and pyridinoid moieties in the molecule and described regio isomer separation of one of the alkylbenzopyridoporphyrazines [9]. We reported a fundamental study on PDT by measuring for the triplet state lifetime of the alkylbenzopyridoporphyrazins and regio isomers [10, 11]. As alkylbenzopyridoporphyrazine exhibited solubility in organic solvents and was expected to have a higher tumor affinity, quaternation of the pyridine nitrogen in the alkylbenzopyridoporphyrazine was done to give solubility in anaqueous media, and to have bioavailability and in vivo distribution [12]. Then, Nyokong et al. reported that phthalocyanine analogues, tetra-2, 3-pyridoporphyrazine and its quaternized compounds have excellent properties compared to zinc phthalocyanine-type photosensitizer [13]. The amphiphilic phthalocyanine derivatives were concluded the best compound for a new generation of photosensitizers for PDT

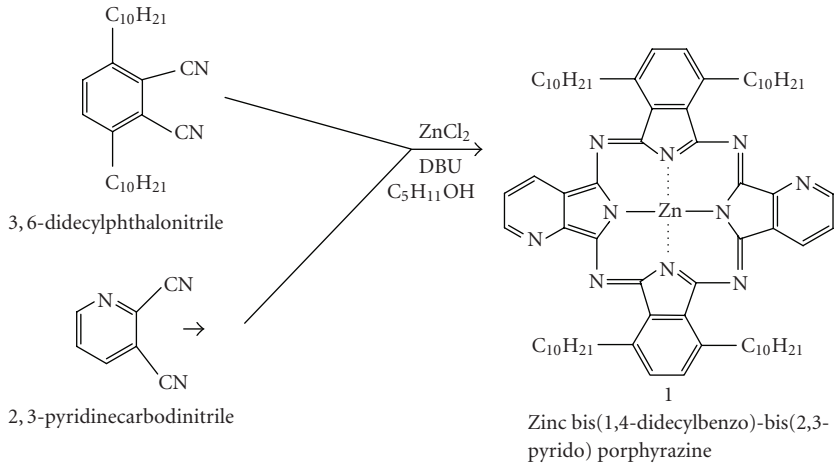

Figure 1: Synthetic pathway of zinc bis(1,4-didecylbenzo)-bis(2,3-pyrido) porphyrazine.

[12]. In our previous papers [9–12], the reported zinc bis(1,4-didecylbenzo)-bis(3,4-pyrido) porphyrazine and its regio isomers were prepared by 1 : 1 mixture of 3,6-didecylphthalonitrile and 3,4-pyridine dicarbonitrile.

In the present study, another type, novel nonperipheral, substituted phthalocyanine derivative, zinc bis(1,4-didecylbenzo)-bis(2,3-pyrido) porphyrazine was synthesized.

In the case of related compounds, 2,3-pyridoporphyrazines are known to have not only longer wavelength but stronger absorption intensity than corresponding phthalocyanines and 3,4-pyridoporphyrazines [14]. In accordance with [14], it is expected that zinc bis(1,4-didecylbenzo)-bis(2,3-pyrido) porphyrazine and its quaternation compounds have stronger absorption intensities than that of zinc bis(1,4-didecylbenzo)-bis(3,4-pyrido) porphyrazines reported before [9–12]. Therefore, the novel compound, zinc bis(1,4-didecylbenzo)-bis(2,3-pyrido) porphyrazine and its quaternation compounds are expected to be excellent photosensitizer for PDT.

2. RESULTS AND DISCUSSION

2.1. Synthesis and quaternization of phthalocyanine derivative

The synthetic procedure used to prepare the novel nonperipheral-substituted phthalocyanine derivative, zinc bis(1,4-didecylbenzo)-bis(2,3-pyrido) porphyrazines, was the same as that used for the preparation of zinc bis(1,4-didecylbenzo)-bis(3,4-pyrido) porphyrazine [9–12]. Zinc bis(1,4-didecylbenzo)-bis(2,3-pyrido) porphyrazine was synthesized in 80% yield using equimolar amounts of 3,6-didecylphthalodinitrile and 2,3-pyridine carbonitrile in the presence of 1,8-diazabicyclo[5.4.0]undec-7-ene (DBU) as basic catalyst (see Figure 1). The target compound, zinc bis(1,4-didecylbenzo)-bis(2,3-pyrido) porphyrazine, and its intermediates were studied using Fourier transformation infrared (IR), proton nuclear magnetic resonance (^{1}H-NMR), ultraviolet-visible (UV-Vis) spectroscopy, and elemental analysis. The analytical data of the compound were in good agreement with the proposed structure.

The synthesized zinc bis(1,4-didecylbenzo)-bis(2,3-pyrido) porphyrazine was anticipated to be a mixture of products, with different numbers of pyridine rings in the molecule. However, the target compound comprised only the proposed constituent as confirmed by thin layer chromatography (TLC). As the target compound had been purified by TLC using benzene as eluent, only one blue-colored constituent was obtained. It is thought that the desired compound was obtained in accordance with the mole ratio of the raw materials used. The same phenomenon has been observed in the case of synthesis of zinc bis(1,4-didecylbenzo)-bis(3,4-pyrido) porphyrazine [9–12].

Zinc bis(1,4-didecylbenzo)-bis(2,3-pyrido) porphyrazine has two alkylbenzenoid and two pyridinoid rings in different locations; thus, it has five regio isomers, three of which have rings adjacent to the pyridinoido rings while the other two have opposed pyridinoid rings. Although we previously reported the separation of regio isomers in alkylbenzopyridoporphyrazine [9–12], no attempt was made in this work to isolate the isomers of zinc bis(1,4-didecylbenzo)-bis(2,3-pyrido) porphyrazine. Of course, the obtained blue-colored constituent will be further separated into five regio isomers by using toluene-pyridine 7 : 3 eluent in accordance with [9–12].

The zinc bis(1,4-didecylbenzo)-bis(2,3-pyrido) porphyrazine reacted with quaternizing agents such as monochloroacetic acid (MCAA), diethyl sulfate (DES), and dimethyl sulfate (DMS) in *N*,*N*-dimethylformamide (DMF) as a solvent at 140°C for 2 hours.

The respective products obtained were greenish-blue-colored powders of which the yields were 24, 21, and 25% for MCAA, DES, and DMS, respectively (see Figure 3). Zinc bis(1,4-didecylbenzo)-bis(2,3-pyrido) porphyrazine was dissolved in toluene, chloroform, pyridine, and methanol but not in water. After reacting with quaternizing agents, the products were also soluble in water.

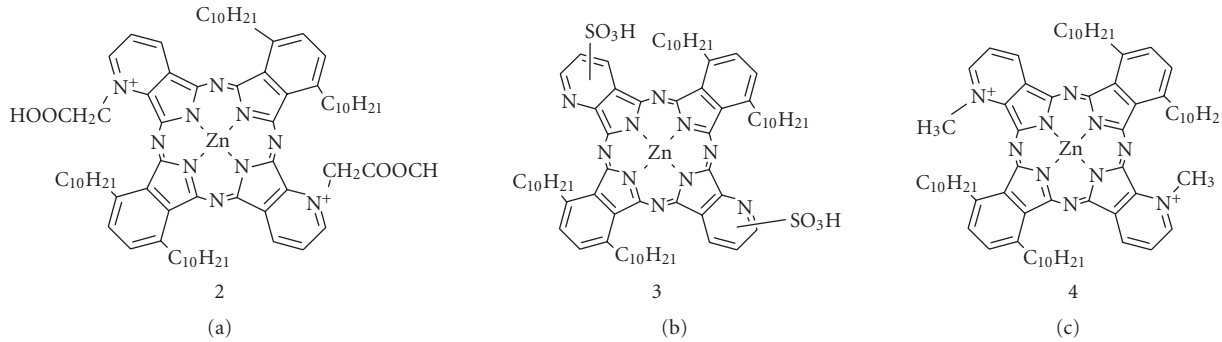

Figure 2: Typical structures of quaternized zinc bis(1,4-didecylbenzo)-bis(2,3-pyrido) porphyrazines.

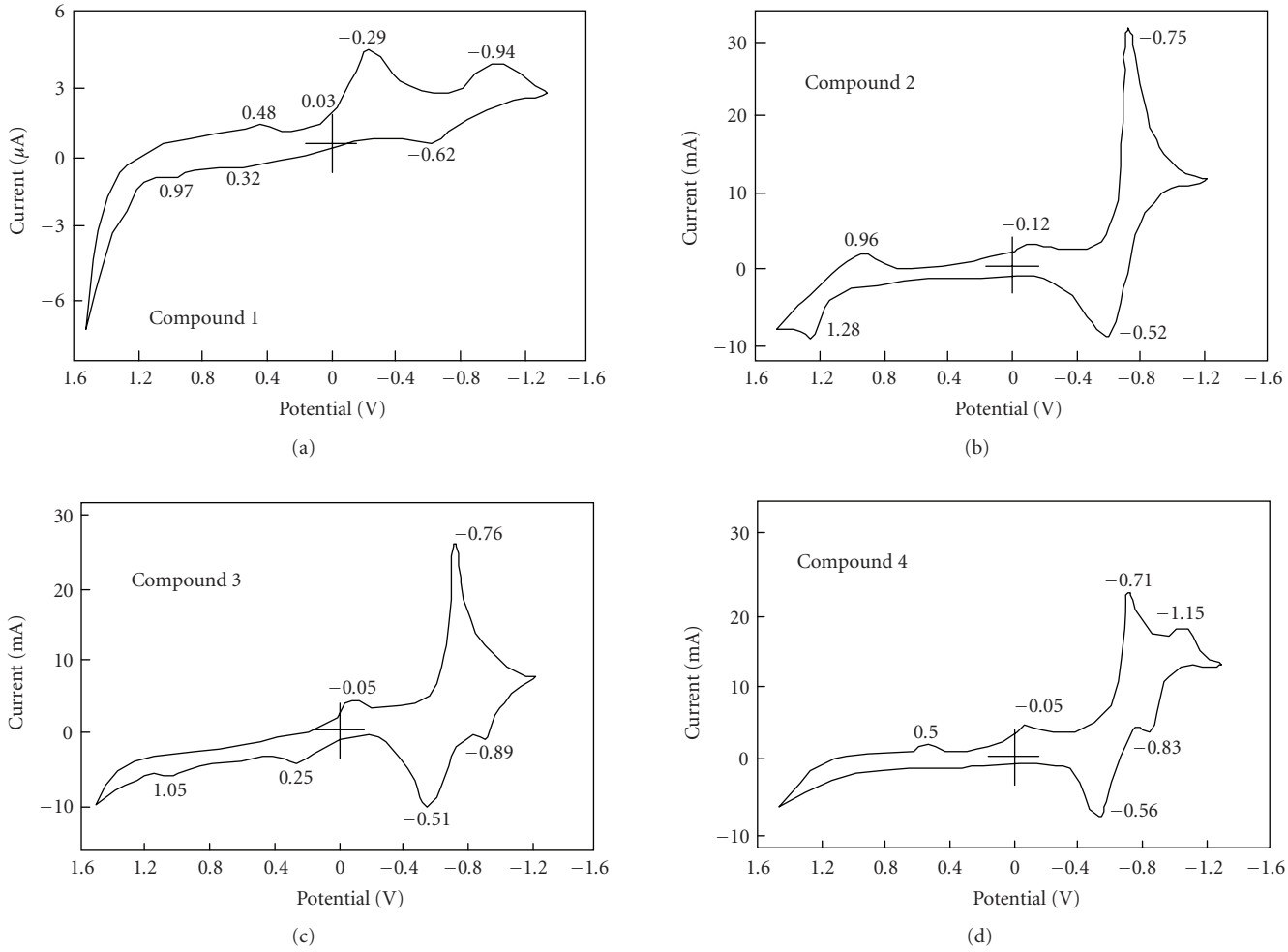

Figure 3: CVs of zinc bis(1,4-didecylbenzo)-bis(2,3-pyrido) porphyrazine.

In the cases of MCAA and DMS, analysis revealed that the structures of the products were in good agreement with those having N-CH_2COOH and N-CH_3 groups, respectively. Whereas when DES was used as a quaternizing agent, no N-CH_2CH_3 singlet peak was present in the ^{1}H-NMR spectrum, S=O stretching in the IR spectrum was observed. Therefore, sulfonation but not quaternization was achieved [12, 15].

After reaction with the quaternizing agents, all compounds possessed amphiphilic properties.

2.2. Spectroscopic and electrochemical properties

The UV-Vis spectrum of zinc bis(1,4-didecylbenzo)-bis(2,3-pyrido) porphyrazines around 700 nm is characteristic

Table 1: UV-Vis and fluorescence spectral data of quaternized zinc bis(1,4-didecylbenzo)-bis(2,3-pyrido) porphyrazine.

Compound	Q-band		Fluorescence	
	λ_{max} pyridine/nm	λ_{max} water/nm	F_{max} pyridine/nm	F_{max} water/nm
1	687	—	694	—
	[2]665	—	—	—
2	[1]679, 650	[1]687, 647	692	688
	[1,2]677, [2]620			
3	[1]693, 658, 628, 597	708, [1]687, 652	698	691
	[2]673, [2]645, [2]605			
4	746, [1]673, 649, 606	723, [1]676, 646	683	688
	[2]738, [1,2]668, [2]641, [2]600			

[1] Main peak.
[2]In toluene.

Table 2: Potentials of quaternized zinc bis(1,4-didecylbenzo)-bis(2,3-pyrido) porphyrazine in DMF with tetrabutylammonium perchlorate.Potentials of reversible wave are midpoint potential of anodic to cathodic peaks for each couple.

Compound	Potential (V versus Ag/AgCl)						
	Reduction (E_{pc})				Oxidation (E_{pa})		
1	–0.94*	–0.62*	–0.29*	–0.03*	0.32*	0.48*	0.97*
ΔE **							
2	–0.75*	–0.52*	–0.12*		0.96*	1.28*	
ΔE **							
3	–0.83	–0.51*	–0.05*		0.25*	1.05*	
ΔE **	0.14						
4	–1.15*	–0.77	–0.14*	–0.05*	0.50*		
ΔE **		0.11					

* Irreversible peak.
** The anodic peak to cathodic peak separation for reversible couple.

ofphthalocyanine analogues, with the Q band attributable to the difference between the highest occupied molecular orbital (HOMO) energy level and the lowest unoccupied molecular orbital (LUMO) energy, that is, the π-π^* transition of the phthalocyanine ring.

The quarternized derivatives of zinc bis(1,4-didecylbenzo)-bis(2,3-pyrido) porphyrazines showed strongest absorption at 676, 687, and 687 nm in water after reaction with DMS, DES, and MCAA, respectively (Table 1); these Q bands were bathochromic compared to the nonquaternized parent compound. As the UV-Vis spectra of the quaternized compounds in water showed very broad peaks, the amphiphilic compounds had excellent molecular association tendency.

Zinc bis(1,4-didecylbenzo)-bis(2,3-pyrido) porphyrazine and its quaternized compounds fluoresced on exposure to ultraviolet light. Although fluorescence spectra generally were known to be mirror images of UV-Vis spectra at the longer wavelengths, the Q bands nearly overlapped with the wavelengths at which fluorescence occurs in the case of zinc bis(1,4-didecylbenzo)-bis(2,3-pyrido) porphyrazine and its quaternized compounds, thus, the differences between λ_{max} of UV-Vis and the F_{max} of fluorescence spectra, called the Storkes shift, were very small between 10 to 20 nm. These observations are similar to that seen with the phthalocyanines zinc bis(1,4-didecylbenzo)-bis(2,3-pyrido) porphyrazine and its quaternized derivatives. These compounds are molecules with high planarity which cannot change their configuration after quaternization.

The important parameters of a cyclic voltammetry (CV) are the reduction (E_{pc}) and oxidation (E_{pa}) potential, the difference between reduction and oxidation potentials, (ΔE_p), and formal reduction potential ($E^{\circ\prime}$) of the observed waves. [Note: $E_{mid} = E^{\circ\prime}$] (Table 2 and see Figure 3).

The potential difference in CVs between the reduction and oxidation correspond to the HOMO-LUMO energy gaps of the compound [16]. Just as chemical reactions occur during the electron transfer between HOMO and LUMO energy levels, photochemical reactions are also based on similar phenomena of energy transfer. Before and after the quaternization, the HOMO-LUMO energy gap of zinc bis(1,4-didecylbenzo)-bis(2,3-pyrido) porphyrazine was unchanged. The shapes of CVs clearly showed that quaternized zinc bis(1,4-didecylbenzo)-bis(2,3-pyrido) porphyrazines had increased electron responsibility.

2.3. Cancer cell study

The uptake of DMS quaternized zinc bis(1,4-didecylbenzo)-bis(2,3-pyrido) porphyrazines was done in IU-002 cells. IU-002 cells were incubated at 37°C. After incubation for

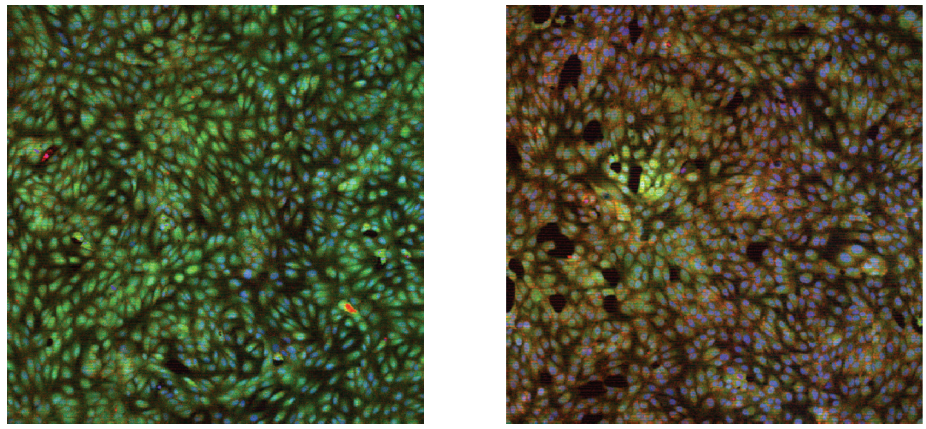

(a) (b)

Figure 4: Fluorescence image of IU-002 cells. (a) Control and (b) Incubated with DMS quaternized zinc bis(1,4-didecylbenzo)-bis(2,3-pyrido)porphyrazine and irradiated with halogen light for 10 minutes.

3 hours, cellular quaternized zinc bis(1,4-didecylbenzo)-bis(2,3-pyrido) porphyrazines was observed with a fluorescence microscope.

A fluorescent substance was noted when the uptake of DMS quaternized zinc bis(1,4-didecylbenzo)-bis(2,3-pyrido) porphyrazines in IU-002 cells was carried out.

Cell rupture can be detected. Intact cells selectively concentrated fluorescence. After exposure to halogen light for 10 minutes showed damage and loss of fluorescence although fluorescence in cells occurred in perinuclear area (see Figure 4).

Concequently, the light exposed DMS quaternized zinc bis(1,4-didecylbenzo)-bis(2,3-pyrido) porphyrazines in cells produces cell disruption that can be detected as a decrease as fluorescence.

2.4. Conclusions

Zinc bis(1,4-didecylbenzo)-bis(2,3-pyrido) porphyrazines were synthesized from an equimolar mixture of 3,6-didecylphthalonitrile and 2,3-pyridine carbonitrile in the presence of basic catalyst.

Zinc bis(1,4-didecylbenzo)-bis(2,3-pyrido) porphyrazines having two pyridine and two alkyl-substituted benzene rings reacted with DMS, DES, and MCAA as quaternizing agents.

When MCAA and DMS were employed as quaternizing agents, zinc bis(1,4-didecylbenzo)-bis(2,3-pyrido) porphyrazines were changed to their quaternized derivatives. However, when DES was employed, we showed that sulfonation but not quaternization was achieved.

Electrochmeical characterization of zinc bis(1,4-didecylbenzo)-bis(2,3-pyrido) porphyrazines and its quaternized derivatives were estimated by CV technique. The shapes of CVs clearly showed that quaternized zinc bis(1,4-didecylbenzo)-bis(2,3-pyrido) porphyrazines had increased electron responsibility.

The uptake of DMS-quaternized zinc bis(1,4-didecylbenzo)-bis(2,3-pyrido) porphyrazines was done in IU-002 cells.

The light-exposed DMS quaternized zinc bis(1,4-didecylbenzo)-bis(2,3-pyrido) porphyrazines in cells produces cell disruption that can be detected as a decrease in fluorescence.

3. EXPERIMENTAL

3.1. Equipment

IR spectra were recorded on a Shimadzu FT-IR 8100A spectrometer using potassium bromide (KBr) pellets. UV-Vis spectra were measured on a Shimadzu UV-2400PC spectrometer; each sample was prepared at 5.0×10^{-5} mol dm^{-3} in pyridine, toluene, and water. Fluorescence spectra were recorded in toluene, pyridine, and water using either a Hitachi F-4500 fluorescence spectrometer or a Jasco (Nihon Bunko) FP-6600 spectrofluorometer. ^{1}H-NMR spectra were measured at 400 MHz on a Bruker Avance 400S in benzene-d_6 (C_6H_6-d_6) or chloroform-d ($CHCl_3$-d) using tetramethylsilane (TMS) as an internal standard. Elemental analyses were carried out using a Perkin-Elmer 2400CHN instrument. Samples for elemental analysis were purified by repeated sublimation; the instrument was calibrated with copper phthalocyanine. CVs were recorded on a BAS CV-50 W voltammetric analyzer at room temperature in 1×10^{-3} mol dm^{-3} acetonitrile solution containing a 0.01 mol dm^{-3} tetrabutylammonium perchlorate (TBAP). CVs were recorded by scanning the potential at a rate of 50 mV s^{-1}. The working and counter electrodes were platinum wires and the reference electrode was a silver/silver chloride- (Ag/AgCl) saturated sodium chloride electrode. The area of the working electrode was 2.0×10^{-2} cm^2.

3.2. Materials

TLC was performed using Merck 60 F_{254} silica gel on aluminium sheets. Merck Silica gel 60, particle size 0.063–0.200 nm 7734 grade was used in chromatographic separations.

Reagents were purchased from Sigma-Aldrich Chemicals (Miss, USA) and were used as received without further purification.

3,6-Didecylphthalonitrile was synthesized from thiophene via 2,5-Didecylthiophene and 2,5-Didecylthiophene-1,1-dioxide, in accordance with our previous reports [9–12]. ^{1}H NMR (δ 400 MHz, $CHCl_3$-d/ ppm) 0.88 (t, 6H), 1.26 (m, 32H), 2.85 (t, 4H), 7.46 (s, 2H); IR(ν KBr/cm^{-1}) 2960 (ν_{C-H}), 2240 ($\nu_{C\equiv N}$), 1560 ($\nu_{C=C}$), 1460 (ν_{C-C}), 1410 (ν_{C-C}), 1230 (δ_{C-H}), 730 (δ_{C-H}); Anal Calcd. for $C_{28}H_4N_2$: C. 82.69: H. 10.85: N.6.86. Found: C.82.26: H. 10.84: N. 6.84.

2,3-Pyridine dicarbonitrile was synthesized from pyridine-2,3-dicarboxylic acid. Pyridine-2,3-dicarboxylic acid (15 g, 0.09 mol) in 200 cm^3 of ethanol was refluxed in 7.5 cm^3 of concentrated sulfonic acid for 48 hours. After the solvent was removed and neutralized with 3 M NaOH solution, the organic layer was extracted with three times of 75 cm^3 of diethyl ether. The extract was dried on calcium chloride and filtered and the solvent evaporated. The residue was distilled to afford pyridine 2,3-dicarboxy ester. The ester was dissolved in concentrated aqueous ammonia and the solution was stirred for 48 hours to afford a white-colored precipitate. The precipitate was filtered off and the corresponding diamide was obtained as m.p. 179–181°C. Thionyl chloride (9.6 g, 0.08 mol) was added dropwise to the diamide (6.6 g, 0.04 mmol) in 56 g of DMF at −10°C. This mixture was allowed to warm to room temperature and was stirred for 24 hours. The solvent was removed by evaporation and water was added to make the thionyl chloride ineffective and then filtered. The product was purified by chromatography over silica gel with benzene-petroleum ether 1 : 1 as eluent, giving a colorless solid (1.97 g, 17%), m.p. 265°C.

^{1}H NMR (δ 400 MHz, $CHCl_3$-d/ppm) 7.26 (s, 1H), 7.75 (s, 1H), 9.09 (s, 1H); IR(ν KBr/cm^{-1}) 3090 (ν_{C-H}), 2240 (ν_{C-N}), 1600 (ν_{C-C}), 1550 (ν_{C-C}), 1470 (ν_{C-C}), 1220 (δ_{C-H}), 750 (δ_{C-H}); Anal Calcd. for $C_7H_3N_3$: C. 65.11: H. 2.34: N.32.55. Found: C.65.12: H. 2.34: N. 32.56.

3.3. Zinc bis(1,4-didecylbenzo)-bis(2,3-pyrido) porphyrazine

3,6-Didecylphthalonitrile (0.12 g, 0.29 mmol) and 2,3-dicyanopyridine (0.04 g, 0.29 mmol) (see Figure 1) were dissolved in pentanol (7 cm^3) and zinc chloride (0.05 g) was added; the ensuing mixture was heated for 4 hours in the presence of DBU as catalyst. After cooling, the reaction mixture was dissolved in toluene (50 cm^3) and filtered; the solvent was removed by evaporation. The product was purified by TLC (eluent : toluene) yielding a blue solid (0.13 g; yield 80%). ^{1}H NMR (δ 400 MHz, C_6H_6-d_6/ppm) 0.9 (m, 12H, CH_3), 1.61–2.61 (m, 64H, CH_2), 4.18–4.36 (m, 8H, α-CH_2), 7.45 (m, 4H, arom), 8.26 (m, 6H, Py); IR(ν KBr/cm^{-1}) 2960 (ν_{C-H}), 1600 (ν_{C-C}), 1500 (ν_{C-C}), 1420 (ν_{C-C}), 1200 (δ_{C-H}), 1100 (δ_{C-H}), 750 (δ_{C-H}); UV-Vis [λ_{max} toluene/nm (log ε_{max})] 665 (5.494); Anal Calcd. for $C_{70}H_{94}N_{10}Zn$: C. 73.68: H. 8.30: N.12.28. Found: C.73.67: H. 8.30: N. 12.28.

3.4. Quaternization of zinc bis(1,4-didecylbenzo)-bis(2,3-pyrido) porphyrazine

Zinc bis(1,4-didecylbenzo)-bis(2,3-pyrido) porphyrazine (0.17 g, 0.15 mmol) reacted with MCAA (0.57 g, 6 mmol), DES (0.1 g, 0.6 mmol) and DMS (0.2 g, 1.5 mmol), respectively, in *N*,*N*-dimetylformamide (DMF) 140°C for 2 hours (see Figures 2 and 3). The reaction mixture was dissolved in acetone (20 cm^3), cooled to room temperature, and the resulting solution was filtered. The solvent was removed and the product was purified by TLC (eluent : THF-toluene, 8 : 2); the product was recovered from the TLC plate via dissolution in pyridine followed by filtration and solvent removal. MCAA:Yield 25%, ^{1}H NMR (δ 400 MHz, C_6H_6-d_6/ppm) 0.87(m, 12H, CH_3), 1.13–1.70(m, 56H, γ-CH_2), 1.82–2.61(m, 8H, β-CH_2), 4.11–4.38(m, 4H, α-CH_2), 6.20(s, 2H, CH_2), 7.14–7.27(m, 4H, Arom), 8.73–.16(m, 6H, Py): IR(ν KBr/cm^{-1}) 3480(ν_{O-H}), 3050, 2970(ν_{C-H}), 1740($\nu_{C=O}$), 1600, 1500, 1400($\nu_{C=C}$), 1210, 1100, 940, 790, 690(δ_{C-H}); DES yield 21%, (δ 400 MHz, C_6H_6-d_6/ppm) 0.86(m, 12H, CH_3), 1.02–1.63(m, 56H, γ-CH_2), 1.88–2.61(m, 8H, β-CH_2), 4.26–4.50(m, 4H, α-CH_2), 7.37(m, 4H, Arom), 8.22(m, 4H, Py): IR(ν KBr/cm^{-1}) 3480(ν_{O-H}), 3050, 2960(ν_{C-H}), 1600, 1460, 1400($\nu_{C=C}$), 1350, 1150($\nu_{S=O}$), 1250, 920, 770(δ_{C-H}), 580(δ_{C-S}); DMS yield 25%, (δ 400 MHz, C_6H_6-d_6/ppm) 0.90(m, 12H, CH_3), 0.95–1.45(m, 56H, γ-CH_2), 1.60–2.41(m, 8H, β-CH_2), 4.05(s, 6H, CH_3), 4.25–4.42(m, 4H, α-CH_2), 7.45(m, 4H, Arom), 8.02(m, 6H, Py): IR(ν KBr/cm^{-1}) 3070, 2980(ν_{C-H}), 1500, 1400($\nu_{C=C}$), 1250, 1100, 950, 810, 660(δ_{C-H}).

3.5. Cell culture

IU-002 cells were maintained in MEM medium supplemented 5% fetal calf serum.

Cells seeded into 96-well tissue culture plates and incubated to allow attachment to the plates. The sensitizer was added to the medium at concentration ranging from $0\ to\ 2 mg cm^3$. Cells were incubated for 3 hours. The medium was removed, the cells were washed with phosphate-buffered saline (PBS), and fresh medium was added. Cells were exposed halogen light for 10 minutes. Appearance of cells was observed used a fluorescence microscope.

ACKNOWLEDGMENTS

The assistance of Miss T. Komoriya in the taking of data for part of cell culture is greatly appreciated. The authors would like to thank Professor Kohono for his helpful advice given to them regarding their paper. This research work wassupported financially by Advanced Research Center for Life Science and Human Environment, Graduate School of Industrial Technology, Nihon University (Narashino-shi, Japan), which was adopted by a project for the promotion of high technology within The Ministry of Education and Science, Japan's Academic Frontier Project.

REFERENCES

[1] N. B. McKeown, *Phthalocyanine Materials—Synthesis Structure and Function*, Cambridge University Press, Cambridge, UK, 1998.

[2] C. C. Leznff and A. B. P. Lever, *Phthalocyanines—Properties and Applications*, vol. 1–4, VCH, New York, NY, USA, 1989, 1993, 1996.

[3] R. Hirohashi, K. Sakamoto, and E. Ohno-Okumura, *Phthalocyanines as Functional Dyes*, ICP, Tokyo, Japan, 2004.

[4] I. Okura, *Photosensitization of Porphyrins and Phthalocyanines*, Kodansya, Tokyo, Japan, 2000.

[5] G. Jory, "Photosensitised processes in vivo: Proposed phototherapeutic applications," *Photochemistry and Photobiology*, vol. 52, pp. 439–443, 1990.

[6] J. Moan, "Properties for optimal PDT sensitizers," *Journal of Photochemistry and Photobiology. B, Biology*, vol. 5, no. 3-4, pp. 521–524, 1990.

[7] M. J. Cook, I. Chambrier, S. J. Cracknell, D. A. Mayes, and D. A. Russell, "Octa-alkyl zinc phthalocyanines: potential photosensitizers for use in the photodynamic therapy of cancer," *Photochemistry and Photobiology*, vol. 62, no. 3, pp. 542–545, 1995.

[8] K. Tabata, K. Fukushima, K. Oda, and I. Okura, "Selective aggregation of zinc phthalocyanines in the skin," *Journal of Porphyrins and Phthalocyanines*, vol. 4, no. 3, pp. 278–284, 2000.

[9] K. Sakamoto, T. Kato, and M. J. Cook, "Position isomer separation of non-peripheral substituted zinc dibenzo-di(3,4-pyrido)porphyrazines," *Journal of Porphyrins and Phthalocyanines*, vol. 5, no. 10, pp. 742–750, 2001.

[10] K. Sakamoto, T. Kato, T. Kawaguchi, et al., "Photosensitizer efficacy of non-peripheral substituted alkylbenzopyridoporphyrazines for photodynamic therapy of cancer," *Journal of Photochemistry and Photobiology A: Chemistry*, vol. 153, no. 1–3, pp. 245–253, 2002.

[11] K. Sakamoto, E. Ohno-Okumura, T. Kato, T. Kawaguchi, and M. J. Cook, "Laser-flash photolysis of dialkylbenzodipyridoporphyrazines," *Journal of Porphyrins and Phthalocyanines*, vol. 7, no. 2, pp. 83–88, 2003.

[12] K. Sakamoto, T. Kato, E. Ohno-Okumura, M. Watanabe, and M. J. Cook, "Synthesis of novel cationic amphiphilic phthalocyanine derivatives for next generation photosensitizer using photodynamic therapy of cancer," *Dyes and Pigments*, vol. 64, no. 1, pp. 63–71, 2005.

[13] I. Seotsanya-mokhosi, N. Kuznetsova, and J. T. Nyokong, "Photochemical studies of tetra-2,3-pyridinoporphyrazines," *Journal of Photochemistry and Photobiology A: Chemistry*, vol. 140, no. 3, pp. 215–222, 2001.

[14] M. Yokote, F. Shibamiya, and S. Shoji, "On the copper phthalocyanine-N-isolog (copper tetra-3,4-pyridoporphyrazine) obtained from Cinchomeronic acid," *Kogyo Kagaku Zasshi*, vol. 67, pp. 166–176, 1964.

[15] K. Sakamoto and F. Shibamiya, "Reaction of copper diberzodipyridoporphyrazine with diethylsulfate," *Journal of the Japan Society of Colour Material*, vol. 59, pp. 517–524, 1986.

[16] K. Kadish, G. Moninot, Y. Hu, et al., "Double-decker actinide porphyrins and phthalocyanines. Synthesis and spectroscopic characterization of neutral, oxidized, and reduced homo- and heteroleptic complexes," *Journal of American Chemical Society*, vol. 115, pp. 8153–8166, 1993.

Hindawi Publishing Corporation
Metal-Based Drugs
Volume 2008, Article ID 498916, 9 pages
doi:10.1155/2008/498916

Research Article

Synthesis and Photophysical Properties of Tetra- and Octasubstituted Phosphorous Oxide Triazatetrabenzcorrole Photosensitizers

Edith M. Antunes and Tebello Nyokong

Department of Chemistry, Rhodes University, Grahamstown 6140, South Africa

Correspondence should be addressed to Tebello Nyokong, t.nyokong@ru.ac.za

Received 27 August 2007; Accepted 10 December 2007

Recommended by Michael J. Cook

The synthesis of phosphorous oxide triazatetrabenzcorroles (TBC) tetra- (**9**, **11**) or octa- (**13**) substituted on the ring with halogenated functional groups is reported. The complexes are not aggregated in dimethylsulfoxide (DMSO) and show solubility in solvents such as pyridine. The *Q* band absorption spectra of the complexes are red-shifted compared to unsubstituted PTBC. The latter complex shows a large triplet lifetime (1.7 milliseconds), higher than for MPc derivatives. The chlorinated derivatives show good triplet yields ($\Phi_T \sim$ 0.46 and 0.36) and relatively long lifetimes (256 and 452 microseconds), respectively, for **11** and **13**.

1. INTRODUCTION

The immense and diverse potential of phthalocyanines (Pc) in a variety of technical (chemical sensors [1], liquid crystals [2], electrocatalysis [3], and nonlinear optics [4]) and medicinal (primarily photodynamic therapy [5–8]) applications has generated a great deal of interest in these macrocyclic compounds. This, together with the extraordinary stability of these complexes, has resulted in considerable research being carried out on the phthalocyanine complex upon incorporation of nearly all metals in the periodic table into the Pc core. Complexes with metalloids and nonmetals of Groups IVA and VA are of particular interest due to the two different valence/oxidation states available to the central atom.

Triazatetrabenzcorroles (TBC) are phthalocyanine-like compounds which have lost one of the bridging nitrogen atoms [9]. The synthesis of Ge, Si, Ga, and Al TBC complexes have been reported [10, 11]. We have recently reported on a microwave synthesis of a sulfonated SnTBC [12]. Gouterman et al. were the first to report on the synthesis and unusual electronic spectra of the PcP^{III} compared to PcP^{V} [9, 13]. It became apparent that upon complexation with the trivalent phosphorous, a bridging nitrogen was lost to form the phosphorous oxide tetrabenzcorroles (PTBC). Since then, a number of octa- and tetrasubstituted PTBC derivatives have been synthesized [14–19]. Most complexes synthesized contained alkyl chain ring substituents. High fluorescence quantum yields [18] and singlet oxygen quantum yields [15] have been reported for the complexes. The water-soluble tetrasulphonated PTBC showed good photodynamic therapy towards HeLa cells [19]. For applications in PDT, high triplet lifetimes and yields are desired; however there are no reports on the triplet-state behavior of the PTBC complexes. In this work, we report on PTBC complexes tetra- or octasubstituted with chloride and bromide ring substituents (see Schemes 1 and 2), since the halogens are expected to enhance intersystem crossing, resulting in high triplet yields due to the heavy atom effect. A PTBC derivative containing a mixture of butoxy and chloro ring substituents has been reported [17], but no photophysical data has been reported for halogenated PTBCs.

2. EXPERIMENTAL PROCEDURES

Materials

Dimethylsulfoxide (DMSO), methanol (MeOH), phosphorous tribromide (PBr_3), deuterated chloroform ($CDCl_3$),

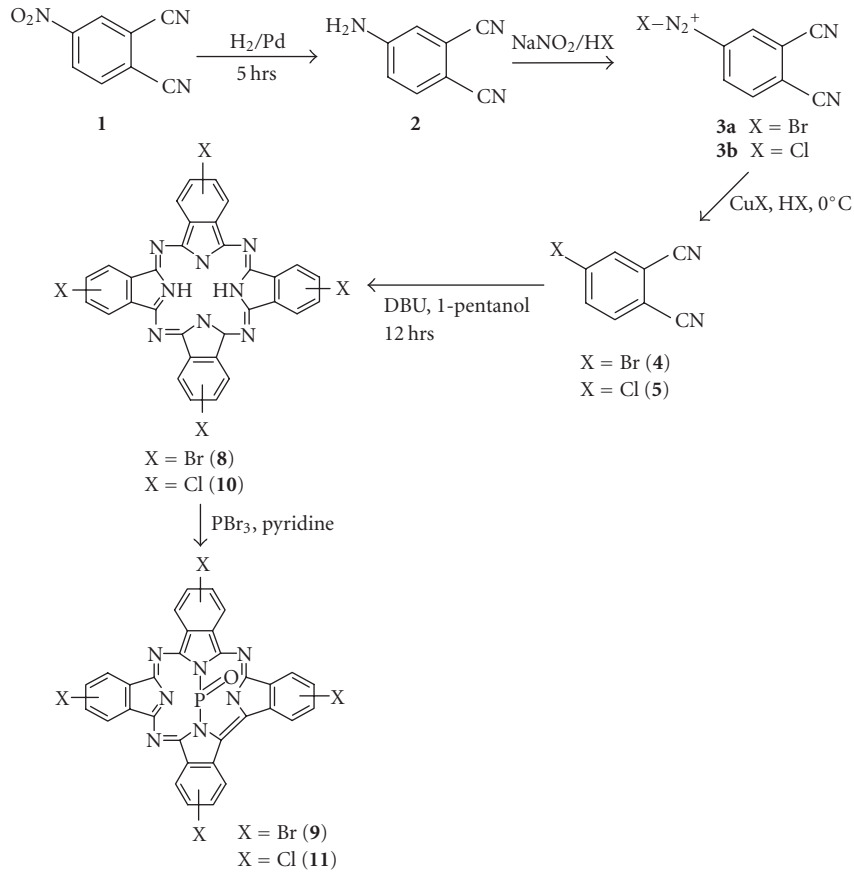

Scheme 1: Synthetic procedure for the tetrasubstituted PTBC complexes.

deuterated dimethylsulfoxide (DMSO-d_6), deuterated pyridine (Pyr-d_5), 4,5 dichlorophthalonitrile, 1,8-diazabicyclo undec-7-ene (DBU), 4-nitrophthalonitrile, copper (I) bromide, copper (I) chloride, hydrobromic acid, hydrochloric acid, palladium on carbon (Pd/C), and dicyanobenzene were purchased from Sigma-Aldrich (Miss, USA) and used as received. Pyridine and 1-pentanol were obtained from Sigma-Aldrich and dried prior to use. Column chromatography was performed on silica gel 60 (0.04–0.063 mm).

Equipment

Ground-state electronic absorption spectra were recorded on a Varian Cary 500 UV-Vis-NIR spectrophotometer. ^{1}H and ^{13}C NMR spectra were obtained using a Bruker AMX 400 MHz and a Bruker Avance II+ 600 MHz NMR spectrometer. Fluorescence emission and excitation spectra were recorded on a Varian Cary Eclipse spectrofluorimeter, while FT-IR spectra (KBr pellets) were recorded on a Perkin-Elmer spectrum 2000 FT-IR spectrometer. MS data was recorded on a Shimadzu KRATOS Maldi MS instrument.

Triplet absorption and decay kinetics were recorded on a laser flash photolysis system, the excitation pulses were produced by an Nd: YAG laser (Quanta-Ray, 1.5 J/90 ns) pumping a dye laser (Lambda Physic FL 3002, Pyridin 1 in methanol). The analyzing beam source was from a Thermo Oriel xenon arc lamp, and a photomultiplier tube was used as detector. Signals were recorded with a two-channel digital real-time oscilloscope (Tektronix TDS 360) where the kinetic curves were averaged over 256 laser pulses. Triplet lifetimes were determined by exponential fitting of the kinetic curves using OriginPro 7.5 software. Solutions for triplet yield and lifetime determinations were degassed with argon before use.

2.1. Syntheses and characterization

4,5-Dichlorophthalonitrile and dicyanobenzene were commercially obtained. Unsubstituted PTBC (**7**) was synthesized from unmetallated phthalocyanine (**6**) and PBr_3 in a 16.4% yield, and characterized as reported in the literature [9, 13, 19]. 4-Aminophthalonitrile (**2**) and 4-bromophthalonitrile (**4**) were synthesised following literature procedures [20, 21] with some minor modifications. 4-Chlorophthalonitrile (**5**) was synthesised by modifying the procedure used for compound **4**.

2.1.1. Preparation of 4-aminophthalonitrile (2)

4-Nitrophthalonitrile (**1**) (1.00 g, 5.78 mmol) was placed in a round bottom flask and 100 mL of ethanol added to obtain a suspension. The catalyst Pd/C (55 mg) was added to the flask,

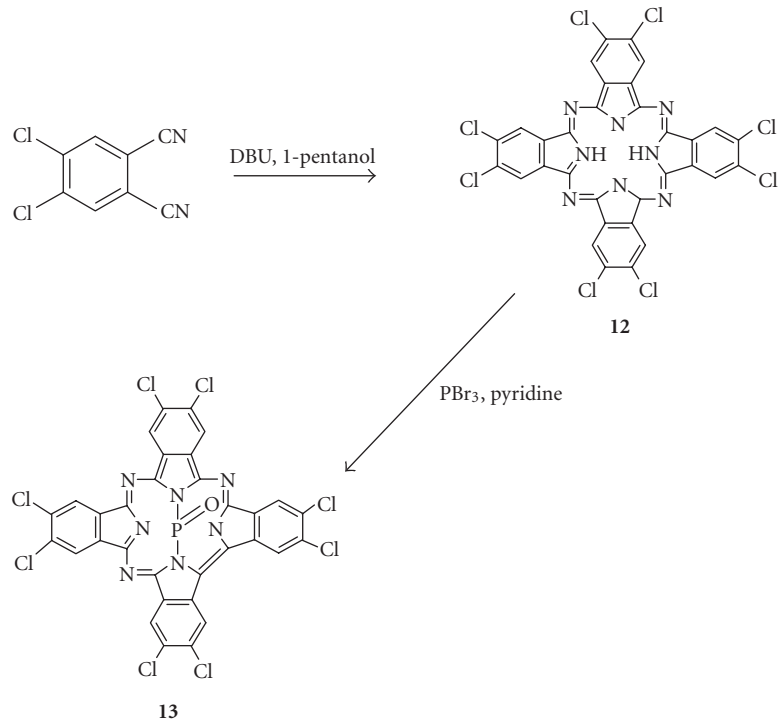

Scheme 2: Synthesis of the octachlorosubstituted PTBC (**13**).

the apparatus evacuated and then filled with hydrogen and the mixture vigorously stirred at room temperature until the absorption of hydrogen had completely stopped. The reaction mixture was subsequently filtered over celite and the solution evaporated in vacuo. Yield: 98%. ^{1}H NMR (400 MHz, DMSO-d_6) δ ppm 7.39 (dd, J = 8.66, 1.34 Hz, 1H), 6.93 (d, J = 2.19 Hz, 1H), 6.81 (dd, J = 8.67, 2.18 Hz, 1H), 6.36 (br s, 2H).

2.1.2. Preparation of 4-bromophthalonitrile (4)

Compound **2** (500 mg, 3.5 mmol) was taken up in a mixture of water (4 mL) and hydrobromic acid (4 mL, 48%) and the solution cooled to 0°C using an ice-salt bath. A solution of sodium nitrite (276 mg, 4 mmol) in water (2 mL) was then added dropwise to the acid mixture to form the diazonium salt **3a** as an intermediate. Copper (I) bromide (1.00 g, 6.97 mmol) was dissolved in HBr (4 mL, 48%) and cooled to 0°C. The cold diazonium salt solution was then added dropwise to the CuBr reagent and the solution stirred for 1 hr at 0°C. After an hour, the solution was left to stand at room temperature overnight. The aqueous solution was then extracted with ethyl acetate (3 × 15 mL), the combined organic extracts washed with brine, dried over magnesium sulphate and concentrated to give 248 mg of **4**. Yield: 34%. ^{1}H NMR (400 MHz, $CDCl_3$) δ ppm 7.96 (d, J = 1.78 Hz, 1H), 7.89 (dd, J = 8.37, 1.89 Hz, 1H), 7.68 (d, J = 8.37 Hz, 1H). ^{13}C NMR (75 MHz, $CDCl_3$) δ ppm 136.6 (d), 136.3 (d), 134.4 (d), 128.1 (s), 117.3 (s), 114.7 (s), 114.5 (s), 114.0 (s).

2.1.3. Preparation of 4-chlorophthalonitrile (5)

A similar procedure to the one above was used to prepare compound **5**. Compound **2** (500 mg, 3.5 mmol) was dissolved in a water (4 mL)/hydrochloric acid (5 mL, 32%) mixture, and the sodium nitrite (276 mg, 4 mmol) in water (2 mL) reagent was added to the amine hydrochloride solution to form the diazonium salt (**3b**). Copper (I) chloride (1.00 g, 10.1 mmol) was dissolved in HCl (5 mL) and cooled to 0°C. The diazonium salt was then added to the CuCl reagent and treated in the same manner as reported above. Compound **5** was thus produced in a 58% yield. ^{1}H NMR (400 MHz, $CDCl_3$) δ ppm 7.80 (d, J = 1.88 Hz, 1H), 7.75 (s, 1H), 7.73 (d, J = 1.87 Hz, 1H). ^{13}C NMR (75 MHz, $CDCl_3$) δ ppm 140.2 (s), 134.5 (d), 133.7 (d), 133.5 (d), 117.4 (s), 114.6 (s), 114.2 (s), 114.1 (s).

2.1.4. Preparation of tetrabromo phosphorous oxide triazatetrabenzcorrole (9, PTBrTBC)

Complex **9** was synthesized from the unmetallated derivative (**8**). The first step was the synthesis of **8**, following established methods [22] as follows: **4** (200 mg, 0.97 mmol) was reacted with DBU (0.36 mL) in 1-pentanol under reflux for 12 hours under a nitrogen atmosphere. The dark green mixture was cooled down to room temperature, then methanol (5 mL) and water (2 mL) were added and the mixture precipitated out and centrifuged. This green solid complex **8**, confirmed to be a phthalocyanine molecule by its UV spectrum, was not purified any further and was employed as is

for the synthesis of complex **9**. Complex **9** was synthesized by heating (under reflux) a mixture of complex **8** (100 mg, 0.12 mmol) and PBr_3 (0.34 mL, 3.60 mmol) in pyridine at 90 to 100°C for 2 hours. The reaction was then allowed to cool to room temperature and poured carefully into water and allowed to stand overnight. The green product obtained was then centrifuged and washed with copious amounts of water. Upon drying, the precipitate was chromatographed on a silica gel column using pyridine as the eluant. The complex was collected as a dark green band, while the unmetallated Pc remained at the top of the column. Yield: 13.5%. UV/Vis (DMSO), λ_{max}/nm ($\log \varepsilon$)]: 662 (4.86), 630 (4.56), 602 (4.29), 578 (3.79), 448 (5.19), 439 (4.94), 418 (4.70). [(KBr) ν_{max}/cm^{-1}]: 3063, 1717, 1608, 1506, 1451, 1396, 1326, 1298 (P=O), 1271, 1151, 1109, 1077, 1043, 967, 956, 832, 813, 758, 723, 691, 578. ^{1}H NMR (600 MHz, Pyr-d_5) δ ppm 10.15–9.92 (m, 4H), 9.83–9.57 (m, 4H), 8.59–8.41 (m, 4H). ^{31}P NMR (162 MHz, Pyr-d_5) δ ppm –198.6. MALDI *m/z*: Calc. 860.8, found 861.1 {Br_4(TBC)P(O)}.

2.1.5. Preparation of tetrachloro phosphorous oxide triazatetrabenzcorrole (11, PTClTBC)

Complex **11** was synthesized as explained above for **9**, except that complex **5** (200 mg, 1.23 mmol) was reacted with DBU (0.24 mL) in 1-pentanol instead of compound **4** to obtain the 4-chloro H_2Pc analogue (complex **10**). The presence of the metal-free Pc was again confirmed by its UV spectrum. Complex **10** was then employed for the synthesis of complex **11** (100 mg, 0.15 mmol) by reacting it with PBr_3 (0.42 mL, 4.50 mmol) in hot pyridine. Yield: 27.7%. UV/Vis (DMSO), λ_{max}/nm ($\log \varepsilon$)]: 661 (4.56), 630 (4.26), 603 (3.99), 447 (4.82), 438 (4.59), 417 (4.39). [(KBr) ν_{max}/cm^{-1}]: 2922, 1717, 1609, 1505, 1456, 1399, 1328, 1297 (P=O), 1143, 1068, 973, 910, 814, 769, 724, 690, 580. ^{1}H NMR (600 MHz, *Pyr-d_5*) δ ppm 9.97–9.66 (m, 8H), 8.45–8.26 (m, 4H). ^{31}P NMR (162 MHz, Pyr-d_5) δ ppm –198.5. MALDI *m/z*: Calc. 682.9, found 682.0 {Cl_4(TBC)P(O)}.

2.1.6. Preparation of octachloro phosphorous oxide triazatetrabenzcorrole (13, POClPBC)

The first step was the synthesis of metal-free complex **12**, using the same procedure as outlined above for the synthesis of **8**, except that 4,5-dichlorophthalonitrile (300 mg 1.53 mmol) was reacted with DBU (0.12 mL) instead of complex **4**. Confirmation of the formation of the H_2Pc (**12**) was provided by the UV spectrum. Complex **13** was then synthesized as described for complexes **9** and **11** using **12** (100 mg, 0.128 mmol) and PBr_3 (0.36 mL, 3.84 mmol). A paucity of proton signals was expected and observed in the ^{1}H NMR spectrum of this octasubstituted complex. Yield: 8.6%. UV/Vis (DMSO), λ_{max}/nm ($\log \varepsilon$)]: 667 (3.47), 635 (3.19), 606 (2.94), 452 (3.83), 442 (3.61), 422 (3.46), 411 (3.42). [(KBr) ν_{max}/cm^{-1}]: 2927, 1726, 1586, 1521, 1349, 1298 (P=O), 1248, 1197, 1138, 948, 908, 837, 743, 602. ^{1}H NMR (600 MHz, Pyr-d_5) δ ppm 8.07 (m, 8H). ^{31}P NMR (162 MHz, Pyr-d_5) δ ppm −197.4. MALDI *m/z*: not observed.

2.2. Photophysical and photochemical parameters

2.2.1. Fluorescence quantum yields and lifetimes

The comparative method was used to determine the fluorescence quantum yields (Φ_F) according to the following equation [23], utilizing unsubstituted ZnPc in DMSO as the standard ($\Phi_F = 0.18$) [24]:

$$\Phi_F = \Phi_{F(\mathrm{Std})} \frac{F \cdot A_{\mathrm{Std}} \cdot \eta^2}{F_{\mathrm{Std}} \cdot A \cdot \eta_{\mathrm{Std}}^2}, \quad (1)$$

where F and F_{Std} are the areas under the fluorescence curve of the sample and the standard, respectively. Similarly, A and A_{Std} are the absorbance of the compound and the standard at the excitation wavelength, η and η_{Std} are the refractive indices of solvents used for the sample and the standard, respectively.

Natural or radiative lifetimes (τ_N) were estimated using PhotochemCAD program which uses the Strickler-Berg equation [25]. The fluorescence lifetimes (τ_F) were evaluated using the following equation:

$$\Phi_F = \frac{\tau_F}{\tau_N}. \quad (2)$$

The rate constants for intersystem crossing from the excited singlet state to the triplet state ($k_{ISC(S-T)}$) were estimated using the following equation [26]:

$$k_{ISC(S-T)} = (1/\tau_f) - (1/\tau_{f^0}), \quad (3)$$

where τ_f and τ_f^0 are the excited singlet-state lifetimes for the halogenated derivatives and unsubstituted PTBC, respectively. Similarly, the rate constants for intersystem crossing from the triplet state to the ground state ($k_{ISC(T-S)}$) were estimated using the following equation:

$$k_{ISC(T-S)} = (1/\tau_T) - (1/\tau_{T^0}), \quad (4)$$

where τ_T and τ_{T^0} are the excited triplet-state lifetime for the halogenated derivatives and unsubstituted PTBC, respectively.

2.2.2. Triplet quantum yields and lifetimes

Solutions of the PTBC complexes were bubbled with argon in a 1 cm pathlength spectrophotometric cell, irradiated at the *Q* band of the respective PTBC complexes, with the triplet quantum yields (Φ_T) determined by the triplet absorption method. The comparative method [27] was applied as in the following equation, using ZnPc in DMSO as the standard:

$$\Phi_T = \Phi_T^{\mathrm{std}} \cdot \frac{\Delta A_T \cdot \varepsilon_T^{\mathrm{Std}}}{\Delta A_T^{\mathrm{Std}} \cdot \varepsilon_T}. \quad (5)$$

Changes in the triplet-state absorbances of the PTBC derivative and the standard are represented by ΔA_T and $\Delta A_T^{\mathrm{Std}}$, respectively; while ε_T and $\varepsilon_T^{\mathrm{std}}$ are the triplet-state molar extinction coefficients for the PTBC derivative and the standard, respectively; while Φ_T^{std} is the triplet quantum yield for the standard ($\Phi_T = 0.65$ for ZnPc in DMSO) [28]. Triplet

lifetimes (τ_T) were determined by exponential fitting of the kinetic curves using OriginPro 7.5 software.

Quantum yields of internal conversion (Φ_{IC}) were obtained from the following equation, which assumes that only three processes (fluorescence, intersystem crossing, and internal conversion) jointly deactivate the excited singlet state of PTBC derivatives:

$$\Phi_{IC} = 1 - (\Phi_F + \Phi_T). \quad (6)$$

3. RESULTS AND DISCUSSION

3.1. Synthesis and characterization

Substituted phthalocyanines are generally prepared by cyclotetramerization of substituted phthalonitriles. 2(3), 9(10), 16(17), 23(24)-Tetrasubstituted phthalocyanines can be synthesized from 4-substituted phthalonitriles [22], while octasubstituted phthalocyanines can be synthesized from 4,5-dichlorophthalonitrile [29]. In the case of tetrasubstituted derivatives, a mixture of four possible structural isomers are obtained, which can be designated by their molecular symmetry as C_{4h}, C_{2v}, C_s, and D_{2h}. In this study, synthesized tetrasubstituted phthalocyanine compounds are obtained as isomer mixtures as expected. No attempt was made to separate the isomers of **9** and **11.**

A variety of halogenated phosphorous oxide triazatetrabenzcorroles (complexes **9**, **11,** and **13**) were prepared by treatment of unmetallated phthalocyanines with PBr_3 in pyridine according to literature procedures [19]. The products thus obtained were then subjected to silica gel column chromatography using pyridine as an eluant.

Generally, phthalocyanine complexes are insoluble in most organic solvents; however introduction of substituents to the ring increases the solubility. The halogenated complexes (particularly **9** and **11**) exhibited excellent solubility in organic solvents such as pyridine and DMSO. For comparative purposes, the unsubstituted PTBC was synthesized and found to be soluble in DMSO, but only sparingly in pyridine.

The new compounds were characterized by UV-vis, IR, mass, and NMR spectroscopies (including ^{31}P NMR) and the analyses were consistent with the predicted structures as shown in Section 2. However, mass spectral data proved to be difficult to obtain for complex **13**. The P=O vibrations were observed at ~1295 cm^{-1} (in accordance with [14]) in the IR spectra, confirming the presence of *O* coordinated to the phosphorous atom. This was corroborated by the ^{31}P NMR shifts obtained, that is, ~−198 ppm, which is typical of a P=O bond [14]. ^{1}H NMR investigations of **9** and **11** gave the characteristic chemical shifts, with three proton signals integrating for a total of 12 for each complex. For complex **13**, a multiplet due to the nonperipheral protons, was observed in the ^{1}H NMR spectrum.

TBC complexes have distinct UV-Vis spectra with a sharp peak at ~450 nm [16–19], which can be employed in their characterization. The formation of the TBC complexes occurs when the MPc molecules no longer retains a Pc moiety as they no longer have the fourth azomethine nitrogen (see Schemes 1 and 2). It is believed [11] that in the presence of excess metal halide, the bridge nitrogen of the Pc is eliminated, forming TBC. In this study, the unmetallated Pc derivatives (**8, 10** and **12**) were formed first, which, upon reaction with PBr_3, resulted in the formation of PTBC derivatives. This was judged spectroscopically by the collapse of the sharp *Q* band in the visible region of unmetallated Pcs to three bands (in the *Q* band region), together with the formation of the sharp Soret band at 440 nm (see Figure 1). The spectra of unmetallated Pcs **6**, **8**, **10,** and **12** in DMSO and pyridine showed a single *Q* band (see Figure 1) which is uncharacteristic of unmetallated Pcs. Typically, unmetallated Pcs show a split *Q* band due to lack of symmetry. Solvation in polar aprotic solvents (such as DMSO and pyridine) occurs through their unshared electrons. Thus, in DMSO (see Figure 1) and pyridine, the spectra of **8**, **10**, and **12** did not show the normal splitting of the *Q* band that is typical of free-base phthalocyanines, showing instead a single sharp *Q* band. The same applies to H_2Pc in pyridine. The nonsplit *Q* band is a result of the basicity of the solvents. It has been documented that in strongly basic solvents, the inner pyrrole hydrogens are acidic enough to dissociate resulting in a charged system (Pc^{-2}) which becomes symmetric and thus possesses an unsplit *Q* band [30].

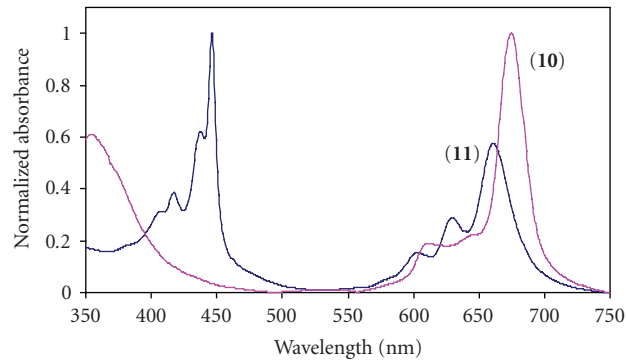

Figure 1: Spectrum of metal-free Pc (**10**) and transformation upon formation of PTClTBC (**11**) in DMSO. Concentration = 3.59 × 10^{-5} mol dm^{-3}.

Figure 2 compares the spectra of the complexes synthesized in this work, while Table 1 lists the *Q* and *B* band maxima. It is clear in Table 1 and Figure 2 that the presence of bromines and chlorines shifts the spectra to the red region. The red shift of spectra on halogenation has been observed before [26] for ZnPc derivatives.

Aggregation in phthalocyanines and related complexes is usually depicted as a coplanar association of rings progressing from monomer to dimer and higher-order complexes. It is dependent upon the concentration of the complex, the nature of the solvent, as well as the nature of the substituents and the complexed metal ions. In this study, the aggregation behavior of the TBC complexes (**7**, **9**, **11**, and **13**) was investigated in DMSO (see Figure 3). The complexes did not show aggregation at concentrations less than 8×10^{-5} mol dm^{-3}. A linear plot of absorbance versus concentration was obtained in this concentration range.

The shapes of the excitation spectra for the TBC complexes were similar to the absorption spectra (see Figure 4).

Table 1: UV-Vis and fluorescence spectral data for the PTBC derivatives.

Compound	$\lambda_{Q\,band}$ (abs)	$\varepsilon(mol^{-1}\cdot L\cdot cm^{-1})$	$\lambda_{Q\,band}$ (abs)	$\lambda_{Q\,band}$ (Em)	$\lambda_{Q\,band}$ (Exc)	Stokes shift (nm)
PTBC (**7**)	655	1.50×10^4	442	660	655	5
PTBrTBC (**9**)	662	7.28×10^4	448	670	661	8
PTClTBC (**11**)	662	4.56×10^4	447	668	659	6
POClTBC (**13**)	667	2.93×10^3	452	675	668	8
ZnPc	672	2.38×10^5 [29]	352	681	672	9

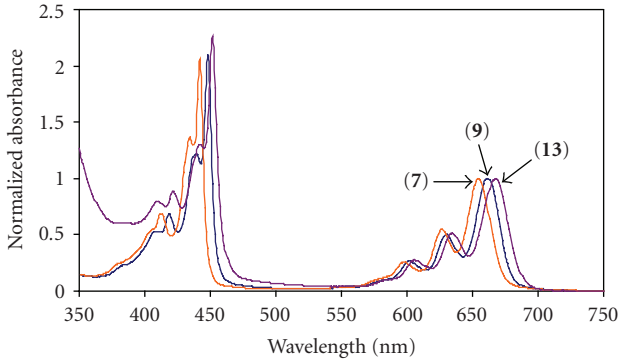

Figure 2: Comparison of the electronic spectra of various PTBC complexes synthesized in DMSO. Concentrations = 8.06×10^{-5} mol dm^{-3}(**7**), 1.95×10^{-5} mol dm^{-3}(**9**), 9.27×10^{-5} mol dm^{-3}(**13**).

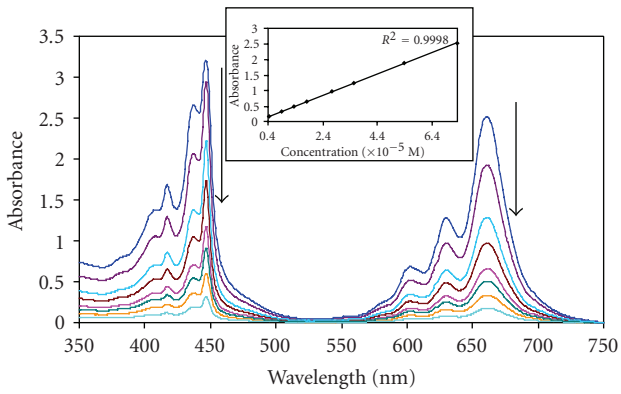

Figure 3: Absorption spectra of (**11**) in DMSO at different decreasing concentrations. Concentrations from 8×10^{-5} to 5×10^{-6} M. Inset: plot of absorbance versus concentration.

However, these spectra were not mirror images of the fluorescence spectra for the PTBC derivatives, in that the emission spectra showed only a single band, while the *Q* band of the absorption spectra has a split *Q* band. The observation of a single-emission band in the *Q* band region is typical of unsymmetric phthalocyanine complexes such as unmetallated derivatives [31–33]. Metal-free Pcs are known to fluoresce with only one main peak in non-aqueous media which has been assigned as the 0–0 transition of the fluorescence [31].

The emission spectra were slightly red-shifted with Stokes shifts ranging from 5 to 9 nm, suggesting no change in nuclear configurations following excitation. The largest shifts were observed for the POClTBC (**13**) and PTBrTBC (**9**),

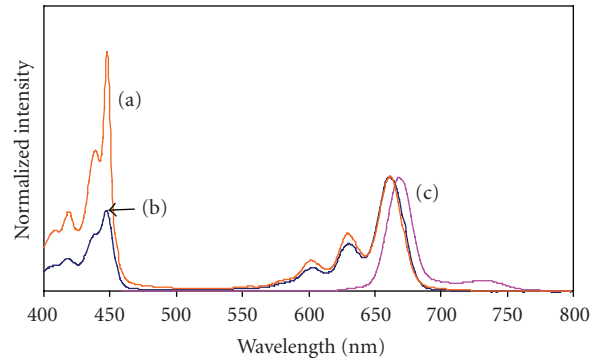

Figure 4: Comparison of the absorbance (a), excitation (b), and emission (c) spectra of complex **9**. Excitation wavelength = 380 nm.

while the smallest shift was observed for the PTBC derivative (**7**).

3.2. Photophysical and photochemical studies

The fluorescence quantum yields (Φ_F) of the PTBC derivatives are given in Table 2. These values are much lower than reported for MPc complexes, except for the unsubstituted PTBC complex, which gives Φ_F values in the range for MPc complexes [34]. The low values obtained for the halogenated derivatives are most likely due to the heavy atom effect of the halide functional group, which encourages intersystem crossing to the triplet state. Halogenation of ZnPc [26] has been reported to give a remarkable decrease in fluorescence quantum yields and lifetimes, since incorporation of a halogen into the photosensitizer increases the level spin-orbit coupling.

Fluorescence lifetimes (τ_F, Table 3) were calculated using the Strickler-Berg equation. Using this equation, a good correlation has been [35] found between experimentally and theoretically determined lifetimes for the unaggregated molecules as found in this work. Thus, we believe that the values obtained using this equation are a good measure of fluorescence lifetimes. Halogenation is expected to decrease fluorescence quantum yields and lifetimes, increase triplet-state formation, and shorten triplet lifetime. Thus, as expected, the τ_F values of the halogenated derivatives were lower than for unsubstituted PTBC and lower than generally observed for MPc complexes [35]. Octasubstitution with chlorines increased the τ_F values compared to tetrasubstituted derivatives when comparing complexes **11** and **13**. It is also interesting to note that a decrease in fluorescence

Table 2: Photophysical and photochemical parameters of the PTBC derivatives in DMSO. References given in square brackets.

Compound[a]	$\tau_T(\mu s)$	Φ_T	τ_F(ns)	Φ_F	Φ_{IC}
PTBC (**7**)	1740	0.27	2.6	0.12	0.61
PTBrTBC (**9**)	657	0.05	0.3	0.03	0.92
PTClTBC (**11**)	452	0.36	0.9	0.07	0.57
POClTBC (**13**)	236	0.46	1.1	0.06	0.48

[a]ZnPc standard: $\tau_T = 353(\mu s)$; $\Phi_T = 0.65$ [28]; $\Phi_F = 0.18$ [24].

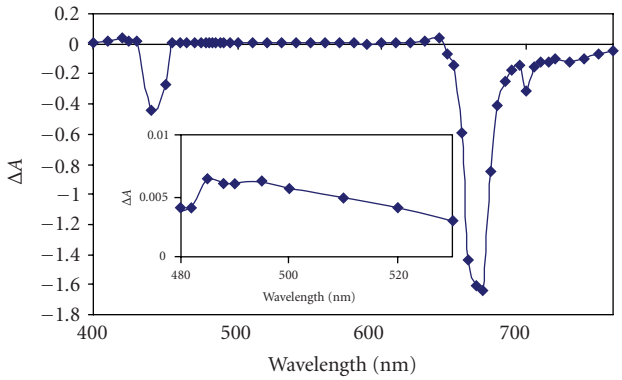

Figure 5: Transient differential spectrum of complex unsubstituted PTBC (**7**) in DMSO. Excitation wavelength = 655 nm. The inset shows the weak transient absorption of the triplet state.

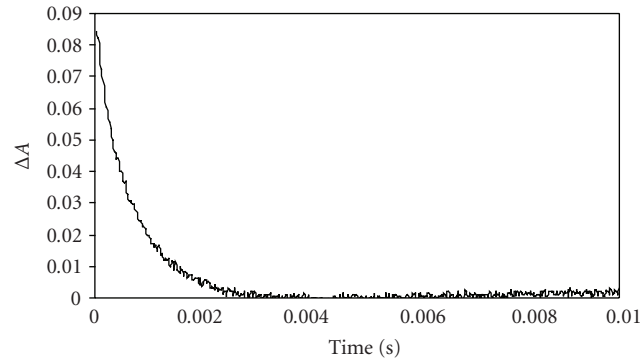

Figure 6: Triplet decay curve of unsubstituted PTBC (**7**) in DMSO at 490 nm. Excitation wavelength = 655 nm.

lifetime was observed upon contraction of the ring in tin tetrasulphonated α,β,γ-tetrabenzcorroles compared to tin tetrasulphonated phthalocyanines [12].

The acquisition of τ_F values allowed us to determine the rate constants for various processes. The rate constant for fluorescence (k_F), Table 3, was highest for complex **9**, which also had the lowest triplet quantum yield as will be discussed below. Likewise, the rate constants for intersystem crossing from the singlet state to the triplet state ($k_{ISC\ (S-T)}$) was the highest for complex **9**, Table 3.

The transient absorption spectra were recorded in argon-degassed solutions by exciting the photosensitizer (in DMSO) in the *Q* band region and recording the transient absorption spectra point by point from 400 to 750 nm (see Figure 5). A representative decay profile is shown in Figure 6. The *Q* and the Soret bands showed a negative absorption (bleaching) and the transient spectra showed a broad positive absorption ~500 nm (see Figure 5).

The triplet lifetimes for the PTBC derivatives, ranging from 256 to 1740 microseconds, are listed in Table 2. The latter value was observed for the unsubstituted PTBC (Table 2) and it is an unusually high triplet lifetime. Such high values are rare for MPc complexes [34]. Values in the millisecond range have been reported for AlPc derivatives, however they are still not as high as the value observed here for unsubstituted PTBC. The presence of the halogens was expected to lower the triplet lifetimes (when compared to unhalogenated PTBC (**7**)), as observed in Table 2; with the octasubstituted complex, **13**, giving the lowest triplet lifetime. Contrary to the heavy atom effect, which results in the decrease in triplet lifetimes with an increase in the size of the halogen [26], this work shows an increase in lifetime on going from the chlorinated (**11**) to brominated (**9**) PTBC derivatives, with the octachlorinated (**13**) complex showing the lowest triplet lifetime. The latter (**13**) could have a lower triplet lifetime than the tetrachlorinated derivative (**11**) due to the plurality of chlorine atoms and the heavy atom effect.

We have recently [12] shown that upon contraction of the ring in tin tetrasulphonated α,β,γ-tetrabenzcorrole compared to tin tetrasulphonated phthalocyanine, there was a decrease in Φ_T values and the triplet lifetimes. However, the lifetimes reported here for PTBC derivatives are high compared to MPc complexes in general.

In general, there is an increase in Φ_T values upon halogenation with a striking exception of the brominated complex (**9**). The octachlorinated derivatives (**13**) gave the highest triplet quantum yield (Φ_T), while surprisingly the bromo substituted complex **9** gave the lowest value. The Φ_T value for **9** is almost ten-fold lower than for **11**. Again, the larger value of Φ_T for **13** could be due to the plurality of chlorines and the heavy atom effect. The low Φ_T value for the brominated derivative compared to the chlorinated one contradicts the heavy atom effect. The increased Φ_T value for the chlorinated derivatives **11** and **13** compared to **9** will result in shorter triplet lifetime for the former, and this is the case in Table 2.

Quantum yields of internal conversion (Φ_{IC}) were calculated using (6) and are high due to low Φ_T values. Using the triplet lifetimes, the rate constants for intersystem crossing from the triplet state to the ground state ($k_{ISC\ (T-S)}$) were determined and are shown in Table 3. The lowest ($k_{ISC\ (T-S)}$)

Table 3: Rate contacts for the photophysical processes occurring in PTBC derivatives in DMSO.

Compound	$^1k_F(s^{-1})$ ($\times 10^7$)	($k_{ISC\ (S-T)}$)($\times 10^9$)	($k_{ISC\ (S-T)}$)(s^{-1})	$^2K_{IC}(s^{-1})$ ($\times 10^8$)
PTBC (**7**)	2.9	—	—	2.3
PTBrTBC (**9**)	10	32	9.5×10^2	31
PTClTBC (**11**)	7.8	9.2	1.6×10^3	6.3
POClTBC(**13**)	5.5	6.7	3.6×10^3	4.4

^1k_F is the rate constant for fluorescence. Values calculated using $k_F = \Phi_F/\tau_F$.
$^2k_{IC}$ is the rate constant for internal conversion. Values calculated using $k_{IC} = \Phi_{IC}/\tau_F$.

value obtained is for complex **9** (Table 3) yet this complex has the lowest triplet quantum yield.

4. CONCLUSIONS

In conclusion, we have synthesized halogenated PTBC derivatives (complexes **9**, **11**, and **13**) and compared their photophysical data with that of the unsubstituted PTBC complex. The latter complex shows a very high triplet lifetime value, higher than that for MPc complexes. However, this complex also has a correspondent low Φ_T value. Complexes **11** and **13** show reasonably high triplet lifetimes and yields, making them possible candidates for PDT. Complex **9** having bromine substituents showed a behavior different from the other halogenated complexes (**11** and **13**) in that it gave a very low triplet quantum yield.

ACKNOWLEDGMENTS

This work is supported by the National Research Foundation of South Africa as well as Rhodes University. Edith M. Autuness wishes to acknowledge Rhodes University and the MRC for funding in the form of a postdoctoral scholarship. The authors thank Hemant Gopee of the University of East Anglia for running the MALDI mass spectra.

Hemant Gopee of the University of East Anglia for running the MALDI mass spectra.

REFERENCES

[1] N. B. McKeown, *Phthalocyanine Materials: Synthesis, Structure and Function*, Cambridge University Press, Cambridge, UK, 1998.

[2] G. Guillaud, J. Simon, and J. P. Germain, "Metallophthalocyanines gas sensors, resistors and field effect transistors," *Coordination Chemistry Reviews*, vol. 178–180, part 2, no. Part 2, pp. 1433–1484, 1998.

[3] T. Nyokong, "Electrodes modified with monomeric M-N4 catalysts for the detection of environmentally important molecules," in *N4-Macrocyclic Metal Complexes: Electrocatalysis, Electrophotochemistry, and Biomimetic Electrocatalysis*, J. H. Zagal, F. Bedioui, and J.-P. Dodelet, Eds., chapter 7, Springer, New York, NY, USA, 2006.

[4] G. de la Torre, T. Tomás, and F. Agulló-López, "The phthalocyanine approach to second harmonic generation," *Advanced Materials*, vol. 9, no. 3, pp. 265–269, 1997.

[5] S. G. Bown, C. J. Tralau, P. D. Coleridge-Smith, D. Akdemir, and T. J. Wieman, "Photodynamic therapy with porphyrin and phthalocyanine sensitisation: quantitative studies in normal rat liver," *British Journal of Cancer*, vol. 54, no. 1, pp. 43–52, 1986.

[6] R. Bonnett, *Chemical Aspects of Photodynamic Therapy*, Gordon and Breach, Amsterdam, The Netherlands, 2000.

[7] I. J. Macdonald and T. J. Dougherty, "Basic principles of photodynamic therapy," *Journal of Porphyrins and Phthalocyanines*, vol. 5, no. 2, pp. 105–129, 2001.

[8] J. D. Spikes, "New trends in photobiology Chlorins as photosensitizers in biology and medicine," *Journal of Photochemistry and Photobiology B*, vol. 6, no. 3, pp. 259–274, 1990.

[9] M. Gouterman, P. Sayer, E. Shankland, and J. P. Smith, "Porphyrins. 41. Phosphorus mesoporphyrin and phthalocyanine," *Inorganic Chemistry*, vol. 20, no. 1, pp. 87–92, 1981.

[10] M. Fujiki, H. Tabei, and K. Isa, "New tetrapyrrolic macrocycle: α,β,γ-triazatetrabenzcorrole," *Journal of the American Chemical Society*, vol. 108, no. 7, pp. 1532–1536, 1986.

[11] J. Li, L. R. Subramaniam, and M. Hanack, "Substituted α,β,γ-triazatetrabenzcorrole: an unusual reduction product of a phthalocyanine," *Chemical Communications*, no. 7, pp. 679–680, 1997.

[12] S. Khene, A. Ogunsipe, E. Antunes, and T. Nyokong, "Microwave synthesis and photophysics of new tetrasulfonated tin(II) macrocycles," *Journal of Porphyrins and Phthalocyanines*, vol. 11, no. 2, pp. 109–117, 2007.

[13] P. Sayer, M. Gouterman, and C. R. Connell, "Metalloid porphyrins and phthalocyanines," *Accounts of Chemical Research*, vol. 15, no. 3, pp. 73–79, 1982.

[14] J. Li, L. R. Subramanian, and M. Hanack, "Studies on phosphorus phthalocyanines and triazatetrabenzcorroles," *European Journal of Organic Chemistry*, vol. 1998, no. 12, pp. 2759–2767, 1998.

[15] J. Liu, Y. Zhao, F. Zhao, F. Zhang, X. Song, and F.-T. Chau, "Study on phosphorus (III) complex of tetrabenzotriazacorrole: a novel phthalocyanine-like photosensitizer," *Journal of Photochemistry and Photobiology A*, vol. 99, no. 2-3, pp. 115–119, 1996.

[16] K. Kasuga, L. Liu, M. Handa, et al., "Preparation and some properties of a phosphorus(V) complex of tetra-*tert*-butylphthalocyanine," *Inorganic Chemistry*, vol. 38, no. 18, pp. 4174–4176, 1999.

[17] J. P. Fox and D. P. Goldberg, "Octalkoxy-substituted phosphorus(V) triazatetrabenzcorroles via ring contraction of phthalocyanine precursors," *Inorganic Chemistry*, vol. 42, no. 25, pp. 8181–8191, 2003.

[18] J. Liu, F. Zhang, F. Zhao, Y. Tang, X. Song, and G. Yao, "Complexation of phosphorus (III) with a novel tetrapyrrolic phthalocyanine-like macrocyclic compound," *Journal of Photochemistry and Photobiology A*, vol. 91, no. 2, pp. 99–104, 1995.

[19] Z. Song, F. Zhang, X. Li, C. Shek-Kiu, F. Zhao, and Y. Tang, "Investigation of a novel triazatetrabenzcorrole photosensitizer," *Journal of Porphyrins and Phthalocyanines*, vol. 6, no. 7-8, pp. 484–488, 2002.

[20] D. R. Beukes, *Structural and Synthetic Investigations of South African Marine Natural Products.*, Ph.D. thesis, Rhodes University, South Africa, 2000.

[21] C. C. Leznoff, Z. Li, H. Isago, A. M. D'Ascanio, and D. Terekhov, "Syntheses of octaalkynylphthalocyanines from halophthalonitriles," *Journal of Porphyrins and Phthalocyanines*, vol. 3, no. 6-7, pp. 406–416, 1999.

[22] C. C. Leznoff, "Syntheses of metal-free substituted phthalocyanines," in *Phthalocyanines: Properties and Applications*, C. C. Leznoff and A. B. P. Lever, Eds., vol. 1, chapter 1, VCH, New York, NY, USA, 1989.

[23] S. Fery-Forgues and D. Lavabre, "Are fluorescence quantum yields so tricky to measure? A demonstration using familiar stationery products," *Journal of Chemical Education*, vol. 76, no. 9, pp. 1260–1264, 1999.

[24] A. Ogunsipe, J. Y. Chen, and T. Nyokong, "Photophysical and photochemical studies of zinc(II) phthalocyanine derivatives—effects of substituents and solvents," *New Journal of Chemistry*, vol. 28, no. 7, pp. 822–827, 2004.

[25] H. Du, R. A. Fuh, J. Li, A. Corkan, and J. S. Lindsey, "PhotochemCAD: a computer-aided design and research tool in photochemistry," *Photochemistry and Photobiology*, vol. 68, no. 2, pp. 141–142, 1998.

[26] X. F. Zhang and H.-J. Xu, "Influence of halogenation and aggregation on photosensitizing properties of zinc phthalocyanine (ZnPC)," *Journal of the Chemical Society, Faraday Transactions*, vol. 89, pp. 3347–3351, 1993.

[27] P. Kubát and J. Mosinger, "Photophysical properties of metal complexes of meso-tetrakis(4-sulphonatophenyl)porphyrin," *Journal of Photochemistry and Photobiology A*, vol. 96, no. 1–3, pp. 93–97, 1996.

[28] T. H. Tran-Thi, C. Desforge, C. Thies, and S. Gaspard, "Singlet-singlet and triplet-triplet intramolecular transfer processes in a covalently linked porphyrin-phthalocyanine heterodimer," *Journal of Physical Chemistry*, vol. 93, no. 4, pp. 1226–1233, 1989.

[29] D. Wöhrle, M. Eskes, K. Shigehara, and A. Yamada, "A simple synthesis of 4,5-disubstituted benzenes and octasubstituted phthalocyanines," *Synthesis*, pp. 194–196, 1993.

[30] M. J. Stillman and T. Nyokong, "Absorption and magnetic circular dichroism spectral properties of phthalocyanines. Part 1: complexes of the dianion Pc(-2)," in *Phthalocyanines: Properties and Applications*, C. C. Leznoff and A. B. P. Lever, Eds., vol. 1, chapter 3, VCH, New York, NY, USA, 1989.

[31] W. Freyer, S. Mueller, and K. Teuchner, "Photophysical properties of benzoannelated metal-free phthalocyanines," *Journal of Photochemistry and Photobiology A*, vol. 163, no. 1-2, pp. 231–240, 2004.

[32] S. I. Yang, J. Li, H. S. Cho, et al., "Synthesis and excited-state photodynamics of phenylethyne-linked porphyrin—phthalocyanine dyads," *Journal of Materials Chemistry*, vol. 10, no. 2, pp. 283–296, 2000.

[33] Y. Kaneko, Y. Nishimura, N. Takane, et al., "Violet emission observed from phthalocyanines," *Journal of Photochemistry and Photobiology A*, vol. 106, no. 1–3, pp. 177–183, 1997.

[34] T. Nyokong, "Effects of substituents on the photochemical and photophysical properties of main group metal phthalocyanines," *Coordination Chemistry Reviews*, vol. 251, no. 13-14, pp. 1707–1722, 2007.

[35] D. Maree, T. Nyokong, K. Suhling, and D. Phillips, "Effects of axial ligands on the photophysical properties of silicon octaphenoxyphthalocyanine," *Journal of Porphyrins and Phthalocyanines*, vol. 6, no. 6, pp. 373–376, 2002.

Hindawi Publishing Corporation
Metal-Based Drugs
Volume 2008, Article ID 469531, 19 pages
doi:10.1155/2008/469531

Research Article

Synthetic Polymers as Drug-Delivery Vehicles in Medicine

Eberhard W. Neuse

School of Chemistry, University of the Witwatersrand, Private Bag 3, WITS 2050, Johannesburg, South Africa

Correspondence should be addressed to Eberhard W. Neuse, eberhard.neuse@wits.ac.za

Received 13 August 2007; Accepted 18 October 2007

Recommended by Jannie C. Swarts

Cancerous diseases present a formidable health problem worldwide. While the chemotherapy of cancer, in conjunction with other treatment modalities, has reached a significant level of maturity, efficacious use of such agents is still restricted by numerous pharmacological deficiencies, such as poor water solubility, short serum circulation lifetimes, and low bioavailability resulting from lack of affinity to cancer tissue and inadequate mechanisms of cell entry. More critically still, most drugs suffer from toxic side effects and a risk of drug resistance. The class of platinum anticancer drugs, although outstandingly potent, is particularly notorious in that respect. Among the countless methods developed in recent years in an effort to overcome these deficiencies, the technology of polymer-drug conjugation stands out as a particularly advanced treatment modality. The strategy involves the bioreversible binding, conjugating, of a medicinal agent to a water-soluble macromolecular carrier. Following pharmacokinetic pathways distinctly different from those of the common, nonpolymeric drugs, the conjugate so obtained will act as a prodrug providing safe transport of the bioactive agent to and into the affected, that is, cancerous cell for its ultimate cell-killing activity. The present treatise will acquaint us with the pharmacological fundamentals of this drug delivery approach, applied here specifically to the metalorganic platinum-type drug systems and the organometallic ferrocene drug model. We will see just how this technology leads to conjugates distinctly superior in antiproliferative activity to cisplatin, a clinically used antitumor agent used here as a standard. Polymer-drug conjugation involving metal-based and other medicinal agents has unquestionably matured to a practical tool to the pharmaceutical scientist, and all indications point to an illustrious career for this nascent drug delivery approach in the fight against cancer and other human maladies.

1. INTRODUCTION

The delivery of medicinal agents to the human body for healing purposes is probably as old as mankind. While in the early days such agents, now generally known as *drugs*, were simply delivered from hand to mouth, perhaps also by rubbing into the skin, or placing on an open wound, we are using more numerous and doubtlessly more complicated modalities of delivery in modern times, simply prompted by the need to control and combat a hugely increased variety of identified infirmities. A new stage of chemotherapeutic development was attained, more than a quarter of a century ago, with the advent of the polymer-drug conjugation paradigm, which teaches the use of polymeric, *that is,* macromolecular compounds as pivotal helpers in drug delivery. Numerous delivery techniques, taking advantage of the functional assistance provided by a macromolecular partner, have since been successfully developed for various routes of administration, not only the time-proven oral route ("just swallow it!"), but more importantly the parenteral routes involving intravenous, intraperitoneal, or intramuscular methods. It is particularly these parenteral administration techniques that have led to the successful use of partaking polymers. We will learn more about those developments further down the road in this paper. Although metal-free drug systems will find due mentioning in this treatise, emphasis will be on metal-containing compounds in accordance with this journal's mission. Before we delve into this core topic, we are prudently advised to take a primer lesson on the pharmacokinetic pathways generally available to a drug—any drug—after its administration to the mammalian organism, especially the human body. Section 2 will guide us leisurely on this learning path.

2. WHAT WE SHOULD KNOW ABOUT DRUG ADMINISTRATION

2.1. The cancer problem

Malignancies and cardiac diseases together provide the main cause of death in the developed world. In the United States, one in every three persons currently alive is estimated to contract some form of cancer, and every fifth person will ultimately succumb to it. A similar pattern of mortality obtains in other Western nations, and an even gloomier prognosis is observed in many developing countries. In South Africa, for example, cancer is the second-most common cause of death in the white, colored, and Asian population, and the third-most common cause in the black population group. Despite major variations among the different racial groups and incomplete registries especially in the black group, statistical data leave no doubt that, on average, South African rates for certain malignancies such as cervical, oesophageal, and skin cancers rank among the highest worldwide. Cancers of the lung and prostate rate among the top six cancers with white and nonwhite males, breast and cervical cancers are among the top six with white and nonwhite females, and melanoma represents one of the top six cancers with white females. Other types of cancer, including the various forms of leukaemia, although of lower incidence, are nonetheless causative for serious concern. The problem will be aggravated in the coming years as increasing urbanization is expected to create environmental and dietary conditions conducive to further initiation and spread of cancers; it will be further compounded by the finding that cancerous afflictions occur in approximately one third of all male and female adult breadwinners in the age bracket of 15–54 years. A novel factor now coming into play is the rapid spread of AIDS; immunodepressed patients will be at special risk to develop early cancerous lesions, and virus-related cancers may well find particularly suitable targets among such patients.

Chemotherapy constitutes an important cancer treatment modality, alone or in conjunction with other treatment regimens. However, despite much progress in drug research, results on average have been highly discouraging. Let us pause for a moment and examine this unsatisfactory state-of-affairs more closely.

Presently used anticancer drugs suffer from a multitude of severe pharmacological deficiencies, all of which continue to contribute to the limitations of effectiveness generally experienced in current clinical practice. Typical pharmacological shortcomings include the following: (i) *lack of cell specificity*, with ensuing drug distribution into both normal and transformed cells, that is, in consequence, drug application will be excessively wasteful; (ii) *inadequate water solubility*, hampering swift, and efficacious drug distribution in the body's aqueous fluid system, with resulting enhanced exposure to macrophage activity; (iii) *decreased serum half-life* as a consequence of catabolism, protein binding by the reticuloendothelial system, or efficacious excretion mechanisms; (iv) monophasic *salt-like* or *charged structure*, inhibiting membrane penetration and cell entry through normal passive diffusion, and resulting from these deficiencies, only a small fraction of the medicinal agent will successfully enter intracellular space for interaction with nuclear DNA or proteinaceous constituents; (v) *excessive systemic toxicity*, which grossly diminishes therapeutic drug efficacy; and (vi) lack of long-term efficaciousness because of inherent or induced *drug resistance*. Both (v) and (vi) are clearly the most aggravating factors added to abovementioned deficiencies, they generally necessitate premature discontinuation of drug-specific therapy, and thus, tend to reactivate tumorous or metastatic growth. As an overall consequence of the cited drug deficiencies, periods of regression tend to be limited, relapses occur frequently, and complete cures of most types of cancer by chemotherapy alone are still the exception rather than the rule.

A rather discomforting outlook indeed! Why then bring up this gloomy topic? Will you, the thoroughly depressed reader, not be prompted to disembark speedily from the wrong ferry boat and run for greener pastures elsewhere? The answer: worldwide efforts in biomedical research are striving to overcome existing chemotherapeutic hurdles through the expediency of developing efficacious cancer-fighting tools, and it is precisely this global development drive in which macromolecular compounds are crucial participants and find their true and foremost destiny. In Section 2.2 we will explore the background to this unique role played by polymers and their outstanding capabilities as delivery vehicles in the chemotherapeutic treatment of cancerous diseases.

2.2. The polymer-drug conjugation concept

To begin with, using text book knowledge, we will examine a typical medicinal agent's pharmacokinetic fate as it unfolds upon the drug's administration by the common intravenous, intramuscular, or oral techniques. For these, Figure 1 depicts exemplifying curves, given in terms of the agent's serum concentration as a function of postadministration time. In typical fashion, the intravenous route (curve A) delivers highest initial concentrations, which decrease more or less asymptotically with time, ultimately to reach zero-concentration level. Intramuscular administration (curve B) needs time for the curve to ascend from zero to a maximum, after which it gradually descends to zero. The oral route (curve C), while likewise providing a concentration maximum (generally below that of curve B), requires time extension for that trend, if one considers the long and obstacle-cluttered gastrointestinal pathway the drug has to follow before entering the blood pool.

At this point, we learn that for any administered drug system there are two critical serum concentration limits, represented by the dashed lines in Figure 2: a lower limit below which the drug has ceased to produce any therapeutic effect, and an upper limit above which the drug exerts various forms of toxicity in the organism. For a drug employed via intravenous injection, which is the administration mode favored for polymer-drug conjugates, curve A allows for drug application devoid of toxic side effects, yet providing limited effectiveness time. In contrast, curve B, representing an increased initial dosis, yields a considerably extended effectiveness period; this, however, does happen at the cost of emerging

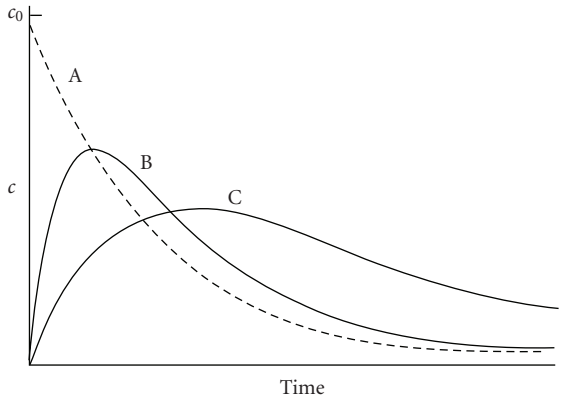

c = serum level (drug concentration in plasma)
A: Intravenous administration
B: Intramuscular administration
C: Oral administration

Figure 1: Drug serum concentration versus time for three administration routes.

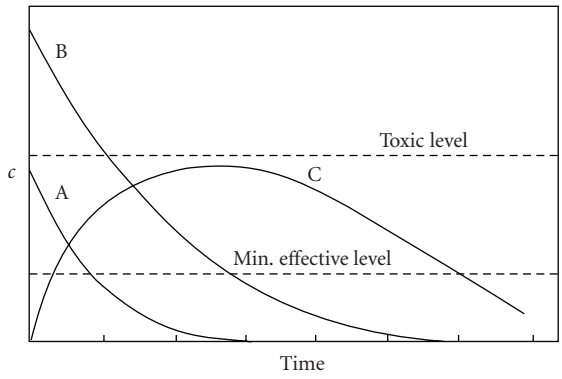

c = drug concentration in plasma
A,B: Conventional application
C: Slow-release application

Figure 2: Drug serum concentration versus time for two different doses.

toxicity. Hence, for a medicinal agent to remain therapeutically efficacious without toxic effects, its serum concentration must stay between the dotted lines over an optimally extended time span as schematically depicted by curve C.

An obvious approach toward achieving this goal of continuous, nontoxic bioactivity, although being tedious and cumbersome, would involve repetitive drug administration within carefully identified time intervals and with doses adjusted so as to maintain serum concentrations just below toxic levels. Better still, one might design a drug delivery construct that would, upon a single bolus administration, allow for a slow and gradual intraserum release of the agent from some sort of depot system. An optimally efficacious concentration trend for this model is schematically shown in Figure 3.

Needless to say, the pharmaceutical community, far from being asleep, has over the past two decades focused research

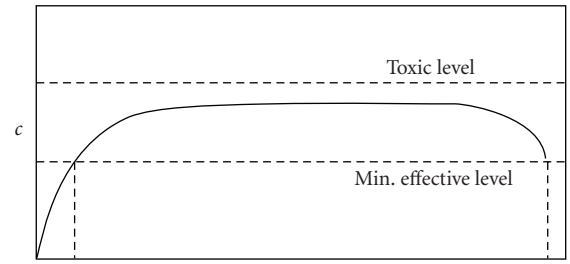

c = drug concentration in plasma

Segment between vertical dotted lines represents effectiveness time

Figure 3: Drug serum concentration versus time for slow-release modality.

activities on a massive scale preferentially on this kind of drug delivery system, generally with highly promising outcomes. Thus, microencapsulated drugs in the form of microspheres, nanospheres, and liposomes have been developed and successfully tested, and so have numerous implantable matrices capable of liberating embedded drugs into the body's fluid system and other body compartments through bioleaching, bioerosion, or simply through matrix biodegradation. These amply discussed drug delivery systems [1–3], all aiming at enhanced therapeutic effectiveness of medicinal agents and by-and-large quite efficacious in their own right, fall outside the definition of the narrow term of polymerdrug conjugation and, hence, outside the scope of the present text.

Deviating in its *modus operandi* from the aforementioned drug delivery constructs, the drug conjugation modality embodies a symbiotic union between two equally contributing partners: the polymer acts as a carrier and transport vehicle (it "knows" how to overcome biological hurdles and deliver the drug load safely at the designated terminal), whereas its "partner in healing", the drug proper, enjoys the safe ride and exerts its bioactivity in the target tissue. The notion of pairing up a bioactive agent with a transporter vehicle, born in the early 1970s, was forcefully advanced by Ringsdorf [4], who defined and refined this paradigm in palpable terms and set in motion broad-based development activities in numerous laboratories, on the strength of which the notion has by now matured to a highly sophisticated pharmaceutical tool. It utilizes the advantageous pharmacokinetic behavior of polymeric compounds in the mammalian body, paired with their enormous compositional versatility allowing for near-limitless structural modifications of these large molecules. In practical terms, the technique comprises the bioreversible binding (*conjugation*) of a bioactive agent, typically an antitumor drug, to a water-soluble macromolecular carrier molecule designed and synthesized in strict conformance with pharmaceutical guidelines. Specifically, the carrier polymer will be composed of the following: (i) subunits containing some molecular entity permitting facilitated cell entry; (ii) other subunits equipped with intra- or extrachain water-solubilizing groups; (iii) still other units featuring a homing device capable of directing the polymer-drug assembly,

the *conjugate*, selectively to the target tissue; and (iv), most importantly, units equipped with functional groups suitable for the critical conjugation step involving bioreversible drug binding to the polymer. The conjugate represents a prodrug, from which the active agent is hydrolytically or enzymatically released into the predestined biological environment, which, for anticancer action, are the cytoplasmic lysosomes and cell nuclei. A conjugate conforming in structure to those specifications will demonstrate therapeutic superiority on account of the following factors.

(i) Even if insoluble in water, the medium providing the circulating blood pool and other fluids, the intraveneously (IV) or intraperitoneally (IP) administered polymer-anchored drug, now perfectly water-soluble, will be swiftly carried into central circulation or the intraperitoneum. This will ensure efficient distribution of the bound drug in the fluid system, a requirement most vital for drug transport within the body.

(ii) While in transit in the central circulation system, the polymer-bound drug, notably if additionally modified by inclusion of oligo(ethylene oxide) units, will experience temporary protection from serum protein binding, enzymatic attack, and other scavenging processes. As a result, renal clearance (i.e., excretion through the kidneys' globular system) will be minimized, while serum life-time and drug bioavailability will be extended as part of a major change in biodistribution.

(iii) The dreaded toxic side effects invariably caused by the common, nonpolymeric medicinal agents will be minimized through carrier attachment, as now the "anchored" agent will be constrained in body and organ distribution while in transit.

(iv) The connecting groups incorporated into the polymer-drug linker for ultimate drug release can be uniquely designed so as to remain intact while the conjugate is on its way to target in the body's ever so slightly basic (ph$\sim$7.5) environment, yet to undergo biofission once the carrier-drug assembly has reached intracellular (specifically lysosomal) space. Such biofission may be mediated by the lysosomal proteolytic enzymes, or else may simply follow a hydrolytic pathway, taking advantage of the acidic (ph$\sim$5) intralysosomal environment. Reduced to monomeric size, the agent so liberated will now be able to undergo extravasation through penetration of the lysosomal membrane (a transport step not generally available to a macromolecular compound) and head for its ultimate destination, which for most anticancer drugs is the cell's nuclear DNA.

(v) The presence of a "homing" (i.e., actively targeting) group will lead to enhanced drug affinity for the transformed, that is,cancerous cell, thus facilitating guided drug transport. To exemplify this process, we wish to take a look at a cancer-targeting system featuring galactosamine as the homing device. This carbohydrate shows affinity for the asialoglycoprotein receptor in hepatocytes and thus, if attached to a cytotoxic agent, directs the latter efficiently to liver tissue, thereby providing cell-killing action against hepatomas, a form of liver malignancies. Other successfully used homing groups are represented by cationic moieties, tracking the conjugate preferentially to neoplastic tissue as a consequence of electrostatic attraction to the negative surface charge displayed by many cancer cells. Still other homing systems utilize the affinity of monoclonal antibodies for specific cancer-associated antigens. This research area, while still hampered by pharmacological problems of solid-state insolubility, immunogenicity, and in-transit vulnerability to side reactions and degradation, has proved eminently promising, and considerable progress has been achieved in recent years.

(vi) The polymer-drug conjugate will experience facilitated endocytotic cell entry, thus circumventing potential problems caused by drug polarity or ionicity in the normal process of membrane crossing by passive diffusion common to nonpolymeric solutes. The mechanism is pinocytotic in nature and thus not subject to the limitations imposed by the reticuloendothelial system on phagocytotically captured particulates. Ideally, adsorptive pinocytosis is utilized by the conjugate for increased efficiency of translocation, and cationic polymers are good examples of compounds so translocated. In cases where excessive P-glycoprotein-mediated drug efflux from endocytic space and consequent resistance problems have developed, the pinocytotic cell entry mechanism, through replenishment of the intracellular drug pool, assumes unique importance as a means of counteracting the dreaded phenomenon of drug resistance and restoring chemotherapeutic drug activity.

(vii) Polymer conjugates, in common with macromolecules in general, tend to accumulate in solid tumors because of enhanced intratumoral vascular permeability, allowing for substantial leakage of the polymeric molecules into the tumor tissue. Whereas, in normal tissues, macromolecules in interstitial space are efficiently recovered and eliminated by the lymphatic system, such lymphatic clearance is grossly retarded in tumorous tissue and so represents a weighty factor contributing to the tumoritropic characteristics of macromolecular compounds. This *enhanced permeability and retention* (EPR) effect associated with polymers provides passive targeting and renders polymer-drug conjugate administration more efficacious while reducing systemic toxicity in other organs.

(viii) Through the expediency of introducing biofissionable segments into the backbone, a polymer can be rendered biodegradable, thus effecting its gradual removal from the body in the form of fragments qualifying for excretion through the body's normal waste removal systems. This process is crucial because high molecular-mass carriers are not readily eliminated from the body and in the longer term may cause additional toxicity.

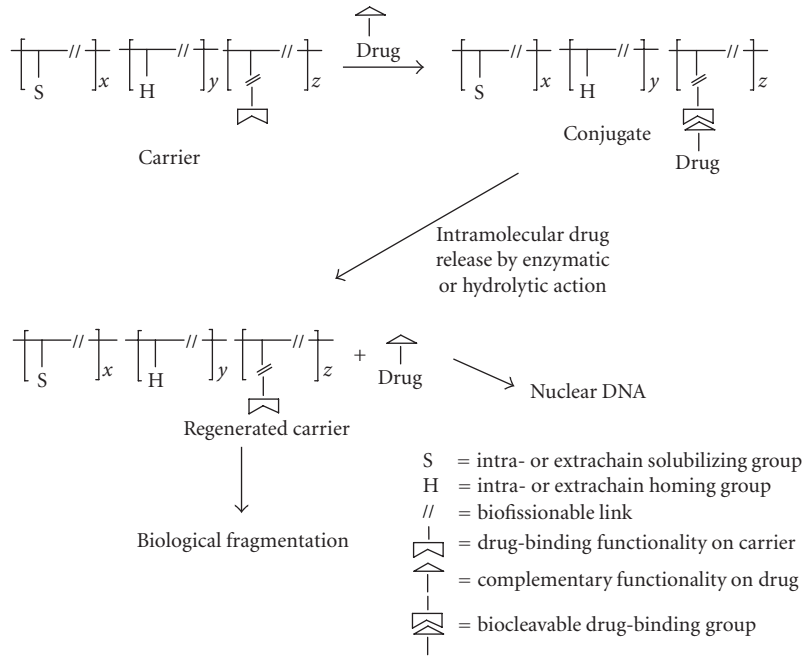

Scheme 1: Pharmacokinetic *in vivo* pathway of polymer-drug conjugate.

A general flow chart depicting the pharmacokinetic pathway of a carrier-anchored antineoplastic agent constructed in conformance with the aforementioned specifications is schematically reproduced in Scheme 1. Most of the earlier papers in the field were concerned with natural macromolecules as carriers, such as carbohydrates or proteinaceous compounds; yet, as pointed out before, immunogenicity and backbone toxicity, premature biodegradation (alternatively, strong resistance to biodegradability), poor stability in the solid state, and other detrimental features are militating against major developments on that front. More recently, in line with the pharmaceutical guidelines discussed further above in this section, synthetic polymers have taken the lead in drug conjugation studies for reasons of synthetic versatility and reproducibility, improved control of physical and chemical behavior patterns, as well as minimization of systemic toxicity and immunogenic properties. Parenthetically (no metal-based constituents being involved here) we wish to introduce the reader to a related, rapidly growing branch of drug conjugation science known as *gene therapy*. In this therapeutic modality, synthetic polymers are used in place of viral vectors as vehicles for the *in vivo* transport of specific nucleic acid agents for the therapeutic manipulation of pivotal genes involved in malignancies and other diseases. Despite existing pharmacological shortcomings, gene therapy is bound to take its well-deserved place in forth-coming therapeutic technology developments [5, 6]. The immensely wide-ranging drug conjugation topic has been amply surveyed over the years in the literature, and some of the most outstanding reviews both of yesteryear [7, 8] and up-to-date [9–14], are recommended to the reader for in-depth studying.

Having thoroughly digested the fundamental principles of polymer-drug conjugation and the significant pharmacological benefits to be derived from this mode of drug delivery, we are ready now for a lecture on the practicalities. Out of a large number of variously structured carrier types developed over the past decade, Section 3 will introduce just three types that have proved to be the predominant role players in the drug conjugation domain, and their structural peculiarities will be highlighted as a helpful prerequisite for the discussion of the drug anchoring strategies covered in Section 4.

3. THE LEADING CARRIER SYSTEMS

The design and construction of a drug carrier represents a pivotal task in polymer-drug conjugation as both the anchoring chemistry and the therapeutic activity of the derived conjugate depend critically on the carrier's solubility behavior and resulting "staying power" in solution upon drug conjugation. Steric accessibility and reactivity of the anchoring sites additionally contribute to the carrier's functional efficacy. A nontoxic chain construction amenable to slow biodegradation in the spent state (i.e., upon drug liberation) is a further requirement for optimal efficaciousness. Lastly, high main-chain flexibility depending on freely rotating single bonds in the backbone and the absence of aromatic or heteroaromatic, sterically blocking units, will be required as this will increase the entropy of solution, thus reinforcing the aforementioned staying power of the assembly in solution. In the following text we will find out if, and to what extent, these prerequisites are met in the structural compositions of the three selected carrier types: (1) the α,β-DL-polyaspartamides, (2) the poly(amidoamines), and (3) the

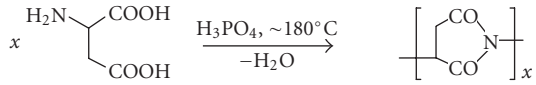

Scheme 2: Synthesis of polysuccinimide from aspartic acid.

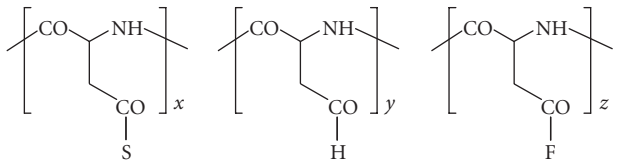

Figure 4: Copolyaspartamide equipped with solubilizing, target-directing, and drug-binding moieties.

2-hydroxypropyl-methacrylate polymers (HPMA). In addition, polyamides obtained by polycondensation processes will cursorily be discussed because of their sporadic use as carriers.

3.1. α,β-DL-polyaspartamides

This carrier type has moved into the limelight of polymer research some three decades ago [15–17]. It is readily accessible synthetically by high-temperature condensation polymerization of DL-aspartic acid in orthophosphoric acid medium, leading to a polysuccinimide intermediate (see Scheme 2).

In subsequent polymer-homologous reactions conveniently performed in a dipolar aprotic solvent such as N,N-dimethylformamide, the intermediary polysuccinimide is treated sequentially with two amine nucleophiles (NH_2–R_1, NH_2–R_2; occasionally a third amine, NH_2–R_3, may be employed in this operation), whereby imide ring opening gives rise to the generation of the ultimate polyaspartamides [18, 19]. These linear polyamides are composed of randomly distributed aspartamide repeat units bearing N-attached substituents (R_1, R_2, etc.) as introduced by the amine nucleophiles chosen. Scheme 3 depicts this sequence of ring opening steps.

It should be noted that here and in subsequent polyaspartamide representations, only the α-peptidic forms are shown for convenience, although the isomeric β-forms, with two carbon atoms (rather than one only) separating –CO and NH–, are also present.

Let us now redraw the structural arrangement in Scheme 3 by substituting a solubilizing entity S for NH–R_1, a homing device H for NH–R_2, and a drug-binding functional group F for NH–R_3 (see Figure 4).

It should be evident from the detailed discussion in the foregoing of structure-function relationships that polyaspartamides complying with this schematic representation will be able to provide an excellent "workhorse" service in drug conjugation studies. Specifically, the following hold. (i) The vital prerequisite of water solubility will be afforded by the numerous freely rotating aliphatic main-chain bonds and, in particular, by the extrachain S units chosen so as to contain *tert*-amine, hydroxyl, or, perhaps, oligo(ethylene oxide) groups [20]. These functionalities will be prone to aquation, that is,hydrogen bond formation with the aqueous solvent, and/or protonation with generation of cationic sites. (ii) Steric accessibility of the anchoring site F is optimized by insertion of a suitably long (say, 8–10 atomic constituents) aliphatic spacer link between F and backbone, thus reducing any steric hindrance potentially provided by the main chain proper. (iii) The chain construction has been rendered nontoxic through use of aspartic acid as the principal molecular backbone source. (iv) The chain is biodegradable hydrolytically at the CO–NH links for catabolic fragment elimination through the globular system of the kidneys upon drug release, a vital detoxification process in light of the fact that, as mentioned before, large nondegradable macromolecules, such as vinyl-type polymers and other carbochain macromolecules, strongly resist excretion and tend to induce toxicity. Such backbone degradation must be slow and controlled, however, so as to ensure stability during serum exposure, yet fragmentation in the endosomal compartment. (see also remarks in Section 2.2). In the polyaspartamide structure, these conditions are ideally met: in the serum environment (pH~7.5) only minimal hydrolytic CO–NH bond fission is observed, whereas in the endosomal space (pH~5) such fragmentation proceeds as expected, albeit slowly. Superimposed on hydrolytic bond fission is the process of enzymatic bond braking, effective both at main-chain NHCO sites and, to a variable extent, also at drug-binding links. Whereas natural polypeptides are prone to rapid degradation (*unzipping*) as a consequence of α-peptidase activity in the serum, such unzipping is grossly impeded by the presence of D-configurated CH groups and β-peptide units in the chain that are inert to α-peptidase attack [21]. Section 4 will show how proper use can be made of these structural features.

3.2. Polyamidoamines

Pioneered in Ferruti's laboratory [22, 23], these macromolecules have proved as versatile as the polyaspartamides, allowing for the construction of a multitude of unique carrier compositions. In the simplest mode of synthesis, a monomer equipped with two activated vinyl groups as in a bis(acryloylamido) compound exemplified by methylenebisacrylamide or bisacryloylpiperazine, is allowed to undergo aqueous-phase Michael addition polymerization with a comonomer that either contains two secondary amino groups for single substitution on each N (see Scheme 4(a)) or else features a primary amine (see Scheme 4(a)), the latter now being doubly N-substituted in the process. The reactions are preferably conducted in aqueous solution and give rise to polymer structures comprising both amide and amine functionalities. In the author's laboratory these studies were extended to include comonomers featuring two primary amino groups that are allowed to enter polymerization by single-step Michael addition at each $–NH_2$ under modified, carefully controlled conditions. This will produce polyamidoamines possessing secondary amino groups in the main chain (see Scheme 4(c)), which, in turn, are destined for drug binding [24]. With R_2 standing for an ethylene residue, the resulting polymer possesses an intrachain

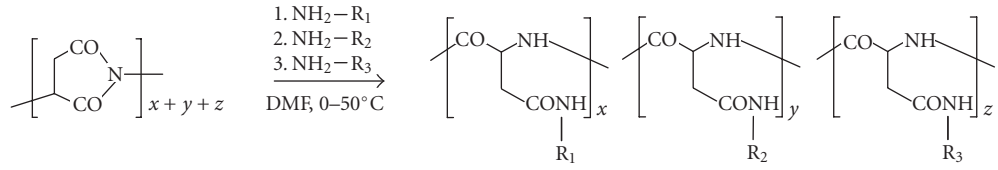

Scheme 3: Aminolytic ring opening in polysuccinimide.

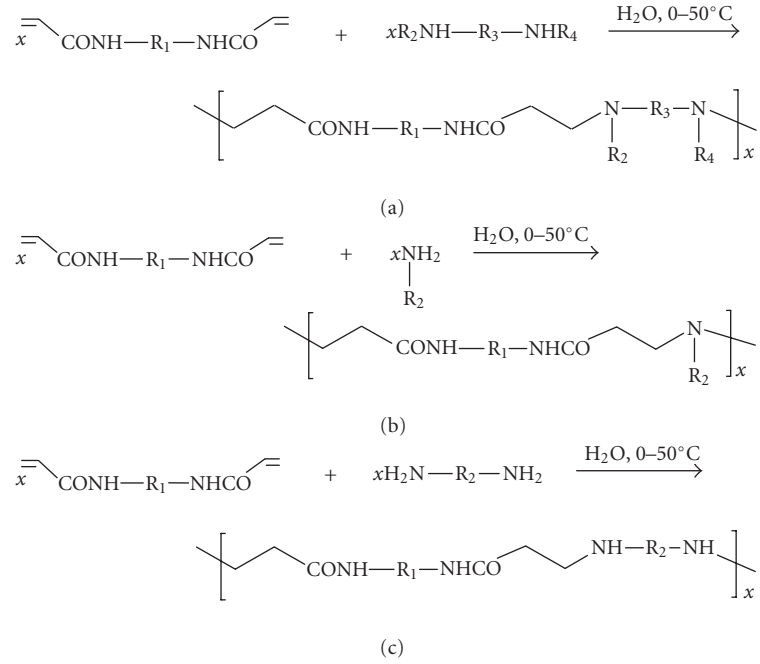

Scheme 4: Different modes of Michael addition polymerization of a bisacrylamide.

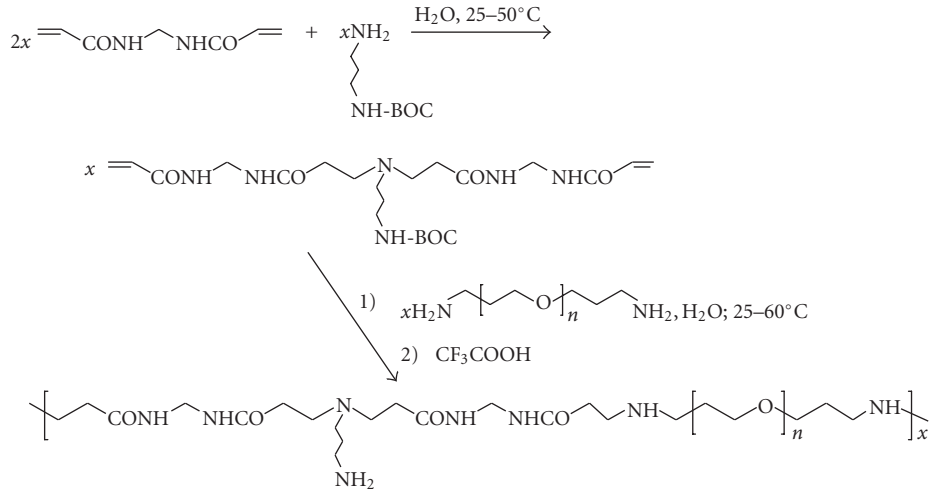

Scheme 5: Michael addition polymerization involving mono-N-protected diamine.

–NH–$(CH_2)_2$–NH segment important for *cis*-N,N chelation of platinum, as will be shown in Section 4.

A special case of sequence (b) in Scheme 4, in which a mono-N-protected diamine takes the place of H_2N–F_3, leads to a polymer possessing the mono-N-protected moiety as a side group. This strategy thus compels primary diamine monomers to be incorporated through just one amine functionality instead of two as in (c). Subsequent N-deprotection

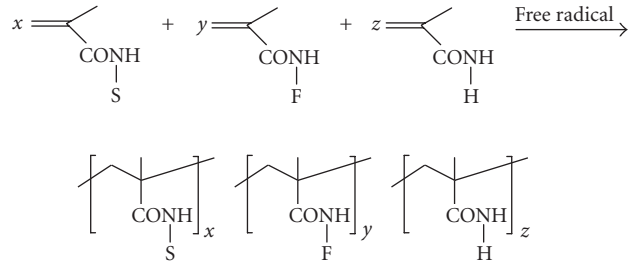

Scheme 6: Synthesis of methacrylamide polymers.

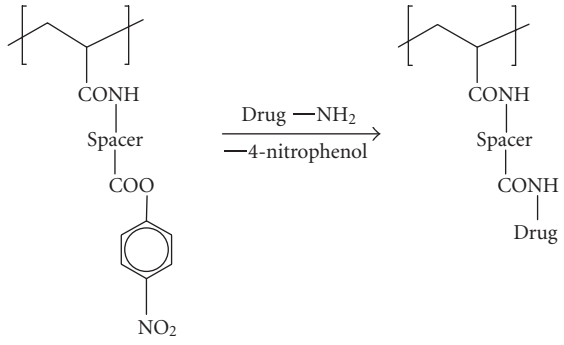

Scheme 7: Drug conjugation with HPMA copolymer.

then provides a polymer featuring a free $–NH_2$ side-chain terminal directly available for drug anchoring [25]. Scheme 5 depicts this reaction course ($n = 3–21$).

It is obvious from these described synthetic strategies that the resultant polyamidoamines in all cases are linear and follow the established rules of construction, in so far as one may vary the intrachain-type segments as well as—more usefully—the extrachain-type side groups, in an effort to provide the vital functions of solubility, target homing, and drug conjugation. In Section 4 we will learn more about the versatile use of the amidoamine polymers.

3.3. N-(2-hydroxypropyl)methacrylamides (HPMA)

The HPMA polymers have followed a glorious development path since early beginnings in 1970s [26]. On the strength of preceding methacrylate polymer research in numerous laboratories, this polymer class, developed almost singularly in the collaborating laboratories of Kopeček (synthesis) and Duncan (biomedical evaluation), has by now most successfully entered the forum of global research in polymer therapeutics [27–29].

The synthetic approach, illustrated in Scheme 6, involves the free-radical copolymerization of two or more methacrylamide monomers bearing substituents S for provision of water solubility (almost always a 2-hydroxypropyl moiety), other substituents, F, for drug anchoring reactions, and still other functionalities, H, as required for specific purposes serving facilitated cell entry, homing to the cancerous target tissue, or in vivo detection and tracing.

The polymers are thus characterized by a carbochain-type backbone composed of substituted 1,2-propylene repeat units, and these are randomly distributed along the main chain. In contrast to the polyaspartamide situation, all basic functionalities are generally preintroduced into the monomers and are automatically polymer-incorporated as the free-radical propagation proceeds. In order to facilitate the drug conjugation step, the respective precursor monomers are methacrylamides substituted with a spacer-separated *para*-nitrophenolate group, the latter acting as a convenient leaving group in the ultimate addition-elimination step leading to the introduction of amine-functionalized drug species with loss of *para*-nitrophenol. A nitrophenolate-terminated repeat unit and its reaction product, the drug-conjugate unit, are shown in Scheme 7.

Selected HPMA conjugates derived from the here-described carriers will be dealt with in Section 4.

3.4. Polyamides prepared by polycondensation reactions

Although of less importance, polycondensation products resulting from interfacial or high-temperature condensation reactions should be included here because monomer variation results in a variety of carrier structures featuring introduction of –NH– groups useful for drug conjugation. Typically, exemplified in Scheme 8, a diacid chloride, such as succinyl chloride, is allowed to react interfacially with a diamine like 1,2-bis(3-aminopropylamino)ethane or the solubilizing commercial Jeff ED-600 (an oligo(ethylene oxide) terminated at both ends with a primary amino group) [30]. High-temperature solution polymerization in polyphosphoric acid provides analogous polyamides, if free diacids are employed in place of the acid chlorides [31]. The $–NH–(CH_2)_2–NH–$ segments in these structures have conveniently been introduced for platinum chelation as pointed out before.

4. SELECTED CARRIER-BOUND DRUG MODELS

Having acquired by now the requisite conceptual tools, we are duly prepared for the ultimate topic: the strategies required to put the carrier-drug assembly together along biomedically prescribed routes. As we delineate the scope of this effort in the forth-coming discussions, we are guided by the requirement to confine the treatment to metal-based polymer systems and, there again, to those systems with a medicinal, specifically therapeutic application potential. Among the considerable number of metal-containing macromolecules that have attracted the bioscientists' interest, we will uniquely focus our attention to the two most actively researched classes: the metal-coordination polymer class belonging to the platinum drug family, and the organometallic class of ferrocene-type iron-containing conjugates. Both classes, as we will see, turn out to be just the right types of "guinea pig" as we set out to explore the broad field of medicinal agents conjugated to macromolecular adjuvants. In addition (you guessed it!), it so happens that it is the development of these two classes to which the

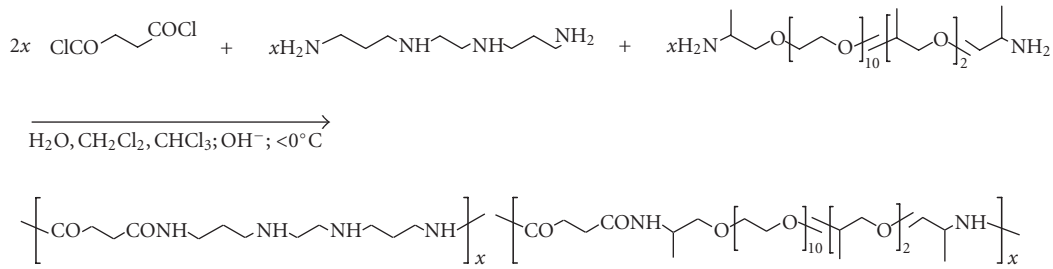

Scheme 8: Synthesis of polyamides by interfacial polymerization.

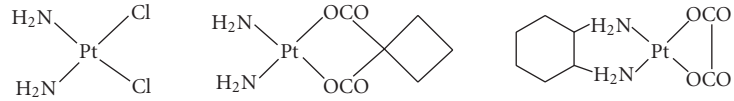

Figure 5: Leading platinum drugs in clinical use.

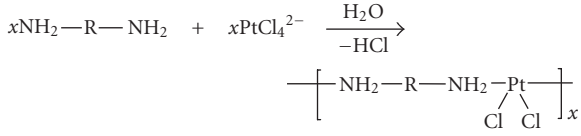

Scheme 9: Polycondensation of diamines with the tetrachloroplatinate dianion.

author's group has been particularly devoted over the past four decades. Other metals, such as titanium or ruthenium, continue to play a role in the field marginal enough as yet to permit us to ignore them within the scope of this text.

4.1. Polymer-platinum conjugates

As metal-based medicinal agents found their way into the oncologist's arsenal of antitumor drugs, several decades ago, platinum containing compounds immediately moved to the forefront with the advent of the prototype, *cisplatin* (*cis*-diamminedichloroplatinum(II)), and its second-generation cousins, *carboplatin* and *oxaliplatin* (see Figure 5).

Their general mechanism of action involves the formation of aquated species upon parenteral administration and subsequent intra- and interstrand crosslinking with intracellular DNA, leading to irreversible lesions in the double-helix and ultimate cell death. The compounds are highly potent against numerous malignancies *per se* and in combination with other antitumor drugs. Set against these highly acclaimed performance criteria, the platinum compounds, just like the metal-free drugs, suffer from severe pharmacological shortcomings, curtailing clinical effectiveness. Thus, residence times in central circulation are generally short, and this is paired with rapid excretion through the urinary tracts and consequent unpredictable variation of drug concentration. Drug action is nonselective, normal and transformed cells being equally affected; this leads to significant, dose-limiting acute and chronic toxicities, and in consequence, therapy discontinuation will frequently be required long before regression-free cure rates are attained. Lastly, and most importantly, various forms of drug resistance tend to build up in the cancerous tissue, which, again, requires treatment termination. In view of these serious deficiencies, active research worldwide has been focused on structural modifications designed to enhance the overall performance profile [32–35]. The polymer-drug conjugation modality is playing an outstanding part in these research endeavors, and, as we will see in the following section, encouraging progress has been made until now. Before going into details, let us remember that the present treatise, far from presenting a comprehensive review, is intended, first and foremost, to provide a didactic lecture on the topic; hence, it will cover only a small number of exemplifying conjugate types selected to mirror general trends in this rapidly expanding field of pharmaceutics. For the student wishing to "dig deeper", Carraher's excellent review chapter with original literature quotes is strongly recommended [36].

4.1.1. Metal coordination involving carrier-bound nitrogen donor ligands

By strict definition of the polymer-drug conjugation concept, the presynthesis of a suitable carrier polymer of biomedically "approved" structure is followed in another reaction step by the bioreversible attachment of the drug. Before we study the exemplifying macromolecules compliant with this definition of drug conjugation, it is only fair to Charles Carraher, the pioneering scientist, that we are acquainted first with a separate synthetic approach deviating from that routine, yet significant in its own right because it is one of the earliest major assaults on the problem of providing biomedically important metal compounds in polymeric form. This approach, developed in meticulous detail in Carraher's laboratory, embodies

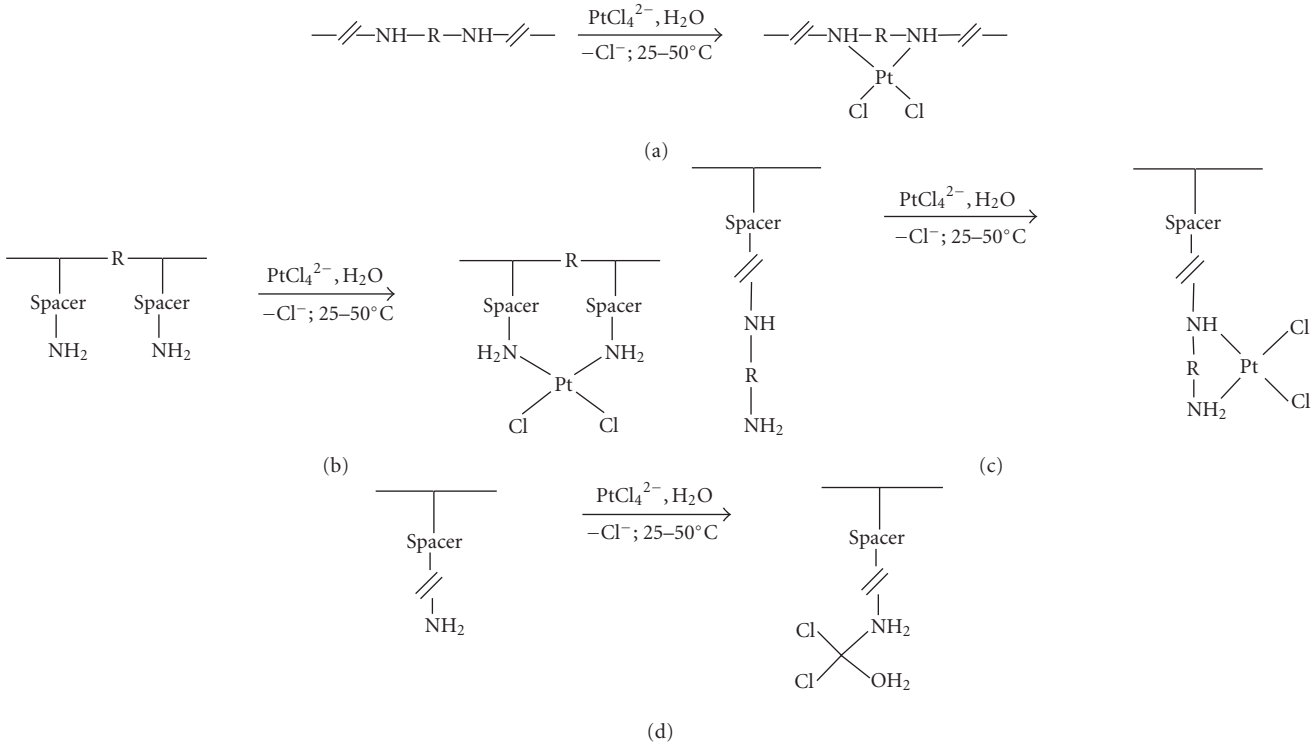

Scheme 10: Platination of amine-functionalized carriers.

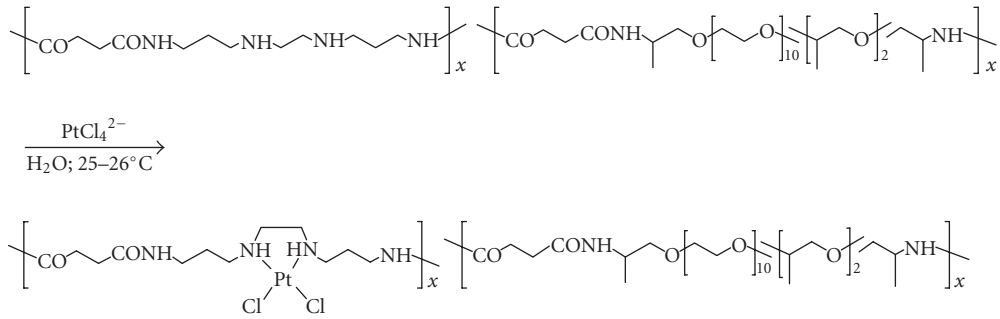

Scheme 11: Platinum atom coordinated by intrachain ethylenediamine segment.

the aqueous-phase polycondensation of the tetrachloroplatinate(II) dianion with diamines, giving polymers with the metal coordinated directly into the main chain in *cis*-diamine fashion, as shown in Scheme 9. The link R in this process stands for a variety of aliphatic, aromatic, and heteroaromatic units, or simply for a direct bond, and molecular masses attain the 10^6 Dalton level. Biological test data, notably for antiviral and antiproliferative performance against a number of cancer cells, at that time demonstrated a "leap forward" in platinum-drug cancer therapy.

This brings us to the main stream of drug conjugate development: the polymerhomologous drug anchoring to presynthesized carrier polymers. In this principal mode, polymer attachment of the square-planar structural element of *cisplatin* can be achieved *via* several reaction paths, in the design of which care must be taken to include suitable cleavage sites in the assembly for *in vivo* liberation of the bioactive agent from the carrier vehicle. In principle, two approaches of metal-binding are available. In the first, the metal center is bound *via* amine ligands attached to the carrier. In the second mode, the metal is polymer-bound *via* the leaving group ligands. In the first case, the result will be a structure comprising a Pt center tightly bound to the carrier, and release of the active complex will require cleavage of a suitable anchoring segment in the side chain. This is a time-dependent process, and the conjugates so constructed should prove most efficacious in long-term administration. In the second case, the active complex is released from the conjugate through (generally hydrolytic) cleavage of the bonds connecting the metal with the leaving groups, resulting in aquation. Release rates will be higher in this model, which should, hence, find optimal utilization in short-term administration,

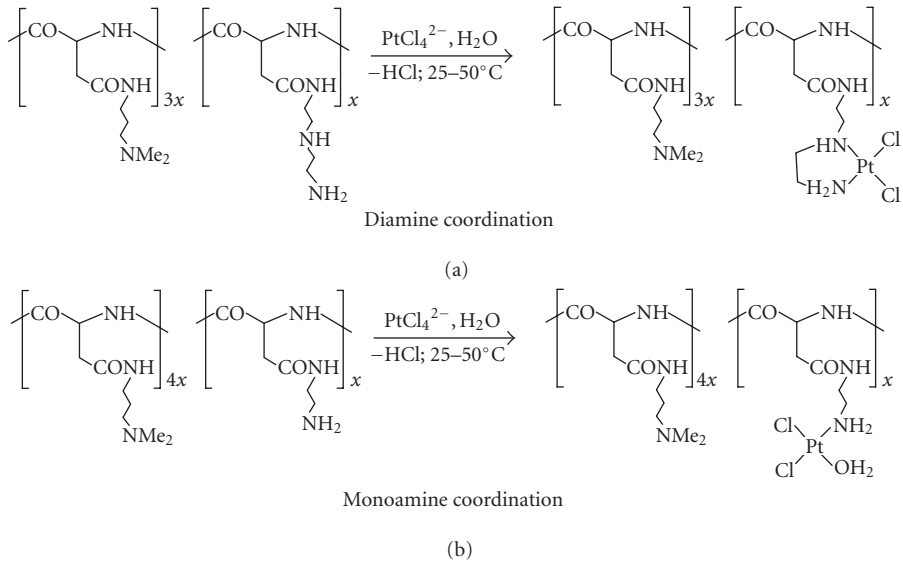

Scheme 12: Platinum conjugation through carrier-attached amine donors.

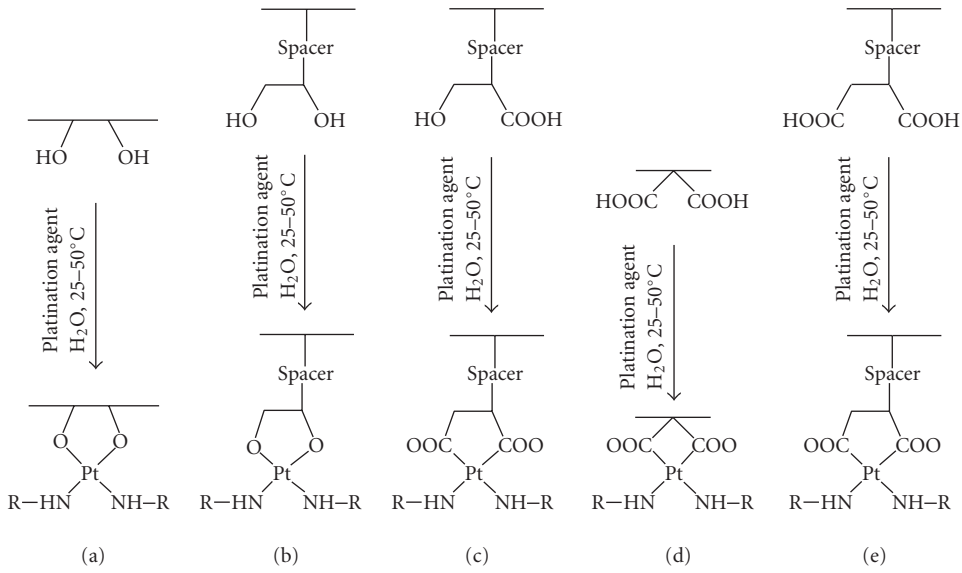

Scheme 13: Platinum chelation patterns.

whenever a boost is required for rapid effects. Let us look at the first case: conjugation *via* carrier-bound amine ligands (see Scheme 10).

In the simplest fashion (type A, with R = CH_2CH_2-), the >Pt$C\ell_2$ moiety is incorporated into a carrier structure containing ethylenediamine as a main-chain segment. Such carriers may be prepared by Michael addition polymerization with selected tetramine comonomers, and Scheme 11 provides an illustrating example. A related metal bonding pattern exists in certain polyethyleneimines prepared by Carraher's group. In conjugates of these structures the *cis*-diamine ligand system is strain-free and thus smoothly generated.

Platination of carriers of type B (see Scheme 10) leads to conjugates in which the entire *cisplatin* skeleton is located outside the main chain. With R standing for a direct bond or, less favorably, no more than a single atomic constituent, metal coordination through chelation with both amino groups would appear to be sterically feasible. Exemplifying product structures have indeed been obtained in Carraher's laboratory [36] by platination of a vinylamine/vinylsulfonate copolymer and of the natural (and hence, biodegradable) polymer chitosan. A special case of type B has been reported by Howell and Walles [37]. These authors *inter alia* presynthesized a *cisplatin* analog with both NH_3 ligands replaced by

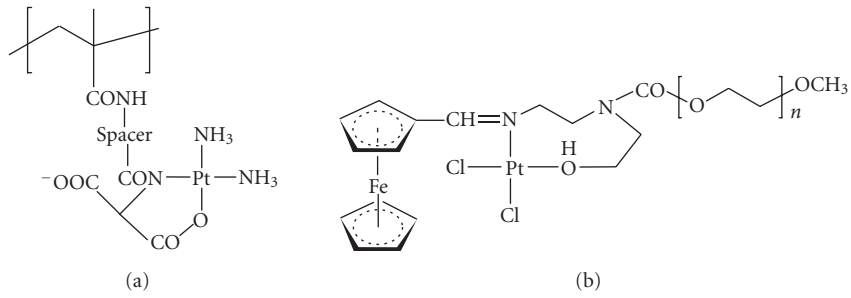

Figure 6: Platinum conjugation through repeat units featuring carrier-attached N- and O-donors.

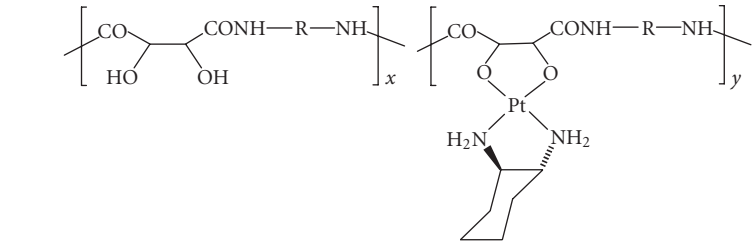

Type A

(a)

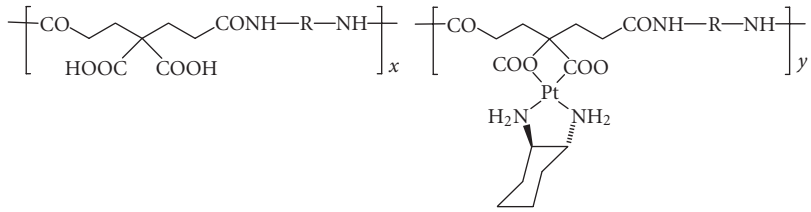

Type D

(b)

Figure 7: Examples of O,O-coordinated platinum in close main-chain proximity.

the two NH_2 groups in 1,2-diamino-4-hydroxybenzene. This reactant was then allowed to bind to poly(vinylpyrrolidone) by molecular complexation, that is, in a form permitting its release from the carrier by simple dissociation [37].

Appreciably more research has been performed with conjugates falling into the pattern of types C and D (see Scheme 10). In the author's laboratory, polyaspartamides prepared per Scheme 3 (yet including only two R-substituted units) were converted to platinated species by treatment with tetrachloroplatinate dianion in aqueous phase. The two platination runs in Scheme 12 exemplify this reaction type. Whereas the upper reaction leads to a conjugate with *cis*-N, N′-coordinated platinum [38, 39], the lower one gives rise to the formation of a structure wherein the metal is polymer-bound through a single N donor ligand [40]. In both cases, the first depicted, potentially cationic repeat unit provides both solubilizing and homing functions. Cell culture tests showed both conjugate types to be equally antitumor-active, and while with the upper conjugate ranked first in a series of cytotoxicity tests [41], the lower one ranked first in an *in vivo* toxicological study, demonstrating some 100-fold lower toxicity than determined for the *cisplatin* standard [42].

Similar platination patterns were reported from Ruth Duncan's prolific laboratory (reviewed [36]), with HPMA polymers used as the carriers. Broad-based biological investigations provided excellent results with respect to release rates, toxicological behavior, and cell-killing properties both *in vitro* and *in vivo*.

Somewhat related to type D is a conjugate synthesized by Gianasi et al. [43] and further investigated by Howell [44, 45], in which only one nitrogen donor ligand, in cooperation with an oxygen donor, partakes in platinum coordination (see Figure 6(a)). The compound, an HPMA derivative, is noteworthy as it features and N,N,N′,O-coordination square around the Pt atom. The compound underwent *in vitro* and Phase I clinical tests with highly promising results, low toxicities being paired with excellent antiproliferative activities [44, 45].

A differently structured polymer type featuring N,O-coordination of the metal has just been reported by

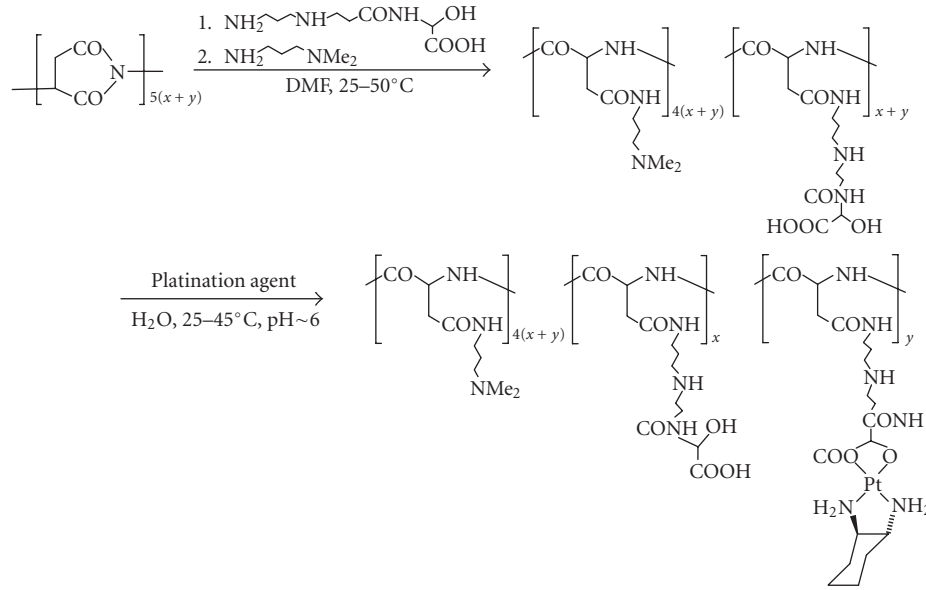

Scheme 14: Synthesis of conjugate featuring extrachain-type 1,2-carboxylatohydroxylato coordination of platinum.

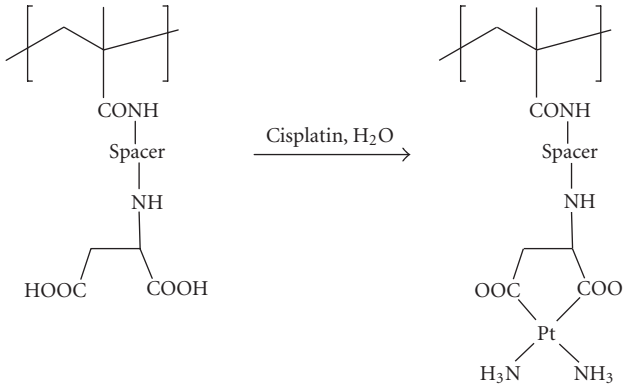

Scheme 15: HPMA-derived dicarboxylato-coordinated platinum.

Bariyanga [46]. Representative compounds contain the Fc−CH=N(R)−Pt(Cl^2)−O− segment (Fc = ferrocenyl) connected to a poly(ethylene oxide) terminal (see Figure 6(b)). These polymers are thus characterized by the presence of both a ferrocene and a platinum complex. While no biomedical test data are available, it would be interesting to find out in future studies whether such compounds display cooperative cytotoxicity between the two drug species.

4.1.2. *Metal coordination through carrier-bound oxygen donor ligands*

In the polymer described in this section the Pt complex is conjugated through two oxygen donor ligands provided by the carrier. Contrasting with those covered in the preceding section, these conjugates follow a release mechanism involving hydrolytic Pt bond cleavage, thus requiring no special biofissionable links in the carrier for drug liberation. In structures of this kind, the anchoring mechanism must be designed with a view to counteracting the inherently limited stability of the O−Pt bond. The preferred approach to this goal involves the construction of 5–7-membered chelate rings connecting the metal atom with the carrier-attached donor ligands. Scheme 13 offers acceptable choices, for which the literature provides exemplifying experiments (reviewed by Carraher [36]); whereas types A and D exemplify carrier binding through directly backbone-attached hydroxylato- or carboxylato-type oxygen donors, the types B, C, and E represent structures with spacers interposed between carrier backbone and oxygen donor. Further work will determine the extent to which biological performance will be affected by the coordinating atoms' special remoteness from the main chain.

Figure 7 provides an example each of type A- and type D-derived conjugates without further comments on the synthetic methodology [47].

Considering now the B- and C-type platination reactions of Scheme 13, the literature provides numerous reaction sequences originating from uniquely functionalized carriers. Scheme 14 represents a prototype reaction starting out from polysuccinimide [47]. In all these exemplifying cases, the platination agent has been *trans*-1,2-diaminocyclohexanediaquaplatinum(II) dinitrate (DACH-Pt), a reactant preferred by us and others over the tetrachloroplatinate dianion on grounds of favorable biological behavior, notably the lack of crossresistance with *cisplatin*.

We will now focus our attention to the bonding pattern of type E (see Scheme 13) which underlies the largest body of recent carrier-Pt conjugation research. Thus, Ohya et al. [48] prepared a water-soluble poly(ethylene oxide) carrying a methoxy terminal and, at the other end, a propylmalonate moiety suitable for platination with hydrolyzed *cisplatin*. The release behavior was examined and

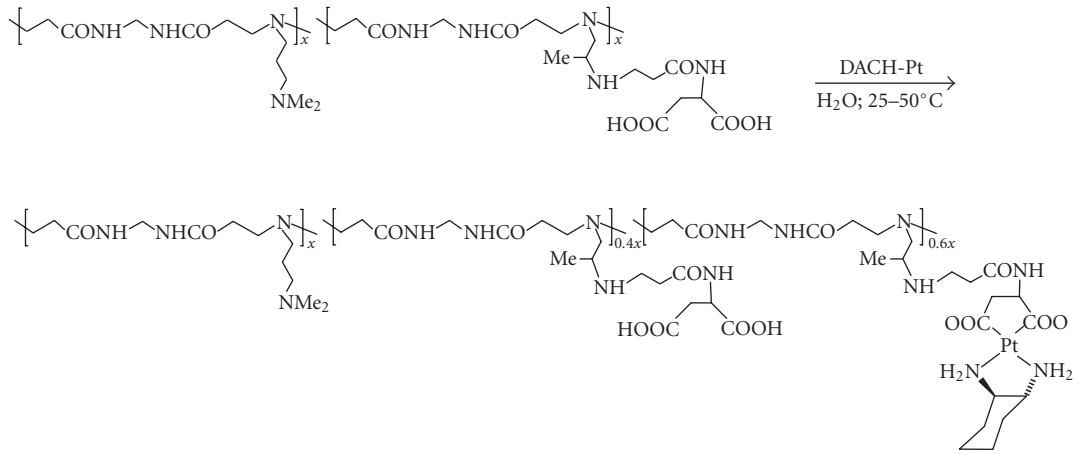

Scheme 16: Polyamidoamine-derived dicarboxylato-coordinated platinum.

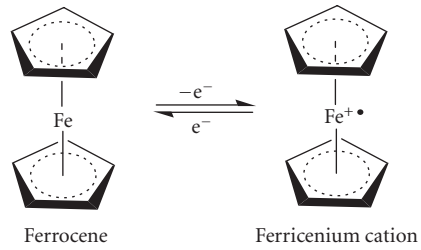

Scheme 17: The ferrocene/ferricenium redox couple.

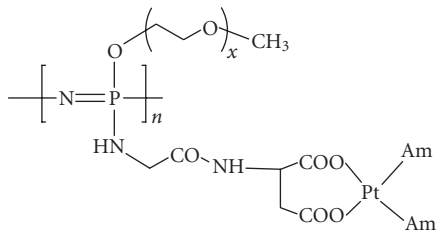

Figure 8: Simplified structure of polyphosphazene repeat unit bearing sidechain-coordinated platinum.

the cytoxicity against lymphocytic leukemia cells was determined. Good activity, although slightly below that of *cisplatin*, was observed. A study by the afore-mentioned group of Duncan et al. produced numerous dicarboxylatoplatinum compounds, among others, HPMA-derived conjugates possessing carrier-attached dicarboxylato ligands [43]. Upon treatment with hydrated *cisplatin*, these converted to highly bioactive *cis*-dicarboxylato-chelated platinum polymers as exemplified in Scheme 15 for the affected repeat unit.

A recent patent, outstanding among the many studies of polymeric phosphazene drugs [49], describes polyphosphazene derivatives of dicarboxylato-coordinated platinum with activity *inter alia* against the gastric tumor YCC-3 [50]. A simplified repeat unit structure is reproduced in Figure 8.

Numerous conjugates of type E have in recent years been synthesized in the author's laboratory, of which only a single example is reproduced in Scheme 16. The carrier educt in this reaction is a polyamidoamine equipped with a solubilizing N,Ndimethylaminopropyl side chain and an aspartic acid-derived dicarboxylate, and platination once more involves treatment with DACH-Pt [47, 51]. This polymer and related structures have shown outstanding antiproliferative performance, on the strength of which, a major development program has been initiated.

This section would be incomplete without a brief treatment of the comprehensive research efforts by the group of Bilha Schechter and collaborators. These workers at the Weizmann Institute of Science have been involved for some decades now in studies aiming at the provision of platinum-containing polymers antibody-modified for immunotargeting to human tumors. Representative compounds are a polyglutamic acid providing chelating capacity of type E (see Scheme 13) and some carboxymethyl derivatives of dextran with similar, albeit less structurally defined metal coordination patterns. Excellent biomedical test results on a broad front attest to the soundness of the development program in Schechter's highly productive laboratory. For in-depth reviews of the Weizmann group's activities, see Siegmann-Louda and Carraher [36], and Chen et al. [52].

4.2. Polymer-ferrocene conjugates

Contrasting with the platinum drugs, which have firmly established their prominent position as antitumor agents in clinical use, research in the realm of ferrocene-based chemotherapy is still at an experimental stage. However, biomedical test data, preliminary as they are, have shown overwhelming promise, stimulating comprehensive investigations currently in progress worldwide. The core organoiron compound, di-(η^5-cyclopentadienyl)iron(II), has been under scientific and technical scrutiny for more than half a century, and numerous topical surveys, including fundamental physical and chemical applications, have appeared in the literature (surveyed in two books [53, 54]). The fascinating

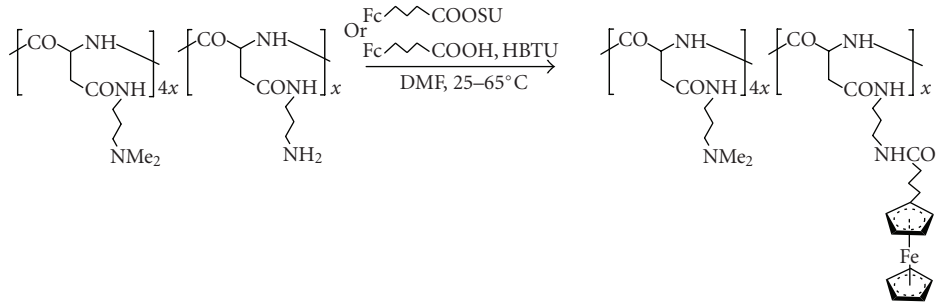

Scheme 18: Polyaspartamide-derived ferrocene conjugate.

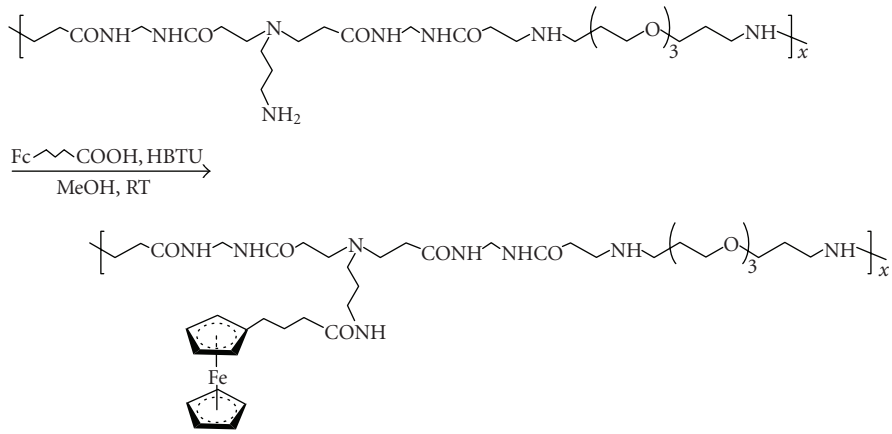

Scheme 19: Poly(amidoamine)-derived ferrocene conjugate.

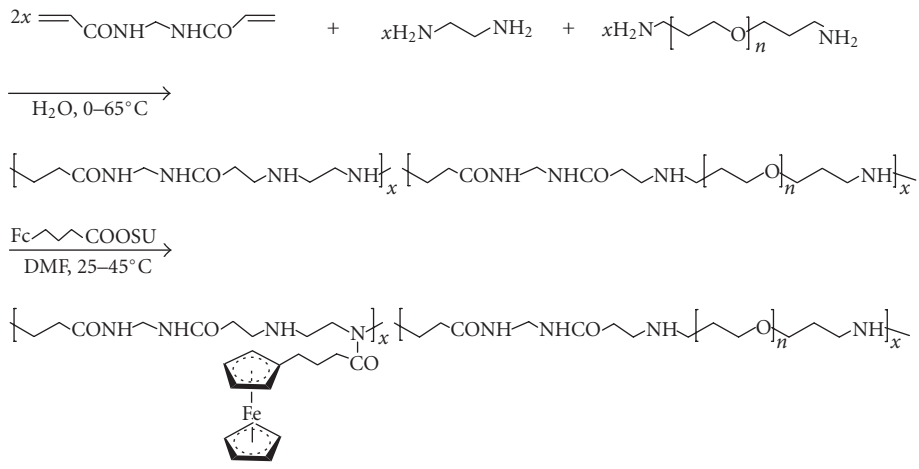

Scheme 20: Ferrocenylation of amidoamine polymer featuring intrachain-type −NH− group.

ferrocene chemistry, pivotally involving the compound's redox equilibrium with its one-electron oxidation product, the ferricenium cation, has prompted wide-ranging investigations of this electrochemical ferrocene/ferricenium couple in the biological environment, with ultimate ramification into the topic of carrier-bound ferrocene conjugates.

The bulk of contributions to these research developments has materialized in the author's laboratory, as attested by more than 50 pertinent papers published by our group until now. The reader is referred to some reviews [54–57] covering this prominent development trend.

Let us look now in detail at the large family of polymer-bound ferrocenes designed for biomedical applications. As we embark on this theme, we realize that, in the "old days" of ferrocene polymer development spanning the 1950–1970 decades, macromolecular ferrocenes and other metallocenes

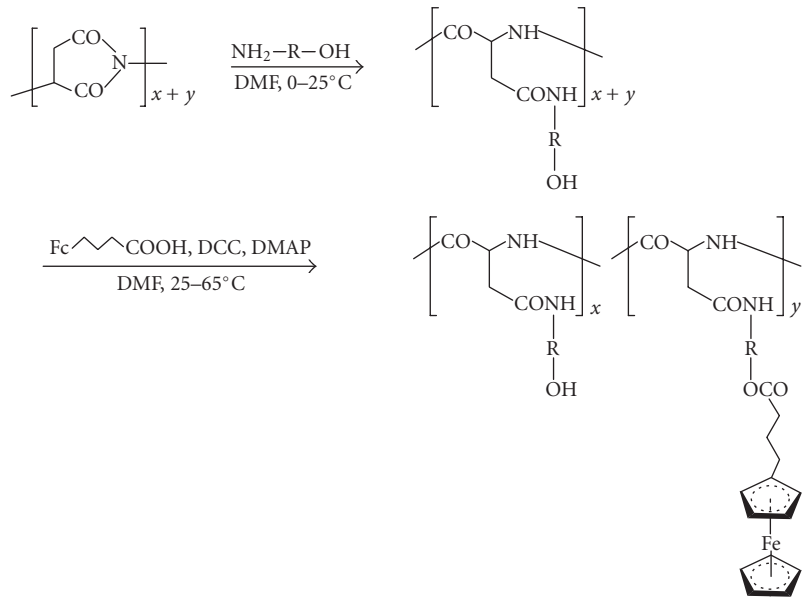

Scheme 21: Ferrocenylation of polyaspartamide featuring extrachain-type hydroxyl groups; R = aliphatic segment.

had been synthesized in huge numbers (reviewed in the book [54] and three book chapters [58–60]), yet most of those were hydrophobic and lacked hydrosolubility and, hence, were not considered in later work. An entirely new concept had to be developed for the purpose of rendering any metallocene polymers qualified for biological examinations. That concept, as we learned in Section 2, originated a decade later. It embodies the technique of conjugation so successfully utilized in the design of polymeric platinum and other drugs, and in the present section it will be seen to be instrumental in the synthesis of carrier-bound ferrocene compounds.

Earlier exploratory studies [61] demonstrated the feasibility of carrier binding and provided a range of variously structured conjugates meeting the crucial requirement of water solubility. Ferrocenylamines, initial candidate agents for ferrocenylation because of their strongly nucleophilic functionality, were soon omitted on electrochemical grounds. Ferrocenyl-carboxylic acids, on the other hand, notably 4-ferrocenylbutanoic acid, emerged in those earlier investigations as suitably functioning compounds providing electrochemically stable ferricenium counterparts [62–64]. The butanoic acid derivative soon became the ferrocenylation agent of choice in all subsequent conjugation developments in preference over other chemically feasible coupling mechanisms. Again, the polyaspartamides introduced in Section 3.1 turned out to be the most versatile and functional carriers; equipped with NH_2-terminated side chains, they soon became, and still are, the "workhorse" carrier polymers in our laboratory, conveniently undergoing coupling reactions in aprotic medium with the ferrocenyl acid via carboxyl group activation, or directly with the aid of strong coupling agents, such as HBTU (O-[1H-benzotriazol-1-yl]-1, 1,3,3-tetramethyluronium hexafluorophosphate). Scheme 18 shows a typical reaction step of this type, singled out here on account of the conjugate's particularly rewarding cytotoxic behavior; *in vitro* screens against the HeLa human cervix epithelial cancer revealed a cell-killing activity (on metal-to-metal equivalent basis) twice that of the *cisplatin* standard, and a fourfold superiority over *cisplatin* against Colo 320 DM, a notoriously drug-resistant human colon cancer line [65]. Interestingly, similar conjugates possessing nonbasic hydroxyalkyl side groups in place of the strongly basic *tert*-amine-terminated solubilizing and homing moiety of the drawn structure gave rather poor results, reflecting the lowered affinity to the cancerous cell (see Section 2.2) because of lacking basicity.

Among the great variety of other carrier types, we cite the primary amine-functionalized amidoamine polymer synthesized by Michael polyaddition (see Section 3.2); readily ferrocenylated with HBTU mediation [66], it converts to a conjugate featuring a long (8 atomic constituents) spacer connecting the metallocene to the main chain as depicted in Scheme 19.

On the other hand, a related amidoamine-type carrier characterized by an additional intrachain −NH−NH− group yet lacking the NH_2-spacer side chain converts to a conjugate by direct N-acylation of the main chain [67] (see Scheme 20). Subjected to the same cell culture tests as cited above, this ferrocene-loaded polymer, again, performed distinctly better than the *cisplatin* standard.

Lastly, we mention an anchoring step involving O-acylation. To this end, various hydroxyalkyl-substituted polyaspartamides were treated in aprotic medium with ferrocenylbutanoic acid in the presence of N, N′-dicyclohexylcarbodiimide coupling agent and 4-(dimethylamino)pyridine (DMAP) catalyst [68]. Scheme 21 shows a representative run, with *x/y* varying from about 3 to 10 as a function of molar reactant ratios.

A conjugate of this type, with *x/y* = 2.6, subjected to an *in vivo* toxicity test, gave a maximum tolerated dose of

0.43 mmol Fe/kg, more than 20-times higher than determined for the *cisplatin* standard [69]. The polymer is thus some 20-fold less toxic than the standard, and comparable toxicity behavior is also displayed by selected amide-linked analogs. These findings, in conjunction with cell-killing properties, augur exceptionally well for the class of ferrocene conjugates as cancer-chemotherapeutic agents, and their future looks highly promising indeed.

5. SUMMARY AND CONCLUSIONS

Mankind, along its arduous development path from early hominids via *Homo erectus* to the present "status" of *Homo sapiens*, has never been spared the experience of bodily injuries and the suffering from debilitating or even lethal diseases. Yet the human spirit has at all times searched for therapeutic weapons to overcome, or at least deter, those inimical adversaries. Even at the sophisticated level of human enterprise attained by now, we have come to accept the limited efficacy of those therapeutic weapons against many serious infirmities and the pressing need for continued forceful research activities to eliminate existing threats to our well-being. Cancerous diseases stand out amid those threats as particularly dreaded adversaries, and on these we have focused our attention in the present discourse.

We have acquainted ourselves with the cancer problem *per se*, with the current chemotherapeutic treatment limitations, and, getting into the core topic, with the promising and highly challenging present research endeavors in the field of polymer-drug conjugation. In doing so, we have followed the development of one of the leading polymer-based chemotherapeutic tools in the fight against cancer, with emphasis on platinum- and iron-based drug systems. We have found out that the expediency of using goal-designed, water-soluble, and biologically acceptable macromolecules as temporary transport vehicles for powerful, yet potentially toxic, and resistance-promoting medicinal agents has, beyond early doubts and objections, matured to a practicable technology. It is to be hoped that the facts and arguments here-presented will encourage many students of the biochemical and pharmaceutical sciences to participate in the global efforts to promote and refine the drug conjugation modality for the future benefit of the victims of neoplastic and other diseases Scheme 17.

ACKNOWLEDGMENTS

This work has been generously supported by the South African Medical Research Council. While other providers of financial support to the author's laboratory have been given due recognition in the individual publications cited, it is his special privilege here as on previous occasions to acknowledge the dedicated and highly professional services rendered at all times by Kitty Banda, Pat Cawthorn, and Agnes Pointeer in the handling of those demanding clerical, artistic, and administrative matters omnipresent in a practical research program. In the execution of current synthetic platinum polymer work, the group has been materially aided by Johnson & Matthey's generous loan of platinum salt, for which the author is most grateful.

REFERENCES

[1] R. L. Juliano, Ed., *Biological Approaches to the Controlled Delivery of Drugs*, vol. 507, New York Academy of Sciences, New York, NY, USA, 1987.

[2] M. S. Sachdeva, "Drug targeting systems for cancer chemotherapy," *Expert Opinion on Investigational Drugs*, vol. 7, no. 11, pp. 1849–1864, 1998.

[3] R. Duncan, "The dawning era of polymer therapeutics," *Nature Reviews, Drug Discovery*, vol. 2, pp. 347–360, 2003.

[4] H. Ringsdorf, "Structure and properties of pharmacologically active polymers," *Journal of Polymer Science: Polymer Symposia*, vol. 51, pp. 135–153, 1975.

[5] J. Kopeček, "Smart and genetically engineered biomaterials and drug delivery systems," *European Journal of Pharmaceutical Sciences*, vol. 20, no. 1, pp. 1–16, 2003.

[6] D. W. Pack, A. S. Hoffman, S. Pun, and P. S. Stayton, "Design and development of polymers for gene delivery," *Nature Reviews, Drug Discovery*, vol. 4, no. 7, pp. 581–593, 2005.

[7] R. Duncan and J. Kopeček, "Soluble synthetic polymers as potential drug carriers," *Advances in Polymer Science*, vol. 57, pp. 51–101, 1984.

[8] C. J. T. Hoes and J. Feijen, "The application of drug-polymer conjugates in chemotherapy," in *Drug Carrier Systems*, F. H. D. Roerdink and A. M. Kroon, Eds., pp. 57–109, John Wiley & Sons, New York, NY, USA, 1989.

[9] S. E. Matthews, C. W. Pouton, and M. D. Threadgill, "Macromolecular systems for chemotherapy and magnetic resonance imaging," *Advanced Drug Delivery Reviews*, vol. 18, no. 2, pp. 219–267, 1996.

[10] F. M. Veronese and M. Morpurgo, "Bioconjugation in pharmaceutical chemistry," *II Farmaco*, vol. 54, no. 8, pp. 497–516, 1999.

[11] H. Maeda, J. Wu, T. Sawa, Y. Matsumura, and K. Hori, "Tumor vascular permeability and the EPR effect in macromolecular therapeutics: a review," *Journal of Controlled Release*, vol. 65, no. 1-2, pp. 271–284, 2000.

[12] R. J. Christie and D. W. Grainger, "Design strategies to improve soluble macromolecular delivery constructs," *Advanced Drug Delivery Reviews*, vol. 55, no. 3, pp. 421–437, 2003.

[13] R. Duncan, M. J. Vicent, F. Greco, and R. I. Nicholson, "Polymer-drug conjugates: towards a novel approach for the treatment of endrocine-related cancer," *Endocrine-Related Cancer*, vol. 12, 1, pp. S189–S199, 2005.

[14] A. Nori and J. Kopeček, "Intracellular targeting of polymer-bound drugs for cancer chemotherapy," *Advanced Drug Delivery Reviews*, vol. 57, no. 4, pp. 609–636, 2005.

[15] P. Neri, G. Antoni, F. Benvenuti, F. Cocola, and G. Gazzei, "Synthesis of α,β-poly[(2-hydroxyethyl)-DL-aspartamide], a new plasma expander," *Journal of Medicinal Chemistry*, vol. 16, no. 8, pp. 893–897, 1973.

[16] J. Drobnik, V. Saudek, J. Vlasák, and J. Kálal, "Polyaspartamide—a potential drug carrier," *Journal of Polymer Science: Polymer Symposia*, vol. 66, no. 1, pp. 65–74, 1979.

[17] J. Kálal, J. Drobnik, J. Kopeček, and J. Exner, "Water soluble polymers for medicine," *British Polymer Journal*, vol. 10, no. 2, pp. 111–114, 1978.

[18] P. Neri and G. Antoni, "α,β-poly(2-Hydroxyethyl)-DL-aspartamide," *Macromolecular Syntheses*, vol. 8, pp. 25–28, 1982.

[19] M. de L. Machado, E. W. Neuse, and A. G. Perlwitz, "Water-soluble polyamides as potential drug carriers, V. Carboxy-functionalized polyaspartamides and copolyaspartamides," *Angewandte Makromolekulare Chemie*, vol. 195, no. 1, pp. 35–56, 1992.

[20] G. Caldwell, E. W. Neuse, and A. G. Perlwitz, "Water soluble polyamides as potential drug carriers. IX. Polyaspartamides grafted with amine-terminated poly(ethylene oxide) chains," *Journal of Applied Polymer Science*, vol. 66, no. 5, pp. 911–919, 1997.

[21] J. Pytela, V. Saudek, J. Drobník, and F. Rypáček, "Poly(N^5-hydroxyalkylglutamines). IV. Enzymatic degradation of n^5-(2-hydroxyethyl)$-_L-$glutamine homopolymers and copolymers," *Journal of Controlled Release*, vol. 10, no. 1, pp. 17–25, 1989.

[22] F. Danusso and P. Ferruti, "Synthesis of tertiary amine polymers," *Polymer*, vol. 11, no. 2, pp. 88–113, 1970.

[23] P. Ferruti, M. A. Marchisio, and R. Duncan, "Poly(amido-amine)s: biomedical applications," *Macromolecular Rapid Communications*, vol. 23, no. 5-6, pp. 332–355, 2002.

[24] G. Caldwell, E. W. Neuse, and A. Stephanou, "Synthesis of water-soluble polyimidoamines for biomedical application. II. Polymers possessing intrachain-type secondary amino groups suitable for side-chain attachment," *Journal of Applied Polymer Science*, vol. 50, no. 3, pp. 393–401, 1993.

[25] D. D. N'Da and E. W. Neuse, "Polyamidoamines as drug carriers: synthesis of polymers featuring extrachain-type primary amino groups as drug-anchoring sites," *South African Journal of Chemistry*, vol. 59, pp. 65–70, 2006.

[26] J. Kopeček and H. Bažilová, "Poly[N-(2-hydroxypropyl)-methacrylamide]—I. Radical polymerization and copolymerization," *European Polymer Journal*, vol. 9, no. 1, pp. 7–14, 1973.

[27] J. Kopeček, P. Kopečková, T. Minko, and Z.-R. Lu, "HPMA copolymer-anticancer drug conjugates: design, activity, and mechanism of action," *European Journal of Pharmaceutics and Biopharmaceutics*, vol. 50, no. 1, pp. 61–81, 2000.

[28] K. D. Jensen, A. Nori, M. Tijerina, P. Kopečková, and J. Kopeček, "Cytoplasmic delivery and nuclear targeting of synthetic macromolecules," *Journal of Controlled Release*, vol. 87, no. 1-3, pp. 89–105, 2003.

[29] O. Hovorka, T. Etrych, V. Šubr, J. Strohalm, K. Ulbrich, and B. Říhová, "HPMA based macromolecular therapeutics: internalization, intracellular pathway and cell death depend on the character of covalent bond between the drug and the peptidic spacer and also on spacer composition," *Journal of Drug Targeting*, vol. 14, no. 6, pp. 391–403, 2006.

[30] E. W. Neuse and G. Caldwell, "cis-diaminedichloroplatinurn-(II) complexes reversibly linked into the main chain of water-soluble polyamides," *Journal of Inorganic and Organometallic Polymers*, vol. 7, no. 3, pp. 163–181, 1997.

[31] J. C. Swarts, E. W. Neuse, A. G. Perlwitz, A. Stephanou, and G. J. Lamprecht, "Water-soluble polyamides as potential drug carriers, VI. Synthesis of amine- and carboxyl-functionalized carrier polymers by high-temperature solution polymerization in polyphosphoric acid," *Angewandte Makromolekulare Chemie*, vol. 207, no. 1, pp. 123–135, 1993.

[32] J. C. Dabrowiak and W. T. Bradner, "Platinum antitumour agents," *Progress in Medicinal Chemistry*, vol. 24, pp. 129–158, 1987.

[33] T. W. Hambley, "The influence of structure on the activity and toxicity of Pt anti-cancer drugs," *Coordination Chemistry Reviews*, vol. 166, pp. 181–223, 1997.

[34] E. W. Neuse, "Platinum coordination compounds in cancer research and chemotherapy," *South African Journal of Science*, vol. 95, no. 11-12, pp. 509–516, 1999.

[35] I. Kostova, "Platinum complexes as anticancer agents," *Recent Patents on Anti-Cancer Drug Delivery*, vol. 1, no. 1, pp. 1–22, 2006.

[36] D. W. Siegmann-Louda and C. E. Carraher Jr., "Platinum-containing polymers for the treatment of cancer," in *Macromolecules Containing Metal and Metal-Like Elements, Vol. 3, Biomedical Applications*, A. S. Abd-El-Aziz, C. E. Carraher Jr., C. U. Pittman Jr., J. E. Sheats, and M. Zeldin, Eds., pp. 119–191, John Wiley & Sons, New York, NY, USA, 2004, chapter 7.

[37] B. A. Howell and E. W. Walles, "cis-dichloro(substituted *o*-phenylenediamine)-platinum(II) compounds," *Inorganica Chimica Acta*, vol. 142, no. 2, pp. 185–186, 1988.

[38] E. W. Neuse, B. B. Patel, and C. W. N. Mbonyana, "cis-diaminedichloroplatinum(II) complexes reversibly bound to water-soluble polyaspartamide carriers for chemotherapeutic applications—I: platinum coordination to preformed, carrier-attached ethylenediamine ligands," *Journal of Inorganic and Organometallic Polymers*, vol. 1, no. 2, pp. 147–165, 1991.

[39] E. W. Neuse, G. Caldwell, and A. G. Perlwitz, "cis-diaminedichloroplatinum(II) complexes reversibly bound to water-soluble polyaspartamide carriers for chemotherapeutic applications—II: platinum coordination to ethylenediamine ligands attached to poly(ethylene oxide)-grafted carrier polymers," *Journal of Inorganic and Organometallic Polymers*, vol. 5, no. 3, pp. 195–207, 1995.

[40] C. W. N. Mbonyana, E. W. Neuse, and A. G. Perlwitz, "Monoamineplatinum (II) complexes conjugated to water-soluble carrier polymers for chemotherapeutic applications," *Applied Organometallic Chemistry*, vol. 7, no. 4, pp. 279–288, 1993.

[41] G. Caldwell, E. W. Neuse, and C. E. J. van Rensburg, "Cytotoxicity of selected water-soluble polymer-cis-diaminedichloroplatinum(II) conjugates against the human HeLa cancer cell line," *Journal of Inorganic and Organometallic Polymers*, vol. 7, no. 4, pp. 217–231, 1997.

[42] B. Schechter, G. Caldwell, M. G. Meirim, and E. W. Neuse, "Preliminary toxicological studies of selected water-soluble polymer-platinum conjugates," *Applied Organometallic Chemistry*, vol. 14, no. 11, pp. 701–708, 2000.

[43] E. Gianasi, R. G. Buckley, J. Latigo, M. Wasil, and R. Duncan, "HPMA copolymers platinates containing dicarboxylato ligands. Preparation, characterisation and in vitro and in vivo evaluation," *Journal of Drug Targeting*, vol. 10, no. 7, pp. 549–556, 2002.

[44] X. Lin, Q. Zhang, J. R. Rice, D. R. Stewart, D. P. Nowotnik, and S. B. Howell, "Improved targeting of platinum chemotherapeutics: the antitumour activity of the HPMA copolymer platinum agent AP5280 in murine tumour models," *European Journal of Cancer*, vol. 40, no. 2, pp. 291–297, 2004.

[45] J. M. Rademaker-Lakhai, C. Terret, S. B. Howell, et al., "A phase I and pharmacological study of the platinum polymer AP5280 given as an intravenous infusion once every 3 weeks in patients with solid tumors," *Clinical Cancer Research*, vol. 10, no. 10, pp. 3386–3395, 2004.

[46] J. Bariyanga, "Synthesis, characterization and biodegradability of poly(ethylene glycol)-bound molecule platinum complex

containing ferrocenyl moiety using MALDI time-of-flight mass spectrometry," *Journal of Bioactive and Compatible Polymers*, vol. 17, no. 1, pp. 37–50, 2002.

[47] E. W. Neuse, N. Mphephu, H. M. Netshifhefhe, and M. T. Johnson, "Synthesis and preliminary in vitro evaluation of polymeric dicarboxylato- and dihydroxylatoplatinum(II) chelates as antiproliferative agents," *Polymers for Advanced Technologies*, vol. 13, no. 10–12, pp. 884–895, 2002.

[48] Y. Ohya, S. Shirakawa, M. Matsumoto, and T. Ouchi, "Design of poly(ethylene glycol) immobilizing platinum complex through chelate-type coordination bond," *Polymers for Advanced Technologies*, vol. 11, no. 8–12, pp. 635–641, 2000.

[49] A. K. Andrianov, "Water-soluble polyphosphazenes for biomedical applications," *Journal of Inorganic and Organometallic Polymers and Materials*, vol. 16, no. 4, pp. 397–406, 2006.

[50] Y. S. Sohn, Y. J. Jun, and J. I. Kim, "Tumor selective and biodegradable polyphosphazene-platinum(II) conjugate antitumor agent, and preparation method thereof," US Patent no. 6951953, 2005.

[51] M. T. Johnson, L. L. Komane, D. D. N'Da, and E. W. Neuse, "Polymeric drug carriers functionalized with pairwise arranged hydroxyl and/or carboxyl groups for platinum chelation," *Journal of Applied Polymer Science*, vol. 96, no. 1, pp. 10–19, 2005.

[52] L. Chen, B. Schechter, R. Arnon, and M. Wilchek, "Tissue selective affinity targeting using the avidin-biotin system," *Drug Development Research*, vol. 50, no. 3–4, pp. 258–271, 2000.

[53] M. Rosenblum, *Chemistry of the Iron Group Metallocenes, Part I*, Wiley-Interscience, New York, NY, USA, 1965.

[54] E. W. Neuse and H. Rosenberg, *Metallocence Polymers*, Marcel Dekker, New York, NY, USA, 1970.

[55] E. W. Neuse, "Polymeric organoiron compounds as prodrugs in cancer research," *Macromolecular Symposia*, vol. 172, pp. 127–138, 2001.

[56] E. W. Neuse, "Polymeric ferrocene conjugates as antiproliferative agents," in *Macromolecules Containing Metal and Metal-Like Elements, Volume 3, Biomedical Applications*, A. S. Abd-El-Aziz, C. E. Carraher Jr., C. U. Pittman Jr., J. E. Sheats, and M. Zeldin, Eds., pp. 89–117, John Wiley & Sons, New York, NY, USA, 2004, chapter 6.

[57] E. W. Neuse, "Macromolecular ferrocene compounds as cancer drug models," *Journal of Inorganic and Organometallic Polymers*, vol. 15, no. 1, pp. 3–32, 2005.

[58] E. W. Neuse, "Metallocene Polymers," *Encyclopedia of Polymer Science Technology*, vol. 8, p. 667, 1968.

[59] E. W. Neuse, "Ferrocene Polymers," *Advances in Macromolecular Chemistry*, vol. 1, p. 1, 1968.

[60] E. W. Neuse, "Polymetallocenylenes-recent developments," *Journal of Macromolecular Science, Part A*, vol. A16, no. 1, pp. 3–72, 1981.

[61] E. W. Neuse and C. W. N. Mbonyana, "Synthesis of polyaspartamide-bound Ferrocene compounds," in *Inorganic and Metal-Containing Polymeric Materials*, J. Sheats, C. Carraher, C. Pittman, M. Zeldin, and B. Currell, Eds., pp. 139–150, Plenum Press, New York, NY, USA, 1990.

[62] N. F. Blom, E. W. Neuse, and H. G. Thomas, "Electrochemical characterization of some ferrocenylcarboxylic acids," *Transition Metal Chemistry*, vol. 12, no. 4, pp. 301–306, 1987.

[63] J. C. Swarts, E. W. Neuse, and G. J. Lamprecht, "Synthesis and characterization of water-soluble polyaspartamide-ferrocene conjugates for biomedical applications," *Journal of Inorganic and Organometallic Polymers*, vol. 4, no. 2, pp. 143–153, 1994.

[64] J. C. Swarts, D. M. Swarts, D. M. Maree, E. W. Neuse, C. La Madeleine, and J. E. van Lier, "Polyaspartamides as water-soluble drug carriers. Part 1: antineoplastic activity of ferrocene-containing polyaspartamide conjugates," *Anticancer Research*, vol. 21, no. 3B, pp. 2033–2037, 2001.

[65] M. T. Johnson, E. Kreft, D. D. N'Da, E. W. Neuse, and C. E. J. van Rensburg, "The cytotoxic activity of macromolecular ferrocene conjugates against the Colo 320 DM human colon cancer line," *Journal of Inorganic and Organometallic Polymers*, vol. 13, no. 4, pp. 255–267, 2003.

[66] D. D. N'Da and E. W. Neuse, "Polyamidoamines as drug carriers: synthesis of polymers featuring extrachain-type primary amino groups as drug-anchoring sites," *South African Journal of Chemistry*, vol. 59, pp. 65–70, 2006.

[67] M. G. Meirim, E. W. Neuse, and G. Caldwell, "Water-soluble polymer-ferrocene conjugates based on polyamide carriers containing intrachain-type secondary amine functions as binding sites," *Journal of Inorganic and Organometallic Polymers*, vol. 8, no. 4, pp. 225–236, 1998.

[68] E. W. Neuse, M. G. Meirim, D. D. N'Da, and G. Caldwell, "Polymer-ferrocene conjugates containing an ester function in the connecting links," *Journal of Inorganic and Organometallic Polymers*, vol. 9, no. 4, pp. 221–230, 1999.

[69] B. Schechter, G. Caldwell, and E. W. Neuse, "A preliminary study of the toxicological properties of selected polymer-ferrocene conjugates," *Journal of Inorganic and Organometallic Polymers*, vol. 10, no. 4, pp. 177–188, 2000.

Hindawi Publishing Corporation
Metal-Based Drugs
Volume 2008, Article ID 217573, 10 pages
doi:10.1155/2008/217573

Research Article

Synthesis and Anchoring of Antineoplastic Ferrocene and Phthalocyanine Derivatives on Water-Soluble Polymeric Drug Carriers Derived from Lysine and Aspartic Acid

M. David Maree,[1] Eberhard W. Neuse,[2] Elizabeth Erasmus,[1] and Jannie C. Swarts[1]

[1] *Department of Chemistry, University of the Free State, Bloemfontein 9300, South Africa*
[2] *School of Chemistry, University of the Witwatersrand, PO WITS 2050, South Africa*

Correspondence should be addressed to Jannie C. Swarts, swartsjc.sci@ufs.ac.za

Received 25 July 2007; Accepted 1 October 2007

Recommended by Michael J. Cook

The general synthetic strategy towards water-soluble biodegradable drug carriers and the properties that they must have are discussed. The syntheses of water-soluble biodegradable copolymers of lysine and aspartic acid as potential drug-delivering devices, having amine-functionalised side chains are then described. Covalent anchoring of carboxylic acid derivatives of the antineoplastic ferrocene and photodynamically active phthalocyanine moieties to the amine-containing drug carrier copolymers under mild coupling conditions has been achieved utilising the coupling reagent O-benzotriazolyl-N,N,N′,N′-tetramethyluronium hexafluorophosphate to promote formation of the biodegradable amide bond. Even though the parent antineoplastic ferrocene and phthalocyanine derivatives are themselves insoluble in water at pH < 7, the new carrier-drug conjugates that were obtained are well water-soluble.

1. INTRODUCTION

In accordance with the goals of this special issue of metal-based drugs, this article deems to fulfil a teaching and guiding role in new anticancer drug research. We hope it will spawn new ideas and new research in the field of anticancer therapy. In what follows, we first create an understanding of why new anticancer drugs are vigorously searched for by highlighting some of the problems associated with a typical chemotherapeutic agent, cisplatin. One possible way to minimise the negative side effects associated with chemotherapeutic agents is to make use of a synthetic polymeric drug delivery system. We explain how such systems may significantly enhance the therapeutic effectiveness of chemotherapeutic agents and highlight some of the structural features they must have. We then develop a general synthetic strategy an experimental chemist may follow to actually synthesise a polymeric drug delivering device and proceed to visualise this strategy utilising a literature example. The need for certain structural features in a delivering device is then motivated by a discussion of the biological mechanism of cell uptake and drug release from the drug carrying device. In conclusion, the synthesis and characterisation of a new example of a polymeric drug delivery system derived from aspartic acid and lysine is presented.

2. PROBLEMS ASSOCIATED WITH CHEMOTHERAPEUTIC DRUGS

Many potentially good pharmaceutical agents are either dose limited, or excluded from use in clinical therapy due to insolubility in an aqueous medium, or because of the many severe side effects that they may exhibit. As far as cisplatin, the most successful metal-containing chemotherapeutic drug of recent times [1], is concerned, these side effects include inter alia:

(a) poor aqueous solubility;
(b) intensive damage to the linings of the intestines, which leads to the loss of appetite (anorexia) and eventually starving in the case of mice and rats [2];
(c) severe nausea, vomiting, and audio toxicity [3];

(d) high toxicity towards the kidneys and bone marrow [4];

(e) being a moderate carcinogen itself. It can induce lung cancer, skin papillomas, and other carcinomas [5].

In general, most if not all chemotherapeutic drug side effects are due to their general inability to differentiate between diseased and healthy cells [6].

Even if a synthetic chemotherapeutic drug has few side effects, it does not imply success in clinical use. One must realize that chemotherapeutic agents usually are poisons, or at the very least, they are foreign to the body. The defence mechanism of the body, the reticuloendothelial system, recognizes them as such and tries to remove them as fast as possible. A fast excretion rate from the body often proves detrimental to chemotherapy. Cisplatin, for example, is eliminated from the body in a biphasic excretion mechanism in such a way that 50% of the initial administered dose is excreted within 20 hours [7]. After 110 hours, 70% of the initial administered amount of drug is removed from the body by the reticuloendothelial system.The principle mode of excretion in mice appears primarily to be through the urine, 90% of the injected dose being excreted within five days after injection. This quick excretion rate causes large drug concentration fluctuations in the body, and hence, also unpredictable therapeutic activity, a highly undesirable situation. The negative impact of such drug concentration fluctuations in the body becomes apparent when one relates it to 50% lethal dosages (LD_{50} values), optimum dosages, and a dosage having no influence on the diseased site at all. For cisplatin [8], the LD_{50} dosage applicable to mice is 14 mg/kg mass of test animal, the optimum dose is half of this, 7 mg/kg test animal, but 3 mg/kg mass of the test animal has absolutely no influence on the diseased site at all. With the excretion profile that cisplatin shows, it is clear that it is extraordinary difficult to maintain drug levels in a patient close to the optimum dose level, but still below the LD_{50} value for prolonged times. The initial required overdose of drug that is required to maintain useful drug levels in the body explains much of the negative side effects of chemotherapeutic drugs.

A further point of consideration in developing and administering anticancer drugs is the development of drug resistance by a tumour after prolonged use.A neoplastic population of cells is not a static entity, but rather an ever-changing one. Tumours display an amazing ability to escape or neutralize the actions of chemotherapeutic agents to which they were initially sensitive [9].Some common examples of this evasive ability are as follows [10]:

(a) the loss of specific receptors;

(b) down-regulation of tumour-associated antigens; and

(c) shedding of antigens into the body fluids.

The metastatic nature of cancer cells thus leads to the development of drug resistance after continued drug dosage [11, 12].

One of the most fundamental barriers to selective drug delivery involves the so-called targeting problem. The central problem of cancer chemotherapy remains one of selective drug action.Ideally, one would like a toxic agent that can discriminate between neoplastic and nonneoplastic cells. This approach presumes the existence of something to aim at, that is, some molecular characteristic that differs between target and nontarget cells. The metastatic nature of cancer cells makes this a formidable task. Even if a target can be identified, or a cell need can be exploited, as has been done in vitro, the problem remains of actually bringing the pharmaceutical agent,in vivo, from the point of administering to the neoplastic growth. To achieve this, many physiological barriers including the reticuloendothelial system of the body have to be bypassed.

Consequently, to improve the treatment of cancer, research today focusses on developing new and better chemotherapeutic agents having less side effects (i.e., drugs that can zoom onto diseased sites) [13], new methods of drug delivery are being researched [6], combination therapy is being investigated in the hope of finding synergistic effects [14], the scope of radiation therapy is broadened, and completely new methods of combating cancer are sought.

New metal-based drugs include members of the titanocene and ferrocene family of compounds [13, 15]. A promising example of a new method of cancer treatment focusses on photodynamic therapy (PDT) [16, 17]. In PDT, the photo-active drugs in themselves are inactive towards both healthy and cancer cells. However, when light of the correct wavelength is shone on them, the drugs become photoactivated and give rise to conditions that kill the cells it is in contact with, normally via the generation of singlet oxygen. A good measure of selective cancer cell killing is therefore induced into the treatment of a patient merely by focussing light from a suitable laser source onto a tumourous growth. Healthy cells will stay largely undamaged provided that light is not shone upon it. If cancer cells would selectively and preferentially absorb the PDT drug, this would lead to a further enhancement of selective cancer cell destruction. Phthalocyanines and related macrocycles are second-generation PDT agents. Many phthalocyanine derivatives have the advantage of being preferentially absorbed by cancer cells. Some of them were found to be distributed upto 90% selectively in cancer cells, and only 10% in healthy cells after a certain induction period [18].

3. SYNTHETIC POLYMERIC DRUG DELIVERY SYSTEMS

Many detrimental properties and side effects of promising anticancer drugs may at least be partially overcome if the pharmaceutical agent is covalently anchored to a polymeric drug carrier. Polymeric or macromolecular drug-carrying devices should be distinguished from sustained drug-release systems. Sustained drug-release systems are normally associated with polymers; frequently insoluble; and in the form of powders, pellets, and capsules from which the slow release of an encapsulated drug from the "container" interior is possible. They normally do not represent systems that may affect target-specific drug delivery as much as they are devices for the continued release of drugs. The term "polymeric drug carrier" describes a polymer or macromolecule that contains covalent *binding sites* that are available to anchor active pharmaceutical units as terminal or pendent groups

protruding from the side of the polymeric chain. Polymeric drug-carrying devices may be synthetic or naturally occurring.The naturally occurring ones such as antibodies [19, 20] induce a high mode of selective drug action onto the polymeric drug-containing device, but usually suffer from a lack of large amounts of drug-anchoring sites. Synthetic polymers on the other hand are more prone to suffer from immunogenic side effects [21], but this may be overcome by copolymerisation with ethylene glycol fragments. Their big advantage is that they can be tailor-made to be suitable for almost any purposes and can be engineered to have a large amount of drug-anchoring sites.

The clinical administration of a polymer bound drug, as compared to the free agent, may significantly enhance the therapeutic effectiveness in terms of the following:

(a) accelerated and unencumbered distribution in the aqueous central circulation system of the body (the blood), thereby reducing the risks of premature degradation and excretion;
(b) they facilitate cell entry via endocytosis—a cell membrane penetration mechanism generally unavailable to nonpolymeric compounds but highly desired for drugs operating intracellularly;
(c) more precisely controlled drug serum levels (i.e., the restriction of the drug concentration to the gap between toxic and minimum effective levels);
(d) an enhanced depot effect through slow drug release from the polymer-drug conjugate.

The structural features of the polymer-drug conjugate required to comply with these attributes include the following:

(a) a highly flexible linear main chain comprising structural entities that can provide water solubility;
(b) a sufficiently large molecular mass to prevent quick excretion from the body (the threshold for elimination via the kidneys is ca. 70 000 g mol^{-1});
(c) a biodegradable carrier backbone prone to catabolic elimination of the "spent" polymer main chain after the payload of drug has been delivered to the target site;
(d) a large amount of reactive functional groups as suitable binding sites for drug attachment, these sites should be distanced from the main chain by short (5–15 constituent atoms) spacer segments to diminish the steric bulk effect of the polymeric carrier backbone, and they should be sufficiently separated from each other along the backbone to prevent intramolecular multifunctional drug binding;
(e) the separation of binding sites on the polymeric backbone requires insertion of side chains on the main chain between active binding sites that lack drug-binding capabilities, but enhance other desirable properties. These may include enhancing the hydrophilic nature of the ultimate polymeric drug-carrying device, the incorporation of moieties that enhance drug-targeting capability (i.e., a tumour homing device), antispasmodic properties, or any other desirable physiological effect;
(f) one or more biofissionable functions (amide, ester, urethane, disulphide, etc.) to be inserted into the carrier-drug connecting link. At least one of these must be sufficiently remote from the main chain to permit enzyme approach and cleavage action to result in effective drug release in a targeted biological compartment;
(g) carrier backbones and spacers which are non toxic per se. They should especially possess absolute minimal immunogenicity so as to preclude carrier-induced pathological effects. This means polymeric drug-carrying devices should be completely biocompatible.

Akey component towards the success of polymeric drug-carrying devices centres around biodegradable bonds and their capability to home preferentially onto a neoplastic growth. Apart from targeting fleeting receptors on a collection of metastatic neoplastic cells, the nutritional needs of such cells may be utilized to gain preferential neoplastic cell access. Neoplastic cells grow much faster than healthy cells, and have a much higher demand for food in the form of amino acids and energy. Hence copolymers constructed at least partially from amino acids are very attractive as polymeric drug delivery devices. They also introduce the biodegradable amide (peptide) bond. Other degradable bonds include nucleotide and sugar bonds. Sugar groups as a source of energy will especially enhance preferential uptake by neoplastic cells. Other biodegradable groups that may be employed include disulphide bonds that may be reduced to thiol groups [22], or, since cell interior has a lower pH than blood plasma, for example, weakly acid-labile groups such as thio-ethers [23].

4. SYNTHETIC STRATEGIES TOWARDS POLYMERIC DRUG DELIVERY SYSTEMS

Although models as those mentioned above for synthetic polymeric drug carriers have been in existence for some time [24], until recently only a few efforts were made to actually prepare such compounds. A review by Neuse [25] describes some of the most recent researches in this field. Scheme 1 illustrates the synthetic approach to actually obtain such polymeric drug-delivering devices. The centre of Scheme 1 serves to visualise the overall strategy. At the left and right ends of Scheme 1 an example for an actual synthesis of a polymeric drug delivery system [26] is highlighted next to each colour-coded step of the general strategy. The use of the water-soluble polyaspartic acid drug carrier not only allowed the water-insoluble parent ferrocene-containing drug to be well soluble in water in concentrations exceeding 100 g dm^{-3} but it also increased the cytotoxicity of the active drug as tested on murine EMT-6 cancer cells from an LD_{90} value of 500 $\mu g/cm^{-3}$ in the case of free 3-ferrocenylbutanoic acid to 80 $\mu g/cm^{-3}$ drug content for the polymeric drug delivery device [27].

At least two factors probably contribute to the enhanced activity of the above-mentioned polymeric drug delivery device. The first must be related to the enhanced aqueous solubility of the ferrocene drug.Free ferrocene itself, which is insoluble in water, has been shown to be completely inactive as

cytotoxic agent. The second factor centres around the use of aspartic acid as monomeric subunit in the main chain of the polymeric drug carrier. As the cancer cells have a large need for nutrients such as amino acids, the use of a polyamino acid as drug carrier may cause the drug carrying device to be absorbed faster and more efficiently by cancer cells than would be the case for the free drug.

A key factor should be observed in the synthetic sequence shown in Scheme 1. The general strategy in the middle shows the use of difunctional monomers. Aspartic acid is trifunctional. The use of tri- or higher-functional polymerization monomers is useful in the synthesis of polymeric drug carriers, as it provides a free arm where the drug may eventually be anchored. Only two of the three or more monomer functionalities should be used to obtain a linear, highly flexible, and soluble monomer. The other functional group(s) ultimately will provide drug attachment sites. However, normally the use of tri- or higher-functionalised monomers will lead to the formation of highly crosslinked, rigid, and insoluble polymers. In the case of aspartic acid, this did not happen because the formation of stable five-membered succinimide rings is thermodynamically highly favoured. It effectively masked the second carboxylic acid functional group of aspartic acid from unwanted crosslinking reactions. For other tri- or higher-functionalized amino acids, such as trifunctionalised lysine or tetrafunctionalised cystine [22], protection of the additional functional groups is required to prevent formation of pharmaceutically undesired crosslinked polymers.

5. MECHANISM OF CELL UPTAKE AND DRUG RELEASE

Uptake by neoplastic (and healthy) cells of the soluble polymeric device, shown in Scheme 1, probably occurs by endocytosis, in particular, by fluid-phase pinocytosis as described by Duncan and Kopeček [6]. As shown in Figure 1, polymers in solution are internalised by means of fluid-phase pinocytosis. Cell internalisation may also occur if the polymeric drug delivery device binds to surface cell receptors by means of adsorptive pinocytosis. They are then internalized as attachments to the infolding membrane. Polymeric drug carriers with porphyrins or phthalocyanines attached to them will probably gain access to neoplastic cells by means of adsorptive pinocytosis as this would be consistent with the selective uptake of these macrocycles by cancer cells. Mixtures of fluid-phase and adsorptive pinocytosis may also occur. It was found that pinocytotic uptake by cells of polymers bearing phenol-containing side chains was greatly enhanced [28]. Once internalized, fusion of the pinocytotic vesicles with primary lysosomes takes place to form secondary lysosomes. Release of the drug from the polymeric drug carrier inside the secondary lysosomes occurs by enzymatic hydrolysis of the biodegradable amide bonds that link the drug, ferrocene in Scheme 1, with the polymeric drug carrier, a polyaspartic acid derivative in Scheme 2. Primary lysosomes may contain more than 50 hydrolytic enzymes that are generated in the Golgi apparatus. Next, the drug and other useful low-molecular-mass degradation products like amino acids are released from the secondary lysosomes for use inside the cell nucleous. Finally, the "spent" polymer main chain and any other nondegradable material leave the cell by exocytosis.

A key factor emerges from this discussion. According to this mechanism, no drug is released outside a living cell because these drugs are not in contact with appropriate hydrolytic enzymes. As the folding pattern of the polymeric drug carrier normally inactivates the drug while polymer-bound, it means no negative side effects can be induced by the drug prior to release from the polymeric main chain. In addition, if the polymeric drug delivery device could be designed in such a way that it is internalized selectively into only neoplastic cells, the negative side effects associated with chemotherapy could be circumvented completely.

6. THE SYNTHESES OF LYSINE-BASED POLYMERIC DRUG CARRIERS

Lysine, **1**, introduces a new dimension into our discussion of the design of polymeric drug carriers. To prevent crosslinking reactions, one of the three lysine functional groups has to be protected. Here we choose to protect an amino group. One can either protect the α- or the ε-amino group, Scheme 2, to obtain lysine derivatives **3** or **4,** respectively. Only α-amino trifluoroacetyl protected lysine, **3**, is obtained by direct treatment of lysine with trifluoroacetic anhydride in trifluoroacetic acid because the ε-amino group is much more basic than the α-amino group [29]. The zwitter-ionic structure of lysine, **1**, implies that the ε-amino group is mainly in the protonated form and thus well protected against acylation reactions. However, treatment of **1** with ethyl thioltrifluoroactetate under basic conditions [30] according to the method described by Schallenberg gave N^{ε}-trifluoroacetyllysine, **4**, in 33% yield after recrystallisation from hot water/ethanol in a 2 : 3 ratio. It is advantageous to use the ε-amino group rather than the α-amino group eventually as the drug-anchoring site because it separates it far enough from the polymer main chain to allow easy enzyme approach to initiate cleavage of amide bonds to facilitate drug release from the eventual drug-carrying devices **11**–**13**.If the α-amino group is protected for later drug-anchoring purposes, the steric bulk effect of the polymeric main chain may be so large that enzyme-induced drug release will become kinetically very slow. In addition, it was also previously demonstrated [26] that drug-anchoring reactions of the type shown in Scheme 2 to generate **11**–**13** via amide bond formation proceed more effectively with compounds possessing longer side chains.

We describe here the syntheses, from N^{ε}-trifluoroacetyllysine **4**, aspartic acid **5**, and polymeric precursors **6** and **7** of polymeric drug carriers **8** and **9**, Scheme 2. We also describe how the ferrocenyl and phthalocyanine moieties may be covalently anchored to the carrier polymers **8** and **9** utilising the coupling agent **10** to obtain the polymeric drug delivery devices **11**, **12**, and **13**.

It was not very easy to predetermine reaction conditions to obtain a specific target x/y ratio in polymer **6** because of a tendency towards homopolymerisation by aspartic acid. In first experiments, **4** and **5** were thermally copolymerised in a monomer mole ratio of 1:10 (**4**:**5**) at 180°C under nitrogen and atmospheric pressure in the presence

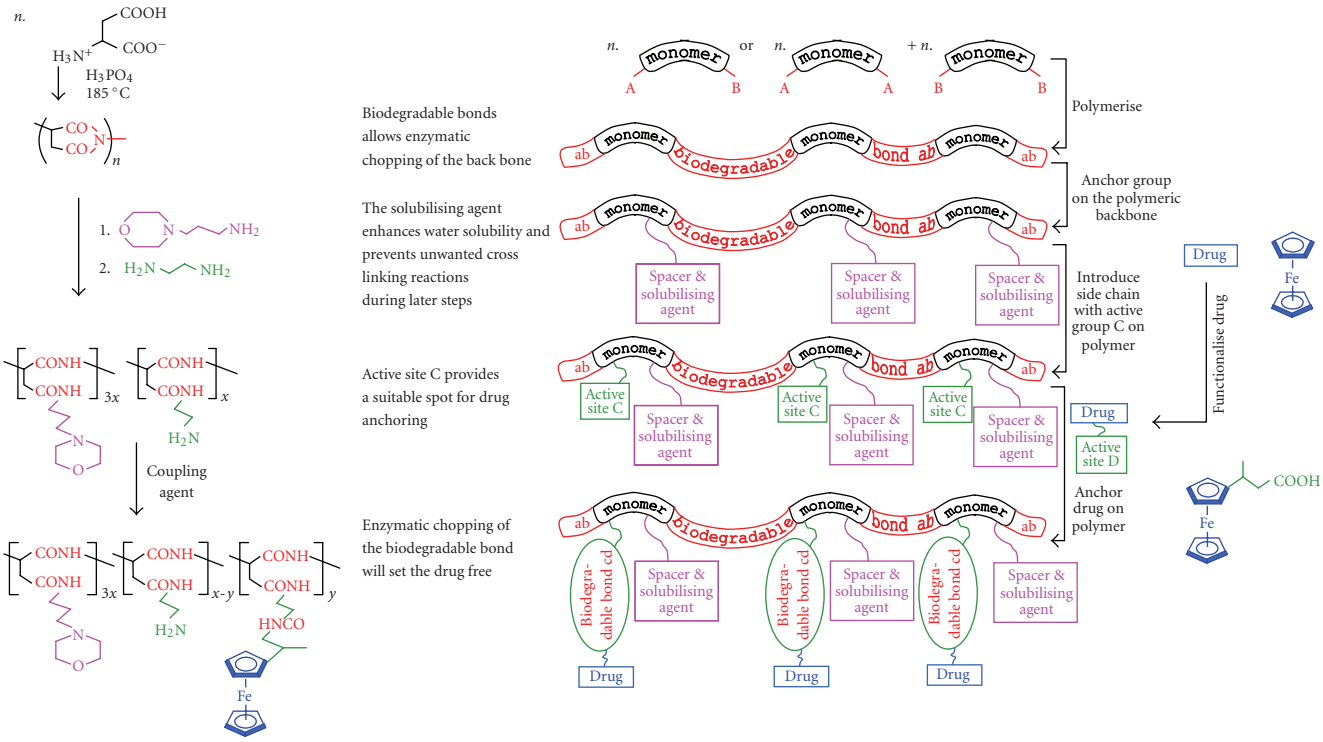

Scheme 1: *Main picture*: Colour-coded general synthetic strategy towards the syntheses of polymeric drug carrier devices. Right, in blue: functionalisation of the antineoplastic drug, ferrocene, to 3-ferrocenylbutanoic acid. Left: The synthesis of a specific ferrocene-containing drug delivery device derived from aspartic acid. The colour codes in the side portions are the same as those used in the central main picture. The main picture was reproduced with permission from copyright owner "International Union of Pure and Applied Chemistry." An adaption of the main part of this scheme was previously published as follows: J. C. Swarts, in *Macromol. Sym.*, Eds. K. Levon and A. Guiseppi-Elie), vol 186, pages 123–128, 2002; Copyright Wiley-VCH Verlag GmbH & Co. KgaA, reproduced with permission.

of a polyphosphoric acid (PPA) mass fraction of 0.8 for 8 hours. Two products were isolated. The first was extracted with water, and after dialysis in an 8,000 molecular mass cut-off membrane tubing, **6** was isolated having an x/y = 2.6/1 ratio, and inherent viscosity η_{inh} = 0.06 dl g^{-1} in 3% yield, m.p = 301°C (dec.). The x/y ratio was established by comparing the ^{1}H NMR signal integrals at 5.1–5.5 ppm (CH of imide, one proton per closed imide unit), 4.4–4.6 ppm (CH of aspartic acid, the integral values showed only 65% ring closure of the aspartic acid recurring unit occurred), with that of the combined β, γ, and δ methylene protons of the lysine recurring unit (6 protons per lysine recurring unit) at 0.9–1.8 ppm.The remaining water-insoluble residue was dissolved in DMF and precipitated with ethanol to yield 56% polymer having η_{inh}(DMF) = 0.07 dl g^{-1}, m.p = 286°C (dec.) In this case, the x/y unit ratio was established by ^{1}H NMR as 22/1. The percentage of aspartic acid ring closure was found to be ca. 97%. The remainder of material had molecular mass <8,000 g mol^{-1}, and was dialysed away.

When **4** and **5** were thermally co-polymerised in a monomer mole ratio of 1:6 = **4**:**5**, other conditions still being the same, the water-soluble fraction was isolated in 8% possessing a monomer ratio of x/y = 1.4/1.The DMF-soluble fraction was isolated in 30% yield having a monomer ratio of x/y = 25/1. In another experiment, when the PPA mass fraction was lowered from 0.8 to 0.5, the water-soluble fraction was very small, but the DMF-soluble fraction was isolated in 50% yield having also a monomer ratio of x/y = 25/1.

The above results showed that **4** and **5** have a tendency to homopolymerise. The low lysine content in each recovered fraction was attributed to the tendency of α-amino acids to form 6-membered diketopiperazine rings upon heating [31]. In the case of **4**, this would result in termination of any polymerisation process, and account also for the large % of low-molecular-mass material that was lost upon dialyses. ^{13}C NMR spectroscopy showed that the trifluoroacetyl protective group did not survive the polymerisation conditions. However, loss of the trifluoroacetyl protective group must have happened in the latter stages of polymerisation, since no insoluble portion was found in the workup of **6**. Crosslinking was, therefore, ruled out as the cause of the relatively moderate yields.

Further experiments focussed exclusively on a 1:2 = **4**:**5** monomer mole ratio in a PPA mass fraction of 0.5 at 180°C for only 2.5 hours at pressures below 2 torr. These conditions resulted in almost no water-soluble fraction (<1%), and a DMF-soluble fraction (18% yield, decomposition temperature = 269°C) having a repeating unit ratio of x/y = 7/1 and 29% of aspartic acid fragments still uncyclised. ^{13}C NMR showed that the trifluoroacetyl protective group remained intact when using these shorter reaction times. By substituting PPA with 85% ortho H_3PO_4, repeated experiments gave

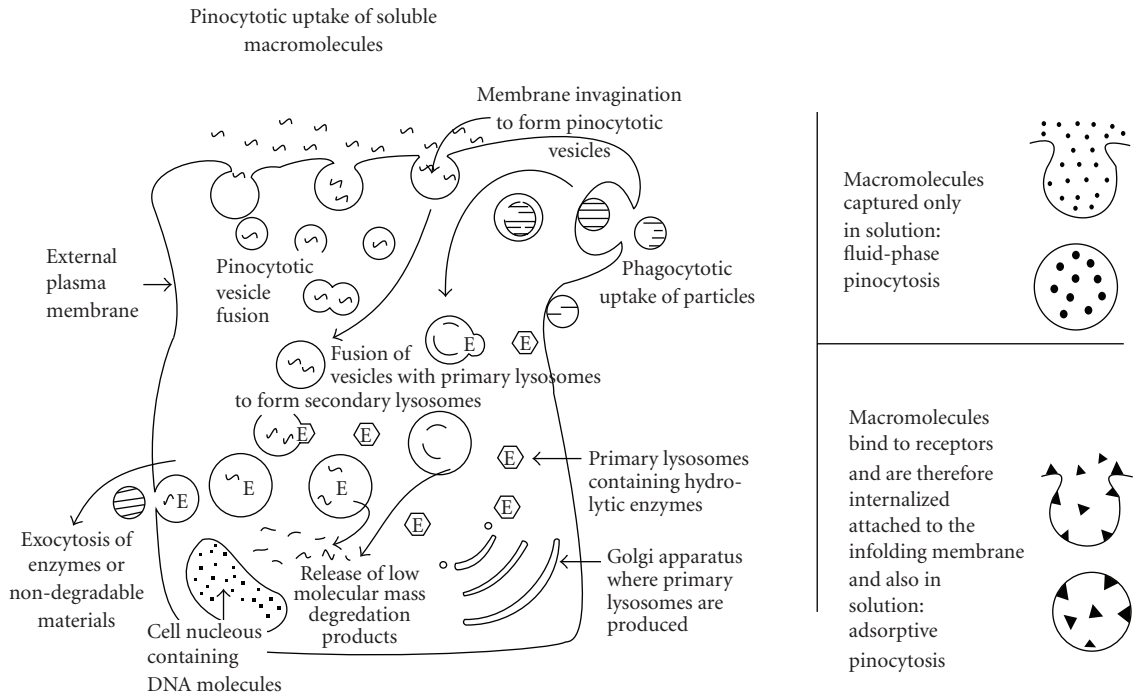

Figure 1: Mechanism of drug uptake and release inside cells. Diagram reproduced with permission from copyright owner "International Union of Pure and Applied Chemistry." It was previously published as follows: J. C. Swarts, in *Macromol. Sym.*, Eds. K. Levon and A. Guiseppi-Elie), vol 186, p123–128, 2002; Copyright Wiley-VCH Verlag GmbH & Co. KgaA, reproduced with permission.

products having recurring unit ratios ranging $2/1 < x/y < 5/1$. Yields were slightly higher (25%). The increase in yield and better recurring unit ratios probably arose because it is easier to mix **4** and **5** to a homogeneous distribution in ortho H_3PO_4 than in PPA. Lower reaction temperatures (140°C) lowered yields substantially to only 6% and virtually the entire product became water-soluble, even after 7 hours of reaction time. Dialyses were again performed in 8,000 molecular mass membrane tubing. The absence of any ^{1}H NMR signals at 5.25 ppm, as well as the presence of the signal at 4.2–4.6 ppm showed that for this product, ring closure of the aspartic acid fragment did not occur. It had a repeating unit ratio of $x/y = 4/1$ as compared to the target of 2/1. ^{13}C NMR showed that the trifluoroacetyl protective group remained intact under these conditions of decreased temperatures even though the reaction time was increased to 7 hours.

Nucleophilic attack of amines on the succinimide rings of polymeric precursor **6** takes place with ease, and the success rate is independent of x/y ratios. By choosing the correct nucleophiles, the solubility properties of choice may be introduced to the carrier polymer. Here, the 3-aminopropyl morpholine unit was used to generate water-soluble **8** in 83% yield after stirring the intermediate product **7** with 2% NaOH solution to remove the trifluoroacetyl protecting group and dialysis in 8,000 molecular mass cutoff membrane tubing. Although intermediate **7** can be isolated *en route* to **8**, this is not necessary. One can go directly from **6** to **8** without isolation of **7**. 2-Phenylethyl amine was used to generate white, water-insoluble **9** in 90% yield after removal of the protective group and slow precipitation with water from a DMF solution.

To demonstrate the carrier capabilities of **8** and **9**, the antineoplastic ferrocenyl moiety [15] and an example of the family of drugs that may be used in photodynamic cancer therapy [17], a phthalocyanine, have been anchored on these polymeric drug carriers. Both ferrocene and phthalocyanine are insoluble in water when not functionalised, or as carboxylic acid derivatives. Even as sodium carboxylates, they are poorly soluble in water. However, once anchored on the polymeric drug carrier **8**, the ferrocene-containing derivative **11** was soluble in excess of 30 g/dm^3, while the phthalocyanine derivative exceeded an aqueous solubility of ca. 5 g dm^{-3} at pH's more extreme than those found in the gastrointestinal system (1–8.5) [32, 33]. However, prior to drug anchoring, the ferrocene and phthalocyanine fragments needed to be modified in such a way that coupling with the available amine active sites on the polymeric drug carriers **8** and **9** is possible. To generate a biodegradable bond between drug and polymeric carrier, formation of a peptide (i.e., amide), saccharide, or nucleotide bonds [34] is desirable. Here, the amide bond was aimed for as a biodegradable bond linking carrier to drug. Thus, 3-ferrocenylbutanoic acid [35] and cobaltotetracarboxyphthalocyanine [36] were prepared according to known procedures for later reaction with the amine-containing polymeric carrier devices **8** and **9**.

Although polymers **8** and **9**, the ferrocene-containing derivatives **11** and **13**, and the phthalocyanine-containing derivative **12** are robust, frequently the drug moiety of

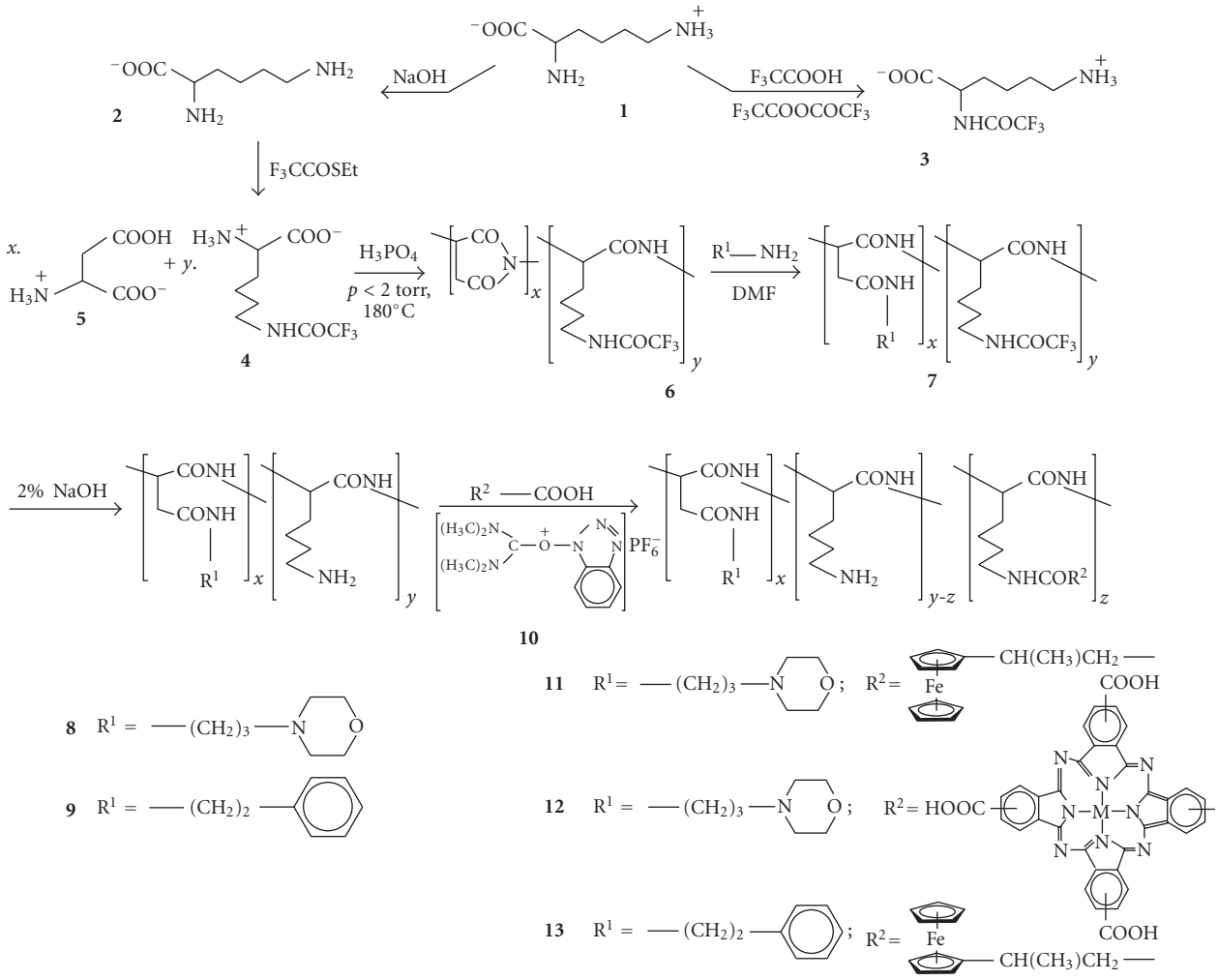

Scheme 2: Syntheses of polymeric drug carrying devices **11**, **12** (M = Co), and **13**. For PDT applications, M = Zn or Cl–Al would be more appropriate [18]. All polymers have a random recurring unit arrangement in the backbone. The indicated structures are meant to show building block ratios rather than block polymers. Opening of the succinimide rings of **6** with nucleophiles R^1-NH_2 lead to a mixture of α and β ring-opened aspartates. For convenience, only the α-form is shown.

interest (as opposed to the drug carrier) may be very labile. It is advantageous, therefore, to be able to anchor the drug onto the polymeric carrying device under very mild conditions in order to preserve labile moieties. Also, coupling procedures need to be developed that will allow coupling in media in which both the water-soluble drug carrier, here **8** and **9**, and poorly soluble or aqueous-insoluble drug may be partially dissolved or suspended. Coupling with the aid of O-benzotriazolyl-N,N,N′,N′-tetramethyluronium hexafluorophosphate, **10**, at room temperaturein DMF or DMSO, sometimes with THF or water as cosolvent, satisfies this requirement [26]. 24-hour reactions between tetracarboxyphthalocyanine and **8** with a x/y ratio of 3/1 in the presence of this coupling agent led to only ca. 10% phthalocyanine binding in **12** as ascertained by ^{1}H NMR utilising the phthalocyanine phenyl aromatic proton signal (12 hours per phthalocyanine group) at ca. 7.3 ppm and the $–CH_2–O–CH_2$ morpholine signals (4 hours per morpholine group) at 3.6 ppm. This result means $z = 0.1y$.

The closeness of the COOH functional group in the phthalocyanine moiety had two effects, both associated with an extremely slow coupling rate due to the closeness of the bulky phthalocyanine core (slow coupling reactions because of steric crowding have already been commented on, and are described in reference 25). Firstly, it explains the low binding efficiency ($z = 0.1y$) of cobaltotetracarboxyphthalocyanine to polymeric drug carrier **8**. Secondly, it explains why crosslinking reactions involving cobaltotetracarboxyphthalocyanine apparently did not take place to a noticeable extent. As ascertained by ^{1}H NMR, no precipitate from the dialysis tubing other than free cobaltotetracarboxyphthalocyanine (i.e., unbound) could be found.

In contrast, 3-ferrocenylbutanoic acid was anchored to a derivative of **8** having a x/y ratio of 2/1 ca. 70–80% effectively (i.e., $z_{\text{average}} = 0.75y$) within 1 hour at room temperature to give **11** as product. This result was obtained by comparing ^{1}H NMR signals (obtained in D_2O) of the $–CH_2–O–CH_2$ morpholine signals (4 hours per morpholine group) at 3.53 ppm

with those of the CH_3 substituent in 3-ferrocenylbutanoic acid at 1.1 ppm (it is a well-defined peak that can be uniquely identified next to the lysine signals), the combined β, γ, and δ methylene protons of the lysine recurring unit (6 protons per lysine recurring unit) at 1.2–1.6 ppm, and the aspartate CH protons at 4.2–4.5 ppm. An atomic absorption iron elemental analysis for **11** with $x/y = 2/1$ showed an iron content of 4.8% which corresponds to $z = 0.67y$. CHN elemental analyses were not performed.

Coupling of 3-ferrocenylbutanoic acid to a derivative of **9** with x/y ratio 3/1 to obtain **13** in DMF as solvent was more successful, probably because there was no solvent water present during the coupling reaction, see experimental. By comparing the integral values of the phenyl group ^{1}H NMR signals (in DMSO-d_{6-x}) at 7.15 ppm with those of the CH_3 substituent in 3-ferrocenylbutanoic acid at 1.2 ppm (it is a well-defined peak that can be uniquely identified between the lysine signals) and the combined β, γ, and δ methylene protons of the lysine recurring unit (6 protons per lysine recurring unit) at 0.9–1.6 ppm, it was ascertained that the ferrocenyl group was anchored 94% efficiently, that is, $z = 0.94y$. An atomic absorption iron elemental analysis for **13** with x/y = 3/1 showed an iron content of 5.08% which corresponds to $z = 0.87y$. CHN elemental analyses were not performed.

The water-insoluble polymer **12** is of particular interest because it demonstrates two separate functional moieties can be supported on the same polymer drug carrier, here phenyl and ferrocenyl. This begs the question: "can more than one antineoplastic group be anchored on the same polymeric drug carrier?" If this would be possible, combination therapy would be possible without administering more than one type of drug in separate doses to a patient. The synergistic effect usually associated with combination therapy [36, 37] would then be potentially obtainable in a single drug dose by binding to the carrier polymer all the drugs required. This topic is at present being researched. Biological studies are at the moment in progress to determine if present lysine-containing polymeric drug-carrying devices **11** and **12** can compare in efficiency with previously described polyaspartic acid drug-delivering systems [26].

7. EXPERIMENTAL

Equipment and materials

All organic solvents were distilled prior to use, water was double-distilled. Chemicals were from Merck & CO., Inc. (NJ, USA) or Sigma-Aldrich and used without further purification. Melting points are uncorrected.NMR measurements, at 298 K, were recorded on a Bruker Advance DPX 300 NMR spectrometer. Chemical shifts are reported as δ values relative to $SiMe_4$ at 0 ppm. Infrared spectra were recorded on a Hitachi 270–50 infrared spectrometer in a KBr matrix. Viscosity measurements were made in a Cannon-Fenske tube at 35.2°C in water or DMF. Dialysis was performed in 8,000 molecular mass cutoff cellulose membrane tubing. Iron analyses were performed on a Varian Techtron atomic absorption spectrometer at 272 nm.

Syntheses

N^{ε}-trifluoroacetyllysine, **4**, [30] and cobalto tetracarboxyphthalocynanine [36] were prepared as described before.

A representative example of the synthesis of polymer **6**: Aspartic acid (1.331 g; 10 mmol), N^{ε}-trifluoroacetyllysine (1.211 g; 5 mmol), and polyphosphoric acid (2.542 g) were thoroughly mixed in a 250 cm^3 round-bottom flask. The flask was mounted on a rotating evaporator, and lowered (while rotating slowly) into an oil bath preheated to 180°. The pressure was reduced after 5 minutes to below 2 torr with the aid of a mechanical pump. After 2.5 hours of slow rotation the reaction mixture was allowed to cool and thoroughly extracted with water. Dialyses of the water extract for 16 hours gave after freeze drying only a negligible quantity of product. The remaining residue after water extraction was dissolved in 20 cm^3 DMF. Precipitation by ethanol afforded 0.38 g (18%) of **6**; η_{inh}(DMF) = 0.08 dl g^{-1}, x/y = 7/1 (see discussion text for conditions to obtain other x/y ratios); m.p. 295°C (dec.). ^{1}H NMR (DMSO-d_{6-x}): 0.9–1.8 (6H; β, γ and δ CH_2's of lysine); 2.1 (3.8 H; CH_2 of open aspartic acid fragment); 2.6–2.9 (4.8 H; CH of succinimide); 3.0–3.4 (4.8 H; CH of succinimide); 4.4–4.6 (1.9 H; CH of aspartic acid fragment); 5.1–5.5 (4.8 H; CH of succinimide). ^{13}C NMR (DMSO-d_{6-x}): 110–122, q, CF_3; 155-156, q, $\underline{CO}CF_3$. IR: 1798, 1720 (C=O); 1219,1189 (CF_3).

Polymers **7**, and **9**: A solution of 0.21 g [0.5 mmol, η_{inh} = 0.08 dl g^{-1}, x/y = 3/1] of **6** and 2-phenylethyl amine (0.202 g; 2 mmol) in 5 cm^3 DMF was stirred for 5 hours at ambient temperature. The newly formed **7** was not isolated (although it can be by precipitation with ethanol or water), but stirred for 5 hours with 20 cm^3 of a 2% NaOH solution. The resulting clear reaction mixture was dialysed for 16 hours, and freeze dried to give 0.24 g (90% yield) of **9** as a white solid which would not redissolve in pure water, but was soluble in DMSO and DMF; η_{inh}(DMF) = 0.07 dl g^{-1}; x/y = 3; m.p 275°C (dec.).

Polymer **8**: This polymer was obtained in exactly the same way as polymer **9**, but by replacing 2-phenylethyl amine with 3-aminopropyl morpholine (0.289 g; 2 mmol), and the x/y ratio of **6** was 2/1. Characterisation data for **8** : yield = 83%; η_{inh} = 0.06 dl g^{-1}; x/y = 2; m.p. 196°C (dec.). Unlike **9**, this polymer remained water-soluble after dialysis and freeze drying.

Polymer **11**: To a solution of 0.2g (0.24 mmol; η_{inh} = 0.06 dl g^{-1}; x/y = 2) of **8** in 1 cm^3 water was added (in the correct order) 0.035 g (0.35 mmol) triethylamine, a solution of 0.068 g (0.25 mmol) 3-ferrocenylbutanoic acid in 1 cm^3 THF (the THF may be replaced with DMF) and 0.114 g (0.3 mmol) of O-benzotriazolyl-N,N,N′,N′-tetramethyluronium hexafluorophosphate, **10**. The mixture was stirred for one hour at room temperature during which time the heterogeneous mixture homogenized. Water (10 cm^3) was added to the reaction mixture before it was centrifuged, dialysed for 16 hours in an 8,000 molecular mas cutoff membrane tubing and freeze dried to give 0.11 g (44%) of **11**; η_{inh} = 0.04 dl g^{-1}; $x : y : z$ = 2.00:0.35:0.65; m.p. 88°C, dec. at 105°C; Fe anal. 4.8% (req. 4.8% for $z = 0.65y$). ^{1}H NMR (D_2O): 1.0–1.2 (0.65 of 3H, CH_3); 1.2–1.6 (6H; β, γ

and δ CH_2's of lysine); 3.53 (8H, CH_2–O–CH_2 of morpholine), 3.9–4.2 (0.65 of 9H, $C_{10}H_9Fe$); 4.2–4.6 (3H, CH of aspartate). IR/cm^{-1}: 1660 (C=O); 1550 (NH).

Polymer **12**: The same procedure was used as for **11** except that the solvents were all DMF, 3-ferrocenylbutanoic acid was replaced with an equivalent amount of cobalto tetracarboxyphthalocyanine and the reaction time was increased to 24 hours. Characterisation data: 44% yield; η_{inh} = 0.04 dl g^{-1}; $x : y : z$ = 2.0:0.9:0.1; m.p. 194°C (dec.); ^{1}H NMR (D_2O): 1.2–1.6 (6H; β, γ and δ CH_2's of lysine); 3.53 (8H, CH_2–O–CH_2 of morpholine); 4.2–4.6 (3H, CH of aspartate) 7.3–8.3 (0.1 of 12H, phthalocyanine aromatics); IR/cm^{-1}: 1720, 1660 (C=O); 1550 (NH).

Polymer **13**: The same procedure was used as for **12**, except that **8** was replaced by an equivalent amount of **9**, tetracarboxyphthalocyanine was replaced with a solution of 0.068 g (0.25 mmol) 3-ferrocenylbutanoic acid dissolved in 1 cm^3 DMF and the reaction was allowed to proceed for 1 hour only. Characterisation data: 64% yield; η_{inh} = 0.04 dl g^{-1}; $x : y : z$ = 3.00:0.13:0.87; m.p. 180°C (dec.); Fe anal. 5.1% (req. 5.1% for $z = 0.87y$. ^{1}H NMR (DMSO-d_{6-x}): 1.2 (0.87 of 3H, CH_3); 0.9–1.6 (6H; β, γ and δ CH_2's of lysine); 4.1-4.2 (0.87 of 9H, $C_{10}H_9Fe$); 4.2–4.6 (4H, CH of aspartate). 7.1–7.3 (15 H, C_6H_5). IR/cm^{-1}: 1655 (C=O); 1553 (NH).

8. CONCLUSIONS

In summary, it was shown that upon using the thermal polymerisation technique, aspartic acid and N^{ε}-trifluoroacetyllysine both have a tendency to homopolymerise. This tendency becomes stronger as reaction conditions become harsher, such as higher temperatures, longer reaction times, or lowering of pressures. Less harsh conditions diminish the tendency to homopolymerisation but also reduce yields. Ring closure of the aspartic acid fragment becomes progressively less efficient when milder reaction conditions are employed. It was also shown that the trifluoroacetyl protective group is less stable at elevated temperatures for prolonged periods of time. Chemical removal of the trifluoroacetyl protective group was achieved under mild alkaline conditions to liberate free amino groups on side chains of lysine-containing potential polymeric drug carriers. Coupling of a carboxylic acid-functionalised ferrocene with the amine-containing polymeric drug carrier was effectively achieved utilising O-benzotriazolyl-N,N,N′,N′-tetramethyluronium hexafluorophosphate as coupling agent. Coupling reactions were more efficient in the absence of water as cosolvent. Coupling of cobaltotetracarboxyphthalocyanine was much less successful. This was presumably due to the poor solubility of cobaltotetracarboxyphthalocyanine in the required solvents.

ACKNOWLEDGMENT

The authors acknowledge financial support from the Central Research Fund of the University of the Free State and the South African NRF under Grant 2054243.

REFERENCES

[1] S. E. Sherman and S. J. Lippard, "Structural aspects of platinum anticancer drug interactions with DNA," *Chemical Reviews*, vol. 87, no. 5, pp. 1153–1181, 1987.

[2] J. M. Ward, M. E. Grabin, E. Berlin, and D. M. Young, "Prevention of renal failure in rats receiving *cis* diamminedichloroplatinum(II) by administration of furosemide," *Cancer Research*, vol. 37, no. 4, pp. 1238–1240, 1977.

[3] M. Rozencweig, D. D. Von Hoff, M. Slavik, and F. M. Muggia, "Cis diamminedichloroplatinum (II). A new anticancer drug," *Annals of Internal Medicine*, vol. 86, no. 6, pp. 803–812, 1977.

[4] M. F. Pera, B. C. Zook, and H. C. Harder, "Effects of mannitol or furosemide diuresis on the nephrotoxicity and physiological disposition of *cis*-dichlorodiammineplatinum-(II) in rats," *Cancer Research*, vol. 39, no. 4, pp. 1269–1278, 1979.

[5] W. R. Leopold, E. C. Miller, and J. A. Miller, "Carcinogenicity of antitumor *cis*-platinum(II) coordination complexes in the mouse and rat," *Cancer Research*, vol. 39, no. 3, pp. 913–918, 1979.

[6] R. Duncan and J. Kopeček, "Soluble synthetic polymers as potential drug carriers," *Advances in Polymer Science*, vol. 57, pp. 51–101, 1984.

[7] W. Wolf and R. C. Manaka, "Synthesis and distribution of ^{195}Pt(m) *cis* dichlorodiammine platinum(II)," *Journal of Clinical Hematology and Oncology*, vol. 7, no. 1, pp. 79–95, 1977.

[8] M. K. Wolpert-DeFillippes, "Antitumor activity of *cis*-dichlorodiammineplatinum(II)," *Cancer Treatment Report*, vol. 63, pp. 1453–1458, 1979.

[9] G. B. Pierce, "Differentiation of normal and malignant cells," *Federation Proceedings*, vol. 29, no. 3, pp. 1248–1254, 1970.

[10] E. Cohen and W. Liang, in *Membranes and Neoplasia*, V. Marchesi, Ed., p. 23, Alan R. Liss, New York, NY, USA, 1976.

[11] J. H. Burchenal, K. Kalaher, T. O'Toole, and J. Chisholm, "Lack of cross resistance between certain platinum coordination compounds in mouse leukemia," *Cancer Research*, vol. 37, no. 9, pp. 3455–3457, 1977.

[12] J. H. Burchenal, K. Kalaher, K. Dew, L. Lokys, and D. G. Gale, "Studies of cross-resistance, synergistic combinations and blocking of activity of platinum derivatives," *Biochimie*, vol. 60, no. 9, pp. 961–965, 1978.

[13] P. Köpf-Maier and H. Köpf, "Non-platinum-group metal antitumor agents: history, current status, and perspectives," *Chemical Reviews*, vol. 87, no. 5, pp. 1137–1152, 1987.

[14] G. R. Gale, L. M. Atkins, and S. J. Meischen, "Chemotherapy of advanced L1210 leukemia with platinum compounds in combination with other antitumor agents," *Cancer Treatment Reports*, vol. 61, no. 3, pp. 445–450, 1977.

[15] P. Köpf-Maier, H. Köpf, and E. W. Neuse, "Ferricenium complexes: a new type of water-soluble antitumor agent," *Journal of Cancer Research and Clinical Oncology*, vol. 108, no. 3, pp. 336–340, 1984.

[16] W. M. Sharman, C. M. Allen, and J. E. van Lier, "Photodynamic therapeutics: basic principles and clinical applications," *Drug Discovery Today*, vol. 4, no. 11, pp. 507–517, 1999.

[17] H. Ali, R. Langlois, J. R. Wagner, N. Brasseur, B. Paquette, and J. E. van Lier, "Biological activities of phthalocyanines—X: syntheses and analyses of sulfonated phthalocyanines," *Photochemistry and Photobiology*, vol. 47, no. 5, pp. 713–717, 1988.

[18] I. Rosenthal and E. Ben-Hur, "Developments in photobiology of phthalocyanines," in *Phthalocyanines, Properties and Applications*, C. C. Leznoff and A. B. P. Lever, Eds., vol. 1, p. 416, VCH, New York, NY, USA, 1989.

[19] P. J. Kelleher, H. L. Mathews, G. E. Moore, and P. Minden, "The use of cellular immunoadsorbents to prepare polyclonal antibodies that distinguish between antigens derived from human melanoma cells and autologous lymphocytes," *Cancer Immunology, Immunotherapy*, vol. 14, no. 3, pp. 191–195, 1983.

[20] M. B. Omary, I. S. Trowbridge, and J. Minowada, "Human cell-surface glycoprotein with unusual properties," *Nature*, vol. 286, no. 5776, pp. 888–891, 1980.

[21] A. Abuchowski, T. van Es, N. C. Palczuk, and F. F. Davis, "Alteration of immunological properties of bovine serum albumin by covalent attachment of polyethylene glycol," *Journal of Biological Chemistry*, vol. 252, no. 11, pp. 3578–3581, 1977.

[22] U. Chiba, E. W. Neuse, J. C. Swarts, and G. J. Lamprecht, "Water-soluble polyamides as potential drug carriers—VII: synthesis of polymers containing intrachain- or extrachain-type amine ligands by interfacial polymerization," *Angewandte Makromolekulare Chemie*, vol. 214, no. 1, pp. 137–152, 1994.

[23] A. S. J. Stewart and C. N. C. Drey, "Selective protection of cysteine with ferrocene derivatives—part 2: synthesis of glutathione," *Journal of the Chemical Society-Perkin Transactions*, no. 1, pp. 1753–1756, 1990.

[24] H. Ringsdorf, "Structure and properties of pharmacologically active polymers," *Journal of Polymer Science*, vol. 51, pp. 135–153, 1975.

[25] E. W. Neuse, "Macromolecular ferrocene compounds as cancer drug models," *Journal of Inorganic and Organometallic Polymers*, vol. 15, no. 1, pp. 3–31, 2005.

[26] J. C. Swarts, E. W. Neuse, and G. J. Lamprecht, "Synthesis and characterization of water-soluble polyaspartamide-ferrocene conjugates for biomedical applications," *Journal of Inorganic and Organometallic Polymers*, vol. 4, no. 2, pp. 143–153, 1994.

[27] J. C. Swarts, D. M. Swarts, M. D. Maree, E. W. Neuse, C. La Madeleine, and J. E. van Lier, "Polyaspartamides as water-soluble drug carriers—part 1: antineoplastic activity of ferrocene-containing polyaspartamide conjugates," *Anticancer Research*, vol. 21, no. 3B, pp. 2033–2037, 2001.

[28] R. Duncan, D. Starling, F. Rypacek, J. Drobnik, and J. B. Lloyd, "Pinocytosis of poly(α,β-(N-2-hydroxyethyl)-DL-aspartamide and a tyramine derivative by rat visceral yolk sacs cultured in vitro. Ability of phenolic residues to enhance the rate of pinocytic capture of macromolecule," *Biochimica et Biophysica Acta*, vol. 717, no. 2, pp. 248–254, 1982.

[29] F. Weygand and R. Geiger, "*N*-Trifluoracetyl-aminosäuren—IV: Mitteil.: *N*-Trifluoracetylierung von Aminosäuren in wasserfreier Trifluoressigsäure," *Chemische Berichte*, vol. 89, no. 3, pp. 647–652, 1956.

[30] E. E. Schallenberg and M. Calvin, "Ethyl thioltrifluoroacetate as an acetylating agent with particular reference to peptide synthesis," *Journal of the American Chemical Society*, vol. 77, no. 10, pp. 2779–2783, 1955.

[31] H. Meislich, H. Nechamkin, and J. Sharefkin, *Theory and problems of Organic Chemistry*, Schaum's Outline Series, McGraw-Hill, New York, NY, USA, 1980.

[32] J. Calam, *Clinicias' Guide to Helicobacter Pylori*, Chapman and Hall Medical, London, UK, 1996.

[33] T. Nogrady, *Medicinal Chemistry*, Oxford University Press, New York, NY, USA, 1988.

[34] C. de Duve, T. de Barsy, B. Poole, A. Trouet, P. Tulkens, and F. Van Hoof, "Commentary. Lysosomotropic agents," *Biochemical Pharmacology*, vol. 23, no. 18, pp. 2495–2531, 1974.

[35] P. da Re and E. Sianesi, "Condensation reactions of formyl- and acetyl-ferrocene," *Experientia*, vol. 21, no. 11, pp. 648–649, 1965.

[36] H. Shirai, M. Maruyama, K. Kobayashi, N. Hojo, and K. Urushido, "Functional metal-porphyrazine derivatives and their polymers .4. synthesis of poly(styrene) bonded Fe(III)-4,4′,4″,4‴ as well as Co(II)-4,4′,4″,4‴-tetracarboxyphthalocyanine and their catalase-like activity," *Makromolekulare Chemie-Macromolecular Chemistry And Physics*, vol. 181, p. 575, 1980.

[37] G. R. Gale, L. M. Atkins, S. J. Meischen, and P. Schwartz, "Synergistic action of high dose hydroxyurea when used with cyclophosphamide and certain new organoplatinum complexes in treatment of advanced L1210 leukemia," *Cancer*, vol. 41, no. 4, pp. 1230–1234, 1978.

Hindawi Publishing Corporation
Metal-Based Drugs
Volume 2008, Article ID 281843, 5 pages
doi:10.1155/2008/281843

Research Article

Phthalocyanine-Based Molecularly Imprinted Polymers as Nucleoside Receptors

Luigia Longo and Giuseppe Vasapollo

Dipartimento di Ingegneria dell'Innovazione, Università del Salento, 73100 Lecce, Italy

Correspondence should be addressed to Giuseppe Vasapollo, giuseppe.vasapollo@unile.it

Received 5 September 2007; Accepted 31 October 2007

Recommended by Jannie C. Swarts

A molecularly imprinted polymer (MIP) for tri-O-acetyladenosine (TOAA), PPM(TOAA), was prepared by the combined use of methacrylic acid (MAA) and Zn(II)tetra(4'-methacryloxyphenoxy) phthalocyanine as functional monomers. This MIP exhibited a higher binding ability for TOAA compared to the MIP prepared using only MAA, PM(TOAA), in batch rebinding tests. Scatchard analysis gave a higher association constant of PPM(TOAA) for TOAA ($2.96 \times 10^4\ M^{-1}$) than that of PM(TOAA) ($1.48 \times 10^4\ M^{-1}$). The MIP prepared using only the zinc-phthalocyanine, PP(TOAA), did not show any binding capacity for TOAA. This means that the phthalocyanine in the MIP contributes to higher affinities, although it barely interacts with TOAA. Since selectivity for this kind of MIPs is more important than binding affinity, the binding of TOAA and a structurally related compound, tri-O-acetyluridine (TOAU), on the polymers was investigated. Both PPM(TOAA) and PM(TOAA) exhibited binding affinities for TOAA while they did not show any binding capacity for TOAU.

1. INTRODUCTION

Molecularly imprinted polymers (MIPs) have received much attention recently as new materials capable of molecular recognition [1]. They have been extensively utilized in solid-phase extraction [2–5], chromatography [6–8], sensing [9, 10], and catalysis [11–13]. During molecular imprinting, crosslinked polymers are formed by free-radical copolymerization of functional monomers with an excess of crosslinker around an analyte that acts as a template. After polymerization, the template is removed leaving in this way selective binding sites in the polymer network that are complementary in form and functionality to the analyte molecules [1].

The main advantages of MIPs, over conventional polymers used as separation material, are the high selectivity and affinity for the target analytes used in the imprinting procedure. Furthermore, MIPs are characterized by superior mechanical and thermal stability, as well as better inertness towards acids, bases, metal ions, and organic solvents compared to enzymes. In addition, imprinting polymerization is a very inexpensive procedure for the development of artificial receptors. In the majority of the cases, the price of an MIP depends entirely on the price of the template used. Moreover, if the template is expensive, it is possible to recover the template and use it again. Alternatively, inexpensive template analogues can be used for the preparation of MIPs [1].

In most studies, methacrylic acid (MAA) was used as functional monomer to synthesize MIPs making the polymer preparation a simple and facile process [14–16]. MAA can form hydrogen bonds with the template molecule in porogen prior to polymerization. A more deliberate approach using synthetically designed functional monomers could enable a better control in the formation of high-affinity binding sites for each corresponding template minimizing, at the same time, the inherent nonspecific binding properties common in noncovalent imprinted polymers.

In this paper, we report for the first time the preparation of MIPs as nucleoside receptors using both methacrylic acid and a zinc-phthalocyanine peripherally substituted with methacrylic groups (Compound 1, Scheme 1) [17] as functional monomers. The receptor site is a three-dimensional cavity around the phthalocyanine plane in crosslinked polymers to which the analyte molecule could be specifically bound via coordination through the metal of the phthalocyanine and hydrogen bonding/electrostatic interaction

with MAA and the modifiers linked to the phthalocyanine (Scheme 1). Such cooperative interaction approach in MIP formation, already proposed for porphyrin derivatives [18–21], was applied here for the first time to phthalocyanine compounds.

An organic soluble nucleoside derivative, tri-O-acetyladenosine (TOAA), was utilized in this work as template in the preparation of phthalocyanine-based MIPs. The development of synthetic receptors that recognize nucleotide bases and their derivatives is an important area in chemistry today. The literature provides many examples of artificial receptors for each of the common nucleoside bases [15, 16, 22–25]. Recently, these receptors have provided insights into DNA-DNA and protein-DNA interactions, and applications are envisioned in the fields of biosensors, drug therapy, separation science, and genetic engineering. TOAA was selected as model template in a previous work [17] where the binding affinity and selectivity of the zinc-phthalocyanine 1 towards different nucleosides were evaluated by UV-vis titration experiments. Binding experiments showed that zinc-phthalocyanine 1 bounds TOAA most strongly, giving a binding constant K_a of 1.35×10^4, 500 times that of 1 to tri-O-acetyluridine (TOAU), showing in this way a high selectivity [17]. The presence of the 2-aminopyridine moiety in the structure of TOAA could be probably responsible for the good binding characteristics of this nucleoside derivative with compounds functionalized with methacrylic groups [15].

An imprinted polymer receptor for TOAA, namely, PPM(TOAA), was prepared using both 1 and MAA as functional monomers. Imprinted polymers were also prepared using either MAA or 1, called PM(TOAA) and PP(TOAA), respectively, and used as references. Corresponding unimprinted blank polymers, PPM(BL), PM(BL), and PP(BL), were prepared using the same monomers in the absence of TOAA. Batch rebinding studies were conducted by UV-vis spectroscopy and the binding characteristics of the MIPs were examined by Scatchard analysis. In order to verify the selectivity of the MIPs, the binding of TOAA and its structurally related compound, TOAU, on the all prepared polymers was investigated.

2. EXPERIMENTAL SECTION

2.1. Materials and methods

Ethylene glycol dimethacrylate (EGDMA), 2′, 3′, 5′-tri-O-acetyladenosine (TOAA), 2′, 3′, 5′-tri-O-acetyluridine (TOAU), and acetic acid were purchased from Sigma-Aldrich (Steinheim, Germany). α-α'-Azoisobutyronitrile (AIBN) and methacrylic acid (MAA) were supplied from Fluka (Steinheim, Germany). Analytical grade dichloromethane and methanol were purchased from J. T. Baker (Deventer, Holland). Zn(II) tetra(4′-methacryloyloxyphenoxy)phthalocyanine (1) was prepared on the basis of a published method [17]. UV-Vis spectra were obtained with a Cary 100 Scan UV-vis spectrophotometer.

2.2. Polymer preparation

The preparation of PPM(TOAA) was carried out as follows: to a solution of TOAA (0,0468 mmol, as template) in dichloromethane (262 μL) were added phthalocyanine 1 (0.0117 mmol, as the first functional monomer) and MAA (0.1758 mmol, as the second functional monomer) in a glass tube. After adding of EGDMA (0.9360 mmol, as cross-linker) and AIBN (0.0112 mmol, as initiator), the mixture was sonicated for 5 minutes flushing with nitrogen gas and then polymerized by heating at 60°C for 16 hours. The resultant polymer was crushed and sieved. The template molecules were removed by washing the polymer first with methanol/acetic acid (7/3 v/v) and then with methanol until no template molecules were detected from the recovered solutions with a UV-vis spectrophotometer. Drying under vacuum afforded particles which were used for rebinding studies. PM(TOAA) and PP(TOAA) were identically prepared using either MAA (0.1758 mmol) or 1 (0.0117 mmol) as functional monomer, respectively. The corresponding blank polymers, PPM(BL), PM(BL), and PP(BL), were prepared in the same manner in the absence of TOAA.

2.3. Batch rebinding experiments and Scatchard analysis

The polymer (20 mg) was added to a dichloromethane solution (3.5 mL) of TOAA of known concentrations ($2.0–8.0 \times 10^5$ M) in vials. The resulting suspension was shaken for 16 hours at room temperature, then the polymer was rapidly removed by filtration and the resulting solution was analyzed by UV-vis spectrophotometer at 258 nm. The amount of TOAA bound to the polymer, B, was calculated by subtraction of the concentration of free TOAA, [TOAA], from the initial TOAA concentration. [TOAA] was determined as an average value of three measurements. Scatchard analysis was provided by the Scatchard equation, $B/[\text{TOAA}] = (B_{\max} - B)\, K_a$, where K_a is the association constant and $B_{\max}$ is the apparent maximum number of binding sites. Therefore, K_a and $B_{\max}$ of the polymer were determined from the slope and the intercept, respectively, by plotting of $B/[\text{TOAA}]$ versus B. Batch rebinding experiments and Scatchard analysis were performed in a similar manner for PPM(TOAA), PM(TOAA), PP(TOAA), and the corresponding blank polymers. The rebinding tests were also carried out incubating the polymers with TOAU in order to verify their binding selectivity.

3. RESULTS AND DISCUSSION

TOAA-imprinted and unimprinted polymers were obtained by the above method. The binding behavior of the prepared MIPs was evaluated by batch rebinding tests and the binding data were processed with Scatchard equation in order to estimate the binding properties of the polymers. Figure 1 shows the Scatchard plot for PPM(TOAA). As can be seen, it is a single straight line, which indicates that there exists one kind of binding sites populated in the MIP. The Scatchard plot is linear also in the case of PM(TOAA). Similar Scatchard plots

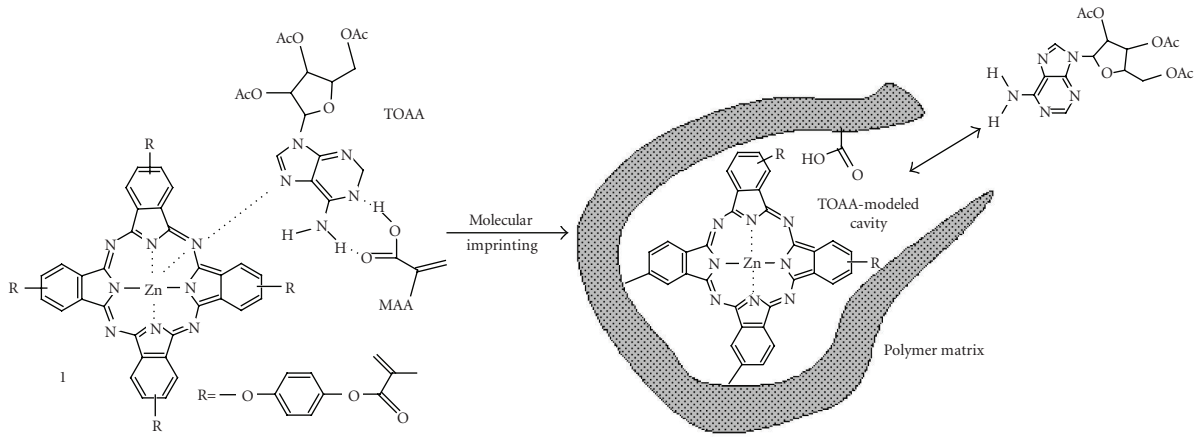

Scheme 1: Schematic representation of the molecular imprinting of TOAA using both 1 and MAA as functional monomers.

Table 1: Association constant (K_a) and maximum number of binding sites (B_{max}) for PPM(TOAA) and PM(TOAA).

Polymer	$K_a(M^{-1})$	B_{max} ($\mu M\, g^{-1}$)
PPM(TOAA)	$(2.96 \pm 0.5) \times 10^4$	6.53
PM(TOAA)	$(1.48 \pm 0.6) \times 10^4$	1.66

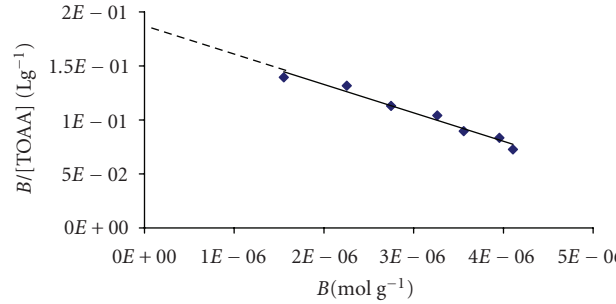

Figure 1: Scatchard plot for PPM(TOAA).

were obtained in a study of Yan et al. [26] with malachite green-imprinted polymers. This fact is very interesting since a nonlinear profile was commonly observed in the Scatchard assessment of MIPs indicating the presence of binding sites that exhibit various affinities to the ligand [18, 20, 21]. Table 1 shows the values of K_a and B_{max} for PPM(TOAA) and PM(TOAA). As shown, the MIP prepared with both functional monomers 1 and MAA, PPM(TOAA), exhibited higher binding affinities for TOAA compared to PM(TOAA), prepared solely with MAA. PP(TOAA), prepared only with 1, did not show any binding capacity for TOAA. This means that phthalocyanine 1 contributes to higher binding affinities, although 1 itself barely interacts with TOAA. The effects of the use of both functional monomers strongly suggest that the imprint that allows the simultaneous multipoint interactions of the template with the carboxylic residues of MAA and the Zn(II) ion of 1 shows a higher binding ability for TOAA than that allowing only the individual template/functional monomer interactions. The corresponding blank polymers, PPM(BL), PM(BL), and PP(BL), showed no binding affinities for TOAA confirming that the selectivity was due to the imprinting of the polymer matrix and not to the intrinsic affinity of the template to the functional monomers alone.

As for the selectivity (Figure 2), both PPM(TOAA) and PM(TOAA) exhibited binding affinities for TOAA while they did not show any binding capacity for TOAU. As expected, also PP(TOAA) did not show any binding capacity for TOAU. The corresponding blank polymers showed no binding affinity for TOAU too. If we examine the chemical structure of TOAA and TOAU, it is clear that TOAA has more chances than TOAU to form hydrogen bonds with the MIPs because of more functional groups that could form hydrogen bonds with the polymers. Consequently, the polymers PPM(TOAA) and PM(TOAA) showed a good binding affinity for TOAA and no binding capacity for TOAU. This is not surprising since the inability of carboxylic acid receptors to bind uracil derivatives appears to be rather general as evidenced in the literature [15, 27, 28].

The higher binding affinity of PPM(TOAA) for TOAA in comparison with PM(TOAA) could be explained considering the possibility of coordination of the Zn(II) ion of 1 with the nitrogen atoms of the 2-amonopyridine moiety of TOAA. Similar multipoint interactions have already been proposed by Takeuchi et al. [18] in a study on the preparation of MIPs for cinchonidine by the combined use of MAA and a vinyl-substituted zinc(II) porphyrin as functional monomers. The coordination of the Zn(II) ion with the nitrogen atoms of TOAA could be explained considering that the zinc(II) ion is the acid with moderate hardness and the nitrogen atom of the 2-aminopyridine moiety is the base with moderate softness [18]. The absence of this kind of nitrogen atom in the chemical structure of TOAU could explain the inability of PPM(TOAA) to bind TOAU. On the other hand, the inability of PP(TOAA) to bind TOAA suggests that the coordination of the Zn(II) ion of the phthalocyanine with the nucleoside is not sufficient alone to assure the recognition and subsequent complementary binding between the receptor and the

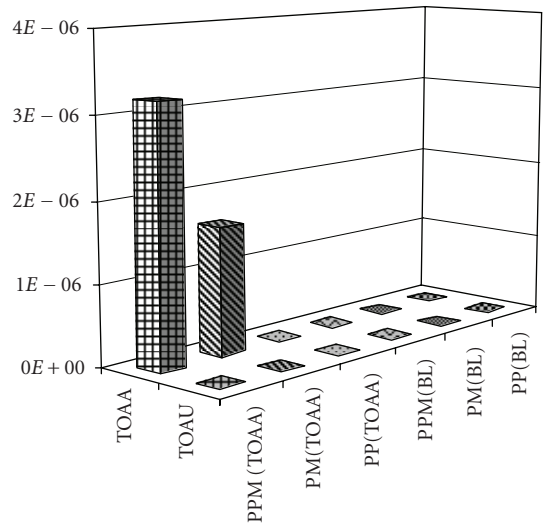

Figure 2: Binding selectivity test of TOAA and TOAU on the MIPs.

nucleoside molecule, confirming in this way that the analyte molecule is specifically bound to the polymer through multipoint interactions.

4. CONCLUSION

A highly specific and selective TOAA-imprinted polymer was prepared by the combination of MAA and a zinc-phthalocyanine substituted with methacrylic groups as functional monomers. The effects of the simultaneous use of the two functional monomers suggest the effective cooperation of the phthalocyanine-based and carboxylic residues rather than independent operation for retaining of TOAA.

Considering these promising results for easily constructed and highly selective MIPs for nucleosides, new investigations are now being directed towards the development of MIP-based sensors arrays for nucleoside discriminations.

ACKNOWLEDGMENT

This work was supported by PRIN 2004-MIUR (No. 20040340210_03).

REFERENCES

[1] S. A. Piletsky and A. P. F. Turner, "New materials based on imprinted polymers and their applications in optical sensors," in *Optical Biosensors: Present and Future*, F. S. Ligler and C. A. Rowe Taitt, Eds., pp. 397–425, Elsevier, Amsterdam, The Netherlands, 2002.

[2] P. Dzygiel, E. O'Donnell, D. Fraier, C. Chassaing, and P. A. G. Cormack, "Evaluation of water-compatible molecularly imprinted polymers as solid-phase extraction sorbents for the selective extraction of sildenafil and its desmethyl metabolite from plasma samples," *Journal of Chromatography B: Analytical Technologies in the Biomedical and Life Sciences*, vol. 853, no. 1-2, pp. 346–353, 2007.

[3] F. G. Tamayo, E. Turiel, and A. Martín-Esteban, "Molecularly imprinted polymers for solid-phase extraction and solid-phase microextraction: recent developments and future trends," *Journal of Chromatography, A*, vol. 1152, no. 1-2, pp. 32–40, 2007.

[4] C. He, Y. Long, J. Pan, K. Li, and F. Liu, "Application of molecularly imprinted polymers to solid-phase extraction of analytes from real samples," *Journal of Biochemical and Biophysical Methods*, vol. 70, no. 2, pp. 133–150, 2007.

[5] J. Haginaka, "Molecularly imprinted polymers for solid-phase extraction," *Analytical and Bioanalytical Chemistry*, vol. 379, no. 3, pp. 332–334, 2004.

[6] Y. C. Lin, H. H. Pan, C. C. Hwang, and W. C. Lee, "Side chain functionality dominated the chromatography of N-protected amino acid on molecularly imprinted polymer," *Journal of Applied Polymer Science*, vol. 105, no. 6, pp. 3519–3524, 2007.

[7] S. Wei and B. Mizaikoff, "Recent advances on noncovalent molecular imprints for affinity separations," *Journal of Separation Science*, vol. 30, no. 11, pp. 1794–1805, 2007.

[8] Y. Luo, L. Liu, L. Li, and Q. Deng, "Chiral resolution of racemic 4-phenyl(benzyl)-2-oxazolidone by use of molecularly imprinted polymers," *Chromatographia*, vol. 65, no. 11-12, pp. 675–679, 2007.

[9] K. Hattori, Y. Yoshimi, and K. Sakai, "Chemical sensors using molecularly imprinted polymers as molecular recognition elements," *Chemical Sensors*, vol. 22, pp. 110–115, 2006.

[10] K. Haupt and K. Mosbach, "Molecularly imprinted polymers and their use in biomimetic sensors," *Chemical Reviews*, vol. 100, no. 7, pp. 2495–2504, 2000.

[11] A. Visnjevski, R. Schomäcker, E. Yilmaz, and O. Brüggemann, "Catalysis of a Diels-Alder cycloaddition with differently fabricated molecularly imprinted polymers," *Catalysis Communications*, vol. 6, no. 9, pp. 601–606, 2005.

[12] R. Kalim, R. Schomäcker, S. Yüce, and O. Brüggemann, "Catalysis of a β-elimination applying membranes with incorporated molecularly imprinted polymer particles," *Polymer Bulletin*, vol. 55, no. 4, pp. 287–297, 2005.

[13] Z. Chen, Z. Hua, J. Wang, Y. Guan, M. Zhao, and Y. Li, "Molecularly imprinted soluble nanogels as a peroxidase-like catalyst in the oxidation reaction of homovanillic acid under aqueous conditions," *Applied Catalysis, A: General*, vol. 328, no. 2, pp. 252–258, 2007.

[14] M. J. Syu, J. H. Deng, and Y. M. Nian, "Towards bilirubin imprinted poly(methacrylic acid-co-ethylene glycol dimethacrylate) for the specific binding of α-bilirubin," *Analytica Chimica Acta*, vol. 504, no. 1, pp. 167–177, 2004.

[15] D. A. Spivak and K. J. Shea, "Binding of nucleotide bases by imprinted polymers," *Macromolecules*, vol. 31, no. 7, pp. 2160–2165, 1998.

[16] D. Spivak, M. A. Gilmore, and K. J. Shea, "Evaluation of binding and origins of specificity of 9-ethyladenine imprinted polymers," *Journal of the American Chemical Society*, vol. 119, no. 19, pp. 4388–4393, 1997.

[17] L. Longo, G. Vasapollo, A. Scardino, R. A. Picca, and C. Malitesta, "Synthesis of a new substituted zinc phthalocyanine as functional monomer in the preparation of MIPs," *Journal of Porphyrins and Phthalocyanines*, vol. 10, no. 8, pp. 1061–1065, 2006.

[18] T. Takeuchi, T. Mukawa, J. Matsui, M. Higashi, and K. D. Shimizu, "Molecularly imprinted polymers with metalloporphyrin-based molecular recognition sites coassembled with methacrylic acid," *Analytical Chemistry*, vol. 73, no. 16, pp. 3869–3874, 2001.

[19] J.-D. Lee, N. T. Greene, G. T. Rushton, K. D. Shimizu, and J.-I. Hong, "Carbohydrate recognition by porphyrin-based

molecularly imprinted polymers," *Organic Letters*, vol. 7, no. 6, pp. 963–966, 2005.

[20] J. Matsui, M. Higashi, and T. Takeuchi, "Molecularly imprinted polymer as 9-ethyladenine receptor having a porphyrin-based recognition center," *Journal of the American Chemical Society*, vol. 122, no. 21, pp. 5218–5219, 2000.

[21] A. Tong, H. Dong, and L. Li, "Molecular imprinting-based fluorescent chemosensor for histamine using zinc(II)-protoporphyrin as a functional monomer," *Analytica Chimica Acta*, vol. 466, no. 1, pp. 31–37, 2002.

[22] K. J. Shea, D. A. Spivak, and B. Sellergren, "Polymer complements to nucleotide bases. Selective binding of adenine derivatives to imprinted polymers," *Journal of the American Chemical Society*, vol. 115, no. 8, pp. 3368–3369, 1993.

[23] K. Yano, K. Tanabe, T. Takeuchi, J. Matsui, K. Ikebukuro, and I. Karube, "Molecularly imprinted polymers which mimic multiple hydrogen bonds between nucleotide bases," *Analytica Chimica Acta*, vol. 363, no. 2-3, pp. 111–117, 1998.

[24] H. Tsunemori, K. Araki, K. Uezu, M. Goto, and S. Furusaki, "Surface imprinting polymers for the recognition of nucleotides," *Bioseparation*, vol. 10, no. 6, pp. 315–321, 2001.

[25] D. A. Spivak and K. J. Shea, "Investigation into the scope and limitations of molecular imprinting with DNA molecules," *Analytica Chimica Acta*, vol. 435, no. 1, pp. 65–74, 2001.

[26] S. Yan, Z. Gao, Y. Fang, Y. Cheng, H. Zhou, and H. Wang, "Characterization and quality assessment of binding properties of malachite green molecularly imprinted polymers prepared by precipitation polymerization in acetonitrile," *Dyes and Pigments*, vol. 74, no. 3, pp. 572–577, 2007.

[27] S. C. Zimmerman, W. Wu, and Z. Zeng, "Complexation of nucleotide bases by molecular tweezers with active site carboxylic acids: effects of microenvironment," *Journal of the American Chemical Society*, vol. 113, no. 1, pp. 196–201, 1991.

[28] G. Lancelot, "Hydrogen bonding between nucleic acid bases and carboxylic acids," *Journal of the American Chemical Society*, vol. 99, no. 21, pp. 7037–7042, 1977.

Hindawi Publishing Corporation
Metal-Based Drugs
Volume 2008, Article ID 289490, 6 pages
doi:10.1155/2008/289490

Research Article

Identification of Proteins Related to Nickel Homeostasis in *Helicobater pylori* by Immobilized Metal Affinity Chromatography and Two-Dimensional Gel Electrophoresis

Xuesong Sun,[1,2] Ruiguang Ge,[2] Jen-Fu Chiu,[3] Hongzhe Sun,[2] and Qing-Yu He[1]

[1] *Institute of Life and Health Engineering, Jinan University, Guangzhou 510632, China*
[2] *Department of Chemistry and Open Laboratory of Chemical Biology, The University of Hong Kong, Hong Kong*
[3] *Department of Anatomy, The University of Hong Kong, Hong Kong*

Correspondence should be addressed to Qing-Yu He, qyhe@hku.hk

Received 28 June 2007; Accepted 21 October 2007

Recommended by Edward N. Baker

Helicobacter pylori (H. pylori) is a widespread human pathogen causing peptic ulcers and chronic gastritis. Maintaining nickel homeostasis is crucial for the establishment of *H. pylori* infection in humans. We used immobilized-nickel affinity chromatography to isolate Ni-related proteins from *H. pylori* cell extracts. Two-dimensional gel electrophoresis and mass spectrometry were employed to separate and identify twenty two Ni-interacting proteins in *H. pylori*. These Ni-interacting proteins can be classified into several general functional categories, including cellular processes (HspA, HspB, TsaA, and NapA), enzymes (Urease, Fumarase, GuaB, Cad, PPase, and DmpI), membrane-associated proteins (OM jhp1427 and HpaA), iron storage protein (Pfr), and hypothetical proteins (HP0271, HP jhp0216, HP jhp0301, HP0721, HP0614, and HP jhp0118). The implication of these proteins in nickel homeostasis is discussed.

1. INTRODUCTION

The human gastric pathogen *Helicobacter pylori* (*H. pylori*) is a microaerophilic, spiral-shaped, Gram-negative bacterium responsible for the majority of peptic ulcer diseases in humans [1]. *H. pylori* has been shown to be the causative agent of type B gastritis and peptic ulcerations [2, 3]. Infection with *H. pylori* increases the risks of developing gastric carcinoma and mucosa-associated lymphoid tissue (MALT) lymphoma [4, 5]. Continuously exposed to acidic pH during the process of colonization in the gastric mucus layer, *H. pylori* requires mechanisms to survive acid shocks and to enable growth in such acidic conditions. This bacterium expresses two nickel-containing enzymes: urease and hydrogenase, both of which is important for its colonization. The *H. pylori* urease consists of 12 UreA and 12 UreB, and activation of this apoenzyme requires the insertion of 24 nickel ions [6]. Urease hydrolyzes urea into carbon dioxide and ammonia, thereby neutralizing the nearby environment [7–9]. [Ni-Fe] hydrogen-uptake hydrogenase contains a heterobimetallic center in the large subunit with nickel coordinating to four cysteines, and permits respiratory-based energy production for the bacteria in the mucosa [10, 11]. Therefore, *H. pylori* needs significant amounts of nickel to satisfy its requirement for the maturation of the nickel-containing enzymes [12].

Two kinds of high-affinity, nickel-specific uptake systems are found in *H. pylori*: ATP-binding cassette (ABC)-type transporter (*abc* ABCD) and nickel-cobalt permease (NixA) [13, 14]. However, when excess nickel ions accumulate, they exhibit toxic effects and thus inhibit bacterial growth [15–17]. *H. pylori* has developed a system to maintain nickel homeostasis, keeping a balance between the import, intracellular storage, and export of nickel ions. Analysis of the *H. pylori* genome sequence has discovered several putative ion binders and membrane transporters involved in metal homeostasis [18]. However, the related nickel-interacting proteins have not been fully identified so far.

Immobilized-metal affinity chromatography (IMAC) is a separation technique commonly used for fractionating proteins based on their different binding affinities of the surface-exposed amino acids towards immobilized metal ions [19, 20]. Ni^{2+} belongs to the group of intermediate metal

ions, preferring coordination to nitrogen, oxygen, and sulfur, and especially favors binding to the proteins with two exposed vicinal histidines [21]. Elution of the target proteins is achieved by lowering the pH or by adding a competing reagent such as imidazole [22]. Two-dimensional gel electrophoresis (2-DE) is a common choice for separating cellular proteins first by their isoelectric point (p*I*) and then by molecular weight (MW). However, low-abundance proteins may not be detected in 2-DE due to its limited separation capacity. IMAC may compensate this, in some way, by specifically serving to enrich the low-abundance metal-binding proteins and to reduce protein complexity.

In this study, proteomic technology was employed for the first time to isolate and identify candidate proteins involved in nickel transport, storage, and utilization in *H. pylori*, by integrating the powerful tools of Ni-IMAC, 2-DE, and matrix-assisted laser desorption time-of-flight mass spectrometry (MALDI-TOF MS). Those proteins with surface active coordinating residues for binding nickel (and maybe other metals with similar coordinating features) were retained, separated, and analyzed. The information obtained from the identification and functional analysis of these nickel-related proteins may improve our understanding of nickel homeostasis in bacteria.

2. MATERIALS AND METHODS

2.1. Bacterial culture conditions

H. pylori strain 11637 was kindly supplied by Dr. H. H-X. Xia (Department of Medicine, The University of Hong Kong), and cultured in the basal medium, Brucella broth (Difco) with 5% (v/v) fetal bovine serum (FBS; GIBCO/BRL Life Technologies), for 72 hours with orbital shaking (100 rpm) at 37°C in an anaerobic jar with a microaerobic gas-generating kit (Oxoid). Solutions used in this study were prepared with ultra-pure water (18.2 MΩ; Millipore).

2.2. Immobilized-nickel affinity

H. pylori 11637 cells grown in 100 mL liquid media to mid-log phase were pelleted at 8000×*g* for 5 minutes at 4°C, and washed three times with 10 mL ice-cold phosphate buffered saline (PBS). Cell pellets were resuspended in 10 mL of ice-cold Buffer A (20 mM sodium phosphate buffer, 500 mM NaCl, 10 mM imidazole, 1 mM PMSF, pH 7.4). Bacteria were ruptured with sonication in the presence of 1% v/v Triton X-100. Proteins were recovered (10,000×*g*, 30 minutes), and the supernatant was filtered through a 0.45 μm cellulose acetate syringe filter (Iwaki Glass, Japan) before being loaded onto a house-made, Buffer A-equilibrated Ni-NTA Agarose column (0.5 mL, Qiagen). After washing with 10 column volumes of Buffer A, proteins were eluted with Buffer B (20 mM sodium phosphate buffer, 500 mM NaCl, 500 mM imidazole, pH 7.4). The fractions were concentrated with Centricon YM-3 (Millipore), and buffer-exchanged into rehydration solutions (8 M urea, 4% CHAPS, 1 mM PMSF, 20 mM DTT, 2% pharmalyte pH 3–11) with PlusOne 2-D Clean-up kit (Amersham Biosciences, Buckinghamshire, UK). Protein concentrations were determined by BCA assay (Bio-Rad, Calif, USA) using BSA as the standard. Cell extractswere used immediately or frozen in aliquots at –80°C.

2.3. 2-DE

2-DE was carried out with an IPGphor II Isoelectric Focusing (IEF) unit and Hoefer SE 600 Ruby electrophoresis unit (Amersham Biosciences) according to the method detailed elsewhere [23]. Briefly, 100 μg of *H. pylori* protein samples were diluted in rehydration solutions containing traces of bromophenol blue. IEF was carried out with precast 13-cm Immobiline DryStrip (IPG strips; Amersham Biosciences) to generate a nonlinear pH gradient of 3–10. Following IEF, strips were immediately used for the second dimensional SDS-PAGE (10). Proteins were visualized with silver stain, and protein molecular weight (MW) was calibrated with prestained SDS-PAGE marker (Broad range; Bio-Rad). To minimize gel to gel variations, two-dimensional gels were run three times for each sample.

2.4. Peptide mass fingerprinting (PMF)

The silver-stained gels were scanned (Image Scanner; Amersham Biosciences) and analyzed with ImageMaster 2D Elite software (Amersham Biosciences) [23]. The normalized intensity (NI) for each protein spot was calculated as the ratio of the spot intensity versus the sum of intensities of the spots present in the whole gel. Protein spots were cut out from the silver-stained gels and enzymatically digested overnight with sequence grade porcine trypsin (Promega) at 37°C. The masses of the digested peptides were determined with a Voyager-DE STR Biospectrometry Workstation (Applied Biosystems, Calif, USA). Protein identification was performed by searching the NCBInr protein database using Protein Prospector (http://prospector.ucsf.edu) (3), with pyroglutamic acid modification of N-terminal glutamine, oxidation of methionine, and protein N-terminal acetylation as permissible modifications. The criteria for searching were set at 50 ppm or better mass accuracy, at least four matching peptide masses, as well as theoretical MW and isoelectric point (p*I*) matching to the estimated values from gels.

3. RESULTS AND DISCUSSION

To investigate nickel binding proteins in *H. pylori* under physiologically relevant conditions, a relatively mild and nondenaturing lysis method was applied prior to Nickel-IMAC (Ni-IMAC) loading. Our previous experiments have shown 1-D gels for the total extract of *H. pylori* 11637 cells and extract fractions eluted from a Ni-IMAC column [24], displaying many protein bands for both cases. We have now further separated and identified nickel-interacting proteins in *H. pylori* using 2-DE.The resulting 2-DE images were visualized by silver staining. The gel image of whole cell extracts of *H. pylori* 11637 (see Figure 1(a)) has a protein distribution very similar to the standard proteome pattern of *H. pylori* 26695 [25]. More than 800 protein spots were separated, with molecular weights ranging from 6 to 200 kDa and

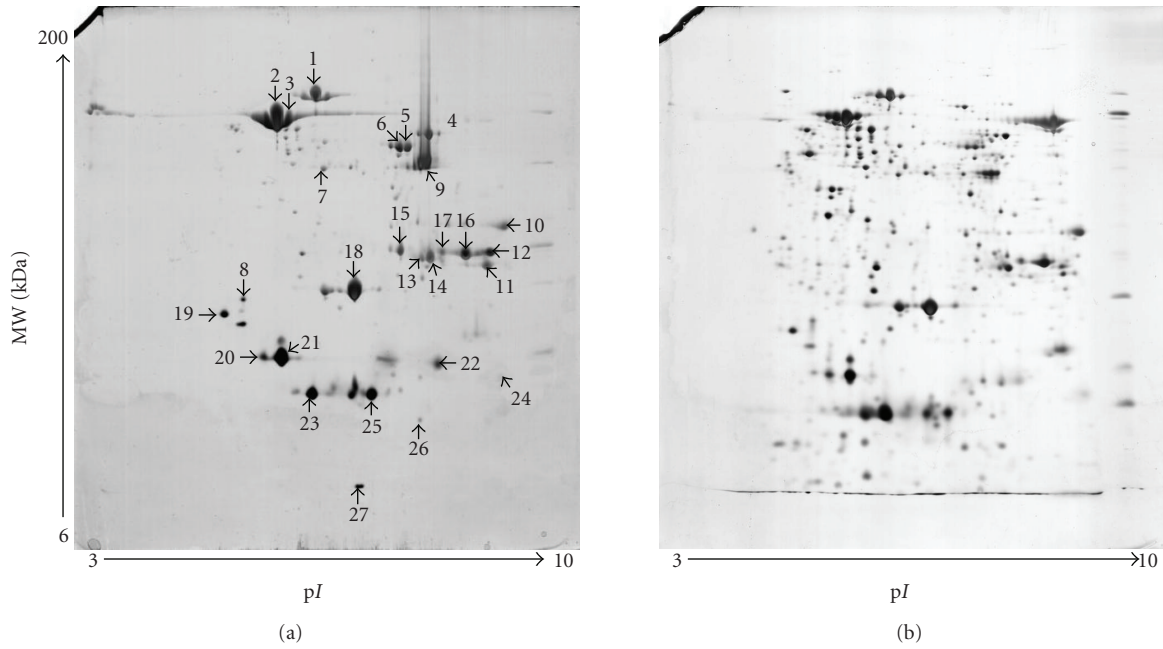

Figure 1: Nickel-interacting proteins in *H. pylori* 11637 analyzed by 2-DE. (a) 2-DE patterns of total Ni-binding proteins in *H. pylori* 11637; (b) 2-DE patterns of *H. pylori* total proteins.

p*I* values from 3 to 10. Figure 1(a) shows a representative gel image of Ni-related proteins in *H. pylori* 11637. The ratio between the number of Ni-binding proteins and total extracted proteins of whole cell lysates was 1 : 57, indicating that nickel specifically binds to a restricted number of proteins. Qualitative comparison of 2-D gels between the Ni-enriched eluates (see Figure 1(a)) and the total extracts (see Figure 1(b)) revealed remarkably different spot patterns.

Ni-binding protein spots were excised, trypsin-digested, and subjected to MALDI-TOF MS sequencing. Mass spectra of tryptic peptides were used to identify proteins by matching to the spectra of the protein sequence databases, and the identification was further verified by comparing to the standard proteomic map of *H. pylori* [25]. In total, twenty two proteins were identified as candidate Ni-interacting proteins, as marked in Figure 1(a) and summarized in Table 1. Some of the protein spots could not be annotated due to no substantial MS signals or inadequate peptide coverage for confident identification. Interestingly, five of the proteins identified,including UreA, HspB, fumarase, Pfr, and hypothetical protein jhp0301, show more than one spot in the 2-DE map, indicating the presence of posttranslational modifications. Protein isoforms typically present themselves as a series of spots that differ slightly in their molecular masses and p*I*, that is, numerous closely spaced spots in 2-DE profiles [26–28]. Five proteins (HspA, HspB, fumarase, TsaA, and NapA) were also identified in the Bi-interacting profile [24], indicating that there was some correlation between Bi^{3+} and Ni^{2+} interactions. The Ni-interacting proteins can be classified into five general functional categories: cellular processes (HspA, HspB, TsaA, and NapA), enzymes (Urease, Fumarase, GuaB, Cad, PPase, and DmpI), membrane-associated proteins (OM jhp1427 and HpaA), iron storage protein (Pfr), and hypothetical proteins (HP0271, HP jhp0216, HP jhp0301, HP0721, HP0614, and HP jhp0118).

Nickel homeostasis is required for the establishment of *H. pylori* infection in animals [7], necessitating a balance in the nickel import, storage, and delivery for the synthesis and activity of nickel-dependent metalloenzymes. Proteins involved in nickel homeostasis are potential drug targets. Consequently, an analysis to identify the nickel-interacting proteins in *H. pylori* may be able to reveal candidate proteins for further characterization and validation to provide drug targets.

In order to live in the acidic gastric environment, *H. pylori* continuously synthesize urease catalyzing the hydrolysis of urea to ammonia and carbamate to elevate pH. Urease is an oligomeric Ni-containing heterodimer of UreA and UreB.Both subunits of urease were observed in the 2-DE gel after Ni-NTA enrichment, suggesting each of them can bind nickel ions (see Figure 1(a)). Expression of active urease is essential for *H. pylori* infection in all animal models and for acid survival in vitro [29]. Urease activity is significantly enhanced in the presence of nickel, additional incorporation of Ni^{2+} into the apoenzyme is thus the major regulating event upon higher Ni^{2+} availability.

Heat shock proteins are a group of highly conserved, abundantly expressed proteins with protective advantage through their functions as molecular chaperones, assisting proper folding of a number of substrate proteins that are otherwise destined to aggregation [30, 31]. Both Chaperones HspA and HspB were isolated by Ni-IMAC. HspA and HspB are also involved in urease activation and protection. Urease activity was increased four folds in *E. coli* when coexpressed with HspA, suggesting that HspA possibly plays an important role in the activation of urease, probably by means of its

Table 1: Summary of nickel-interacting *H. pylori* proteins identified by peptide mass fingerprinting.

Protein no.	Protein name	Identified peptides	% Sequence coverage	MOWSE score	MW (kDa)/p*I*	
					Theor.	Obs.
1*	UreB	21	42	1.595e+10	61.4/5.5	65.5/5.8
2*	60 kDa chaperonin (HspB)	65	75	1.199e+15	58.2/5.5	59.3/5.3
3	60 kDa chaperonin (HspB)	19	37	9.875e+04	58.2/5.5	56.7/5.5
4	Inosine-5′-monophosphate dehydrogenase (GuaB)	24	51	2.559e+09	51.8/7.7	56.2/8.0
5	Fumarase	22	51	1.097e+11	51.0/6.5	52.6/7.4
6	Fumarase	20	45	1.800e+10	51.0/6.5	52.6/7.0
7	Putative aminotransferase	26	55	2.466e+12	42.4/5.8	40.4/6.2
8	Hypothetical protein HP0271 (fragment)	4	12	980	38.6/5.0	21.1/4.8
9	Cinnnamyl-alcohol dehydrogenase ELI3-2 (Cad)	15	36	1.912e+09	38.6/7.0	40.7/7.8
10	Cell binding factor 2	21	48	5.030e+06	34.0/9.3	31.9/9.8
11	Outer membrane protein jhp1472	11	32	6.291e+04	30.2/9.1	26.7/9.3
12	Hypothetical protein jhp0216	15	57	7.869e+05	29.5/9.1	27.4/9.4
13	Hypothetical protein jhp0301	7	24	1.027e+04	28.6/7.8	27.1/8.0
14	Hypothetical protein jhp0301	19	61	2.461e+05	28.6/7.8	27.1/8.1
15	Putative neuraminyllactose-binding hemagglutinin homolog (HpaA)	13	50	2.381e+05	28.3/7.9	27.0/7.2
16	Urease alpha subunit (UreA)	14	68	1.280e+07	26.5/8.5	27.2/9.0
17	Urease alpha subunit (UreA)	4	88	1.846e+11	26.5/8.5	27.2/8.5
18	Putative alkyl hydroperoxide reductase (TsaA)	12	54	1.297e+07	21.9/5.7	19.9/6.2
19	Inorganic pyrophosphatase (PPase)	4	23	575	14.7/5.0	20.7/4.7
20	Non-heme iron containing ferritin (Pfr)	2	23	369	19.3/5.4	14.4/5.2
21	Non-heme rion containing ferretin (Pfr)	8	56	2.190e+07	19.3/5.4	14.4/5.5
22	Hypothetical protein HP0721	13	44	1.692e+04	17.6/8.9	14.4/8.5
23	Neutrophil activating protein (NapA)	6	48	1.570e+05	16.8/5.7	10.2/6.2
24	Hypothetical protein jhp0118	4	32	1.620e+03	16.6/9.3	12.2/9.8
25	Chaperonin groES (HspA)	6	44	146	13.0/6.1	10.2/6.4
26	Hepothetical protein HP0614	13	56	1.557e+05	13.0/7.0	7.7/8.0
27	4-oxalocrotonate tautomerase (DmpI)	10	85	3.420e+05	7.5/6.0	5.5/6.4

* Confirmed with 2-DE images of *H. pylori* 26695 (http://www.mpiib-berlin.mpg.de/2D-PAGE/EBP-PAGE/index.html).

Ni-binding domain in the C-terminus [32]. HspA has two distinct Ni^{2+}-binding sites: a high-affinity site ($K_d \approx 2.8\,\mu$M) and a lower affinity site ($K_d \approx 30\,\mu$M). The *H. pylori* GroEL homologue HspB belongs to the HSP60 family [33], and has been shown to increase the risk of gastric carcinoma, possibly by directly inducing the hyperproliferation of gastric cells [34]. HspB also was suggested to be responsible for the protection and regulation of urease activity [33].

Many identified Ni-interacting proteins in *H. pylori* are involved in antioxidant, antitoxic, and antiinflammation machinery. *H. pylori* TsaA is a major component of the thioredoxin-dependent thiol-specific antioxidant (TSA) system that catalyzes the reduction of hydroperoxides [35] and peroxynitrite [36]. The cleavage of TsaA suppresses the protecting response of *H. pylori* cells against oxidative stress in two possible ways: directly by the way of nucleophilic attacking the peptide bond through metal-bound hydroxide ions, and/or indirectly by way of stimulating the activities of specific proteases. NapA is also directly involved in cell defense in response to oxidative stress.It was named because of its ability to mediate neutrophil adhesion to endothelial cells [37], and to bind to mucin and neutrophil glycosphingolipids [38]. NapA was identified as a 150 kDa DNA-binding dodecamer that protects cells from DNA damage caused by free radicals under oxidative stress [39, 40]. NapA was found to be positively regulated by iron, repressed by ferric uptake regulator (Fur) [40], and unaffected by copper, nickel, or zinc [41]. An excess of iron is potentially harmful as it catalyzes the formation of toxic reactive oxygen species (ROS) via Fenton chemistry. Ferritin protein Pfr, the major iron storage protein of *H. pylori*, is also regulated by iron, nickel, zinc, and copper. The accumulation of this protein under iron-rich conditions allows *H. pylori* to maximize the iron storage capacity in response to an increase in iron availability [44]. It is essential for the bacteria to adapt to low-iron conditions [42–45]. Obviously, Ni-IMAC is also able to trap Pfr with its cation binding affinity.

4. CONCLUSION

Immobilized-nickel affinity chromatography and proteomic analysis were integrated to separate and identify the Ni-interacting proteins in *H. pylori*. The results suggest that Ni-interacting proteins are mainly involved in cellular processes, oxidative stress, and metabolism of the bacteria. This study demonstrated that metalloproteomic technique can be utilized to efficiently identify metal-related proteins that may play crucial roles in metal homeostasis. These proteins may be potential targets for designing and constructing drugs to suppress the bacterial infection.

ACKNOWLEDGMENTS

This work was partially supported by Hong Kong Research Grants Council, Grants HKU 7512/05M (to Q. Y. He) and HKU703904P (to H. Sun), and the Areas of Excellence Scheme of Hong Kong University Grants Committee.

REFERENCES

[1] B. J. Marshall and J. R. Warren, "Unidentified curved bacilli in the stomach of patients with gastritis and peptic ulceration," *Lancet*, vol. 1, no. 8390, pp. 1311–1315, 1984.

[2] M. J. Blaser, "*Helicobacter pylori* and the pathogenesis of gastroduodenal inflammation," *Journal of Infectious Diseases*, vol. 161, no. 4, pp. 626–633, 1990.

[3] M. J. Blaser, "Gastric Campylobacter-like organisms, gastritis, and peptic ulcer disease," *Gastroenterology*, vol. 93, no. 2, pp. 371–383, 1987.

[4] J. Parsonnet, S. Hansen, L. Rodriguez, et al., "*Helicobacter pylori* infection and gastric lymphoma," *New England Journal of Medicine*, vol. 330, no. 18, pp. 1267–1271, 1994.

[5] D. Forman, D. G. Newel, F. Fullerton, et al., "Association between infection with *Helicobacter pylori* and risk of gastric cancer: evidence from a prospective investigation," *British Medical Journal*, vol. 302, no. 6788, pp. 1302–1305, 1991.

[6] D. J. McGee, "Mechanisms of *Helicobacter pylori* infection: bacterial factors," *Current Topics in Microbiology and Immunology*, vol. 241, pp. 155–180, 1999.

[7] S. B. Mulrooney and R. P. Hausinger, "Nickel uptake and utilization by microorganisms," *FEMS Microbiology Reviews*, vol. 27, no. 2-3, pp. 239–261, 2003.

[8] L.-T. Hu and H. L. T. Mobley, "Purification and N-terminal analysis of urease from *Helicobacter pylori*," *Infection and Immunity*, vol. 58, no. 4, pp. 992–998, 1990.

[9] B. E. Dunn, G. P. Campbell, G. I. Perez-Perez, and M. J. Blaser, "Purification and characterization of urease from *Helicobacter pylori*," *Journal of Biological Chemistry*, vol. 265, no. 16, pp. 9464–9469, 1990.

[10] J. W. Olson and R. J. Maier, "Molecular hydrogen as an energy source for *Helicobacter pylori*," *Science*, vol. 298, no. 5599, pp. 1788–1790, 2002.

[11] R. J. Maier, C. Fu, J. Gilbert, F. Moshiri, J. Olson, and A. G. Plaut, "Hydrogen uptake hydrogenase in *Helicobacter pylori*," *FEMS Microbiology Letters*, vol. 141, no. 1, pp. 71–76, 1996.

[12] K. Stingl and H. De Reuse, "Staying alive overdosed: how does *Helicobacter pylori* control urease activity?" *International Journal of Medical Microbiology*, vol. 295, no. 5, pp. 307–315, 2005.

[13] J. K. Hendricks and H. L. T. Mobley, "*Helicobacter pylori* ABC transporter: effect of allelic exchange mutagenesis on urease activity," *Journal of Bacteriology*, vol. 179, no. 18, pp. 5892–5902, 1997.

[14] P. Bauerfeind, R. M. Garner, and H. L. T. Mobley, "Allelic exchange mutagenesis of nixA in *Helicobacter pylori* results in reduced nickel transport and urease activity," *Infection and Immunity*, vol. 64, no. 7, pp. 2877–2880, 1996.

[15] M. Misra, R. Olinski, M. Dizdaroglu, and K. S. Kasprzak, "Enhancement by L-histidine of nickel(II)-induced DNA-protein cross-linking and oxidative DNA base damage in the rat Kidney," *Chemical Research in Toxicology*, vol. 6, no. 1, pp. 33–37, 1993.

[16] S. Kawanishi, S. Inoue, S. Oikawa, et al., "Oxidative DNA damage in cultured cells and rat lungs by carcinogenic nickel compounds," *Free Radical Biology and Medicine*, vol. 31, no. 1, pp. 108–116, 2001.

[17] S. K. Chakrabarti, C. Bai, and K. S. Subramanian, "DNA-protein crosslinks induced by nickel compounds in isolated rat lymphocytes: role of reactive oxygen species and specific amino acids," *Toxicology and Applied Pharmacology*, vol. 170, no. 3, pp. 153–165, 2001.

[18] J.-F. Tomb, O. White, A. R. Kerlavage, et al., "The complete genome sequence of the gastric pathogen *Helicobacter pylori*," *Nature*, vol. 388, no. 6642, pp. 539–547, 1997.

[19] X. Sun, J.-F. Chiu, and Q.-Y. He, "Application of immobilized metal affinity chromatography in proteomics," *Expert Review of Proteomics*, vol. 2, no. 5, pp. 649–657, 2005.

[20] J. Porath, J. Carlsson, I. Olsson, and G. Belfrage, "Metal chelate affinity chromatography, a new approach to protein fractionation," *Nature*, vol. 258, no. 5536, pp. 598–599, 1975.

[21] E. Sulkowski, "The saga of IMAC and MIT," *BioEssays*, vol. 10, no. 5, pp. 170–175, 1989.

[22] M. Zachariou, "Immobilized metal ion affinity chromatography of proteins," *Methods in Molecular Biology*, vol. 251, pp. 89–102, 2004.

[23] Q.-Y. He, G. K. K. Lau, and Y. Zhou, "Serum biomarkers of hepatitis B virus infected liver inflammation: a proteomic study," *Proteomics*, vol. 3, no. 5, pp. 666–674, 2003.

[24] R. Ge, X. Sun, Q. Gu, et al., "A proteomic approach for the identification of bismuth-binding proteins in *Helicobacter pylori*," *Journal of Biological Inorganic Chemistry*, vol. 12, no. 6, pp. 831–842, 2007.

[25] K.-P. Pleißner, T. Eifert, S. Buettner, et al., "Web-accessible proteome databases for microbial research," in *Proteomics*, vol. 4, no. 5, pp. 1305–1313, May 2004.

[26] W. Schlags, B. Lachmann, M. Walther, M. Kratzel, and C. R. Noe, "Two-dimensional electrophoresis of recombinant human erythropoietin: a future method for the European Pharmacopoeia?" *Proteomics*, vol. 2, no. 6, pp. 679–682, 2002.

[27] F. Lasne and J. De Ceaurriz, "Recombinant erythropoietin in urine," *Nature*, vol. 405, no. 6787, p. 635, 2000.

[28] A. Caldini, G. Moneti, A. Fanelli, et al., "Epoetin alpha, epoetin beta and darbepoetin alfa: two-dimensional gel electrophoresis isoforms characterization and mass spectrometry analysis," *Proteomics*, vol. 3, no. 6, pp. 937–941, 2003.

[29] M. Clyne, A. Labigne, and B. Drumm, "*Helicobacter pylori* requires an acidic environment to survive in the presence of urea," *Infection and Immunity*, vol. 63, no. 5, pp. 1669–1673, 1995.

[30] P. A. Lund, A. T. Large, and G. Kapatai, "The chaperonins: perspectives from the archaea," *Biochemical Society Transactions*, vol. 31, no. 3, pp. 681–685, 2003.

[31] P. A. Lund, "The roles of molecular chaperones in vivo," *Essays in Biochemistry*, vol. 29, pp. 113–123, 1995.

[32] I. Kansau, F. Guillain, J.-M. Thiberge, and A. Labigne, "Nickel binding and immunological properties of the C-terminal domain of the *Helicobacter pylori* GroES homologue (HspA)," *Molecular Microbiology*, vol. 22, no. 5, pp. 1013–1023, 1996.

[33] S. Suerbaum, J.-M. Thiberge, I. Kansau, R. L. Ferrero, and A. Labigne, "*Helicobacter pylori* hspA-hspB heat-shock gene cluster: nucleotide sequence, expression, putative function and immunogenicity," *Molecular Microbiology*, vol. 14, no. 5, pp. 959–974, 1994.

[34] A. De Luca, A. Baldi, P. Russo, et al., "Coexpression of *Helicobacter pylori*'s proteins CagA and HspB induces cell proliferation in AGS gastric epithelial cells, independently from the bacterial infection," *Cancer Research*, vol. 63, no. 19, pp. 6350–6356, 2003.

[35] L. M.S. Baker, A. Raudonikiene, P. S. Hoffman, and L. B. Poole, "Essential thioredoxin-dependent peroxiredoxin system from *Helicobacter pylori*: genetic and kinetic characterization," *Journal of Bacteriology*, vol. 183, no. 6, pp. 1961–1973, 2001.

[36] R. Bryk, P. Griffin, and C. Nathan, "Peroxynitrite reductase activity of bacterial peroxiredoxins," *Nature*, vol. 407, no. 6801, pp. 211–215, 2000.

[37] N. Yoshida, D. N. Granger, D. J. Evans Jr., et al., "Mechanisms involved in *Helicobacter pylori*-induced inflammation," *Gastroenterology*, vol. 105, no. 5, pp. 1431–1440, 1993.

[38] S. Teneberg, H. Miller-Podraza, H. C. Lampert, et al., "Carbohydrate binding specificity of the neutrophil-activating protein of *Helicobacter pylori*," *Journal of Biological Chemistry*, vol. 272, no. 30, pp. 19067–19071, 1997.

[39] D. J. Evans Jr., D. G. Evans, T. Takemura, et al., "Characterization of a *Helicobacter pylori* neutrophil-activating protein," *Infection and Immunity*, vol. 63, no. 6, pp. 2213–2220, 1995.

[40] C. Cooksley, P. J. Jenks, A. Green, A. Cockayne, R. P. H. Logan, and K. R. Hardie, "NapA protects *Helicobacter pylori* from oxidative stress damage, and its production is influenced by the ferric uptake regulator," *Journal of Medical Microbiology*, vol. 52, pt. 6, pp. 461–469, 2003.

[41] W. G. Dundon, A. Polenghi, G. Del Guidice, R. Rappuoli, and C. Montecucco, "Neutrophil-activating protein (HP-NAP) versus ferritin (Pfr): comparison of synthesis in *Helicobacter pylori*," *FEMS Microbiology Letters*, vol. 199, no. 1, pp. 143–149, 2001.

[42] B. A. Frazier, J. D. Pfeifer, D. G. Russell, et al., "Paracrystalline inclusions of a novel ferritin containing nonheme iron, produced by the human gastric pathogen *Helicobacter pylori*: evidence for a third class of ferritins," *Journal of Bacteriology*, vol. 175, no. 4, pp. 966–972, 1993.

[43] Y. H. Choe, T. S. Hwang, H. J. Kim, S. H. Shin, S. U. Song, and M. S. Choi, "A possible relation of the *Helicobacter pylori* pfr gene to iron deficiency anemia?" *Helicobacter*, vol. 6, no. 1, pp. 55–59, 2001.

[44] S. Bereswill, U. Waidner, S. Odenbreit, et al., "Structural, functional and mutational analysis of the pfr gene encoding a ferritin from *Helicobacter pylori*," *Microbiology*, vol. 144, pt. 9, pp. 2505–2516, 1998.

[45] S. Bereswill, S. Greiner, A. H. M. Van Vliet, et al., "Regulation of ferritin-mediated cytoplasmic iron storage by the ferric uptake regulator homolog (Fur) of *Helicobacter pylori*," *Journal of Bacteriology*, vol. 182, no. 21, pp. 5948–5953, 2000.

Hindawi Publishing Corporation
Metal-Based Drugs
Volume 2008, Article ID 275084, 8 pages
doi:10.1155/2008/275084

Research Article

DNA Binding and Photocleavage Studies of Cobalt(III) Ethylenediamine Pyridine Complexes: $[Co(en)_2(py)_2]^{3+}$ and $[Co(en)_2(mepy)_2]^{3+}$

Penumaka Nagababu,[1] D. Aravind Kumar,[2] Kotha Laxma Reddy,[1] K. Ashwini Kumar,[1] Md. B. Mustafa,[1] Mynam Shilpa,[1] and S. Satyanarayana[1]

[1] *Department of chemistry, Faculty of Science, Osmania University, Hyderabad 500 007, Andhra Pradesh, India*
[2] *Indian Institute of Chemical Technology, Taranaka, Hyderabad 500 007, India*

Correspondence should be addressed to S. Satyanarayana, ssnsirasani@yahoo.com

Received 7 May 2007; Accepted 4 July 2007

Recommended by Jannie C. Swarts

Two novel cobalt(III) pyridine complexes (**1**) $[Co(en)_2(py)_2]^{3+}$ and (**2**) $[Co(en)_2(mepy)_2]^{3+}$ (en=ethylenediamine, py=pyridine, and mepy=methylpyridine) have been synthesized and characterized. The interaction of these complexes with calf thymus DNA was investigated by absorption, emission spectroscopy, viscosity measurements, DNA melting, and DNA photocleavage. Results suggest that the two complexes bind to DNA via groove mode and complex **2** binds more strongly to CT DNA than complex **1**. Moreover, these Co(III) complexes have been found to promote the photocleavage of plasmid DNA pBR322 under irradiation at 365 nm, cytotoxicity results of complexes are also showing anticancer activity.

1. INTRODUCTION

The interaction of transition metal polypyridyl complexes with DNA has received a great deal of attention during the past decade [1–3]. Many complexes have been synthesized. These complexes can bind to DNA in noncovalent modes such as electrostatic, intercalative, and groove binding [4, 5]. The cationic metal complexes possessing planar aromatic ligands may bind to DNA by intercalation which involves stacking of the planar ligand in between adjacent base pairs of the DNA duplex [6–9]. In the early 1980s, Barton demonstrated that tris phenanthroline complexes of ruthenium (II) display enantiomeric selectivity in binding to DNA, which can be served as spectroscopic probes in solution to distinguish right- and left-handed DNA, helices [10]. Then they found that tris (phenanthroline) complexes of cobalt(III) could cleave DNA when irradiated at 254 nm. Furthermore, they conducted the cleavage reactions by using high stereo specificity of tris (diphenyl penanthroline) (DIP) metal isomers. The cleavage reaction is also stereo specific. These findings underscore the importance of an intimate association of the metal ion with the duplex. The high level of recognition of DNA conformation by these chiral inorganic complexes suggested the powerful application of stereo specificity in DNA drug design [11]. According to [12], *cis*- and *trans*-$[PtCl_2(pyridine)_2]$ complexes show anticancer activity and inhibit DNA synthesis, implying a role for DNA binding in their mechanism of action, and *cis* complex implies more binding with CT DNA than trans complex.

A series of dichloro(ethylenediamine)-type platinum complexes bearing ester-, amide-, and ether-bonded alkyl straight chains were prepared as a model for the prodrug of *cis*-diamminedichloroplatinum [13] and the cytotoxic activity of the complexes against the S-180 cell line was investigated. Schonenberger et al. presented antitumor active (1,2-diphenylethylenediamine)-platinum (II) complex compounds [14]. Ring-substituted diaqua(1,2-diphenylethylenediamine) platinum(II) sulfate was prepared [15] and mode of binding to the DNA was studied. A series of isomeric[1,2-*bis* (difluorophenyl) ethylenediamine] dichloroplatinum (II) complexes and *cis*-platin were tested on the P388 leukemia and on the murine

mammary carcinoma for evaluating antineoplastic activity against breast cancer in vivo [16]. The activity of 1,2-*bis*(2,6-difluoro-3-hydroxy-phenyl)ethylenediamine] platinum(II) complexes against breast cancer was investigated in [17].

Our group has synthesized some Ruthenium(II) and Cobalt(III) ethylenediamine mixed-polypyridyl complexes, which bind to DNA through an intercalative and groove mode and promote cleavage of plasmid pBR 322 DNA [18–21]. Herein we chose to concentrate on the cobalt(III)ethylenediamine complexes, because they have same interesting characteristics of metallointercalation. In this paper, we are reporting the synthesis and characterization of the complexes 1 and 2 in which 2 possesses a greater binding affinity and their DNA-binding properties are revealed by electronic absorption, emission spectra, viscosity measurement, and DNA melting curve. The photochemical DNA cleavage of the complexes is also demonstrated. These studies are necessary for further comprehension of binding of transition metal complexes to DNA. The cytotoxicity studies of 1 and 2 complexes were discussed in this paper.

2. EXPERIMENTAL

Materials. All materials were purchased and used without further purification unless otherwise noted. Pyridine, ethylenediamine, and CT DNA were purchased from *Aldrich*. All the experiments involving interaction of the complexes with DNA were carried out in BPE buffer (5 mM Tris-HCl, 50 mM NaCl, pH 7.0). A solution of calf thymus DNA in the buffer gave a ratio of UV absorbance at 260 and 280 nm of about 1.90 indicating that the DNA was sufficiently free of protein [22]. The DNA concentration per nucleotide was determined by absorption spectroscopy using the molar absorption coefficient (6600 $M^{-1}cm^{-1}$) at 260 nm [23].

3. SYNTHESIS OF COMPLEXES

3.1. $[Co(en)_2(py)_2]^{3+}$

A mixture of *cis*-$[Co(en)_2Cl_2]Cl$ (1.43 g) was prepared by the procedure available in the literature (see [24]). Complexes 1 and 2 were prepared by literature methods [25–27] as follows. A mixture of *trans*-$[Co(en)_2Cl_2]Cl$ {4.28 g, 0.015 mol} and pyridine {2.7 g, 0.015 mol} taken in distilled H_2O (20 cm^3) was heated at 100°C for 30 minutes. A saturated NaBr solution was added to the cooled solution, which was kept overnight. After filtration to remove $[Co(en)_3]Br_3$, Me_2CO (200 cm^3) was added, resulting in precipitation of a mixture of $[Co(en)_2(py)_2]Br_3$ and $[Co(en)(py)_4]Br_3$. This was dissolved in H_2O and the complex $[Co(en)_2(py)_2]Br_3$ was reprecipitated by addition of EtOH. $[Co(en)_2(Mepy)_2]Br_3$, (2) was prepared similarly using methylpyridine. UV/Vis: 361,470 and 618 nm Isosbestic points: 438 and 576 nm IR: 1457 (C=C), 1578 (C=N), 469 (Co−N (en)), 578 cm^{-1} (Co−N (L)). Formula: Co $N_6H_{26}C_{14}Br_3$Anal. Calc. H 4.54, C 29.14, N 14.56 found: H 4.01, C 29.0, N 14.02. ^{1}H-NMR (D_2O), 3.1,(dd, $2CH_2$ $(en)_2$, 2.55(m,$2CH_2(en)_2$, 7.69 (d, 2H), 8.210 (d, 2H), 7.990(t, 1H).

3.2. $[Co(en)_2(mepy)_2]^{3+}$

UV/Vis: 312, 447 and 617 nm, Isosbestic points: 449 and 578 nm IR: 1448 (C=C), 1577 (C=N), 467 (Co−N (en)), 555 cm^{-1} (Co−N (L)). Formula: Co $N_6H_{30}C_{16}Br_3$, Anal. Calc. H 5.00, C 31.76 N 13.89 found: H 4.8 C 30.56 N 12.18. ^{1}H-NMR (D_2O), 2.7,(dd, $2CH_2$ $(en)_2$, 2.89(m, $2CH_2(en)_2$, 7.412(d, 2H), 8.036(d,2H) 4.412(s, 3H).

3.3. Physical measurements

UV-Visible spectra were recorded on *Elico Bio*-spectrophotometer model *BL198*, emission spectra were recorded on a *Shimadzu Rf-2000* luminescence spectrometer at room temperature. IR spectra were recorded, in KBr phase on *Perkin-Elmer FTIR-1605* spectrophotometer; ^{1}H-NMR spectra were measured on a *Varian XL-300* MHz spectrometer with D_2O as a solvent at room temperature and tetramethylsilane (TMS) as the internal standard, Microanalyses (C, H, N) were carried out on a *Perkin-Elmer* 240 elemental analyzer.

For the absorption spectra titrations were carried out at room temperature to determine the binding affinity between DNA and complex. Initially, 3000 μL solutions of the blank buffer and the cobalt complex sample (20 μM) were placed in the reference and sample cuvettes (1 cm path length), respectively, and then first spectrum was recorded in the range of 200–600 nm. During the titration, aliquot (1–10 μL) of buffered DNA solution (concentration of ∼5 to 10 mM in base pairs) was added to each cuvette to eliminate the absorbance of DNA itself, and the solutions were mixed for ∼5 minutes, the absorption spectra were recorded. The titration processes were repeated until there was no change in the spectra indicating that binding saturation had been achieved. The changes in the metal complex concentration due to dilution at the end of each titration were negligible. The cobalt (III) complexes on other hand, showed additional MLCT bands between 400–500 nm [28].

Emission measurements were carried out by using a HitachiF 4500 Fluorescence Spectrometer. Tris-buffer was used as a blank to make preliminary adjustments. The excitation wavelength was fixed and the emission range was adjusted before measurements. All measurements were made at 25° in a thermostated cuvette holder with 5 nm entrance slit and 5 nm exit slit. Emission titration experiments were performed at a fixed metal complex concentration (20 μM) to which increments of a stock DNA solution (0–160 μM) containing the same concentration of the metal complexes were added. The emission enhancement factors were measured by comparing the intensities at 559 nm in the absence and presence of CT DNA.

Viscosity experiments were carried out using an Ostwald viscometer maintained at a constant temperature 30.0 ± 0.1° in a thermostatic water bath. Calf thymus DNA samples, approximately 200 base pairs in average length, were prepared by sonicating in order to minimize complexities arising from DNA flexibility [29]. Data were presented as $(\eta/\eta_0)^{1/3}$ versus the concentration of Co(III) complexes, where η is the viscosity of DNA in presence of complexes and η_0 is the viscosity

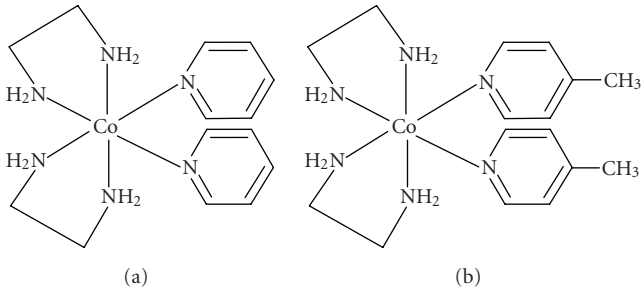

Figure 1: Molecular structure of complexes.

of DNA alone. Viscosity values were calculated from the observed flow time of DNA-containing solution ($t > 100$ seconds) corrected for flow time of buffer alone (t_0), $\eta = t - t_0$ [30]. The DNA melting experiments were done by controlling the temperature of the sample cell with a *Shimadzu* circulating bath while monitoring the absorbance at 260 nm.

Thermal denaturation studies were carried out with a *Elico Bio*-spectrophotometer model *BL198*, equipped with temperature-controlling programmer (±0.1°C). The absorbance at 260 nm was continuously monitored for solutions of CT-DNA (100 μM) in the absence and presence of the cobalt(III) complex (10 μM). The temperature of the solution was increased by 1°C min^{-1}. For the gel electrophoresis experiments, super coiled pBR322 DNA (100 μM) was treated with Co(III) complexes in pH = 7.2, and the solutions were incubated for 1 hour h in the dark. The samples were analyzed by electrophoresis for 2.5 hours at 40 V on a 0.8% agarose gel in buffer, pH 7.2. The gel was stained with 1 μg/ml ethidiumbromide and then photographed under UV light.

3.4. Spectroscopic characterization

Molecular structures of the complexes are given in Figure 1. The IR spectral data for the complexes are given. The complexes clearly exhibit a band at 1458 cm^{-1}and 1578–1590 cm^{-1} corresponding to C=C and C=N of the ring, respectively. A band at around 589 cm^{-1} and 590 cm^{-1} corresponding to Co−N(en) and Co−N of NH_2(en) bending exhibits around 1650 cm^{-1}. In the ^{1}H-NMR spectra of the Co(III) complexes, the peaks due to various protons of pyridine shifted downfield compared to the free ligand suggesting complexation. As expected the signal for pyridine appeared in the range between 6.5 to 9.2, CH_2 of ethylenediamine gave peaks at 3.1 (br, 4 H, CH_2(en)).

3.5. Cell viability MTT assay

All cell culture reagents and media were purchased from Sigma-Aldrich and used without further purification unless otherwise noted. Cytotoxicity assay were performed using Chinese hamster ovarian (CHO) in order to assess the cancer chemotherapeutic potential of the cells. Cells were grown as monolayers in Eagle's minimum essential medium, supplemented with 2 mM L-glutamine and Earle's balanced salt solution, containing 1.5 g dm^{-3}, sodium bicarbonate, 0.1 mM nonessential amino acids, 1.0 mM sodium pyruvate, 100 cm^{-3} penicillin, and 100 μgcm^{-3} streptomycin supplemented to contain 10% (v/v) foetal bovine serum. All cells were grown at 37°C in a humidified atmosphere, in the presence of 5% CO_2, and were in the exponential phase of growth at the time of assay. Cytotoxicity was assessed using MTT assay. Cells (100 μL) were seeded at a density of 5×10^4 cells cm^{-3} into sterile 96 well flat-bottomed plates (Falcon, Plastics, Becton, Dickinson) and grown in 5% CO_2 at 37°C. Test compounds were dissolved in culture media. Each drug solution (100 μL) was added to replicate wells in the concentration range of 0.1–100 μM and incubated for 72 hours. A miniaturized viability assay using 3-(4,5-dimethylthiazol-2-yl)-2,5-diphenyl tetrazolium bromide (MTT) was carried out according to method described by Mosmann [31]. The IC_{50} value, defined as the drug concentration causing a 50% reduction in cellular viability was calculated for each drug. Each assay was carried out using five replicates and repeated on at least three separate occasions. Viability was calculated as a percentage of solvent-treated control cells, and expressed as a percentage of the control. The significance of any reduction in cellular viability was determined using one-way ANOVA (analysis of variance). A probability of .05 or less was deemed statistically significant.

4. RESULTS AND DISCUSSION

4.1. Absorption spectral studies

Absorption titration experiments of Co(III) complexes in buffer were performed by using fixed cobalt complex concentration to which increments of the DNA stock solution were added. The calf thymus DNA was added to a ratio of 8:1 [DNA]/[Co]. Cobalt solutions were allowed to incubate for 10 minutes before the absorption spectra were recorded (see Figures 2(a) and 2(b)). As the DNA concentration is increased, the MLTC transition bands of complex at 618 nm exhibit hypochromism and as well as an insignificant bathochromism, showing isosbestic points at 438, 576 and 449, 578 complexes 1 and 2, respectively. Based on the observations of complexes, we presume that there are some interactions between complexes and DNA. To know quantitatively the binding strength of the complexes, the intrinsic binding constant K_b of the complexes with CT-DNA were obtained by monitoring the changes in absorbance at 618 and 617 nm for complexes (1 and 2, resp.) with increasing concentration of DNA using the following function equation [32], which has been applied to describe the binding of high-affinity complexes to DNA assuming noncooperative binding to discrete sites:

$$[\mathrm{DNA}]/(\epsilon_a - \epsilon_f) = [\mathrm{DNA}]/(\epsilon_b - \epsilon_f) + 1/(\mathrm{K}(\epsilon_b - \epsilon_f)), \quad (1)$$

where [DNA] is the concentration of DNA in base pairs, the apparent absorption coefficients ϵ_a, ϵ_f and K_b correspond to A_{obs}/[Co], the extinction coefficient for cobalt complexes in the free and fully bound form, respectively. In plots [DNA]/($\epsilon_a - \epsilon_f$) versus [DNA]. K is given by the ratio of slope

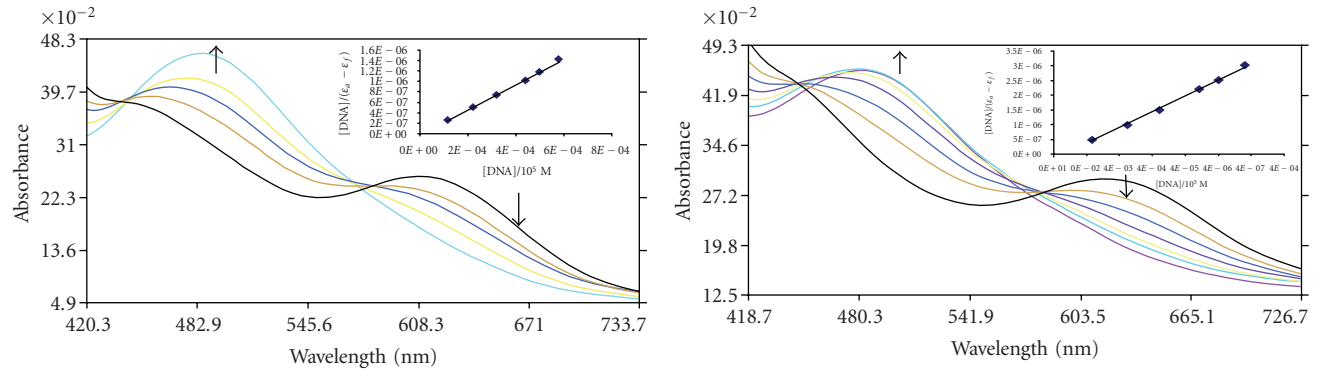

FIGURE 2: Absorption spectra of complexes: (a) complex 1, (b) complex 2, in tris-HCl buffer. Upon addition of CT DNA to complex absorption decreases [Co] = 10 μM; [DNA] = 0–126 μM. Insert: plots of $(\epsilon_a - \epsilon_f)/(\epsilon_b - \epsilon_f)$ versus [DNA] for the titration of DNA with Co(III) complexes. Isosbestic points at 438, 576 for complex 1. Isosbestic points at 449, 578 for complex 2.

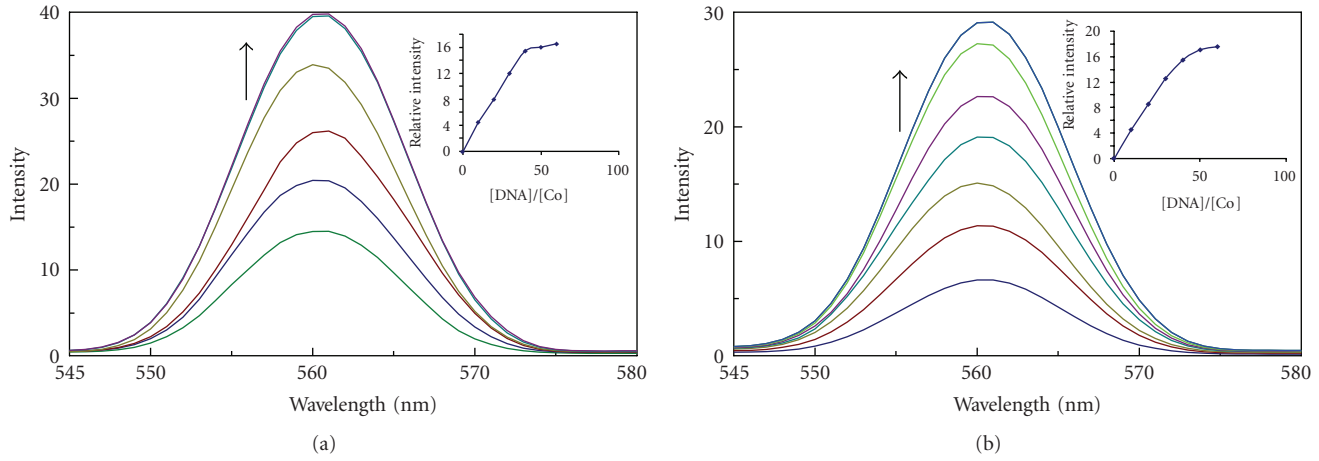

FIGURE 3: Fluorescence emission spectra of complexes: (a) complex 1, (b) complex 2 in tris-HCl buffer. Fluorescence intensity increases upon increasing CT DNA concentrations (5 μl, 10 μl, 15 μl, 20 μl, ...). Insert: plots of relative emission intensity versus [DNA]/[Co].

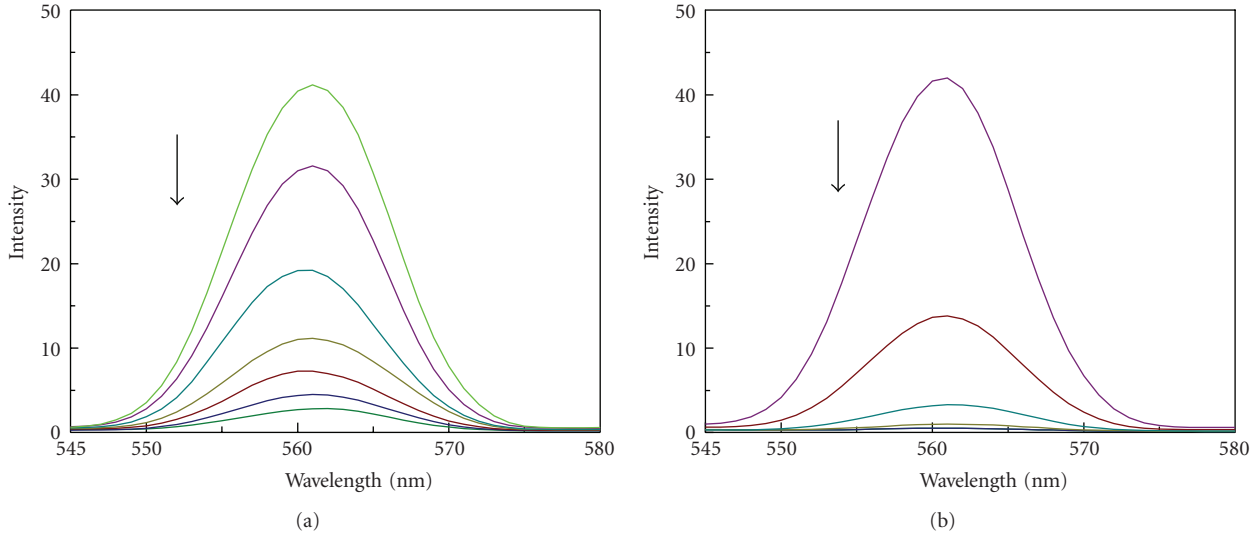

FIGURE 4: Fluorescence quenching curves of DNA + complex by ferrocyanide: (a) complex 1 + DNA; (b) complex 2 + DNA.

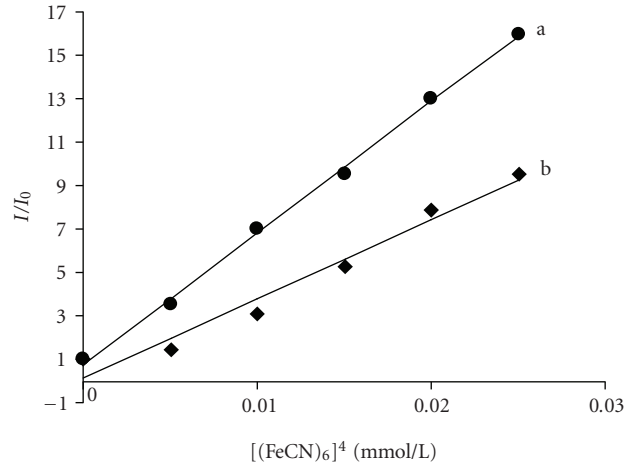

Figure 5: Quenching of fluorescence emission of Co(III) complex + DNA with Ferro cyanide: (a) complex1 + DNA, (b) complex 2 + DNA.

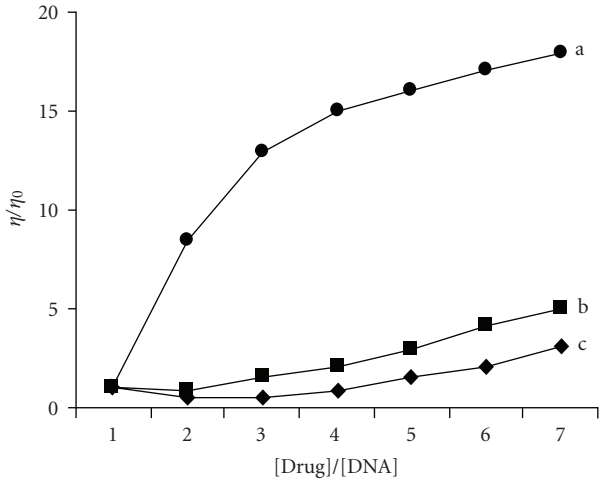

Figure 6: Effect of increasing amount of complexes on the relative viscosities of CT DNA at $25 \pm 0.1^\circ$: (a) EtBr, (b) complex 2, (c) complex 1.

to intercept. Intrinsic binding constants K obtained about $2.7 \pm 0.2 \times 10^3$ and $3.5 \pm 0.2 \times 10^3$ of complexes 1 and 2, respectively, from the decay of the absorbance. The binding constants indicate that complex 2 binds more strongly than 1 to CT DNA.

4.2. Emission studies

In the absence of DNA, complexes can emit luminescence in Tris buffer with emission maximum appearing at 562 nm. Upon addition of CT DNA (= Calf thymus DNA), the emission intensities of the complexes increase when compared to the intensity of complexes alone shown in Figures 3(a) and 3(b). This implies that complexes can strongly interact with DNA and be protected by DNA efficiently, since the hydrophobic environment inside the DNA helix reduces the accessibility of solvent water molecules to the duplex and the complexes mobility is restricted at the binding site, lead to decrease the vibrational modes of relaxation.

This observation is further supported by the fluorescence quenching experiments using $[Fe(CN)_6]^{4-}$ as quencher. The ion $[Fe(CN)_6]^{4-}$ has been shown to be able to distinguish differentially bound Co(III) species and positively charged free complex ions should be readily quenched by $[Fe(CN)_6]^{4-}$. The complexes bound to DNA can be protected from the quencher, because highly negatively charged $[Fe(CN)_6]^{4-}$ would be repelled by the negative DNA phosphate backbone, hindering quenching of the emission of the bound complex. The method essentially consists of titrating a given amount of DNA-metal complexes with increasing the concentration of $[Fe(CN)_6]^{4-}$ and measuring the change in fluorescence intensity (see Figure 4). The ferro-cyanide quenching curves for these complexes in the presence and absence of CT DNA are shown in Figure 5. Obviously, complex 2 inserts into DNA much deeper than 1. The absorption and fluorescence spectroscopy studies determine the binding of complexes with DNA.

4.3. Viscosity studies

Mode of interaction between the metal complexes and DNA was clarified by viscosity measurements. Optical photophysical probes are necessary, but not sufficient to support a binding model. Hydrodynamic measurements are sensitive to length change (i.e., viscosity and sedimentation) are regarded as the least ambiguous and the most critical tests of binding in solution in the absence of crystallographic structural data [33]. A classical intercalation model results in unwinding of the DNA helix, which would lead to an increase in viscosity. In contrast, a partial and/or nonclassical intercalation of ligand could bend (or kink) the DNA helix, reduce its effective length and concomitantly, its viscosity [30]. Effect of the complexes on the viscosity of rod-like DNA is shown in Figure 6. The viscosity of DNA is not increased with the increase of the concentration of complexes, in contrast to that of proven DNA intercalator EtBr (= ethidium bromide). Based on the viscosity results, it was observed that these complexes bind with DNA through groove binding, result from DNA melting experiment further supported the above result.

4.4. DNA melting studies

As intercalation of the complexes into DNA base pairs causes stabilization of base stacking and hence raises the melting temperature of the double-stranded DNA, the DNA melting experiment is useful in establishing the extent of intercalation [34]. The complexes were incubated with CT DNA and their temperature raised from 25 to 85° and the absorbance at 260 nm was monitored. Conductivity and pH measurements were also carried out before and after heating the complexes to 85° through 1 hour [35]. The presence of monophasic melting curves with no change in pH. ΔT_m values of the DNA in presence of complexes is shown in Table 1, revealing avid DNA binding [36]. The complexes show ΔT_m values of 3° which is characteristic of a nonintercalative binding

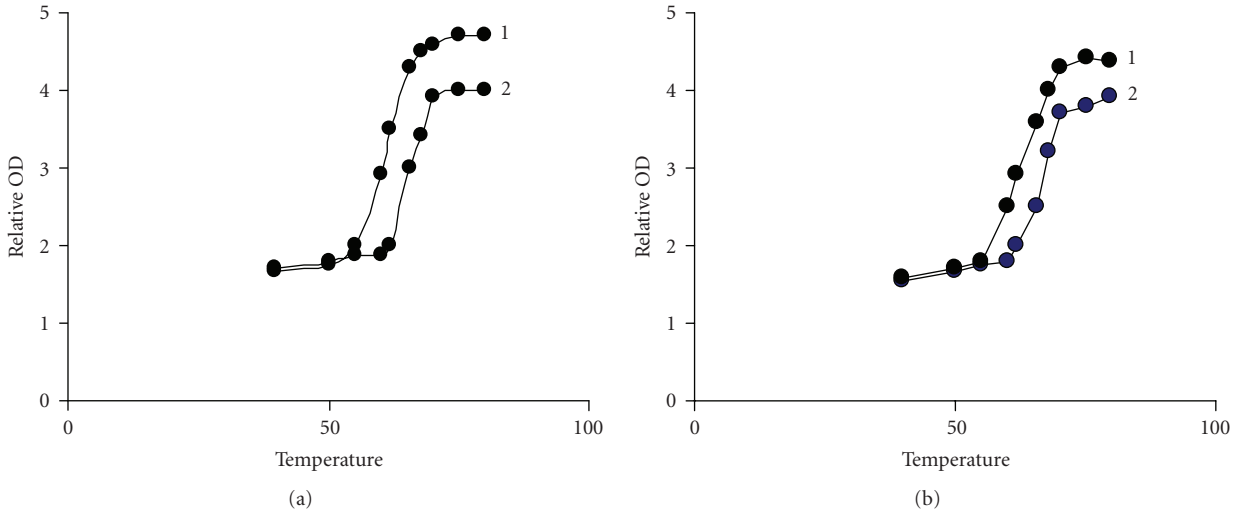

Figure 7: Plots of A/A_0 versus temperature for the melting of CT DNA: (a) 1 only DNA spectra 2 DNA + complex 1, (b) 1 only DNA 2 DNA + complex 2.

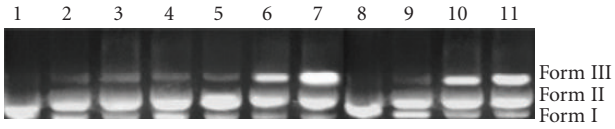

Figure 8: Photocleavage of pBR 322 DNA: lane 1 control plasmid DNA (untreated pBR 322), lanes 2–11 addition of complex (1) in amounts of 5, 10, 20, 30... μl. Line 8 at 0 time lanes 7–10, + 5 μm complex up on irradiation (λ_{irrd} = 360 nm) at 5 minutes, 10 minutes, 20 minutes, 30 minutes.

Table 1: ΔT_m values of the DNA and complex + DNA.

Compound	T_M°C
CT DNA	60
$[Co(en)_2(py)_2]^{3+}$	63
$[Co(en)_2(mepy)_2]^{3+}$	63

Table 2: IC_{50} values of complexes 1, 2.

Complexes	IC_{50}(nm) Mean±SEM
$[Co(en)_2(mepy)_2]Br_3$	1.8 μM
$[Co(en)_2(py)_2]Br_3$	1.75 μM

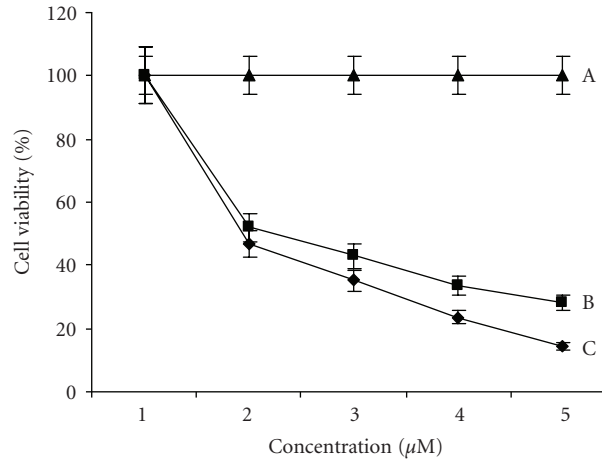

Figure 9: Effects of complex 2 [C], 1[B], and control [A] on the viability of CHO cells (human hepatocellular), following continuous incubation for 72 hours, with increasing drug concentration (0.1–500 μM). Bars indicate standard error of the mean (SEM) and results were statistically significant from control at $P < .05$. Results are representative of three independent experiments ($n = 3$).

behavior (see Figure 7). viscosity experiments further support the nonintercalative binding.

4.5. Photocleavage of pBR322 DNA by Co(III) complexes

There has been considerable interest in DNA endonucleolytic cleavage reactions which are activated by metal ions [37]. The delivery of high concentrations of metal ion to the helix, in locally generating oxygen or hydroxide radicals, yields an efficient DNA cleavage reaction. DNA photocleavage was monitored by relation of supercoiled circular pBR 322 (form I) into nicked circular (form II) and linear (form III). When circular plasimd DNA is subjected to electrophoresis, relatively fast migration will be observed for the supercoiled form (form I). If scission occurs on one strand (nicking), the supercoils will relax to generate a slower-moving open circular form (form II) [38]. If both strands are cleaved, a linear form (III) will be generated that migrates between forms I and II. Figure 8 shows the gel electrophoretic separations of plasmid pBR 322 DNA after incubation and irradiation at 360 nm with complex 1. This is the result of single stranded photocleavage of pBR322 DNA. That incubation with Co(III) without light yields significant strand scission. It is most likely that the reduction of Co(III) is the important

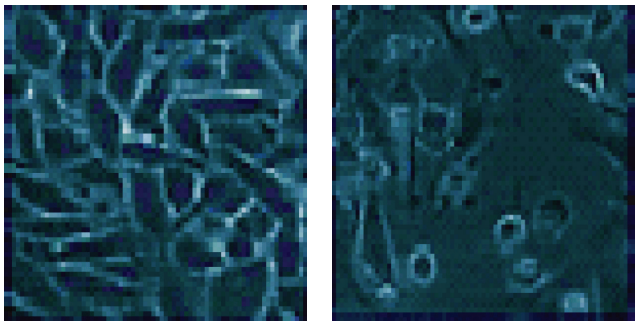

(a) (b)

Figure 10: The morphological effects exerted by complexes on CHO cells 24 hours after treatment. Photographs were taken using a Nikon inverted light microscope (20X objective). (a) shows the untreated cells and while (b) shows cells treated with 0.5 mM of complex 2.

step leading to DNA cleavage. Further study required to find out the path of reaction mechanism.

4.6. Anticancer studies

The ability of the cobalt complexes 1 and 2 to kill human-derived cancer cells was investigated using CHO cells and a standard bioassay, MTT. Cells were continuously exposed to test agent for 72 hours, and their effects on cellular viability was evaluated. It was intended that the results from these studies would allow the identification of those derivatives with cancer chemotherapeutic potential. Therefore, profiles of cell viability against complex concentration were established Figure 9 and were used to calculate the IC_{50} values for each derivative (see Table 2). Comparison of IC_{50} values allowed the relative potency of each of the test complexes to be determined and ranked. Photographs of treated and untreated CHO cells are presented in Figure 10. Both complexes screened displayed a concentration dependent cytotoxic profile. The order of the observed cytotoxicity was seen as complex 2 appearing as the potent.

5. CONCLUSIONS

In this study, we have attempted to unravel the DNA interaction of ethylenediamine pyridine Co(III) complexes. The binding behavior of complexes with DNA was characterized by absorption titration, fluorescence, and fluorescence quenching and viscosity measurements. The experimental results indicate that the complexes can bind to DNA through groove and Co(III) complex can efficiently cleave the plasmid pBR322. Overall, the results described explain to the DNA-binding, cleavage ability. The complex containing py ligand shows better anticancer activity than mepy. The efficiency of these complexes on various cancerous cell lines is presently being studied in our laboratory.

ABBREVIATIONS

CT DNA:	Calf thymus DNA
py:	Pyridine
mepy:	Methylpyridine
en:	ethylenediamine
EtBr:	Ethedium bromide

ACKNOWLEDGMENT

We are grateful to UGC-MJRP, India, for providing financial support.

REFERENCES

[1] K. E. Erkkila, D. T. Odom, and J. K. Barton, "Recognition and reaction of metallointercalators with DNA," *Chemical Reviews*, vol. 99, no. 9, pp. 2777–2795, 1999.

[2] M. Demeunynck, C. Bailly, and W. D. Wilson, Eds., *DNA and RNA Binders: From Small Molecules to Drugs*, Wiley-VCH, Weinheim, Germany, 2003.

[3] M. Gielen and E. R. T. Tiekink, Eds., *Metallotherapeutic Drugs and Metal-Based Diagnostic Agents: The Use of Metals in Medicine*, John Wiley & Sons, New York, NY, USA, 2005.

[4] J. A. Cowan, "Chemical nucleases," *Current Opinion in Chemical Biology*, vol. 5, no. 6, pp. 634–642, 2001.

[5] L.-N. Ji, X.-H. Zou, and J.-G. Liu, "Shape- and enantioselective interaction of Ru(II)/Co(III) polypyridyl complexes with DNA," *Coordination Chemistry Reviews*, vol. 216-217, pp. 513–536, 2001.

[6] J. K. Barton, "Metals and DNA: molecular left-handed complements," *Science*, vol. 233, no. 4765, pp. 727–734, 1986.

[7] C. S. Chow and J. K. Barton, "Shape-selective cleavage of $tRNA^{Phe}$ by transition-metal complexes," *Journal of the American Chemical Society*, vol. 112, no. 7, pp. 2839–2841, 1990.

[8] X. Qu and J. B. Chaires, "Hydration changes for DNA intercalation reactions," *Journal of the American Chemical Society*, vol. 123, no. 1, pp. 1–7, 2001.

[9] Y. Xiong and L.-N. Ji, "Synthesis, DNA-binding and DNA-mediated luminescence quenching of Ru(II) polypyridine complexes," *Coordination Chemistry Reviews*, vol. 185-186, pp. 711–733, 1999.

[10] J. K. Barton, "Tris (phenanthroline) metal complexes: probes for DNA helicity," *Journal of Biomolecular Structure & Dynamics*, vol. 1, no. 3, pp. 621–632, 1983.

[11] J. K. Barton and A. L. Raphael, "Photoactivated stereospecific cleavage of double-helical DNA by cobalt(III) complexes," *Journal of the American Chemical Society*, vol. 106, no. 8, pp. 2466–2468, 1984.

[12] N. Farrell, L. R. Kelland, J. D. Roberts, and M. Van Beusichem, "Activation of the trans geometry in platinum antitumor complexes: a survey of the cytotoxicity of trans complexes containing planar ligands in murine L1210 and human tumor panels and studies on their mechanism of action," *Cancer Research*, vol. 52, no. 18, pp. 5065–5072, 1992.

[13] Y. Kageyama, Y. Yamazaki, and H. Okuno, "Novel approaches to prodrugs of anticancer diaminodichloroplatinum(II) complexes activated by stereoselective enzymatic ester hydrolysis," *Journal of Inorganic Biochemistry*, vol. 70, no. 1, pp. 25–32, 1998.

[14] H. Schonenberger, B. Wappes, M. Jennerwein, E. von Angerer, and J. Engel, "(1,2-diphenyl)-ethylenediamine-platinum (II) complex compounds," US4598091, 1986.

[15] F. Bernges and E. Holler, "Ring-substituted diaqua(1,2-diphenylethylenediamine)platinum(II) sulfate reacts with DNA through a dissociable complex," *European Journal of Biochemistry*, vol. 208, no. 3, pp. 573–579, 1992.

[16] T. Spruss, G. Bernhardt, E. Schickaneder, and H. Schönenberger, "Different response of murine and human mammary tumour models to a series of diastereoisomeric [1,2-bis(difluorophenyl) ethylenediamine]dichloroplatinum(II) complexes," *Journal of Cancer Research and Clinical Oncology*, vol. 117, no. 5, pp. 435–443, 1991.

[17] S. Schertl, R. W. Hartmann, C. Batzl-Hartmann, et al., "[1,2-bis(2,6-difluoro-3-hydroxyphenyl)ethylene-diamine]platinum (II) complexes, compounds for the endocrine therapy of breast cancer - mode of action II: contribution of drug inactivation, cellular drug uptake and sterical factors in the drug-target interaction to the antitumor activity," *Archiv der Pharmazie*, vol. 337, no. 6, pp. 349–359, 2004.

[18] P. Nagababu, J. N. L. Latha, and S. Satyanarayana, "DNA-binding studies of mixed-ligand (ethylenediamine)ruthenium (II) complexes," *Chemistry & Biodiversity*, vol. 3, no. 11, pp. 1219–1229, 2006.

[19] P. Nagababu and S. Satyanarayana, "DNA binding and cleavage properties of certain ethylenediamine cobalt(III) complexes of modified 1,10-phenanthrolines," *Polyhedron*, vol. 26, no. 8, pp. 1686–1692, 2007.

[20] P. Nagababu and S. Satyanarayana, "DNA binding and photocleavage studies of cobalt(III) polypyridine complexes: $[Co(en)_2PIP]^{3+}$, $[Co(en)_2IP]^{3+}$, and $[Co(en)_2phen\text{-}dione]^{3+}$," *Bioinorganic Chemistry and Applications*, vol. 2007, Article ID 54562, 8 pages, 2007.

[21] P. Pallavi, P. Nagababu, and S. Satyanarayana, "Biomimetic model of coenzyme B_{12}: aquabis(ethane-1,2-diamine-$\kappa N, \kappa N'$)ethylcobalt(III) - its kinetic and binding studies with imidazoles and amino acids and interactions with CT DNA," *Helvetica Chimica Acta*, vol. 90, no. 3, pp. 627–639, 2007.

[22] B. P. Sullivan, D. J. Salmon, and T. J. Meyer, "Mixed phosphine 2,2′-bipyridine complexes of ruthenium," *Inorganic Chemistry*, vol. 17, no. 12, pp. 3334–3341, 1978.

[23] J. Marmur, "A procedure for the isolation of DNA from microorganisms," *Journal of Molecular Biology*, vol. 3, pp. 208–218, 1961.

[24] W. C. Fernelius, Ed., *Inorganic Syntheses: Volume 2*, McGraw-Hill, New York, NY, USA, 1946.

[25] A. C. Barve, S. Ghosh, A. A. Kumbhar, A. S. Kumbhar, and V. G. Puranik, "DNA-binding studies of mixed ligand cobalt(III) complexes," *Transition Metal Chemistry*, vol. 30, no. 3, pp. 312–316, 2005.

[26] R. D. Gillard, R. E. E. Hill, and R. Maskill, "Optically active co-ordination compounds—part XX: reactions of 1,10-phenanthroline co-ordinated to cobalt(III)," *Journal of the Chemical Society A*, vol. 707, pp. 1447–1451, 1970.

[27] A. M. Funston, R. W. Gable, W. D. McFadyen, and P. A. Tregloan, "The preparation of a mixed-ligand cobalt(III) complex of DPPZ and ethylenediamine: crystal structures of $[Co(en)_2(DPPZ)](ClO_4)_3.0.5H_2O$, $[Co(en)_2(bpy)]Br(ClO_4)_2$ and $[Co(en)_2(phen)]Br_3$," *Australian Journal of Chemistry*, vol. 52, no. 8, pp. 817–822, 1999.

[28] D. M. Roundhill, *Photochemistry and Photophysics of Metal Complexes*, Plenum Press, New York, NY, USA, 1994.

[29] J. B. Chaires, N. Dattagupta, and D. M. Crothers, "Selfassociation of daunomycin," *Biochemistry*, vol. 21, no. 17, pp. 3927–3932, 1982.

[30] S. Satyanarayana, J. C. Dabrowiak, and J. B. Chaires, "Tris(phenanthroline)ruthenium(II) enantiomer interactions with DNA: mode and specificity of binding," *Biochemistry*, vol. 32, no. 10, pp. 2573–2584, 1993.

[31] T. Mosmann, "Rapid colorimetric assay for cellular growth and survival: application to proliferation and cytotoxicity assays," *Journal of Immunological Methods*, vol. 65, no. 1-2, pp. 55–63, 1983.

[32] A. Wolfe, G. H. Shimer Jr., and T. Meehan, "Polycyclic aromatic hydrocarbons physically intercalate into duplex regions of denatured DNA," *Biochemistry*, vol. 26, no. 20, pp. 6392–6396, 1987.

[33] S. Satyanarayana, J. C. Dabrowiak, and J. B. Chaires, "Neither Δ- nor Λ-tris(phenanthroline)ruthenium(II) binds to DNA by classical intercalation," *Biochemistry*, vol. 31, no. 39, pp. 9319–9324, 1992.

[34] J. M. Kelly, A. B. Tossi, D. J. McConnell, and C. OhUigin, "A study of the interactions of some polypyridylruthenium(II) complexes with DNA using fluorescence spectroscopy, topoisomerisation and thermal denaturation," *Nucleic Acids Research*, vol. 13, no. 17, pp. 6017–6034, 1985.

[35] E. Tselepi-Kalouli and N. Katsaros, "The interaction of $[Ru(NH_3)_5CI]^{2+}$ and $[Ru(NH_3)_6]^{3+}$ ions with DNA," *Journal of Inorganic Biochemistry*, vol. 37, no. 4, pp. 271–282, 1989.

[36] R. B. López, B. L. Loeb, T. Boussie, and T. J. Meyer, "Synthesis of a new phenanthroline derived ligand with acceptor properties," *Tetrahedron Letters*, vol. 37, no. 31, pp. 5437–5440, 1996.

[37] D. R. Graham, L. E. Marshall, K. A. Reich, and D. S. Sigman, "Cleavage of DNA by coordination complexes. Superoxide formation in the oxidation of 1,10-phenanthroline-cuprous complexes by oxygen - relevance to DNA-cleavage reaction," *Journal of the American Chemical Society*, vol. 102, no. 16, pp. 5419–5421, 1980.

[38] J. K. Barton and A. L. Raphael, "Photoactivated stereospecific cleavage of double-helical DNA by cobalt(III) complexes," *Journal of the American Chemical Society*, vol. 106, no. 8, pp. 2466–2468, 1984.

Hindawi Publishing Corporation
Metal-Based Drugs
Volume 2008, Article ID 495123, 10 pages
doi:10.1155/2008/495123

Review Article

Metallocene Antimalarials: The Continuing Quest

Margaret A. L. Blackie[1] and Kelly Chibale[1,2]

[1] *Department of Chemistry, University of Cape Town, Rondebosch 7701, South Africa*
[2] *Institute of Infectious Disease and Molecular Medicine, UCT Faculty Of Health Sciences, University of Cape Town, Observatory 7925, South Africa*

Correspondence should be addressed to Kelly Chibale, kelly.chibale@uct.ac.za

Received 20 June 2007; Accepted 23 August 2007

Recommended by Jannie C. Swarts

Over the last decade, a significant body of research has been developed around the inclusion of a metallocene moiety into known antimalarial compounds. Ferroquine is the most successful of these compounds. Herein, we describe our contribution to metallocene antimalarials. Our approach has sought to introduce diversity sites in the side chain of ferroquine in order to develop a series of ferroquine derivatives. The replacement of the ferrocenyl moiety with ruthenocene has given rise to ruthenoquine and a modest series of analogues. The reaction of ferroquine and selected analogues with $Au(PPh_3)NO_3$, $Au(C_6F_5)(tht)$, and $[Rh(COD)Cl_2]$ has resulted in a series of heterobimetallic derivatives. In all cases, compounds have been evaluated for in vitro antiplasmodial activity in both chloroquine-sensitive and chloroquine-resistant strains of *Plasmodium falciparum*. Preliminary structure-activity relationships have been delineated.

1. INTRODUCTION

The ongoing battle against malaria is far from over. In the 1950s and 1960s, there was a massive drive to try and eradicate malaria worldwide following the successful eradication of the disease in the United States. The population at risk from malaria was reduced to 10%. However, the banning of dicophane (DDT) and the concurrent emergence of chloroquine resistance led to the collapse of this campaign. A quarter of a century later, over 300 million clinical cases of malaria occur annually and over 40% of the world's population is at risk of contracting the disease. Of these cases, over one million will prove fatal [1]. The greatest tragedy of malaria is that 90% of fatalities occur in sub-Saharan Africa, and the overwhelming majority of those fatalities are children under the age of 5. Malaria is still essentially a tropical disease, but continues to claim the title of one of the leading killers among infectious diseases. The importance of developing new antiplasmodial drugs cannot be overemphasised. The Roll Back Malaria campaign which began in 1998 has yet to show a decrease in malaria mortality rates [2].

Over the last decade, there has been an increasing interest in metal-containing antiplasmodials. This trend was in part initiated by the successes of metal-containing antitumour drugs such as cisplatin. In the 1980's and 1990's, interest in coordination complexes of known chemotherapeutic agents began to emerge [3, 4]. It was not long before coordination complexes of chloroquine were synthesised and evaluated for efficacy against both chloroquine-sensitive and chloroquine-resistant strains of *P. falciparum* [5–7]. It is not surprising that antiplasmodial efficacy proved to be somewhat dependent on both metal and ligand.

The incorporation of a metallocene into compounds with medicinal application was rare prior to the 1980's. The low cytotoxicity of ferrocene, coupled with its lipophilicity ($\log P_{octanol/water} = 3.28$) and its electrochemical behaviour (redox potential of the ferrocene/ferrocenium couple, $E_0 = +0.400$ V versus SCE (Saturated Calomel Electrode)), suggested that this compound could yield interesting results if incorporated into a known drug [8]. Indeed there are several reported successes of increased efficacy of ferrocenyl analogues of known drugs. Ferrocifen, the ferrocenyl analogue of tamoxifen, has shown antiproliferation effects in both hormone-dependent and hormone-independent tumours. Tamoxifen and other established chemotherapeutic agents fail to exhibit such antiproliferative effects in both hormone-dependent and hormone-independent cell lines [9].

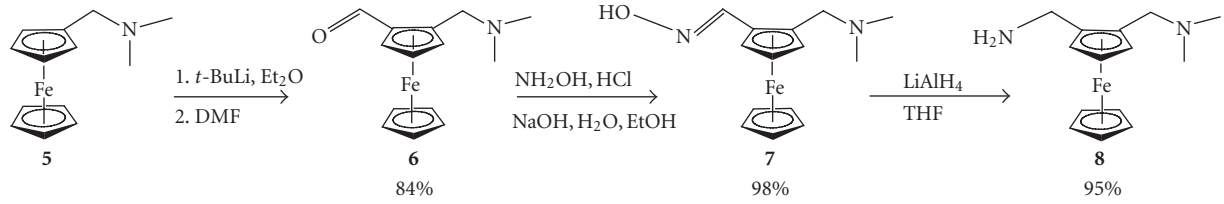

Scheme 1: Synthesis of [(*N*,*N*-dimethylamino)methyl] ferrocenecarboxaldehyde (**6**), and 2-[(*N*,*N*-dimethylamino)methyl] ferrocenemethylamine (**8**).

Ferroquine and other ferrocenyl chloroquine analogues have been shown to be efficacious in vitro in both chloroquine-sensitive and chloroquine-resistant *P. falciparum* across a variety of strains [10–12].

The purpose of this paper is to draw together some of the research carried out within our laboratories in the field of metal-containing chloroquine derivatives. This research, together with work published recently by other researchers, will hopefully shed some light on the role of ferrocene in ferroquine and related compounds.

2. FERROQUINE ANALOGUES AND DERIVATIVES

Brocard and colleagues have developed a number of ferrocene-containing chloroquine analogues [10]. Ferrocene was incorporated as an integral part of the side chain; as a terminal component of the side chain; and bonded through the quinoline nitrogen [11–13]. They have shown that incorporation of a ferrocenyl moiety as an integral part of the side chain of chloroquine between the two nitrogens had superior efficacy to other analogues in which the moiety was terminal on the side chain or bonded to the quinoline nitrogen. Some analogues of the compound were produced bearing different alkyl groups on the terminal tertiary nitrogen. They established that the dimethylamino terminal group was superior in efficacy [10].

Building on this foundation, we decided to explore the possibility of developing other analogues of ferroquine in which a reactive secondary amine group between the quinoline and ferrocenyl moieties would serve as a site for introducing further chemical diversity. We reasoned that this would facilitate the exploration of structure-activity relationships. The role of the length of the methylene spacer between the two nitrogens in chloroquine analogues has been shown to have an influence on efficacy in chloroquine-resistant strains of *P. falciparum* [14]. Krogstad and coworkers have shown that aminoquinolines with short (2-3 carbons) and long (10–12 carbons) methylene side chains are equipotent against chloroquine-sensitive, chloroquine-resistant, and multidrug-resistant strains of *P. falciparum*. Whilst aminoquinolines with side chains of intermediate length (4–8 carbons) showed efficacy against chloroquine-sensitive strains of *P. falciparum*, they showed a significant decrease in efficacy against chloroquine-resistant strains of *P. falciparum* [15]. For this reason, we decided to explore the influence of chain length on ferroquine analogues. The parallel series of urea derivatives was also synthesised and evaluated at the same time. The introduction of structural diversity via the urea functionality is a well-established strategy in the development of new biologically active compounds [16].

Synthesis of the ferroquine-type compounds was achieved via the synthetic strategy shown in Schemes 1–3. The reaction of **5** with *n*-butyllithium gave the desired product in a reasonable yield (70%) [10]. However, the use of *tert*-butyllithium had the effect of reducing the reaction time and improving the yield [17]. The presence of the dimethylaminomethyl substituent on the ferrocene results in a high regioselectivity for the 1,2-disubstituted product **6**.

Ferroquine (**2**) was synthesised from 2-[(*N*,*N*-dimethylamino)methyl] ferrocenemethylamine (**8**) and 4,7-dichloroquinoline. The published procedure uses dichloromethane and brine for the workup, in order to extract the product from 1-methylpyrrolidinone [10]. We favoured the use of ethyl acetate rather than dichloromethane as it was more time efficient. This had little impact on the moderate yield of the reaction (53%).

Synthesis of compound **10** was achieved from 4,7-dichloroquinoline and the appropriate 1,n-alkyldiamine. The two starting materials were simply reacted together in the melt to form the product [18]. Compound **10** was then reacted with the ferrocenecarboxaldehyde (**6**) in methanol, to form the imine (Schiff base) which was then reduced in situ with sodium borohydride to deliver compound **3** which was in turn reacted with phenyl isocyanate in dichloromethane at room temperature (see Scheme 3).

Consistent with previous observations [15, 16], the length of the methylene spacer was found to have an influence on antiplasmodial activity. In the chloroquine-sensitive D10 strain, the longer the methylene spacer, the lower the efficacy. A distinguishable pattern was not quite so clear in the chloroquine-resistant K1 strain, but the methylene spacer length appeared to have an impact on efficacy with compound **3b** (3-carbon spacer) showing the greatest efficacy [19]. For the urea derivatives, the chain length made no significant difference to efficacy in D10, but a decrease in efficacy with an increase in the length of the methylene spacer was observed in the K1 strain [19].

Given the distinctive redox chemistry of ferrocene, we decided to establish the electrochemical behaviour of the analogues we had synthesised (see Table 2). It was postulated that the half-wave potential $E_{1/2}$ or ΔE value could provide a cheap and quick method of screening for potential biological activity if this could be correlated to the in vitro antiplasmodial activity. Unfortunately, no discernable trend

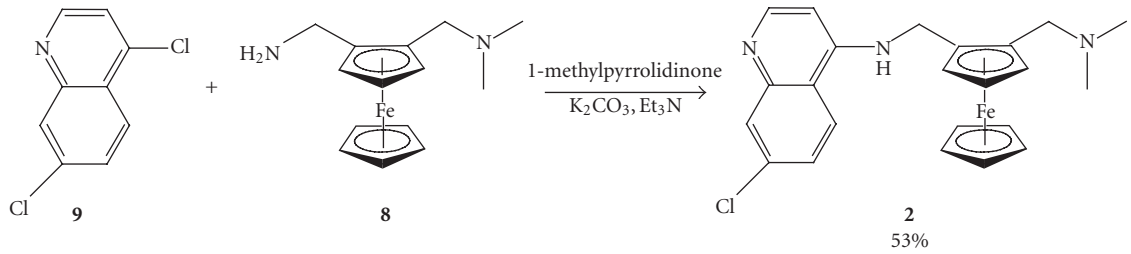

Scheme 2: Synthesis of ferroquine (**2**).

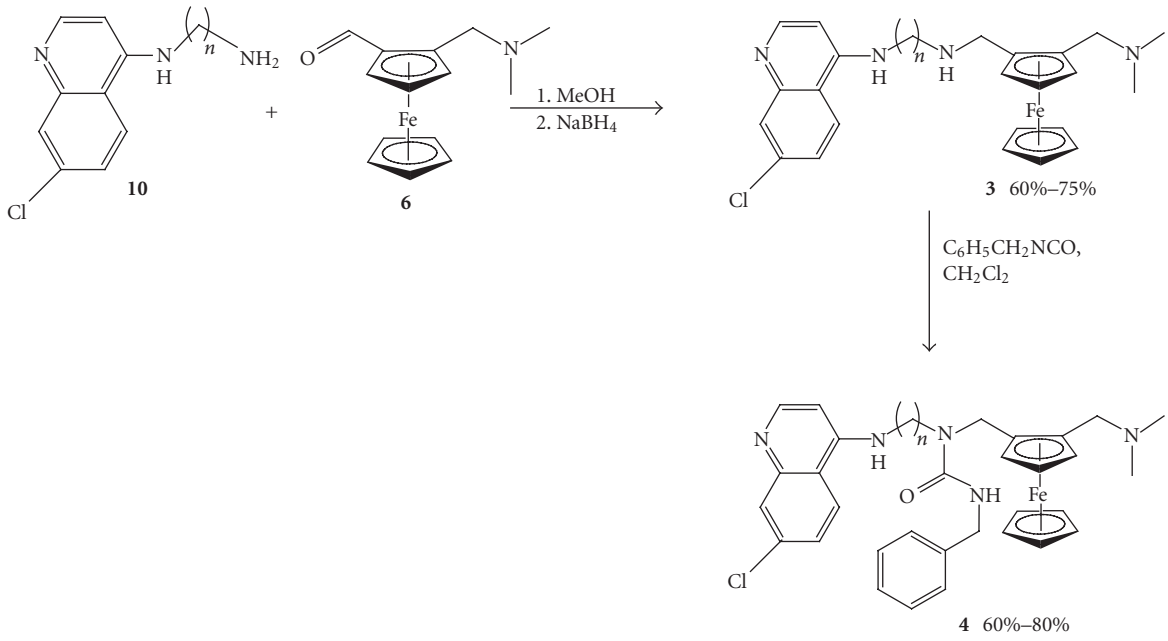

Scheme 3: Synthesis of ferroquine analogues (**3a–d**) and urea derivatives (**4a–d**).

was observed relating either of these values with in vitro efficacy in either strain of *P. falciparum*. However, it was noted that the presence of the reactive secondary amine centre had a marked effect on the redox chemistry of the ferrocenyl moiety. Ferroquine exhibits a fully reversible one-electron oxidation. The curve is similar to that of ferrocene (see Figure 2) although the ferrocenyl moiety in ferroquine is significantly more difficult to oxidise ($E_{1/2}$ for FQ = 147; $E_{1/2}$ for Fc = 79).

Compounds **3a–d** showed, at best, a quasireversible oxidation. The cathodic peak current was significantly smaller than the anodic peak current (see Figure 2). The ease of reversibility of oxidation increases with an increase in carbon chain length, as demonstrated by the decrease in ΔE_p values (see Table 2). A fully reversible one-electron oxidation requires a peak separation, ΔE_p, of 70–90 mV. In compounds **4a–d**, the reversibility of the one-electron oxidation event in the ferrocenyl moiety was restored. As with ferroquine, these compounds are significantly more difficult to oxidise than ferrocene, as demonstrated by the increase in half-wave potential $E_{1/2}$ values (see Table 2).

3. RUTHENOQUINE ANALOGUES

The chemistry of ferrocene is similar to the chemistry of ruthenocene. In order to begin to probe the role of ferrocene in ferroquine derivatives, we reasoned that it would be of interest to synthesise the ruthenocene analogues of selected derivatives (see Figure 3). The antiproliferative properties of ferrocifen and its ruthenocene analogue have proven quite different. This difference in efficacy has been attributed to the stability of the ferrocenium ion relative to the ruthenocenium ion. The presence of the ferrocenium ion allows for a change in chemical reactivity at another point in the molecule as a result of the highly conjugated system present in the ferrocifen molecule. The instability of the ruthenocenium ion does not allow for this change in chemical reactivity [9]. It is clear that a similar through-bond effect is not available in ferroquine or ruthenoquine as there is no conjugation accessible to the metallocene moiety in these compounds. However, it was thought that some insight into the role of ferrocene could be gained by examining the biological activity of the ruthenocene analogues.

Table 1: In vitro antiplasmodial activities of ferroquine analogues.

Compound	n	Reactive secondary amine substituent	D10 (CQS) IC_{50} (nM)	K1 (CQR) IC_{50} (nM)
CQ			41.86 ± 1.25	125.38 ± 4.53
3a	2	H	41.7 ± 2.6	73.46 ± 6.4
3b	3	H	51.37 ± 3.85	36.93 ± 1.7
3c	4	H	61.16 ± 1.53	111.5 ± 12.9
3d	6	H	86.92 ± 7.3	81.39 ± 5.57
4a	2	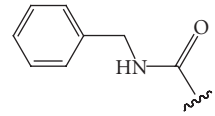	21.35 ± 1.99	37.5 ± 7.35
4b	3	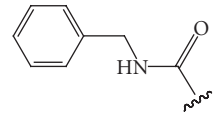	16.2 ± 0.54	47.41 ± 2.41
4c	4	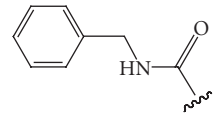	16.74 ± 4.25	75.23 ± 8.49
4d	6	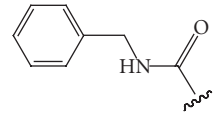	19.01 ± 6.24	110.2 ± 9.46

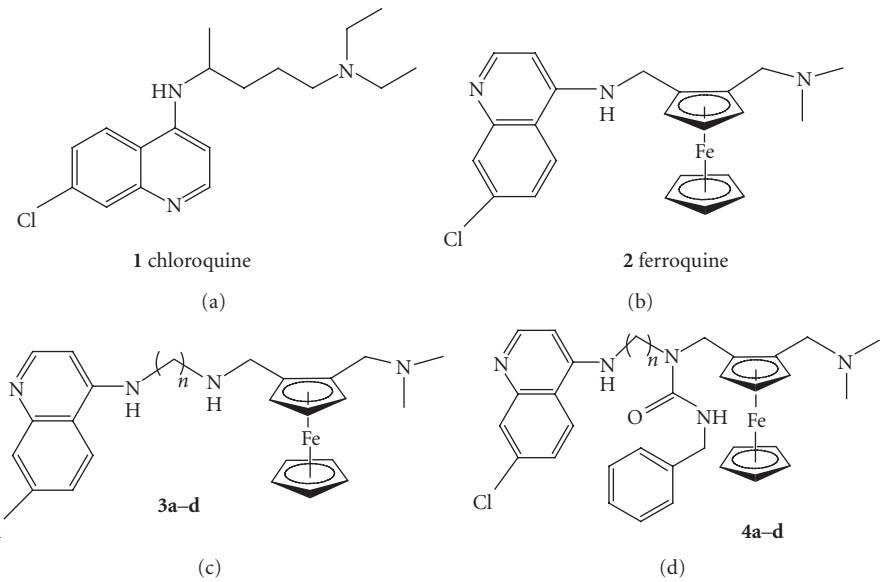

Figure 1: Structure of ferroquine analogues.

It was envisioned that a similar synthetic strategy could be employed to synthesise the compounds **2Ru** and **3aRu**, as had been used for the ferrocene analogues and described in Schemes 1–3. However, the ruthenocene system proved more complicated [20]. Firstly, (*N*,*N*-dimethylaminomethyl) ruthenocene is not commercially available and had to be synthesised using Eschenmoser's salt ($[CH_2{=}NMe_2]I$) [21]. Secondly, in the ferrocenyl system, high regioselectivity for the 1,2-disubstituted product **6** is observed. In the ruthenocenyl system, when using

Table 2: Cyclic voltametry measurements on antimalarial ferroquine analogues.

Compound	n	Reactive secondary amine substituent	E_{pa}	E_{pc}	[a]$E_{1/2}$	[b]ΔE_p
Ferrocene			123	34	79	89
FQ	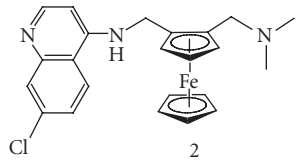		181	113	147	70
3a	2	H	150	(30)		120
3b	3	H	120	(13)		107
3c	4	H	106	(14)		92
3d	6	H	[c]—	(12)		
4a	2	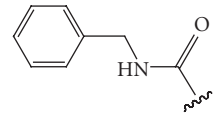	198	115	156.5	83
4b	3	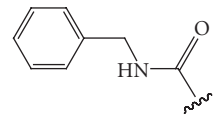	171	91	131	80
4c	4	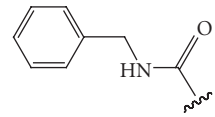	149	82	115.5	67
4d	6	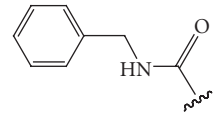	164	81	122.5	83

[a]$E_{1/2} = (E_{pa} + E_{pc})/2$; [b]$\Delta E_p = E_{pa} - E_{pc}$; [c]$E_{pa}$ indistinct.

n-butyllithium to achieve deprotonation, significant quantities of the 1,1′-monoaldehyde **11**, and the dialdehyde **12** were formed (see Scheme 4). Isolation of **11** led to the synthesis of isoruthenoquine, **2′Ru**, and **3a′Ru.** It was later discovered that the use of *tert*-butyllithium affords **6-Ru** exclusively. However, by this stage, **2′Ru** and **3a′Ru** had already been synthesised and found to show antiplasmodial activity [21]. In order to create a better comparison of the efficacies of the ferrocene and ruthenocene compounds, the 1,1′-ferrocenyl derivatives were also synthesised. The synthesis of the 1,1′-ferrocene compounds required a fairly lengthy synthetic procedure which is discussed in full elsewhere [22].

All compounds tested exhibited a good efficacy in both chloroquine-sensitive and chloroquine-resistant strains. Consistent with previous findings, the addition of the metallocene was advantageous in overcoming chloroquine resistance. These results indicate that the 1,2-disubstituted compounds (**2Fe**, **2Ru**, **3aFe**, and **3aRu**) are more efficacious than the 1,1′-disubstituted analogues (**2′Fe**, **2′Ru**, **3a′Fe**, and **3a′Ru**) in the chloroquine-resistant K1 strain. It has not been established why this trend should be observed, but the crystal structures of these compounds clearly show that there is a significant increase in distance between the 4-aminoquinoline nitrogen and the terminal nitrogen when moving from the 1,2- to 1,1′-disubstituted product [21, 23]. It has been previously established that this distance is significant in the observed efficacy of 4-aminoquinolines [15, 16]. It is noteworthy that barring compounds **3a′Fe** and **3a′Ru**, there is no significant difference in efficacy between ferrocenyl and ruthenocenyl analogues. This may suggest that the difference in redox chemistry and chemical reactivity of these moieties is not a factor in the efficacy of these compounds. The observed efficacy may be associated with the lipophilicity or physical bulk of the metallocene group.

Comparative studies on the behaviour of chloroquine and ferroquine have led to the conclusion that the effect of shape, volume, lipophilicity, basicity, and electronic profiles of the ferrocenyl moiety leads to a modification of the pharmacological behaviour of the analogue [23]. It has yet

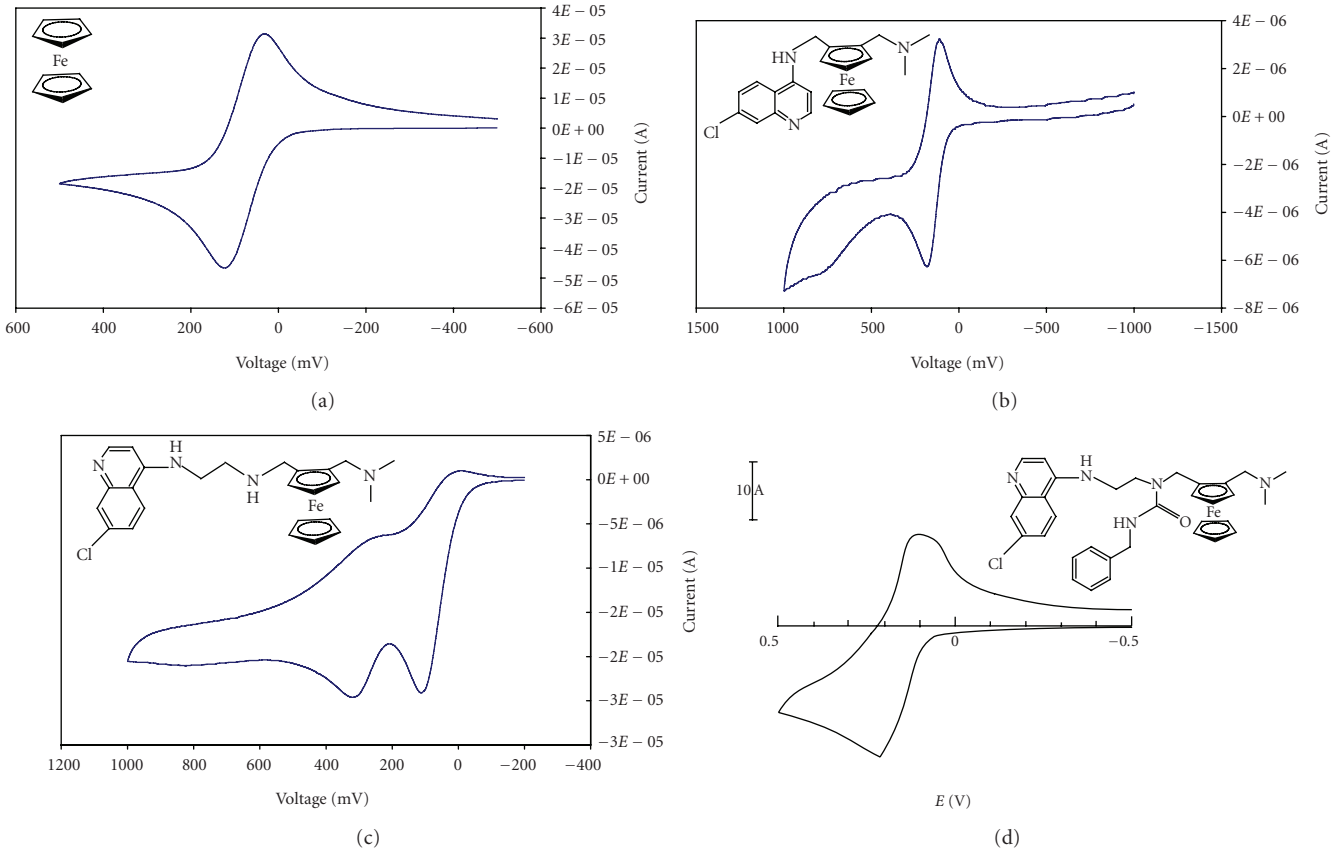

Figure 2: Cyclic voltammograms of selected ferrocene, ferroquine, **3a**, and **4a**.

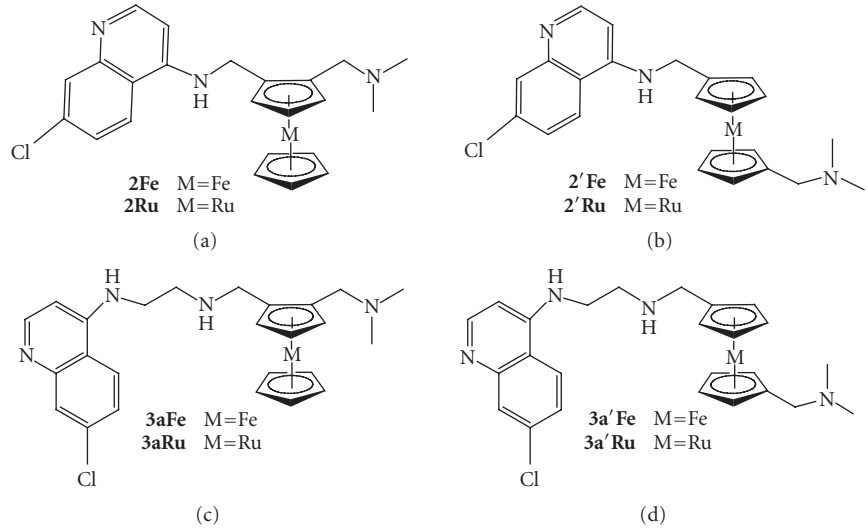

Figure 3: Ferrocene and ruthenocene analogues of ferroquine.

to be established which of these factors is most significant. In chloroquine-resistant strains of *P. falciparum*, a transporter protein, *P. falciparum* chloroquine resistance transporter (PfCRT), has been identified which allows the efflux of chloroquine from the food vacuole. It has been noted that ferroquine resistance cannot be induced under drug pressure in the W2 strain of *P. falciparum*. This has led to the conclusion that the bulky lipophilic ferrocene moiety overcomes PfRCT resistance, thereby maintaining ferroquine in the food vacuole. In addition, ferroquine retains all the features that have been identified as necessary in the structure of chloroquine (see Figure 4) [23]. The similarity of behaviour

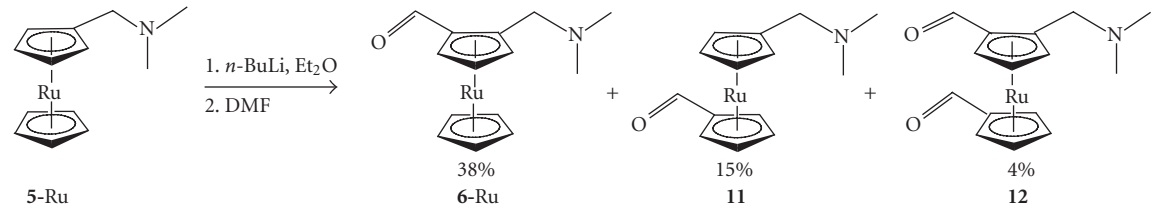

Scheme 4

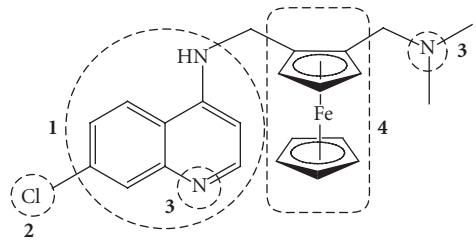

1. Interaction with hematin: 4-aminoquinoline needed for stacking interaction with hematin

2. Beta-hematin inhibition: 7-chloro group required for correct charge distribution

3. Accumulation in the food vacuole: weak basicity afforded by quinoline and terminal tertiary amine assist in vacuolar accumulation through pH trapping

4. Maintenance in food vacuole: ferrocene moiety overcomes PfCRT resistance, thereby maintaining FQ in food vacuole (note that CQ and FQ both exhibit **1**–**3**)

Figure 4: Proposed structure-activity relationships for ferroquine [23].

Table 3: Results of in vitro antimalarial tests conducted on the chloroquine-sensitive (D10) and chloroquine-resistant (K1) strains of *P. falciparum*.

Compound	D10 IC_{50}/nM	K1 IC_{50}/nM
$CQ \cdot 2H_3PO_4$	23	352
2Fe	18	14
2Ru	19	13
2′Fe	19	49
2′Ru	25	29
3aFe	33	37
3aRu	20	20
3a′Fe	16	65
3a′Ru	34	127

of the ruthenoquine and ferroquine molecules opens an interesting avenue of research. Ruthenium is known to be a good contrasting agent in electron microscopy [24]. It is reasonable, in the absence of data to the contrary, to postulate that the mechanism of action of ruthenoquine and ferroquine is similar. The sites of accumulation of ruthenoquine can be established easily using scanning electron microscopy. In mice infected with *Plasmodium berghei* N and treated with ruthenoquine, the drug has been found to accumulate close to the malaria pigment and in the parasitic membrane. Chloroquine exhibits no such accumulation in the parasitic membrane [25]. It is possible that ferroquine exhibits a similar pattern of accumulation to ruthenoquine, although this has yet to be established. The reason for this accumulation of ruthenoquine in the membrane has not been ascertained, but it may well be associated with the increase in lipophilicity afforded by the metallocene moiety.

4. COORDINATION COMPLEXES

A number of transition metals have been used to form coordination complexes of chloroquine. These coordination complexes have been shown to exhibit improved efficacy in both chloroquine-sensitive and chloroquine-resistant strains of *P. falciparum* compared to chloroquine [6, 7, 26]. The $[Ru(Cl)_2(CQ)]_2$ dimeric complex showed considerably better in vivo efficacy than was expected on the basis of the in vitro results [6]. The same study reports that both $[Rh(COD)Cl]_2$ and $RuCl_2(DMSO)_4$ failed to exhibit any antiplasmodial activity. As the metal complexes of chloroquine showed improved efficacy against both chloroquine-sensitive and chloroquine-resistant strains of the parasite, it was concluded that the coordination of a metal to the quinoline nitrogen enhanced the efficacy of chloroquine in vitro. However, a decade after the advent of these and other chloroquine-metal coordination complexes, the mode of action of these complexes is still poorly understood. It has not been established whether these complexes reach the site of action intact or not. Furthermore, it has not been established whether the inhibition of β-haematin formation is possible with the presence of a coordinated metal. This question is relevant as it has been established that the 7-chloro-4-aminoquinoline structure is crucial for this mode of action in chloroquine [27].

Given that the ferroquine derivatives could give rise to an analogous series of ferroquine coordination complexes, we thought it would be interesting to examine the effect of coordination of a second metal. To our knowledge, no such heterobimetallic coordination complexes of chloroquine had been synthesised and tested for antiplasmodial efficacy [28]. Four ligands (**1**–**4**), in Figure 5, were selected for preliminary comparative studies.

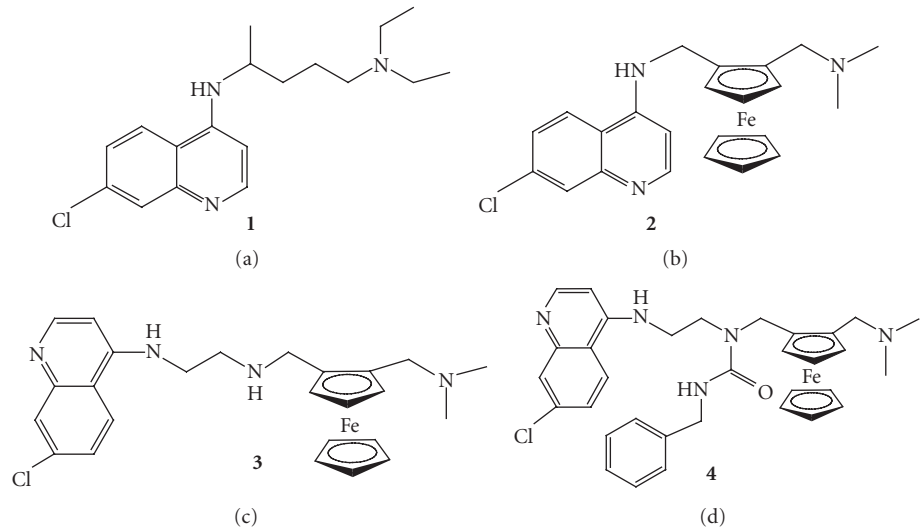

Figure 5: Ligands for coordination.

Table 4: In vitro activity of coordination complexes and the free 4-aminoquinoline ligands in chloroquine-sensitive (D10) and chloroquine-resistant (K1) strains of *P. falciparum*.

Compound	D10 (CQ sensitive) IC_{50}(nM)	K1 (CQ resistant) IC_{50} (nM)
L1	37.10	570.0
[Au(**L1**)(PPh_3)]NO_3	21.09	61.53
[Au(C_6F_5)(**L1**)]	18.07	61.09
[Rh(Cl)(COD)(**L1**)]	21.50	81.31
L2	16.30	4.96
[Au(**L2**)(PPh_3)]NO_3	10.50	5.68
[Au(C_6F_5)(**L2**)]	10.08	3.96
[Rh(Cl)(COD)(**L2**)]	15.80	10.55
L3	11.30	12.56
[Au(**L3**)(PPh_3)]NO_3	33.27	33.89
[Au(C_6F_5)(**L3**)]	13.70	14.65
[Rh(Cl)(COD)(**L3**)]	202.00	597.59
L4	16.54	15.54
[Au(**L4**)(PPh_3)]NO_3	30.32	31.09
[Au(C_6F_5)(**L4**)]	23.36	12.92
[Rh(Cl)(COD)(**L4**)]	56.10	47.70

The results shown in Table 4 indicate that the chloroquine complexes [Au(CQ)(PPh_3)]NO_3, [Au(C_6F_5)(CQ)], and [Rh(Cl)(COD)(CQ)] all show comparable efficacy to chloroquine in the chloroquine-sensitive strain. In the chloroquine-resistant strain, these complexes exhibit an efficacy 7 to 9 times better than chloroquine. However, it is noteworthy that efficacy of these compounds dropped up to three times in moving from sensitive to resistant strain suggesting that some cross-resistance may occur. Unfortunately, the metal complexes of the ferrocenyl-4-aminoquinolines did not perform so well. At best, addition of the second metal had little effect on the efficacy of the parent ligand (as in pentafluorophenyl gold complexes of **L2**, **L3**, and **L4**), whilst at worst, there appeared to be a significant antagonistic effect (as in the cyclooctadiene rhodium complexes of **L3** and **L4**). Whilst the reason for this antagonistic effect was not explored, it was noted that the presence of the second metal made the ferrocenyl moiety far more difficult to oxidise. This was evidenced by the increase in half-wave potential, $E_{1/2}$, in the complexes of **L2** and **L4** when compared with the free ligand. In the case of **L3**, where no fully reversible one-electron oxidation was observed, the significant increase in cathodic peak potential suggests that the ferrocenyl moiety is more difficult to oxidise. Once again we found no discernible correlation between redox activity and antiplasmodial efficacy.

5. DISCUSSION

The ferrocenyl moiety has several characteristics which make it a good addition to known drug molecules. Its lipophilicity, electron density, relative thermal and chemical stability, and interesting redox behaviour are all favourable in this respect. We have shown that altering the structure of the ferroquine analogue can have a significant effect on the redox behaviour of the ferrocenyl moiety. However, there is no discernible correlation between the differences in redox behaviour, whether ease of oxidation or reversibility of oxidation, and the efficacy of a compound against either chloroquine-sensitive or chloroquine-resistant strain of *P. falciparum*. It is worth noting that ferrocene and ruthenocene have quite different redox chemistry. The ruthenocenyl analogue of the antitumour agent ferrocifen has been shown to have a significantly different range of efficacy which is attributed principally to this difference in redox chemistry and the effect on the highly conjugated molecule to which the metallocene is bonded. No such difference in antiplasmodial efficacy is observed here between ferrocenyl and ruthenocenyl analogues of ferroquine. This, together with our cyclic voltammetric studies and the lack of correlation with antiplasmodial efficacy,

Table 5: Cyclic voltametry of gold triphenylphosphine complexes and the parent ligands.

Compound	[a]E_{pa}(mV)	[b]E_{pa}(mV)	[c]$E_{1/2}$(mV)	E_{pa}-E_{pc}(mV)
L2	181	113	147	70
[Au(**L2**)(PPh_3)]NO_3	252	162	207	90
L3	150	30	—	120
[Au(**L3**)(PPh_3)]NO_3	294	186	—	108
L4	198	115	158	83
[Au(**L4**)(PPh_3)]NO_3	219	141	180	78

[a] anodic potential; [b] cathodic potential; [c] half wave potential $(E_{pa} + E_{pc})/2$.

suggests that the redox behaviour of the metallocene is not a significant factor in the efficacy of these compounds. Some study of the redox chemistry of the ruthenoquine analogues would be useful to determine the accuracy of this supposition.

The incorporation of a ferrocenyl moiety into chloroquine has yielded fruitful results in terms of overcoming chloroquine resistance. Ferroquine continues to undergo testing to ascertain its suitability as a candidate for full-scale human clinical trials [8]. However, the results of incorporation of a ferrocenyl moiety into other known antimalarial drugs such as mefloquine, quinine [29], or artemisinin [30] have proved far less rewarding. This raises a question as to whether there is any inherent antiplasmodial toxicity associated with the ferrocenyl moiety. It may be that the changes in lipophilicity and pK_a values and other physicochemical effects of the incorporation of the ferrocenyl moiety into chloroquine are the primary factor in the enhanced efficacy of ferroquine. This may also explain the antagonistic effects exhibited by the heterobimetallic complexes of ferroquine and its analogues. The presence of the complexed metal and associated ligands may have adverse effects on the influence of the ferrocenyl moiety.

The role of the ferrocenyl moiety in the ability of ferroquine to overcome chloroquine resistance has still not been fully determined, although its role in overcoming PfCRT resistance seems supported by experimental evidence [24]. The continuing biological success of ferroquine means that this avenue of research must remain open and active. If we are to overcome the problem of malaria in sub-Saharan Africa, a potent, cheap alternative to chloroquine must be found.

ACKNOWLEDGMENTS

The authors would like to thank their coworkers, Paul Beagley and John R. Moss, with whom they published most of the work discussed here. They would also like to thank Alan Hutton for help with the interpretation of cyclic voltammetry data; Simon L. Croft and Peter Smith for antimalarial testing. Christophe Biot, Jacques Brocard, and their coworkers are acknowledged for their contribution to the field of metallocene antimalarials. The Claude Leon Foundation is gratefully acknowledged for funding (MB).

REFERENCES

[1] "World Health Report," 2002.

[2] G. Yamey, "Roll back Malaria: a failing global health campaign," *British Medical Journal*, vol. 328, no. 7448, pp. 1086–1087, 2004.

[3] N. P. Farrell, J. Williamson, and D. J. M. McLaren, "Trypanocidal and antitumour activity of platinum-metal and platinum-metal-drug dual-function complexes," *Biochemical Pharmacology*, vol. 33, no. 7, pp. 961–971, 1984.

[4] R. A. Sánchez-Delgado, K. Lazardi, L. Rincón, J. A. Urbina, A. J. Hubert, and A. N. Noels, "Toward a novel metal-based chemotherapy against tropical diseases. 1. Enhancement of the efficacy of clotrimazole against *Trypanosoma cruzi* by complexation to ruthenium in $RuCl_2$(clotrimazole)$_2$," *Journal of Medicinal Chemistry*, vol. 36, no. 14, pp. 2041–2043, 1993.

[5] N. Wasi, H. B. Singh, A. Gajanana, and N. Raichowdhary, "Synthesis of metal complexes of antimalarial drugs and in vitro evaluation of their activity against *plasmodium falciparum*," *Inorganica Chimica Acta*, vol. 135, no. 2, pp. 133–137, 1987.

[6] R. A. Sánchez-Delgado, M. Navarro, H. Pérez, and J. A. Urbina, "Toward a novel metal-based chemotherapy against tropical diseases. 2. synthesis and antimalarial activity in vitro and in vivo of new ruthenium- and rhodium-chloroquine complexes," *Journal of Medicinal Chemistry*, vol. 39, no. 5, pp. 1095–1099, 1996.

[7] M. Navarro, H. Pérez, and R. A. Sánchez-Delgado, "Toward a novel metal-based chemotherapy against tropical diseases. 3. synthesis and antimalarial activity in vitro and in vivo of the new gold-chloroquine complex [Au(PPh_3)(CQ)]Pf_6," *Journal of Medicinal Chemistry*, vol. 40, no. 12, pp. 1937–1939, 1997.

[8] C. Biot, "Ferroquine: a new weapon in the fight against Malaria," *Current Medicinal Chemistry - Anti-Infective Agents*, vol. 3, no. 2, pp. 135–147, 2004.

[9] S. Top, A. Vessières, C. Cabestaing, et al., "Studies on organometallic selective estrogen receptor modulators (SERMs). Dual activity in the hydroxy-ferrocifen series," *Journal of Organometallic Chemistry*, vol. 637–639, pp. 500–506, 2001.

[10] C. Biot, G. Glorian, L. A. Maciejewski, et al., "Synthesis and antimalarial activity in vitro and in vivo of a new ferrocene-chloroquine analogue," *Journal of Medicinal Chemistry*, vol. 40, no. 23, pp. 3715–3718, 1997.

[11] C. Biot, W. Daher, C. M. Ndiaye, et al., "Probing the role of the covalent linkage of ferrocene into a chloroquine template," *Journal of Medicinal Chemistry*, vol. 49, no. 15, pp. 4707–4714, 2006.

[12] C. Biot, L. Delhaes, C. M. N'Diaye, et al., "Synthesis and antimalarial activity in vitro of potential metabolites of ferrochloroquine and related compounds," *Bioorganic & Medicinal Chemistry*, vol. 7, no. 12, pp. 2843–2847, 1999.

[13] C. Biot, L. Delhaes, H. Abessolo, et al., "Novel metallocenic compounds as antimalarial agents. Study of the position of ferrocene in chloroquine," *Journal of Organometallic Chemistry*, vol. 589, no. 1, pp. 59–65, 1999.

[14] R. G. Ridley, W. Hofheinz, H. Matile, et al., "4-aminoquinoline analogs of chloroquine with shortened side chains retain activity against chloroquine-resistant *Plasmodium falciparum*," *Antimicrobial Agents and Chemotherapy*, vol. 40, no. 8, pp. 1846–1854, 1996.

[15] D. De, F. M. Krogstad, L. D. Byers, and D. J. Krogstad, "Structure-activity relationships for antiplasmodial activity among 7-substituted 4-aminoquinolines," *Journal of Medicinal Chemistry*, vol. 41, no. 25, pp. 4918–4926, 1998.

[16] G. A. Patani and E. J. LaVoie, "Bioisosterism: a rational approach in drug design," *Chemical Reviews*, vol. 96, no. 8, pp. 3147–3176, 1996.

[17] S. Picart-Goetgheluck, O. Delacroix, L. Maciejewski, and J. Brocard, "High yield synthesis of 2-substituted (*N*, *N*-dimethylaminomethyl) ferrocenes," *Synthesis*, vol. 2000, no. 10, pp. 1421–1426, 2000.

[18] D. De, L. D. Byers, and D. J. Krogstad, "Antimalarials: synthesis of 4-aminoquinolines that circumvent drug resistance in Malaria parasites," *Journal of Heterocyclic Chemistry*, vol. 34, no. 1, pp. 315–320, 1997.

[19] K. Chibale, J. R. Moss, M. A. L. Blackie, D. van Schalkwyk, and P. J. Smith, "New amine and urea analogs of ferrochloroquine: synthesis, antimalarial activity in vitro and electrochemical studies," *Tetrahedron Letters*, vol. 41, no. 32, pp. 6231–6235, 2000.

[20] P. Beagley, M. A. L. Blackie, K. Chibale, C. Clarkson, J. R. Moss, and P. J. Smith, "Synthesis and antimalarial activity in vitro of new ruthenocene-chloroquine analogues," *Journal of the Chemical Society, Dalton Transactions*, no. 23, pp. 4426–4433, 2002.

[21] R. Sanders and U. T. Mueller-Westerhoff, "The lithiation of ferrocene and ruthenocene: a retraction and improvement," *Journal of Organometallic Chemistry*, vol. 512, no. 1-2, pp. 219–224, 1996.

[22] P. Beagley, M. A. L. Blackie, K. Chibale, et al., "Synthesis and antiplasmodial activity in vitro of new ferrocene chloroquine-analogues," *Dalton Transactions*, no. 15, pp. 3046–3051, 2003.

[23] C. Biot, D. Taramelli, I. Forfar-Bares, et al., "Insights into the mechanism of action of ferroquine. Relationship between physicochemical properties and antiplasmodial activity," *Molecular Pharmaceutics*, vol. 2, no. 3, pp. 185–193, 2005.

[24] J. H. Luft, "Ruthenium red and violet. I. Chemistry, purification, methods of use for electron microscopy and mechanism of action," *Anatomical Record*, vol. 171, no. 3, pp. 347–368, 1971.

[25] S. M. Dzekunov, L. M. B. Ursos, and P. D. Roepe, "Digestive vacuolar pH of intact intraerythrocytic *P. falciparum* either sensitive or resistant to chloroquine," *Molecular and Biochemical Parasitology*, vol. 110, no. 1, pp. 107–124, 2000.

[26] M. Navarro, F. Vásquez, R. A. Sánchez-Delgado, H. Pérez, V. Sinou, and J. Schrével, "Toward a novel metal-based chemotherapy against tropical diseases. 7. Synthesis and in vitro antimalarial activity of new gold-chloroquine complexes," *Journal of Medicinal Chemistry*, vol. 47, no. 21, pp. 5204–5209, 2004.

[27] C. H. Kaschula, T. J. Egan, R. Hunter, et al., "Structure-Activity relationships in 4-aminoquinoline antiplasmodials. The role of the group at the 7-position," *Journal of Medicinal Chemistry*, vol. 45, no. 16, pp. 3531–3539, 2002.

[28] M. A. L. Blackie, P. Beagley, K. Chibale, C. Clarkson, A. T. Hutton, J. R. Moss, and P. J. Smith, "Synthesis and antimalarial activity in vitro of new heterobimetallic complexes: Rh and Au derivatives of chloroquine and a series of ferrocenyl-4-amino-7-chloroquinolines," *Journal of Organometallic Chemistry*, vol. 688, no. 1-2, pp. 144–152, 2003.

[29] C. Biot, L. Delhaes, L. A. MacIejewski, et al., "Synthetic ferrocenic mefloquine and quinine analogues as potential antimalarial agents," *European Journal of Medicinal Chemistry*, vol. 35, no. 7-8, pp. 707–714, 2000.

[30] L. Delhaes, C. Biot, L. Berry, et al., "Novel ferrocenic artemisinin derivatives: synthesis, in vitro antimalarial activity and affinity of binding with ferroprotoporphyrin IX," *Bioorganic & Medicinal Chemistry*, vol. 8, no. 12, pp. 2739–2745, 2000.

Hindawi Publishing Corporation
Metal-Based Drugs
Volume 2008, Article ID 754358, 7 pages
doi:10.1155/2008/754358

Research Article

Synthesis and Cytotoxicity Studies of Titanocene C Analogues

Megan Hogan, James Claffey, Eoin Fitzpatrick, Thomas Hickey, Clara Pampillón, and Matthias Tacke

Conway Institute of Biomolecular and Biomedical Research, The UCD School of Chemistry and Chemical Biology, Centre for Synthesis and Chemical Biology (CSCB), University College Dublin, Belfield, Dublin 4, Ireland

Correspondence should be addressed to Matthias Tacke, matthias.tacke@ucd.ie

Received 12 June 2007; Accepted 23 July 2007

Recommended by Jannie C. Swarts

From the carbolithiation of 6-*N*,*N*-dimethylamino fulvene (**3**) and 2,4[bis(*N*,*N*-dimethylamino)methyl]-*N*-methylpyrrolyl lithium (**2a**), *N*-(*N*′,*N*′-dimethylaminomethyl)benzimidazolyl lithium (**2b**)' or *p*-(*N*,*N*-dimethylamino)methylphenyl lithium (**2c**), the corresponding lithium cyclopentadienide intermediate (**4a–c**) was formed. These three lithiated intermediates underwent a transmetallation reaction with $TiCl_{4'}$ resulting in *N*,*N*-dimethylamino-functionalised titanocenes **5a–c**. When these titanocenes were tested against a pig kidney epithelial cell line (LLC-PK), the IC_{50} values obtained were of 23, and 52 μM for titanocenes **5a** and **5b**, respectively. The most cytotoxic titanocene in this paper, **5c** with an IC_{50} value of 13 μM, was found to be approximately two times less cytotoxic than its analogue Titanocene **C** (IC_{50} = 5.5 μM) and almost four times less cytotoxic than cisplatin, which showed an IC_{50} value of 3.3 μM when tested on the LLC-PK cell line.

1. INTRODUCTION

Titanium-based reagents have significant potential against solid tumors. Budotitane ([cis-diethoxybis(1-phenylbutane-1,3-dionato)titanium(IV)]) looked very promising during its preclinical evaluation, but did not go beyond Phase I clinical trials, although a Cremophor EL-based formulation was found for this rapidly hydrolysing molecule [1]. Much more robust in this aspect of hydrolysis is titanocene dichloride (Cp_2TiCl_2), which shows medium antiproliferative activity in vitro but promising results in vivo [2, 3]. Titanocene dichloride reached clinical trials, but the efficacy of Cp_2TiCl_2 in Phase II clinical trials in patients with metastatic renal cell carcinoma [4] or metastatic breast cancer [5] was too low to be pursued.

More recently, novel methods starting from fulvenes [6–17] and other precursors [18–20] allow direct access to highly substituted titanocenes via reductive dimerisation, carbolithiation, or hydridolithiation of the fulvene followed by transmetallation in the last two cases.

Titanocene **Y** was obtained using hydridolithiation of fulvene, and it showed an IC_{50} value of 21 μM [12]. The antiproliferative activity of Titanocene **Y** has been studied in 36 human tumor cell lines [21] and in explanted human tumors [22]. These in vitro and ex vivo experiments showed that prostate, cervix, and renal cell cancers are prime targets for these novel classes of titanocenes, whereas the IC_{50} values for the breast cancer cell lines were very promising as well. These results were underlined by first mechanistic studies concerning the effect of these titanocenes on apoptosis and the apoptotic pathway in prostate cancer cells [23]. Furthermore, first animal studies have been published recently, reporting the successful treatment of xenografted Ehrlich's ascites tumor in mice with an ansa-titanocene [24] and xenografted Caki-1 tumors with Titanocene **Y** [25], showing that the effect of Titanocene **Y** against xenografted Caki-1 tumors in mice was superior to cisplatin. The structure of Titanocene **Y** is shown in Figure 1.

So far, our most cytotoxic titanocene, Titanocene **C** (bis-(*N*,*N*-dimethylamino-2(*N*-methylpyrrolyl)methylcyclo pentadienyl) titanium (IV) dichloride, was obtained through carbolithiation of fulvenes, which has been published recently [26]. It has an IC_{50} value of 5.5 μM when tested on the LLC-PK cell line. Its structure is shown in Figure 1. This meant significant progress, since Cp_2TiCl_2 exhibits an IC_{50} value of only 2000 μM against LLC-PK, which explains partly the failed Phase II clinical trials against renal cell carcinoma. The main idea behind the research presented in this paper was to improve the cytotoxicity of Titanocene **C** by adding extra dimethylamino groups using

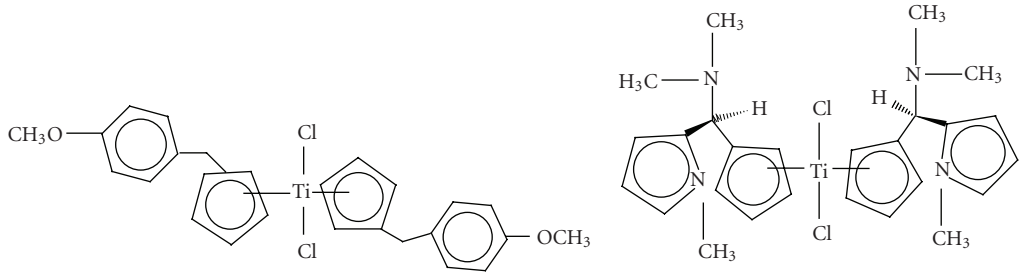

Figure 1: Structure of Titanocenes **Y** and **C**.

the well-established Mannich reaction. Within this paper, we present a new series of chiral titanocenes, their synthesis, and preliminary cytotoxicity studies.

2. EXPERIMENTAL

2.1. General conditions

Titanium tetrachloride (1.0 M solution in toluene) and butyl lithium (2.0 M solution in pentane) were obtained commercially from Aldrich Chemical Co. (Wis, USA). THF was dried over Na and benzophenone, and it was freshly distilled and collected under an atmosphere of argon prior to use. Manipulations of air and moisture sensitive compounds were done using standard Schlenk techniques under an argon atmosphere. NMR spectra were measured on either a Varian 300 or a 400 MHz spectrometer. Chemical shifts are reported in ppm and are referenced to TMS. IR spectra were recorded on a Perkin Elmer Paragon 1000 FT-IR Spectrometer employing a KBr disk. UV/Vis spectra were recorded on a Unicam UV4 Spectrometer, while CHN analysis was done with an Exeter Analytical CE-440 Elemental Analyser.

2.2. Synthesis

6-(N,N-dimethylamino) fulvene (**3**) was synthesised according to the already published procedure [27].

Synthesis of bis-(3-[2,4-di(N,N-dimethylamino)methyl]-N-methylpyrrolyl-(N,N-dimethylamino)-methylcyclopentadienyl) titanium (IV) dichloride, $\{\eta^5$–C_5H_4–$CH[N(CH_3)_2][C_4H_2(CH_2$–$N(CH_3)_2)_2N(CH_3)]\}_2TiCl_2$ ***(5a)***

To a Schlenk flask with 2,4[bis(N,N-dimethylamino) methyl]-N-methyl pyrrole (1.61 g, 8.25 mmol), 20 ml of THF were added until a transparent solution was formed, while stirring at room temperature. The solution was cooled down to −78°C for 15 minutes and 4.8 mL (8.25 mmol) of butyl lithium were added. The solution was allowed to warm up to 0°C for 20 minutes, resulting in the formation of the yellow lithium intermediate.

In a second Schlenk flask, 6-(N,N-dimethylamino) fulvene (1.00 g, 8.25 mmol) was dissolved in THF, and the resultant orange solution was added via cannula at −78°C to the Schlenk flask containing the lithiated intermediate. The reaction mixture was then allowed to warm up to room temperature and left stirring for 40 minutes. Titanium tetrachloride (4.1 ml, 4.13 mmol) was added afterwards in situ at room temperature, and the mixture was refluxed for 20 hours. Subsequently, the solvent was removed under vacuum, resulting in the formation of a dark brown oil that was dissolved in dichloromethane and filtered through Celite to remove the LiCl. The black filtrate was filtered additionally twice by gravity filtration. The solvent was removed under reduced pressure forming a shiny dark red solid, which was washed with 20 ml of pentane and then dried in vacuo (1.44 g, 1.93 mmol, 46.8% yield).

^{1}H NMR (δ ppm $CDCl_3$, 400 MHz): 6.36 (m, 8 H, $C_5\underline{H}_4$); 6.05 (s, 2 H, $[C_4\underline{H}(CH_2$–$N(CH_3)_2)_2N(CH_3)]$); 3.8–2.6 (m, 14 H, $[C_4H(CH_2$–$N(C\underline{H}_3)_2)_2N(C\underline{H}_3)]$, $[C_4H(CH_2$–$N(CH_3)_2)_2N(C\underline{H}_3)]$, $[C_4H(C\underline{H}_2$–$N(CH_3)_2)_2N(C\underline{H}_3)]$); 2.36 (s, 26 H, $C_4\underline{H}(CH_2$–$N(C\underline{H}_3)_2)_2N(CH_3)$).

^{13}C NMR (δ ppm $CDCl_3$, 125 MHz, proton decoupled): 138, 135, 132, 126, 121, 119, 108 [$\underline{C}_5H_4$ and $\underline{C}_4H(CH_2$–$N(CH_3)_2)_2N(CH_3)$]; 52 [C_5H_4–$\underline{C}H$–$(N(CH_3)_2)(C_4H(CH_2$–$N(CH_3)_2)_2N(CH_3)$]; 34, 32 [$N(\underline{C}H_3)_2$ and $C_4H(\underline{C}H_2$–$N(\underline{C}H_3)_2)_2N(\underline{C}H_3)$].

IR absorptions (cm^{-1} KBr): 3414, 2917, 2769, 1620, 1466, 1382, 1018.

Anal. Calc. for $C_{38}H_{62}N_8TiCl_2$: C, 60.87; H, 8.35; N, 14.95; Cl, 9.46; Found: C, 59.80; H, 8.29; N, 14.18; Cl, 9.45.

UV-Vis (CH_2Cl_2): λ 244 nm (ε 10 833), λ 330 nm (ε 12 996), λ_{max} 510 nm (weak).

Synthesis of bis-[(N,N-dimethylaminomethyl-2-benzimidazolyl)(N',N' dimethylamino) methylcyclopentadienyl]titanium (IV) dichloride, $\{\eta^5$–C_5H_4–$CH[N(CH_3)_2][C_{10}H_{12}N_3]\}_2TiCl_2$ ***(5b)***

To a Schlenk flask with N-(N',N'-dimethylaminomethyl) benzimidazol (1.45 g, 8.25 mmol), 20 ml of THF were added until a transparent solution was formed, while stirring at room temperature. The solution was cooled down to −78°C for 15 minutes and 14.0 ml (8.25 mmol, 1.7 M) of butyl lithium were added. The solution was allowed to warm up

to 0°C for 20 minutes, resulting in the formation of the yellow lithium intermediate.

In a second Schlenk flask, 1.00 g (8.25 mmol) of 6-*N*,*N*-dimethylamino fulvene was dissolved in THF, and the resultant red solution was added via cannula at −78°C to the Schlenk flask containing the lithiated intermediate. The reaction mixture was then allowed to warm up to room temperature and left stirring for 40 minutes. Titanium tetrachloride (4.1 ml, 4.13 mmol) was added afterwards in situ at room temperature and the mixture was refluxed for 20 h. Subsequently, the solvent was removed under vacuum, resulting in the formation of a dark green oil that was dissolved in dichloromethane and filtered through Celite to remove the LiCl. The black filtrate was filtered additionally twice by gravity filtration. The solvent was removed under reduced pressure forming a shiny black solid, which was washed with 20 ml of pentane and then dried in vacuo (1.97 g, 2.77 mmol, 67.3% yield).

^{1}H NMR (δ ppm $CDCl_3$, 400 MHz): 7.80–7.82 [m, 4H, $C_5H_4-CH[N(CH_3)_2]-C-N-C-C\underline{H}-CH-CH-C\underline{H}-C-N(CH_2N(CH_3)_2)$]; 7.49–7.51 [m, 4 H, $C_5H_4-CH[N(CH_3)_2]-C-N-C-CH-C\underline{H}-C\underline{H}-CH-C-N(CH_2N(CH_3)_2]$; 6.42–6.71 [m, 8H, $C_5\underline{H}_4-CH[N(CH_3)_2]-C_7H_4NN-CH_2{-}N\ (CH_3)_2]$; 4.85 [s, 4H, $C_5H_4-CH[N(CH_3)_2]-C_7H_4NN-C\underline{H}_2{-}N(CH_3)_2]$; 4.00 [m, 2H, $C_5H_4-C\underline{H}[N(CH_3)_2]-C_7H_5N_2-CH_2{-}N-(CH_3)_2]$; 2.16, 2.23, 2.34 [s, 24 H, $C_5H_4-CH[N(C\underline{H}_3)_2]-C_7H_5N_2-CH_2{-}N-(C\underline{H}_3)_2]$.

^{13}C NMR (δ ppm $CDCl_3$, 125 MHz, proton decoupled): 144, 142, 136, 135, 132, 126, 123, 122, 121, 120, 119, 112[$\underline{C}_5H_4-CH[N(CH_3)_2]-\underline{C}_7H_5N_2-CH_2{-}N-(CH_3)_2$]; 69, 68,64,44,43,36,34,32,23,28,19,14,13[$C_5H_4-\underline{C}H[N(\underline{C}H_3)_2]-C_7H_5N_2-\underline{C}H_2{-}N-(\underline{C}H_3)_2$].

IR absorptions (cm^{-1} KBr): 3429, 2926, 1635, 1456, 1270, 1039, 861, 743.

Anal. Calc. for $C_{36}H_{46}N_8TiCl_2$: C, 60.93; H, 6.53; N, 15.79; Cl, 9.99 Found: C, 59.99; H, 6.52; N, 15.72; Cl, 9.99.

UV-Vis (CH_2Cl_2): λ 230 nm (ε 22 770), λ 402 nm (ε 2020), λ 499 nm (ε 210), λ_{max} 523 nm (weak).

Bis-(N,N-dimethylamino)-p-(N,N-dimethylamino)methylphenylcyclopentadienyl) titanium (IV) dichloride, $\{\eta^5$-C_5H_4–$CH[N(CH_3)_2][C_6H_4CH_2N(CH_3)_2]\}_2TiCl_2$ ***(5c)***

To a Schlenk flask with 0.37 g (1.73 mmol) *p*-(*N*,*N*-dimethylamino)methylphenylbromide, 14 ml of THF were added until a transparent solution was formed, while stirring at room temperature. The solution was cooled down to −78°C and 1.02 ml (1.73 mmol, 1.7 M) of *t*-butyl lithium were added. The solution was allowed to warm up to 0°C for 20 minutes, resulting in the formation of the yellow lithium intermediate.

In a second Schlenk flask, 0.21 g (1.73 mmol) of 6-(*N*,*N*-dimethylamino) fulvene was dissolved in THF, and the resultant red solution was added via cannula at −78°C to the Schlenk flask containing the lithiated intermediate. The reaction mixture was then allowed to warm up to room temperature and left stirring for 40 minutes. Titanium tetrachloride (0.86 ml, 0.86 mmol) was added afterwards in situ at room temperature and the mixture was refluxed for 20 h. Subsequently, the solvent was removed under vacuum, resulting in the formation of a dark brown oil that was dissolved in dichloromethane and filtered through Celite to remove the LiCl. The black filtrate was filtered additionally twice by gravity filtration. The solvent was removed under reduced pressure forming a shiny dark brown solid, which was washed with 150 ml of pentane and then dried in vacuo (0.45 g, 0.71 mmol, 82.7% yield).

^{1}H NMR (δ ppm $CDCl_3$, 300 MHz): 7.73–7.43 [m, 8H, $C_6\underline{H}_4CH_2N(CH_3)_2$]; 6.70–6.40 [m, 8H, $C_5\underline{H}_4$]; 3.14 [s, 2H, $C_5H_4-C\underline{H}-(N(CH_3)_2(C_6H_4CH_2N(CH_3)_2)$]; 4.25–4.21 [s, 4H, $C_5H_4-CH-(N(CH_3)_2(C_6H_4C\underline{H}_2N(CH_3)_2)$]; 2.84–2.81 [s, 12H, $C_5H_4-CH-(N(C\underline{H}_3)_2(C_6H_4CH_2N(CH_3)_2)$]; 2.81–2.77 [s, 12H, $C_5H_4-CH-(N(CH_3)_2(C_6H_4CH_2N(C\underline{H}_3)_2)$].

^{13}C NMR (δ ppm $CDCl_3$, 125 MHz, proton decoupled): 146, 138, 136, 132, 131, 129, 127, 124, 120 [($\underline{C}_6H_4CH_2N(CH_3)_2$) and ($\underline{C}_5H_4$)]; 61 [$C_5H_4-\underline{C}H-(N(CH_3)_2(C_6H_4CH_2N(CH_3)_2)$)]; 60 [$(C_6H_4\underline{C}H_2N(CH_3)_2)$]; 42 [$C_5H_4-CH-(N(\underline{C}H_3)_2(C_6H_4CH_2N(\underline{C}H_3)_2)$)].

IR absorptions (cm^{-1} KBr): 3444, 3391, 2958, 2670, 2470, 1621, 1467, 1411, 1261, 1164, 1071, 1013, 943, 798.

Anal. Calc. for $C_{34}H_{46}N_4TiCl_2$: C, 64.90; H, 7.37; N, 8.91; Cl, 11.27 Found: C, 64.88; H, 7.36; N, 8.90; Cl, 11.27.

UV-Vis (CH_2Cl_2): λ 263 nm (ε 86 000), λ 275 nm (ε 94 000), λ 298 nm (ε 98 000), λ 320 nm (ε 108 000), λ 340 nm (ε 72 000), λ 390 nm (ε 35 000), λ_{max} 455 nm (weak).

3. RESULTS AND DISCUSSION

3.1. Synthesis

6-(*N*,*N*-dimethylamino) fulvene (**3**) was synthesised according to the already published procedure [27], and its structure is shown in Scheme 1.

The use of aryl lithium in the synthesis of other metallocenes is well known [28–30], and it has recently been used for the synthesis of chiral titanocene dichlorides [26].

This time, the carbolithiation method led to the synthesis of a new group of titanocenes that contain stereo centres (**5a–c**).

The first step of the reaction consists of the formation of the functionalised lithium intermediates (**2a–c**) by reacting the corresponding heterocycles (**1a–c**) with *tert*-butyl lithium. Side reactions were avoided by cooling the reaction down to −78°C during the addition of *tert*-butyl lithium, and subsequent warming up to 0°C.

This step was followed by a nucleophilic addition of the lithiated intermediate to the double bond of 6-*N*,*N*-dimethylamino fulvene at −78°C. Then the reaction mixture was allowed to warm up to 0°C, resulting in the formation of the appropriately substituted lithium cyclopentadienyl intermediates **4a–c**. This reaction occurs with no stereo-selectivity, and the intermediates **4a–c** already contain a stereogenic carbon.

After stirring the reaction mixture for 40 minutes, two molar equivalents of **4a**, **4b** or **4c** underwent a transmetallation reaction when reacted with $TiCl_4$ under reflux over 20 h in THF to give titanocenes **5a–c**.

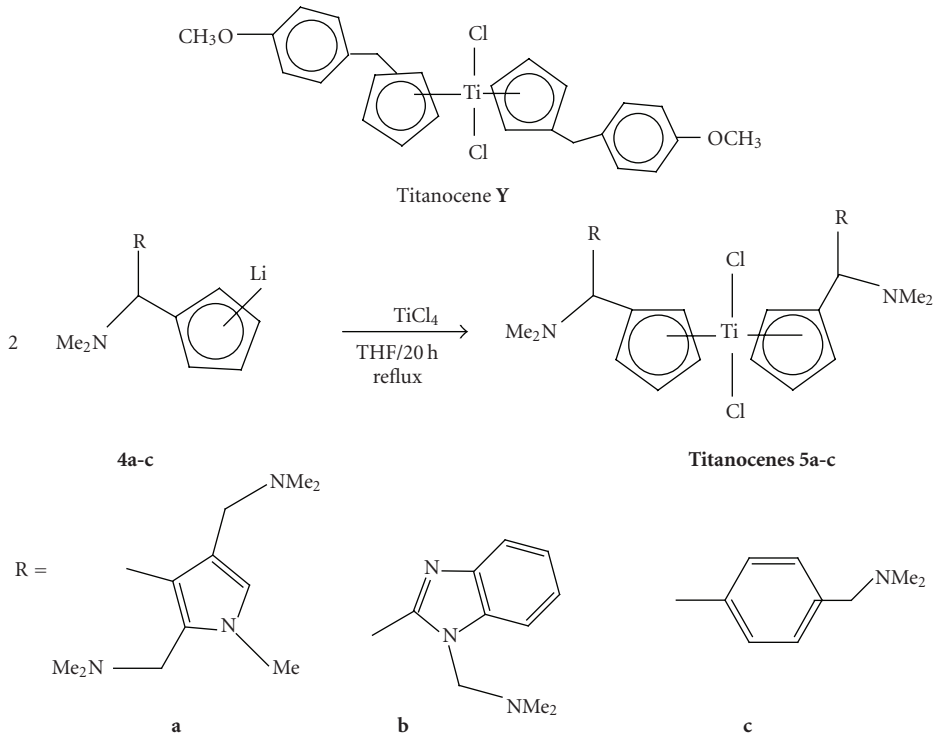

Scheme 1: Synthesis of Titanocenes **5a–c**.

The compounds obtained are shiny dark red solids. The synthesis of these compounds is shown in Scheme 1.

All three titanocenes shown in this paper have different isomers as seen in Figure 1. As a result of this, three different signals should be seen for every proton and carbon in the ^{1}H and ^{13}C NMR spectra. The R,R and S,S isomers are enantiomers and thus give identical NMR spectra, whereas for protons or carbons corresponding to the R,S (same as S,R) isomer, two signals can be observed as the environment of the two cyclopentadienyl rings is different. A relation of 2 : 1 : 1 for S,S and R,R, and the two signals for the S,R (or R,S) isomers can be observed in the integration pattern.

3.2. Cytotoxicity studies

Preliminaryin vitro cell tests were performed on LLC-PK cells in order to compare the cytotoxicity of the compounds presented in this paper. This cell line was chosen based on their long-lasting growth behavior, similar to the one shown in carcinoma cells. It was obtained from the ATCC (american tissue cell culture collection) and maintained in Dulbecco's modified Eagle medium containing 10% (v/v) FCS (foetal calf serum), 1% (v/v) penicillin streptomycin, and 1% (v/v) L-glutamine. Cells were seeded in 96-well plates containing 200 μl microtiter wells at a density of 5,000-cells/200 μl of medium and were incubated at 37°C for 24 h to allow for exponential growth. Then the compounds used for the testing were dissolved in the minimalamount of DMSO (dimethylsulfoxide) possible and diluted with medium to obtain stock solutions of 5×10^{-4} M in concentration and less than 0.7% of DMSO. The cells were then treated with varying concentrations of the compounds and incubated for 48 hours at 37°C. Then the solutions were removed from the wells, the cells were washed with PBS (phosphate buffer solution), and fresh medium was added to the wells. Following a recovery period of 24 h incubation at 37°C, individual wells were treated with a 200 μl of a solution of MTT (3-(4,5-dimethylthiazol-2-yl)-2,5-diphenyltetrazolium bromide) in medium. The solution consisted of 30 mg of MTT in 30 ml of medium. The cells were incubated for 3 hours at 37°C. The medium was then removed and the purple formazan crystals were dissolved in 200 μL DMSO per well. Absorbance was then measured at 540 nm by a Wallac Victor (Multilabel HTS Counter) Plate Reader. Cell viability was expressed as a percentage of the absorbance recorded for control wells. The values used for the dose response curves of Figure 2 represent the values obtained from four consistent MTT-based assays for each compound tested.

As seen in Figure 2, Titanocenes **5a–c** showed an IC_{50} value of 23, 52, and 13 μM, respectively.

When compared to unsubstituted titanocene dichloride (IC_{50} value = 2000 μM), titanocene **5c** shows a major decrease in magnitude in terms of the IC_{50} value, and approximately a fourfold increase in magnitude with respect to cisplatin itself (IC_{50} value = 3.3 μM). However, titanocene **5c** shows a decrease in cytotoxicity with respect to Titanocene **C**. The increased polarity of the new titanocenes together with

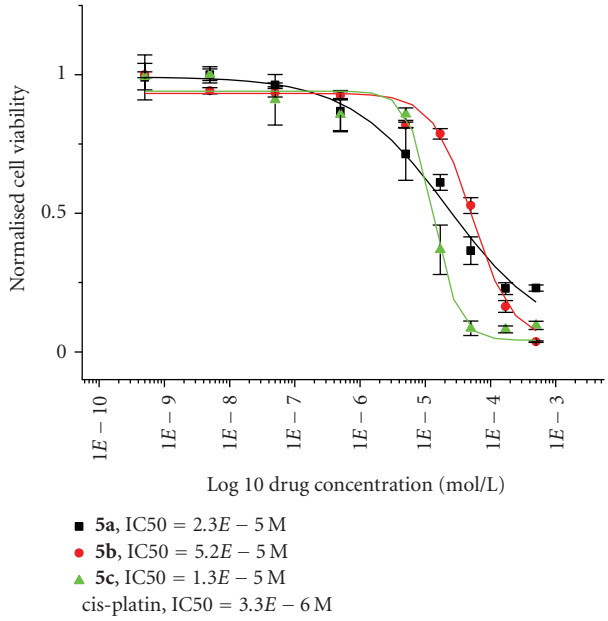

Figure 2: Cytotoxicity studies of Titanocenes **5a–c** against LLC-PK cells.

an increase in size might be the cause of the decrease in cytotoxicity shown.

3.3. *Structural DFT discussion*

Despite our efforts to crystallise these three titanocenes, no crystal structures were obtained. This might be explained by the existence of different isomers in the racemic mixture. In order to overcome this problem, density functional theory (DFT) calculations were carried out for titanocene **5c** at the B3LYP level using the 6-31G** basis set [31], and compared with that of Titanocene **C** [26].

Selected bond lengths of the optimised structure of titanocenes **5a** and **C** are listed in Table 1 (for atom numbering, see Scheme 2). The calculated structure of **5c** is presented in Figure 3.

The length of the bond between the metal centre and the cyclopentadienyl carbons is slightly different for the different Cp rings (251.3 and 248.5 pm, resp.). The same applies for the carbon-carbon bonds of the cyclopentadienyl rings with bond lengths between 140.2 and 143.4 pm.

The bond length between the methylic carbon centre and the carbon centre of the Cp group is of 152.2 and 152.0 pm, respectively. As well, the length of the bond between the methylic carbon and the nitrogen of the dimethylamino group is almost identical in all cases, and between 152.0 and 148.2 pm, respectively. The steric impediment of the dimethylamino groups attached to the methylic carbons causes a lengthening of the bond, in order to relieve the resultant steric strain.

The Cl–Ti–Cl angle was calculated to be 95.1°. The angle formed between C_1 and $C_{1'}$, the respective methylic carbons (C_6 or $C_{6'}$), and C_7 or $C_{7'}$, respectively, was of 11.42° in both cases, and almost identical to the one formed between each nitrogen of the dimethylamino group, C_6 or $C_{6'}$, and C_1 and $C_{1'}$, respectively.

The DFT calculated structure of **5a** was then compared to the calculated structure of its mono-*N*-methylpyrrolyl-substituted analogue, Titanocene **C** [26]. In this complex, the length of the bond between the titanium centre and the two Cl atoms appeared to differ in only 1 pm approximately from the one found for **5c**, and of 234.9 and 236.1 pm, respectively. The same applies to the bond length between the N_1 or N_2 and C_6 or $C_{6'}$, respectively, and to the length of the bond between the Cp carbon atoms and the titanium centre.

The Cl–Ti–Cl angle in Titanocene **C** is very similar to the one calculated for **5c**, and of 94.9°, and so is the angle formed between the titanium centre and the centre of the Cp rings (with a difference of 0.3°).

Selected bond lengths from the calculated DFT structure of Titanocene **C** are listed in Table 1, while atom numbering can be seen in Scheme 2.

Table 1: Selected bond lengths from the DFT-calculated structure of **5c** and DFT-calculated structure of Titanocene **C**.

	DFT structure (**5c**) Bond length (pm)	DFT structure Titanocene **C** Bond length (pm)
$Ti-C_1$	251.3	250.4
$Ti-C_2$	242.9	242.8
$Ti-C_3$	244.2	240.0
$Ti-C_4$	240.4	237.4
$Ti-C_5$	243.2	242.9
$Ti-C_{1'}$	248.5	247.8
$Ti-C_{2'}$	239.1	239.0
$Ti-C_{3'}$	234.2	233.1
$Ti-C_{4'}$	245.6	243.7
$Ti-C_{5'}$	250.2	249.3
C_1-C_2	143.4	143.2
C_2-C_3	141.6	141.5
C_3-C_4	141.2	141.3
C_4-C_5	142.3	142.3
C_5-C_1	141.4	141.4
$C_{1'}-C_{2'}$	141.4	141.4
$C_{2'}-C_{3'}$	142.2	142.4
$C_{3'}-C_{4'}$	142.3	142.2
$C_{4'}-C_{5'}$	140.2	140.2
$C_{5'}-C_{1'}$	143.0	143.0
C_1-C_6	152.2	152.2
$C_{1'}-C_{6'}$	152.2	152.0
$C_6-C_{6'}$	559.5	559.5
C_6-C_7	151.5	152.0
$C_{6'}-C_{7'}$	152.0	151.5
C_6-N_1	152.0	148.3
$C_{6'}-N_2$	149.7	148.4
$Ti-Cl_1$	240.5	234.9
$Ti-Cl_2$	234.1	236.1

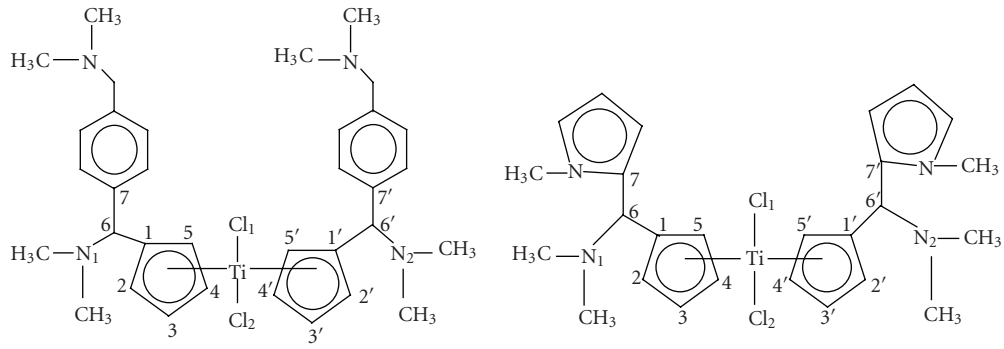

Scheme 2: Numbering scheme of **5c** and Titanocene **C** for the structural DFT discussion of **5c**.

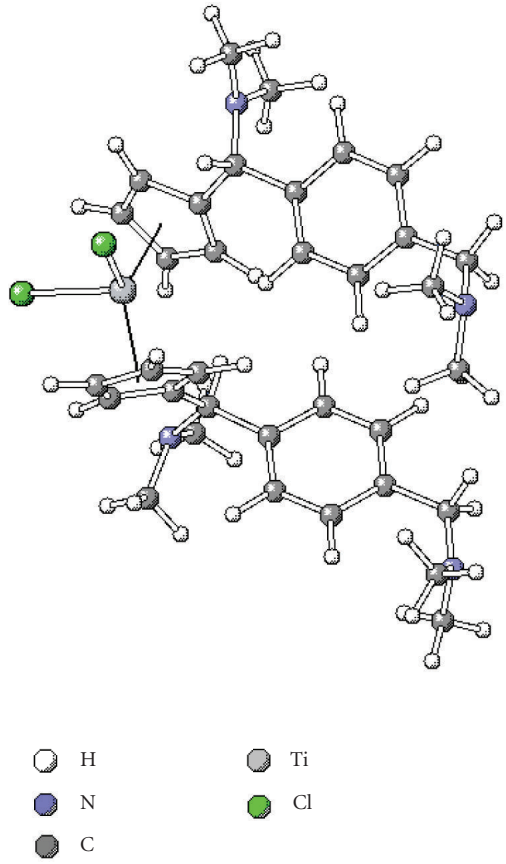

Figure 3: DFT calculated structure of **5c**.

The cartesian coordinates for the DFT optimised structure of titanocene 5C can be observed in the supplementary material, where the energy of optimisation is also found.

4. CONCLUSIONS AND OUTLOOK

The carbolithiation of 6-(*N*,*N*-dimethylamino) fulvene with Mannich-functionalised lithiated species followed by transmetallation offers a general way into the synthesis of new chiral *N*,*N*-dimethylamino-functionalised metallocenes. Derivative **5c** exhibits an impressive cytotoxicity with an IC_{50} value of 13 μM against LLC-PK cells, but is slightly less active with respect to Titanocene **C** that shows the highest cytotoxicity for a published titanocene so far.

ACKNOWLEDGMENTS

The authors thank the Higher Education Authority (HEA), the Centre for Synthesis and Chemical Biology (CSCB), UCD, and COST D39 for funding.

REFERENCES

[1] T. Schilling, K. B. Keppler, M. E. Heim, et al., "Clinical phase I and pharmacokinetic trial of the new titanium complex budotitane," *Investigational New Drugs*, vol. 13, no. 4, pp. 327–332, 1995.

[2] E. Meléndez, "Titanium complexes in cancer treatment," *Critical Reviews in Oncology/Hematology*, vol. 42, no. 3, pp. 309–315, 2002.

[3] F. Caruso and M. Rossi, "Antitumor titanium compounds and related metallocenes," *Metal Ions in Biological Systems*, vol. 42, pp. 353–384, 2004.

[4] G. Lümmen, H. Sperling, H. Luboldt, T. Otto, and H. Rübben, "Phase II trial of titanocene dichloride in advanced renal-cell carcinoma," *Cancer Chemotherapy and Pharmacology*, vol. 42, no. 5, pp. 415–417, 1998.

[5] N. Kröger, U. R. Kleeberg, K. Mross, L. Edler, G. Saß, and D. Hossfeld, "Phase II clinical trial of titanocene dichloride in patients with metastatic breast cancer," *Onkologie*, vol. 23, no. 1, pp. 60–62, 2000.

[6] J. Eisch, X. Shi, and F. Owuor, "Novel synthesis of *ansa*-metallocenes via the reductive dimerization of fulvenes with group 4 metal divalent halides," *Organometallics*, vol. 17, no. 24, pp. 5219–5221, 1998.

[7] S. Fox, J. Dunne, M. Tacke, and J. F. Gallagher, "Novel derivatives of *ansa*-titanocenes procured from 6-phenylfulvene: a combined experimental and theoretical study," *Inorganica Chimica Acta*, vol. 357, no. 1, pp. 225–234, 2004.

[8] M. Tacke, L. Allen, L. Cuffe, et al., "Novel titanocene anticancer drugs derived from fulvenes and titanium dichloride," *Journal of Organometallic Chemistry*, vol. 689, no. 13, pp. 2242–2249, 2004.

[9] F.-J. Rehmann, L. Cuffe, O. Mendoza, et al., "Heteroaryl substituted *ansa*-titanocene anti-cancer drugs derived from fulvenes and titanium dichloride," *Applied Organometallic Chemistry*, vol. 19, no. 3, pp. 293–300, 2005.

[10] M. Tacke, L. Cuffe, W. Gallagher, et al., "Methoxy-phenyl substituted *ansa*-titanocenes as potential anti-cancer drugs derived from fulvenes and titanium dichloride," *Journal of Inorganic Biochemistry*, vol. 98, no. 12, pp. 1987–1994, 2004.

[11] F.-J. Rehmann, A. Rous, O. Mendoza, et al., "A trimethoxyphenyl substituted *ansa*-titanocene: a possible anti-cancer drug," *Polyhedron*, vol. 24, no. 11, pp. 1250–1255, 2005.

[12] N. Sweeney, O. Mendoza, H. Müller-Bunz, et al., "Novel benzyl substituted titanocene anti-cancer drugs," *Journal of Organometallic Chemistry*, vol. 690, no. 21-22, pp. 4537–4544, 2005.

[13] C. Pampillón, O. Mendoza, N. Sweeney, K. Strohfeldt, and M. Tacke, "Diarylmethyl substituted titanocenes: promising anti-cancer drugs," *Polyhedron*, vol. 25, no. 10, pp. 2101–2108, 2006.

[14] C. Pampillón, N. Sweeney, K. Strohfeldt, and M. Tacke, "Diheteroarylmethyl substituted titanocenes: a novel class of possible anti-cancer drugs," *Inorganica Chimica Acta*, vol. 359, no. 12, pp. 3969–3975, 2006.

[15] N. Sweeney, W. M. Gallagher, H. Müller-Bunz, C. Pampillón, K. Strohfeldt, and M. Tacke, "Heteroaryl substituted titanocenes as potential anti-cancer drugs," *Journal of Inorganic Biochemistry*, vol. 100, no. 9, pp. 1479–1486, 2006.

[16] K. Strohfeldt, H. Müller-Bunz, C. Pampillón, N. Sweeney, and M. Tacke, "Glycol methyl ether and glycol amine substituted titanocenes as antitumor agents," *European Journal of Inorganic Chemistry*, vol. 2006, no. 22, pp. 4621–4628, 2006.

[17] N. Sweeney, J. Claffey, H. Müller-Bunz, C. Pampillón, K. Strohfeldt, and M. Tacke, "The synthesis and cytotoxic evaluation of a series of benzodioxole substituted titanocenes," *Applied Organometallic Chemistry*, vol. 21, no. 2, pp. 57–65, 2007.

[18] O. Allen, L. Croll, A. Gott, R. Knox, and P. McGowan, "Functionalized cyclopentadienyl titanium organometallic compounds as new antitumor drugs," *Organometallics*, vol. 23, no. 2, pp. 288–292, 2004.

[19] P. Causey, M. Baird, and S. P. C. Cole, "Synthesis, characterization, and assessment of cytotoxic properties of a series of titanocene dichloride derivatives," *Organometallics*, vol. 23, no. 19, pp. 4486–4494, 2004.

[20] R. Meyer, S. Brink, C. van Rensburg, G. Jooné, H. Görls, and S. Lotz, "Synthesis, characterization and antitumor properties of titanocene derivatives with thiophene containing ligands," *Journal of Organometallic Chemistry*, vol. 690, no. 1, pp. 117–125, 2005.

[21] G. Kelter, N. Sweeney, K. Strohfeldt, H.-H. Fiebig, and M. Tacke, "In-vitro anti-tumor activity studies of bridged and unbridged benzyl-substituted titanocenes," *Anti-Cancer Drugs*, vol. 16, no. 10, pp. 1091–1098, 2005.

[22] O. Oberschmidt, A.-R. Hanauske, F.-J. Rehmann, K. Strohfeldt, N. Sweeney, and M. Tacke, "Activity of [1,2-di(cyclopentadienyl)-1,2-di(*p*-*N*,*N*-dimethylaminophenyl)-ethanediyl] titanium dichloride against tumor colony-forming units," *Anti-Cancer Drugs*, vol. 16, no. 10, pp. 1071–1073, 2005.

[23] K. O'Connor, C. Gill, M. Tacke, et al., "Novel titanocene anticancer drugs and their effect on apoptosis and the apoptotic pathway in prostate cancer cells," *Apoptosis*, vol. 11, no. 7, pp. 1205–1214, 2006.

[24] M. Valadares, A. Ramos, F.-J. Rehmann, et al., "Antitumour activity of [1,2-di(cyclopentadienyl)-1,2-di(*p*-*N*,*N*-dimethylaminophenyl)-ethanediyl] titanium dichloride in xenografted Ehrlich's ascites tumour," *European Journal of Pharmacology*, vol. 534, no. 1–3, pp. 264–270, 2006.

[25] I. Fichtner, C. Pampillón, N. Sweeney, K. Strohfeldt, and M. Tacke, "Anti-tumor activity of Titanocene Y in xenografted Caki-1 tumors in mice," *Anti-Cancer Drugs*, vol. 17, no. 3, pp. 333–336, 2006.

[26] C. Pampillón, N. Sweeney, K. Strohfeldt, and M. Tacke, "Synthesis and cytotoxicity studies of new dimethylamino-functionalised and heteroaryl-substituted titanocene anti-cancer drugs," *Journal of Organic Chemistry*, vol. 692, no. 11, pp. 2153–2159, 2007.

[27] T. Suzuka, M. Ogasawa, and T. Hayashi, "Asymmetric synthesis of metallocenes through enantioselective addition of organolithium reagents to 6-(dimethylamino)fulvene," *Journal of Organic Chemistry*, vol. 67, no. 10, pp. 3355–3359, 2002.

[28] Y. Qian, J. Huang, J. Yang, et al., "Syntheses, structures and reactions of some new benzyl-substituted cyclopentadienyl titanium complexes," *Journal of Organometallic Chemistry*, vol. 547, no. 2, pp. 263–279, 1997.

[29] M. Horáček, P. Štěpnička, S. Gentil, et al., "Syntheses and properties of some *exo,exo*-bis(isodicyclopentadienyl)titanium low-valent complexes," *Journal of Organometallic Chemistry*, vol. 656, no. 1-2, pp. 81–88, 2002.

[30] S. Knüppel, C. Wang, G. Kehr, R. Fröhlich, and G. Erker, "Bis(enamino-Cp) Group 4 metal complex chemistry: developing a Mannich-type carbon-carbon coupling reaction at the bent metallocene famework," *Journal of Organometallic Chemistry*, vol. 690, no. 1, pp. 14–32, 2005.

[31] Gaussian '03, *Revision C.02*, Gaussian, Wallingford, Conn, USA, 2004.

Hindawi Publishing Corporation
Metal-Based Drugs
Volume 2008, Article ID 864653, 5 pages
doi:10.1155/2008/864653

Research Article

The In Vitro Antitumour Activity of Novel, Mitochondrial-Interactive, Gold-Based Lipophilic Cations

Sherika Mahepal,[1] Richard Bowen,[2] Messai Adenew Mamo,[2] Marcus Layh,[2] and Constance Elizabeth Jansen van Rensburg[1]

[1] *Department of Pharmacology, University of Pretoria, P.O. Box 2034, Pretoria 0001, South Africa*
[2] *School of Chemistry, University of the Witwatersrand, Private Bag 3, Johannesburg 2050, South Africa*

Correspondence should be addressed to C. E. J. van Rensburg, cmedlen@postillion.up.ac.za

Received 18 July 2007; Accepted 1 October 2007

Recommended by Jannie C Swarts

In this study we compared the effects of two previously described antimitochondrial gold complexes, that is, [A] $[Au(dppe)_2]Cl$ and [B] $[Au(d4pype)_2]Cl$ with two novel lipophilic cations, that is, [C] $[Au(dpmaaH_2)(dpmaaSnMe_2)]Cl$ and [D] $[Au(dpmaaSnMe_2)_2]Cl$ as antimitochondrial agents. The results of this study indicate that [C] and [D] have intermediate partition coefficients and exhibited a selective uptake by cells. They exhibited a higher selectivity for the various cell lines than [A] but were more cytotoxic than [B]. There is a significant correlation between the cytotoxic potential of [A], [B], [C], and [D] and their octanol/water partition coefficients in both MCF-7 (breast cancer) and MCF-12A (nonmalignant breast) cells, whereas their cytotoxic potential and ability to induce the release of cytochrome c correlated only in the case of the MCF-12A cells. Complexes [C] and [D] are promising new chemotherapeutic drugs. These compounds target the mitochondrial membranes of certain cancer cells exploiting the differences between the mitochondrial membrane potential of these cells and normal cells. Although the concentrations of these compounds necessary to eradicate cancer cells are very high, the results provide a basis for the synthesis of a new family of compounds with intermediate partition coefficients compared to [A] and [B] but with increased activity against cancer cells.

1. INTRODUCTION

The successful chemotherapy of cancer has been hindered by the acquired resistance of tumour cells to clinical drugs, which has necessitated the use of multidrug therapy with a higher potential for adverse drug effects. The use of relatively nonselective compounds results in the eradication of normal cells in addition to tumour cells. Previous studies have indicated that $[Au(dppe)_2]Cl$ (see Figure 1) exhibits antitumour activity in a wide range of tumour models in mice [1]. Since the lipophilic cationic properties of $[Au(dppe)_2]Cl$ promote its nonselective uptake into the mitochondria of all cells, strategies were adopted to synthesize more hydrophilic analogues that retained antitumour activity while being less toxic to the mitochondria.

The lipophilicity of gold(I) phosphine complexes can be controlled by an appropriate substitution at the quaternary centre or alkyl backbone that enables the modification of the compound to achieve greater selectivity for tumour cells [2]. This has led to the synthesis of the 3- and 4-pyridyl substituted analogues of $[Au(dppe)_2]Cl$ by the replacement of some or all of the phenyl substituents in dppe with hydrophilic pyridyl groups [3]. The lipophilicity of these tetrahedral bis(dipyridylphosphino) gold(I) complexes plays a key role in determining their cellular uptake [4]. It is therefore necessary to retain the lipophilicity of the compound within a certain octanol-water coefficient range in order to facilitate the uptake of a drug and determine the degree of protein binding [2].

Although the precise mechanism of action of these gold-containing lipophilic aromatic compounds is poorly understood, several studies have suggested a mitochondrial mode of action as well as the occurrence of DNA strand breaks and DNA-protein crosslinks in tumour cells [1, 2, 4, 5].

Tumour cells possess one of the highest mitochondrial transmembrane potentials [6, 7], which may be due to the inability of tumour cells to use mitochondria to fulfil their demands for ATP. Normal cells rely on oxygen consumption

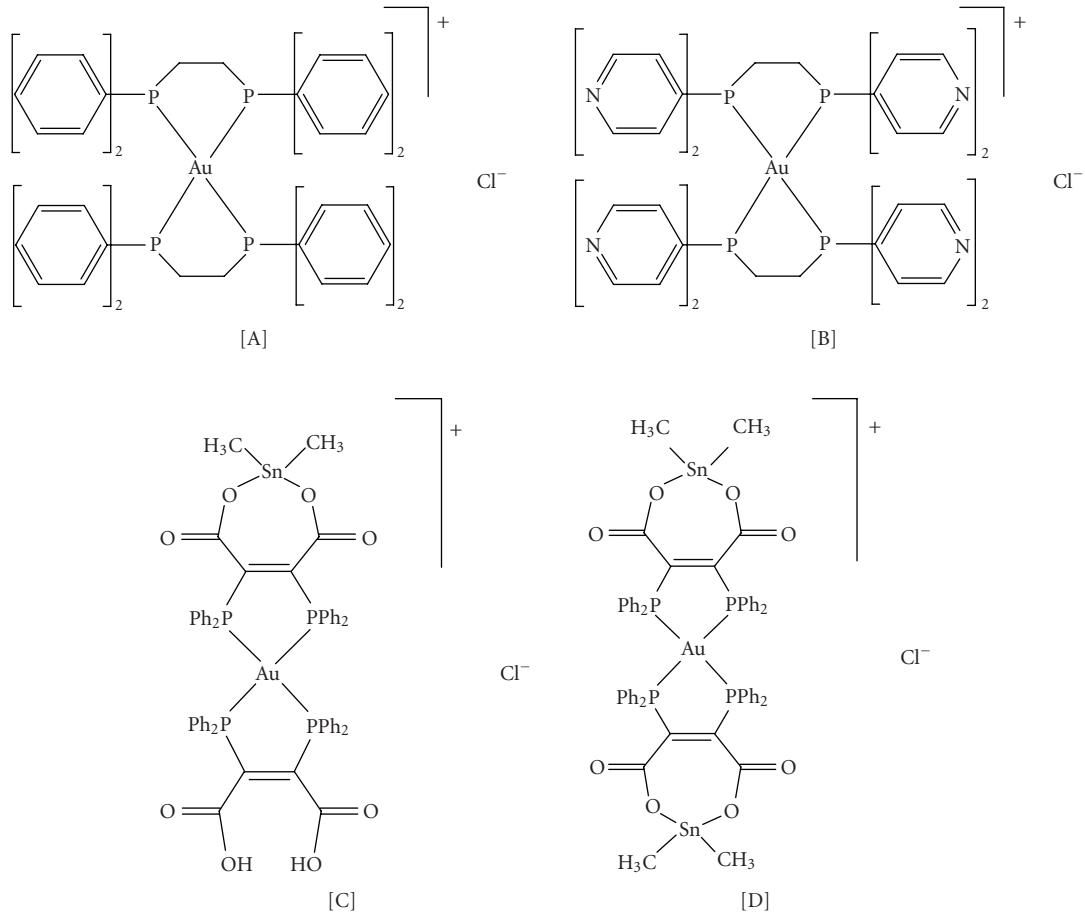

Figure 1: Structure of the experimental compounds: $[Au(dppe)_2]Cl$ [A], $[Au(d4pype)_2]Cl$ [B], $[Au(dpmaaSnMe_2)(dpmaaH_2)]Cl$ [C], and $[Au(dpmaaSnMe_2)_2]Cl$ [D]. (50 μM).

and oxidative phosphorylation for ATP production that takes place in the mitochondria, whereas tumour cells rely primarily on glycolysis for ATP production that takes place in the cytosol of the cell [4]. Lipophilic cations that possess a positive charge are able to penetrate the hydrophobic barriers of the plasma and mitochondrial membranes [8]. These compounds accumulate in the mitochondria in response to a negative transmembrane potential, which is the rationale behind the use of lipophilic cations as anticancer agents.

According to Davis et al. the uptake of a lipophilic cation is dependent on both the plasma and mitochondrial membrane potentials. The plasma membrane preconcentrates the drug in the cytoplasm and the mitochondrial membrane, in turn, concentrates the drug within the mitochondria [9]. These facts provide the perfect opportunity for drug accumulation in tumour cells and the feasibility for the use of tumour selective antimitochondrial compounds in human cancer chemotherapy.

The $[Au(d4pype)_2]Cl$ complex (see Figure 1), which is hydrophilic, exhibited a higher tumour uptake and a smaller in vivo liver/tumour ratio in treated mice with advanced Colon 38 adenocarcinoma tumours than $[Au(dppe)_2]Cl$ [10]. McKeage et al. [4] corroborated that compounds with an intermediate lipophilicity when compared to more lipophilic or hydrophilic compounds displayed significant antitumour activity, less dose-limiting toxicity, and a higher plasma concentration of gold. A correlation between the lipophilicity of the drug and the degree of selectivity and cytotoxic potency of the compounds has been established [10]. This denotes that an enhanced selectivity is achieved with greater hydrophilicity but an increase in the potency of the drug can be observed with a greater lipophilicity.

The common occurrence of drug-resistant tumour cells and the lack of selectivity of cancer drugs in differentiating between tumour cells and normal cells are two overriding problems in cancer chemotherapy [10]. In an attempt to combat this lack of selectivity, an investigation was initiated into two new aromatic cations, that is, $[Au(dpmaaSnMe_2)(dpmaaH_2)]Cl$ [C] and $[Au(dpmaaSnMe_2)_2]Cl$ [D] (see Figure 1). The simultaneous presence of gold and tin in aromatic cations should offer the advantage of reducing the development of resistance in cancer cells.

2. MATERIALS AND METHOD

2.1. Octanol/water partition coefficient

60 μM stock solutions of $[Au(dppe)_2]Cl$ [A], $Au(d4pype)_2]$-Cl [B], $[Au(dpmaaSnMe_2)(dpmaaH_2)]Cl$ [C], and

[Au-(dpmaaSnMe$_2$)$_2$]Cl [D] were prepared in octanol (Merck, Darmstadt, Germany). Water-saturated octanol and octanol-saturated water were prepared by shaking equal volumes of octanol and water for 15 minutes and allowing the mixture to separate into the respective phases for 20 hours. The absorbance of the initial drug concentration in the water-saturated octanol at 20 μM, 40 μM, and 60 μM was analysed by UV spectrophotometry. Five millilitres of the octanol-saturated water were then added to 5 ml of the drug/octanol solutions to obtain a final volume of 10 ml. These solutions were shaken vigorously for 15 minutes, thereafter they were left to separate into an octanol and aqueous phase for 20 hours. The aqueous phase was separated ensuring that there was no contamination from the octanol phase, and each of these solutions was analysed by UV spectrophotometry in 1 cm quartz cuvettes to obtain the absorbance of the compounds.

2.2. Cell cultures

Cytotoxicity assays were performed on the following cell cultures: human ovarian carcinoma (A2780)-(ECACC93112519) and its cisplatin-resistant subline (A-2780cis)(ECACC93112517), breast carcinoma (MCF-7)-(HTB-22), colon cancer (CoLo 320 DM)(CCL-220), cervical carcinoma cells (HeLa)(CCL-2), mouse melanoma (B16)(ECACC92101203), primary human fibroblasts (CCL-171), and a breast nontumourogenic cell line (MCF-12A)(CRL-10782). A2780, A2780cis and CoLo 320 DM were maintained in RPMI; B16, HeLa cells, and the primary fibroblasts were maintained in EMEM. B16 cells were maintained in DMEM. MCF-7 cells were maintained in DMEM supplemented with 2% nonessential amino acids and MCF-12A cells were maintained in a 1 : 1 mixture of DMEM and HAMS F12 medium with hydrocortisone (10 mg/mL), cholera toxin (1 mg/mL), insulin (20 mg/mL), 10% foetal calf serum (FCS), and epidermal growth factor (100 mg/mL). All media were supplemented with 1% solution of penicillin and streptomycinand 10% heat inactivated FCS.

2.3. Cell growth assay

A metabolic assay based on the reactivity of MTT (3-[4, 5-dimethylthiazol-2-yl)-2,5-diphenyl-tetrazolium bromide), originally described by Mosmann [11] with modifications [12], was used to determine the effects of the experimental compounds on cell growth after a 7-day treatment period in 96 well-round bottom microtiter plates.

2.4. Cellular uptake of gold

MCF-7 and MCF-12A cells were prepared in supplemented DMEM at a stock concentration of 5×10^6 cells/mL. The cells were exposed to the various compounds at concentrations that lead to 80–90% of cell death in the above-mentioned assay for 30 minutes at 37°C, centrifuged for 10 minutes at 185 g, and the pellets washed with Hank's balanced salt solution (HBSS). The gold content of the pellets was determined on an inductively coupled plasma mass spectrometer (ICP-MS) using standard procedures.

Table 1: Average octanol/water partition coefficients of the experimental compounds as well as the mean log octanol/water partition coefficient ± standard error mean (SEM).

Octanol/water partition coefficient and mean log octanol/water partition coefficient ± SEM		
Experimental compounds	Average[1] octanol/water partition coefficient value	Mean log octanol/water partition coefficient ± SEM
[A]	12.06	1.07 ± 0.104
[B]	0.038	−1.568 ± 0.149
[C]	2.3	−0.012 ± 0.317
[D]	1.67	0.09 ± 0.155

[1]Average of 9 experiments at three different concentrations.

2.5. Release of cytochrome c

A suspension of MCF-7 and MCF-12A cells (2×10^6 cells/mL) was prepared in supplemented DMEM. The cells were exposed to a concentration of the various compounds that lead to 80–90% of cell death for 30 minutes at 37°C, centrifuged for 10 minutes at 185 g, and the pellets washed with HBSS and assayed according to the manufacturers' instructions for cytochrome c using an assay kit (Sigma Chemical Co, St. Louis, Mo, USA).

2.6. Statistical analysis

The Pearson correlation coefficient (±95% confidence interval) was calculated and used to determine correlations between the various assay results.

3. RESULTS

3.1. Octanol/water partition coefficient

The average octanol/water partition coefficient values and the mean log octanol/water partition coefficient values are summarised in Table 1. The results indicate that [A] has a mean log octanol/water partition coefficient of 1.07, making it a lipophilic compound whereas [B] is hydrophilic with a very low log octanol/water partition coefficient of −1.57. The octanol/water partition coefficients of both [C] and [D] (−0.012 and 0.09, resp.) are intermediate to that of [A] and [B].

3.2. Cytotoxicity assays

The IC_{50} values of the compounds for the various cell lines are summarised in Table 2. All eight cell cultures were more sensitive to [A] than any of the other compounds tested. [B] was more selective for certain cell types such as MCF-7. This cell line was 8-9 times more sensitive for this compound than the colon cancer cell line (CoLo 320DM) and the primary fibroblast culture. [C] and [D] also exhibited some selectivity

Table 2: Mean drug concentration (μM) causing 50% cell death (IC_{50}) after treatment of various cell lines with the five experimental compounds.

Cell lines	[A][1]	[B]	[C]	[D]
MCF-7	2.31	20.327	5.33	6.508
MCF-12A	2.424	160	25.639	16.58
A2780	1.158	22.244	12.996	17.277
A2780cis	2.58	37.663	10	20
HeLa	1.407	63.793	11.476	12.264
CoLo	7.686	200	31.141	26.234
Primary fibroblasts	0.887	170	11.874	8.046
B16	0.115	49.89	4.999	2.738

[1]Average of 3–5 experiments.

Table 3: Gold uptake (mg/L) by MCF-7 and MCF-12 [A] cells treated with the experimental compounds.

	Gold Uptake (mg/L)[1]			
Cell lines	[A]	[B]	[C]	[D]
MCF-7	5.27	5.19	2.85	2.68
MCF-12A	6.51	6.83	3.3	2.63

[1]Average of 3 different experiments.

for certain cell types viz [D] acted on the B16 cells at a concentration that was 9.5 times lower than what was necessary to inhibit the growth of CoLo 320DM.

3.3. Cellular uptake of experimental compounds

The average amount of gold taken up by MCF-7 and MCF-12A cells after treatment with the various experimental compounds is summarised in Table 3. The cells treated with [A] and [B] accumulated almost twice the percentage of gold than cells treated with [C] and [D].

3.4. Release of cytochrome c

The average percentage of cytochrome c release by MCF-7 and MCF-12A cells is summarised in Table 4. The results indicate that the outer membrane of mitochondria of cells treated with [A] incurred the greatest amount of damage as only 2-3% of the cells had undamaged mitochondrial membranes after treatment. There were no significant differences between the sensitivity of the mitochondrial membranes of MCF-7A and MCF-12A for the experimental drugs.

3.5. Pearson's correlation coefficient

(i) There is a significant correlation ($P < .05$) between the cytotoxic potential of [A], [B], [C], and [D] and their octanol/water partition coefficients in both MCF-7 and MCF-12A cells.

(ii) There is a significant correlation ($P < .05$) between the cytotoxic potential of [A], [B], [C] and [D] and their ability to induce the release of cytochrome c in MCF-12A cells.

Table 4: Mitochondria of MCF-7 and MCF-12A cells with undamaged membranes after treatment with experimental compounds.

	Percentage mitochondria with undamaged membranes calculated as the invert of the percentage cytochrome c release[1]				
Cell line	Untreated	[A]	[B]	[C]	[D]
MCF-7	60.75	3	61.75	39.5	41.0
MCF-12A	70.25	2.25	76.5	48.0	46.25

[1]Average of 3–5 experiments.

4. DISCUSSION

Results from this study have indicated that [B], [C], and [D] have octanol/water partition coefficients that are lower than that of [A]. These compounds exhibit more selectivity for different cell types but are less intrinsically potent. The lower octanol/water partition coefficients facilitate the more selective uptake of these compounds. On the other hand, Berners-Price et. al. [13] described a related compound, that is, $[Au(dpmaaH_2)_2]Cl$, to be hydrophilic with no significant activity against cancer cells indicating the important role lypophilicity plays in the design of antitumour compounds.

A significant correlation between drug uptake and the octanol/water partition coefficient of compounds has been established [10]. Although [C] and [D] have intermediate partition coefficients we failed to obtain a significant correlation between drug uptake and the octanol/water partition coefficient.

McKeage et al. [4] affirmed that compounds with an intermediate lipophilicity displayed significant antitumour activity, less dose-limiting toxicity, and a higher plasma concentration of gold when compared to more lipophilic or hydrophilic compounds. Similarly, we found a significant correlation between lipophilicity and cytotoxicity. However, results from this study suggest that the cellular uptake of these compounds is not dependent on the lipophilicity of the compound.

The mere fact that cytochrome c is being released indicates that the cell will eventually undergo apoptosis. The uncoupling of oxidative phosphorylation results in the swelling of the mitochondria [5], which consequently causes the outer membrane of the mitochondria to rupture, leading to the release of cytochrome c [7]. In this study, we found a significant correlation between lipophilicity and mitochondrial damage only in the case of the nontumourogenic breast cell line (MCF-12A) and not the breast cancer cell line (MCF-7) indicating a possible selectivity of less lipophilic compounds for mitochondrial cell membranes.

Furthermore, cytotoxicity results indicate that MCF-7 is more sensitive than MCF-12A to [B], [C], and [D].

The results from this study suggest that [C] and [D] act more selectively against a breast cancer and myeloma cell line than [B] but possess less overall cytotoxicity compared to [A], which is an important characteristic in selecting anticancer agents. These compounds possess an intermediate partition coefficient compared to [A] and [B], which plays an important role in their uptake by both normal and cancer cells. Future work will include experimental studies to obtain

a clear understanding of the mechanism of action of [C] and [D] and the influence of tin in this regard. Although the high IC_{50} values obtained with [C] and [D] against malignant cell lines are not achievable in vivo, it provides a basis for the synthesis of a new family of compounds with intermediate partition coefficients compared to [A] and [B] but increased activity against cancer cells.

ACKNOWLEDGMENTS

This project was funded by AuTEK Biomed (Mintek and Harmony Gold, Johannesburg, South Africa), the Cancer Association of South Africa and the Department of Trade and Industry Technology and Human Resources for Industry Programmes (THRIP) (Pretoria, South Africa).

REFERENCES

[1] S. J. Berners-Price, C. K. Mirabelli, R. K. Johnson, et al., "In vivo antitumor activity and in vitro cytotoxic properties of bis[1,2-bis(diphenylphosphino)ethane]gold(I) chloride," *Cancer Research*, vol. 46, no. 11, pp. 5486–5493, 1986.

[2] M. J. McKeage, S. J. Berners-Price, P. Galettis, et al., "Role of lipophilicity in determining cellular uptake and antitumour activity of gold phosphine complexes," *Cancer Chemotherapy and Pharmacology*, vol. 46, no. 5, pp. 343–350, 2000.

[3] R. J. Bowen, A. C. Garner, S. J. Berners-Price, I. D. Jenkins, and R. E. Sue, "Convenient synthetic routes to bidentate and monodentate 2-, 3- and 4-pyridyl phosphines: potentially useful ligands for water-soluble complex catalysts," *Journal of Organometallic Chemistry*, vol. 554, no. 2, pp. 181–184, 1998.

[4] M. J. McKeage, L. Maharaj, and S. J. Berners-Price, "Mechanisms of cytotoxicity and antitumor activity of gold(I) phosphine complexes: the possible role of mitochondria," *Coordination Chemistry Reviews*, vol. 232, no. 1-2, pp. 127–135, 2002.

[5] P. F. Smith, G. D. Hoke, D. W. Alberts, et al., "Mechanism of toxicity of an experimental bidentate phosphine gold complexed antineoplastic agent in isolated rat hepatocytes," *Journal of Pharmacology and Experimental Therapeutics*, vol. 249, no. 3, pp. 944–950, 1989.

[6] V. R. Fantin, M. J. Berardi, L. Scorrano, S. J. Korsmeyer, and P. Leder, "A novel mitochondriotoxic small molecule that selectively inhibits tumor cell growth," *Cancer Cell*, vol. 2, no. 1, pp. 29–42, 2002.

[7] P. Bernardi, L. Scorrano, R. Colonna, V. Petronilli, and F. Di Lisa, "Mitochondria and cell death. Mechanistic aspects and methodological issues," *European Journal of Biochemistry*, vol. 264, no. 3, pp. 687–701, 1999.

[8] J. S. Modica-Napolitano and J. R. Aprille, "Delocalized lipophilic cations selectively target the mitochondria of carcinoma cells," *Advanced Drug Delivery Reviews*, vol. 49, no. 1-2, pp. 63–70, 2001.

[9] S. Davis, M. J. Weiss, J. R. Wong, T. J. Lampidis, and L. B. Chen, "Mitochondrial and plasma membrane potentials cause unusual accumulation and retention of rhodamine 123 by human breast adenocarcinoma-derived MCF-7 cells," *Journal of Biological Chemistry*, vol. 260, no. 25, pp. 13844–13850, 1985.

[10] S. J. Berners-Price, R. J. Bowen, P. Galettis, P. C. Healy, and M. J. McKeage, "Structural and solution chemistry of gold(I) and silver(I) complexes of bidentate pyridyl phosphines: selective antitumour agents," *Coordination Chemistry Reviews*, vol. 185-186, pp. 823–836, 1999.

[11] T. Mosmann, "Rapid colorimetric assay for cellular growth and survival: application to proliferation and cytotoxicity assays," *Journal of Immunological Methods*, vol. 65, no. 1-2, pp. 55–63, 1983.

[12] C. E. J. van Rensburg, R. Anderson, M. S. Myer, G. K. Joone, and J. F. O'Sullivan, "The riminophenazine agents clofazimine and B669 reverse acquired multidrug resistance in a human lung cancer cell line," *Cancer Letters*, vol. 85, no. 1, pp. 59–63, 1994.

[13] S. J. Berners-Price, R. J. Bowen, M. A. Fernandes, et al., "Gold(I) and silver(I) complexes of 2,3-bis-(diphenylphosphino)maleic acid: structural studies and antitumour activity," *Inorganica Chimica Acta*, vol. 358, no. 14, pp. 4237–4246, 2005.

Hindawi Publishing Corporation
Metal-Based Drugs
Volume 2008, Article ID 362105, 11 pages
doi:10.1155/2008/362105

Research Article

Synthesis, Structure, Electrochemistry, and Spectral Characterization of Bis-Isatin Thiocarbohydrazone Metal Complexes and Their Antitumor Activity Against Ehrlich Ascites Carcinoma in Swiss Albino Mice

M. P. Sathisha,[1] V. K. Revankar,[1] and K. S. R. Pai[2]

[1] *P. G. Department of Studies in Chemistry, Karnatak University, Dharwad 580 003, India*
[2] *Department of Pharmacology, Manipal College of Pharmaceutical Sciences, Manipal Academy of Higher Education, Manipal 576 104, India*

Correspondence should be addressed to V. K. Revankar, vkrevankar@rediffmail.com

Received 10 May 2007; Revised 7 July 2007; Accepted 6 August 2007

Recommended by Jannie C. Swarts

The synthesis, structure, electrochemistry, and biological studies of Co(II), Ni(II), Cu(II), and Zn(II) complexes of thiocarbohydrazone ligand are described. The ligand is synthesized starting from thiocarbohydrazide and isatin. It is evident from the IR data that in all the complexes, only one part of the ligand is coordinated to the metal ion resulting mononuclear complexes. The ligand coordinates essentially through the carbonyl oxygen of the isatin fragment, the nitrogen atom of the azomethine group, and sulfur atom after deprotonation to give five membered rings. ^{1}H NMR spectrum of the ligand shows only one set of signals for the aromatic protons, while the NH of isatin and NH of hydrazone give rise to two different singlets in the 11–14 ppm range. The formulations, $[Cu(L)Cl]\cdot 2H_2O$, $[Cu(L)(CH_3COO)]\cdot 2H_2O$, [Ni(L)Cl], $[Ni(L)(CH_3COO)]$, $[Co(L_2)]$, and $[Zn(L_2)]\cdot 2H_2O$ are in accordance with elemental analyses, physical, and spectroscopic measurements. The complexes are soluble in organic solvents. Molar conductance values in DMF indicate the nonelectrolytic nature of the complexes. Copper complex displays quasireversible cyclic voltametric responses with *Ep* near −0.659 v and 0.504 v Vs Ag/AgCl at the scan rate of 0.1 V/s. Copper(II) complexes show a single line EPR signals. For the observed magnetic moment and electronic spectral data possible explanation has been discussed. From all the available data, the probable structures for the complexes have been proposed. The compounds synthesized in present study have shown promising cytotoxic activity when screened using the in vitro method and at the same time were shown to have good activity when tested using the Ehrlich ascites carcinoma (EAC) model. The antimicrobial screening showed that the cobalt complex possesses enhanced antimicrobial activity towards fungi.

1. INTRODUCTION

Although ligands having oxygen and nitrogen as donor atoms are by far the most extensively studied, interest in sulfur donor chelating agents has grown over the years and the number of chemical studies in this area has increased considerably [1]. Interest in complexes of these ligand systems now covers several areas, ranging from general considerations of the effect of sulfur and electron delocalization in transition metal complexes to potential biological activity and practical application [2–4].

The aim of the present work is to synthesize new thiocarbohydrazone ligand, and to study its coordination behavior with Co(II), Ni(II), Cu(II), and Zn(II) ions. N, N′-Thiocarbohydrazide condenses easily with two molecules of carbonyl compounds *viz*., isatin, on the N^1H_2 and N^4H_2 hydrazine amino groups to produce the desired ligand shown in Figure 1. The tautomerism in this ligand and also the well-known tendency of oxygen and sulfur donors to act as bridging sites [5, 6] allows various structural possibilities for the corresponding metal complexes.

A considerable number of metal complexes are now known to possess antitumor activity [7]. There are reports that sulphur-containing ligands [8] and platinum complexes of sulphur-containing amino acids were found to have inhibitory action against tumors [9]. However, since the

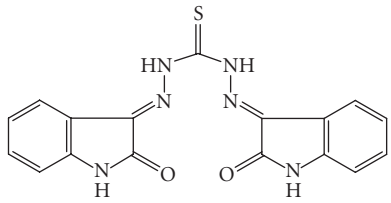

Figure 1: Representative structure of the ligand.

class of sulphur-containing compounds such as thiosemicarbazones, an structural analogue of the thiocarbohydrazone, have been reported to have anticancer activity owing to the specific and unique properties of their metal chelate [10], it is suggested that the present compounds, being similar in structure and character, may be acting by virtue of their chelating properties at the cellular level thereby exerting their anticancer activity. Hence, it was considered worthwhile to subject the presently studied complexes for evaluation of their anticancer activity.

The antimicrobial properties of metals have been recognized for centuries and have represented some of the most fundamental breakthroughs in medicinal history [11]. Many studies stressed the role of metal ions in important biological processes, whereas the inorganic pharmacology started to be an important field with more than 25 inorganic compounds, being used in therapy as antibacterial, antiviral, and anticancer drugs [12, 13]. Kirschner et al. [14] have suggested that the transfer of the metal ion from the ligand to the cancer-associated viruses was an important mechanism for designing new anticancer therapies. The inverse process, that is, coordinating a metal ion from an important biomolecule, such as, for instance, a zinc finger protein, has recently been used to design novel antiviral therapies, targeted against human immunodeficiency (HIV) and human papilloma virus (HPV) infections [15]. We have already drawn attention to the strong relationship between metals or their complexes [16–18], and antibacterial [19], antitumour [20], and anticancer [21] activities. A number of in vivo studies have indicated [22] that biologically active compounds become more bacteriostatic and carcinostatic upon chelation.

2. EXPERIMENTAL

2.1. Materials, analytical methods, and physical measurements

All chemicals used were of reagent grade. Solvents were distilled prior to use. The metal content of the complexes were estimated after decomposition with mixture of HCl and $HClO_4$ by gravimetric method (copper and nickel) and EDTA titration method (cobalt and zinc). Magnetic susceptibility of complexes were measured at room temperature on a Faraday balance using $Hg[Co(SCN)_4]$ as a calibrant. Electronic spectra were recorded using VARIAN CARY 50 Bio UV-Visible spectrophotometer in DMSO. The IR spectra of ligand and its complexes were recorded as KBr pellets in the region 4000–400 cm^{-1} on Nicolet 170 SX FT-IR spectrometer. The ^{1}H-NMR spectra of ligand and its zinc (II) complex were recorded in DMSO-d_6 on Bruker 300 MHz spectrometer using TMS as an internal standard. The cyclic voltammetry experiments were carried out with a three-electrode apparatus using a CHI1110A electrochemical analyzer (USA). The EPR spectra of copper (II) complexes were recorded at room temperature on Varian E-4 X-band spectrometer using TCNE as *g*-marker. Conductivity measurements were made on 10^{-3} M solutions of complexes in DMSO using ELICO-CM82 conductivity bridge provided with a cell having cell constant 0.51.

2.2. Synthesis of N, N′-Thiocarbohydrazone bis (isatin)

A solution of isatin 5.8 g (0.04 mol) in ethanol (30 ml) was added drop wise to a refluxing solution of thiocarbohydrazide 2.1 g (0.02 mol) in the same solvent (40 ml). Few drops of glacial acetic acid were added to the reaction mixture and was refluxed for 2 hours. At the end of the reaction, monitored by TLC (n-hexane/ethyl acetate 2 : 3), a yellow-orange powder was filtered and washed with warm ethanol and then with diethyl ether. Yield 75%. M.P. 284°C (Scheme 1).

The thiocarbohydrazide was prepared as described in the literature [23].

2.3. Synthesis of metal (II) chloride and acetate complexes

In a representative preparation, the complex was prepared by the addition of ethanolic solution of metal (II) chloride or aqueous ethanolic solution of metal (II) acetates (0.003 mol) with constant stirring to the corresponding amount of the ligand (0.003 mol) in the same solvent. The mixture was heated to reflux for 1 hour. The product was filtered off, washed several times with ethanol, and dried in vacuum over P_2O_5 (Scheme 2).

2.4. Brine shrimp lethality bioassay [24]

The brine shrimp lethality test was used to predict the presence of cytotoxic activity. The brine shrimp (Artemia salina) eggs were procured from www.brineshrimp.com. The brine shrimp eggs were hatched in artificial sea water at room temperature under constant aeration for 48 hours. After hatching, 10 larvae were placed in a vial containing 5 ml of artificial sea water. A drop of dry yeast suspension (3 mg in 5 ml sea water) was added to each vial as food for shrimps. Test compounds in different concentrations (10, 100, and 1000 ppm) were added to the vials before making up the final volume to 5 ml with sea water. The control group had shrimp in artificial sea water. The vials were maintained under illumination with 40 W electric bulb. The experiments were done in triplicate and mean of three readings was taken as final result. After 24 hours, the survivors were counted using a 3X magnifying glass, and the percent deaths and LC_{50} (Lethal concentration for half the population) values wear calculated by using Finney computer program.

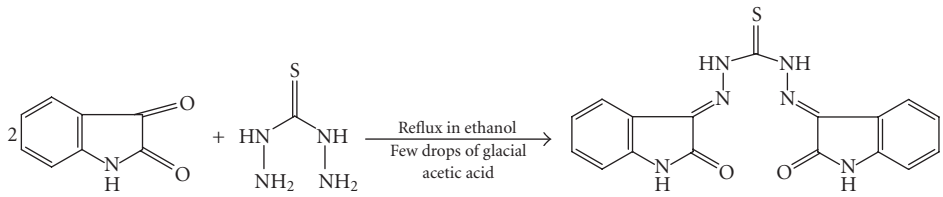

Scheme 1: Synthesis of ligand.

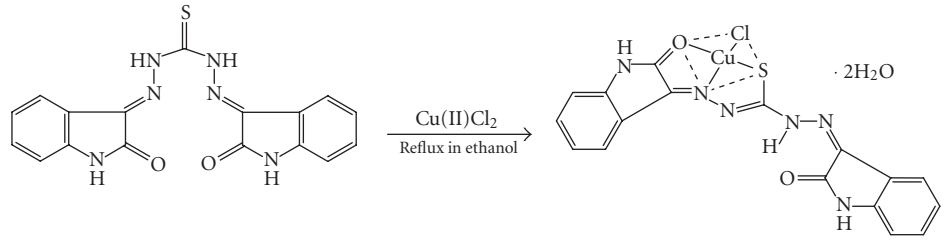

Scheme 2: Representative synthesis of copper chloride complex.

2.5. Cell lines

Cancer cell lines viz. Ehrlich ascitic carcinoma (EAC), to induce cancer in animal model (mice) were obtained from (Amala Cancer Research Center, Amala Nagar, Kerala, India.) The cells were maintained as ascites tumor in Swiss Albino mice by intraperitoneal inoculation of 1×10^6 viable cells.

2.6. Animals

Six-to-eight week old female Swiss Albino mice (25 ± 5 g body weight) were selected from (Central Animal Facility, Manipal Academy of Higher Education, Manipal, Karnataka, India.) The animals were acclimatized to the experimental room having temperature $23 \pm 2^\circ$C, controlled humidity conditions, and 12 : 12 hour light and dark cycle. The mice were housed in sterile polypropylene cages containing sterile paddy husk as bedding material with a maximum of 4 animals in each cage. The mice were fed on autoclaved standard mice food pellets (Hindustan Lever) and had access to water *ad libitum*. The animal experiments were performed according to the rules and regulations of the Institutional Animal Ethics Committee (IAEC).

2.7. Preparation of test solution of compounds

The compounds (dose 50 mg/kg), suspended in 4% gum acacia (gummy exudates from the bark of Acacia senegal, an inactive substance, which forms a mucilage with water) were administrated intraperitoneally, daily once for 5 days from day 10 posttumor inoculation in a volume of 0.1 ml/10 g mouse. The dose of cisplatin selected was 3.5 mg/kg. This was calculated from the human dose using an appropriate conversion factor [25].

3. ANTITUMOR ACTIVITY

3.1. Determination of cytotoxicity of compounds to EAC cells (in vitro studies) Tryphan blue exclusion method (cell viability test)

In vitro short-term cytotoxic activity of drug was determined using EAC cells. The EAC cells that were collected from the animal peritoneum by aspiration were washed repeatedly with phosphate buffered saline (PBS) to free it from blood. The viability of the cells was checked in a haemocytometer. The cells (1×10^6 in 0.1 ml PBS) were incubated in clean sterile tubes with the test compounds (0.01 ml, 1–50 μg/ml in dimethyl sulfoxide (DMSO)) for 3 hours at 37°C, keeping the final volume at 0.9 ml. The volume of DMSO was pegged below 0.1% of the total volume. The control tube had 10 μl of solvent. The final volume was made up to 0.9 ml with PBS. To each tube 100 μl of Tryphan blue solution was added. The live (without stain) and dead (with blue stain) cells were counted using haemocytometer and percent cell death was calculated using the formula:

$$\%\ \text{Cytotoxicity} = 100 \times \left(T_{\text{dead}} - C_{\text{dead}}\right)/T_{\text{tot}}, \quad (1)$$

where T_{dead} is the number of dead cells in the treated group, C_{dead} is that in the control group, and T_{tot} is the total number of dead and live cells in the test compound treated group. Cisplatin was used as the standard [26].

3.2. Induction of Ehrlich Ascites Carcinoma [27]

Antitumor activity of the compounds was determined using Ehrlich ascites carcinoma (EAC) tumor model in mice. Female Swiss Albino mice were divided into groups of 12 animals each. ((a) Normal mice for hematological studies, (b) Tumor-bearing mice, (c) Tumor-bearing mice treated with one dose of cisplatin, (d) Tumor-bearing mice groups

treated with compounds for 5 days.) The ascitic carcinoma-bearing mice (donor) were used for the study, 15 days after tumor transplantation. The ascitic fluid was drawn using an 18-gauge needle into sterile syringe. A small amount was tested for microbial contamination. Tumor viability was determined by Tryphan blue exclusion test and cells were counted using haemocytometer. The ascitic fluid was suitably diluted in normal saline to get a concentration of 10^6 cells/ml of tumor cell suspension. This was injected intraperitoneally to obtain ascitic tumor. The mice were weighed on the day of tumor inoculation and then once in three days thereafter. Treatment was started on the tenth day of tumor inoculation. Cisplatin (one dose) was injected on tenth day intraperitoneally. The compounds were administered from tenth day for 5 days intraperitoneally. After the administration of last dose followed by 18-hour fasting, six mice from each group were sacrificed for the study of antitumor activity and hematological parameters. The remaining animals in each of the groups were kept to check the mean survival time (MST) of the tumor-bearing hosts. Antitumor effects of compounds were assessed by observation of following parameters.

3.3. Percentage increase in weight as compared to day-0 weight

Upon weighing the animal on the day of inoculation and after once in three days in the postinoculation period, the percentage increase in weight was calculated using the formula: % Increase in weight = [(animal weight on respective day/animal weight on day-0) -1] $\times 100$ [28].

3.4. Median survival time and increase in lifespan [% ILS]

Total number of days an animal survived from the day of tumor inoculation was counted. Subsequently, the median and mean survival time were calculated. The percentage increase in lifespan (% ILS) was calculated using the formula: ILS (%) = [(mean survival time of treated group/mean survival time of control group) -1]$\times 100$ [26].

3.5. Hematological parameters [29]

In order to detect the influence of compounds on the hematological status of EAC-bearing mice, comparison was made amongst groups of mice for each compound on the fourteenth day after transplantation. Blood was drawn from each mouse from retro orbital under ether anesthesia and the white blood cell (WBC) total count, differential leukocyte counts, red blood cell (RBC) total count, and hemoglobin content parameters were evaluated.

3.6. Statistical analysis

Results were analyzed by one-way ANOVA by Scheffe's post-hoc test using SPSS computer package.

4. EVALUATION OF ANTIBACTERIAL AND ANTIFUNGAL ACTIVITIES

4.1. Antibacterial activity

Antibacterial activity of test compounds was assessed against *Bacillus cirroflgellosus* by cup-plate method [30].

4.1.1. Materials

(1) Nutrient agar.
(2) Sterilized petridishes and pipettes.
(3) 20–24-hour old subcultures in nutrient agar medium.
(4) Sterilized test tubes containing solution of the test compounds in desired concentration.

4.1.2. Preparation of inoculation medium

The definite volumes of peptone (0.5%), yeast extract (0.15%), beef extract (0.15%), sodium chloride (0.35%), dipotassium phosphate (0.36%), and potassium dihydrogen phosphate (0.13%) were dissolved in distilled water and the *p*H was adjusted to 7.2. This solution was sterilized by autoclaving at 15 p.s.i. for 20 minutes.

4.1.3. Preparation of subcultures

One day prior to these tests, inoculation of above bacterial cultures was made in the inoculation medium as described above and incubated at 37°C for 18–24 hours.

4.1.4. Preparation of base-layer medium

Base-layer medium was prepared by dissolving definite volumes of peptone (0.6%), yeast extract (0.3%), beef extract (0.13%), and agar (2.5%) in distilled water. The *p*H of this medium was also adjusted to 7.2 and sterilized by autoclaving at 15 p.s.i. for 20 minutes.

4.1.5. Preparation of test compounds

Each test compounds (5 mg) was dissolved in dimethylformamide (5 ml) to give a solution of 1000 μg/ml. Out of this 0.1 ml. of solution was used for antimicrobial testing.

4.1.6. Testing method

Base-layer was obtained by pouring about 10–15 ml of base-layer medium into each sterilized petridishes and were allowed to attain room temperature. This solid layer after attaining room temperature is called base-layer. Over-night grown sub-cultures of bacteria were mixed with seed layer medium and immediately poured into petridishes containing the base-layer and then allowed to attain room temperature.

The cups were made by scooping out nutrient agar with a sterile cork borer. To these cups, solutions of test compounds (0.1 ml) were added using sterile pipettes and these plates were subsequently incubated at 37°C for 36 hours. The zone

of inhibitions, if any, was measured in mm for the particular compound. Norfloxacin was used as positive-control and solvent-control was also used to know the activity of the solvent. The results of antibacterial testing are summarized in Table 8.

4.2. Antifungal activity

Fungicidal activity of test compounds was assessed against *Aspergillus niger* and *Candida albicans* by cup-plate method.

4.2.1. Materials

(1) Nutrient agar.
(2) Sterilized Petri dishes and pipettes.
(3) 16–18 hours old sub-cultures in nutrient agar medium supplemented with 1% glucose.
(4) Sterilized test tubes containing solutions of the compounds in desired concentration.

4.2.2. Preparation of inoculation medium

Inoculation medium was prepared by dissolving definite volumes of peptone (1.0%), yeast extract (0.6%), sodium chloride (0.5%), potassium dihydrogen phosphate (0.3%), and glucose (1.0%) in distilled water. The *p*H of the medium was adjusted to 6.0 and sterilized at 15 p.s.i. for 20 minutes.

4.2.3. Preparation of sub-cultures

One day before testing, inoculation of fungi, were made in the inoculation medium and incubated at 37°C for 18–24 hours.

4.2.4. Preparation of base-layer medium

The definite volumes of peptone (4.0%), yeast extract (0.6%), sodium chloride (0.5%), potassium dihydrogen phosphate (0.3%), glucose (1.0%), and agar (2.5 %) were dissolved in distilled water. The *p*H of the medium was adjusted to 6.0 and sterilized by autoclaving at 15 p.s.i. for 20 minutes.

4.2.5. Preparation of seed layer medium

The definite volumes of peptone (4.0%), yeast extract (0.6%), sodium Chloride (0.5%), potassium dihydrogen phosphate (0.3%), glucose (1.0%) and agar (2.5%) were dissolved in distilled water. The *p*H of medium was adjusted to 6.0 and was sterilized separately by autoclaving at 15 p.s.i. for 20 minutes.

4.2.6. Testing method

The method of testing for antifungal activity is the same as that adopted for assessing antibacterial activity. Grisofulvin was used as a positive control and solvent content was also used to know the activity of the solvent. The fungicidal results are summarized in Table 8.

5. RESULT AND DISCUSSION

The ligand was synthesized by acid catalysed condensation of thiocarbohydrazide with the isatin in ethanol (Scheme 1); the condensation proceeds, as usual, selectively on the carbonyl in position 3 in the isatin ring. The ligand is characterized by means of IR, ^{1}H NMR spectroscopy, and elemental analysis. In the ^{1}H NMR spectrum of the ligand there is only one set of signals for the aromatic protons, while the NH of isatin and NH of hydrazone give rise to two different singlets in the 11–14 ppm range. The presence of the NH groups is confirmed in the IR spectra by a broad peak around 3200 cm^{-1}; the C=O groups absorb near 1690 cm^{-1}.

The reactions between the metal(II) chlorides/acetates and the ligand (1:1) lead to formation of complexes, (Scheme 1). The growth of single crystals of these complexes for X-ray studies is very difficult owing to their amorphous nature and we were unsuccessful in our attempts to do so. The elemental analyses of these complexes reveal 1:1 ligands to metal stoichiometry in case of Cu(II) and Ni(II). Copper forms the complexes of the type $[Cu(L)Cl]\cdot 2H_2O$ with Cu(II) chloride and $[Cu(L)OAc]\cdot 2H_2O$ in case of Cu(II) acetate. Nickel forms [Ni(L)Cl] type complex with Ni(II) chloride and [Ni(L)OAc] with acetate. Both cobalt and zinc chloride and acetates form the same complexes with the 2 : 1 ligand to metal stoichiometry, with general formula, $[M(L_2)]$. The complexes are found to be soluble in dimethylformamide, dimethylsulphoxide, and acetonitrile but insoluble in common organic solvents such as ethanol, methanol, benzene, acetone, and so forth. The composition and coordination geometry of these complexes has been established on the following experimental observations. The molar conductance values in dimethylsulphoxide fall in the expected range (10–32 $cm^2\Omega^{-1}mol^{-1}$) of nonelectrolytes [31]. The complexes were analyzed for metal, nitrogen, carbon, hydrogen and chloride. The analytical, conductivity, and magnetic moment data of the complexes are summarized in Table 1.

5.1. Infrared spectral studies

The IR spectral data of the ligand N, N′-*bis*(isatin)thiocarbohydrazone shows a sharp absorption band around 3200 cm^{-1} attributed to the presence of NH group and a very strong band near 1690 cm^{-1} assigned to (C=O) stretching vibration. The band at 1619 cm^{-1} is assigned to the azomethine (C=N) stretching. The Ir spectral assignment of metal complexes was aided by comparison with the vibration frequencies of the free ligand. The broad band that appears in the range of 3160–3210 cm^{-1} is assigned to the stretching vibration of ring (N−H). There is only one band in the ν(C=O) region and it does not differ significantly from the band in the ligand; suggesting that the carbonyl groups are weakly involved in the coordination. Although there is coordination of nitrogen atom of the azomethine group to the central metal atom, we could not appreciably conclude from the Ir data, because of remaining uncoordinated azomethine group that absorbs at a just lower frequency near 1614-1615 cm^{-1} as compared to their ligand [32]. The band corresponding to the stretching vibration of the C=S group appears at 1200–1194 cm^{-1}

Table 1: Elemental analysis, molar conductance, and magnetic moment measurements.

Compounds	Found (Calc.) %					Molar conductance	Magnetic moment BM
	C	H	N	M	CI	$\lambda_m(cm^{-1}\Omega^{-1}mol^{-1})$	
Ligand	55.8(56.1)	2.8(3.2)	23.0(23.1)	—	—	—	—
$[Co(L_2)]$	50.9(51.1)	2.8(2.2)	21.4(20.7)	7.2(7.5)	—	2.1	4.98
[Ni(L)Cl]	43.5(44.7)	2.0(2.4)	17.9(18.4)	12.2(12.8)	7.3(7.7)	3.5	3.55
[Ni(L)OAc]	40.3(41.8)	2.3(2.8)	15.7(16.2)	10.9(11.4)	—	2.6	2.92
$[Cu(L)Cl]\cdot 2H_2O$	39.6(40.8)	2.3(2.8)	16.1(16.8)	11.9(12.7)	6.7(7.1)	2.2	1.91
$[Cu(L)OAc]\cdot 2H_2O$	43.1(43.6)	2.9(3.4)	15.9(16.1)	11.8(12.2)	—	2.8	1.89
$[Zn(L_2)]\cdot 2H_2O$	46.8(47.2)	1.9(2.5)	18.6(19.4)	7.1(7.5)	—	0.7	—

in the ligand [33]. The absence of this band in the Ir spectra of the metal complexes can be explained by the tautomerism of the C=S group with one of the imino groups to form the C−SH and the coordination of sulphur after deprotonation. The band that appears in the range of 690–750 cm^{-1} is thus assigned to the ν (C−S) in the Ir spectra of the metal complexes. The Ir spectra of the complexes derived from copper and nickel acetate, show an absorption bands in the region 1665–1650 cm^{-1} which is assigned to ν_8 (C−O) antisymmtric stretching of acetate group and another in the region 1297–1258 cm^{-1} and which can be assigned to ν_3 (C−O) symmetric stretching vibration of acetate. Difference $\nu_8 - \nu_3$ which is around 407–493 cm^{-1} indicates the unidentate coordination of the acetate group [34]. The complexes show a broad band around 3400 cm^{-1}, which is assigned to the $\nu(H_2O)$ absorption. The ν(M−N) and ν(M−O) stretching vibrations are observed at about 490 and 455 cm^{-1}, respectively, in the spectra of the complexes [35].

5.2. ^{1}H NMR spectral studies

The ^{1}H NMR spectrum of the ligand shows only one set of signals for the aromatic protons around 6.93–7.60 ppm, while the NH of isatin and NH of hydrazone give rise to two different singlets in the 11–14 ppm range.

The ^{1}H NMR spectrum of the Zn(II) complex is less informative, the presence of the hydrazonic proton is confirmed by a peak at about 13 ppm, which is slightly shifted to down field after complexation. Peak due to ring NH and remaining signals of the ligand remain substantially unchanged upon complexation.

5.3. Electronic spectral studies

Electronic spectral data of the ligand and their transition metal complexes were recorded in DMF solutions. In the electronic spectrum of the ligand, three prominent absorption bands at 266, 382, and 670 nm were characterized. The band at 266 nm corresponds to the $\pi \rightarrow \pi^*$ transition of the C=S group [36]. The band at 382 nm corresponds to the transition of azomethine group and the band at 670 nm corresponds to the $n \rightarrow \pi^*$ transition from the amide oxygen of the isatin moiety to the azomethine group [37].

In case of complexes, the bands appeared in the almost same position as they were appeared in ligand. Followed by these, the bands displayed at 485, 485 and 495 nm in case of Cu(II), Ni(II) and Co(II) complexes respectively are assigned to ligand to metal charge transfer transitions (LMCT). Apart from these, the bands around 899, 780 nm in case of Cu(II) and Ni(II) complexes were assigned as d-d transition bands.

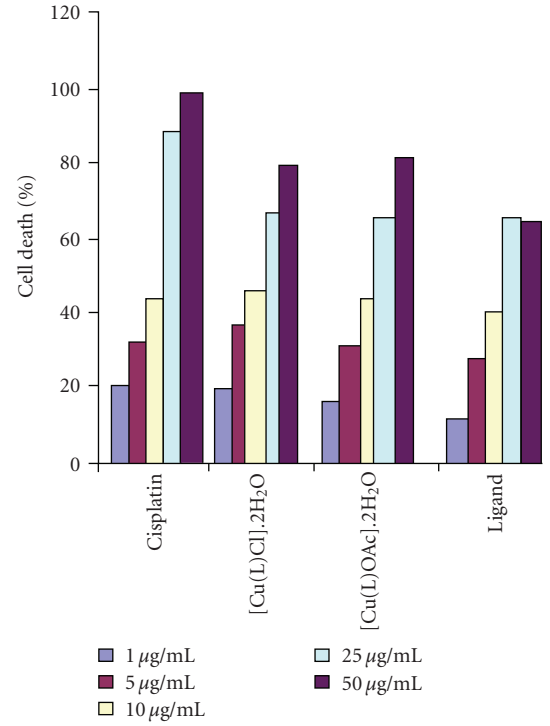

Figure 2: Short-term in vitro cytotoxicity of compounds towards EAC cells.

5.4. Cyclic voltametric studies

The electrochemical behavior of copper(II) complex has been investigated in DMSO containing 0.1 M tetraethyl ammonium chloride supporting electrolyte, using glassy carbon working electrode and Ag/AgCl, Pt electrodes as reference and counter electrodes, respectively. The complex involves single redox step corresponding to Cu(II)→Cu(I), quasireversible electrode process at $Epc = -0.659$ V and the

Table 2: Brine shrimp bioassay results of compounds.

SL. no	Compound	Percentage deaths at 24 hr			LC_{50} mg/ml
		5 mg/ml	10 mg/ml	20 mg/ml	
1	$[Cu(L)Cl]\cdot 2H_2O$	40	72	100	6.17
2	$[Cu(L)OAc]\cdot 2H_2O$	27.27	66.66	100	7.26
3	Ligand	9.1	25	90	11.83

Table 3: Short-term in vitro cytotoxicity of compounds towards EAC cells.

Compounds	Percentage cell-death at different concentrations after 3 hours					$LC_{50}\mu$g/mL
	1 μg/mL	5 μg/mL	10 μg/mL	25 μg/mL	50 μg/mL	
Cisplatin	20	32	44	88	98	6.6377
$[Cu(L)Cl]\cdot 2H_2O$	19	37	46	67	79	11.1475
$[Cu(L)OAc]\cdot 2H_2O$	16	31	43	65	82	10.9732
Ligand	12	28	40	56	64	19.1815

Table 4: Effect of drugs on body weight changes in tumor-induced mice.

Group	Dose (mg/Kg) i.p.	% increase in weight as compared to Day-0 (mean ± SE)				
		Day-3	Day-6	Day-9	Day-12	Day-15
Control	—	4.46 ± 1.98	7.04 ± 2.19	16.13 ± 1.75	17.15 ± 1.89	19.15 ± 2.22
Cisplatin	3.5	4.51 ± 1.15	12.04 ± 1.38	19.16 ± 1.34	9.91 ± 2.12[a]	1.32 ± 4.23[a]
$[Cu(L)Cl]\cdot 2H_2O$	50	5.45 ± 1.25	16.27 ± 3.29	22.13 ± 5.76	15.35 ± 1.88	4.56 ± 2.56[a]
$[Cu(L)OAc]\cdot 2H_2O$	50	5.55 ± 1.83	14.19 ± 2.37	21.09 ± 2.42	15.24 ± 2.65	6.36 ± 2.55[a]
Ligand	50	4.88 ± 2.02	14.33 ± 4.37	24.69 ± 4.99	16.54 ± 2.35	7.76 ± 3.43[a]

[a] $P < .05$ versus Control.

associated anodic peak at $Epa = 0.504$ V [38] suggesting the tetrahedral environment of the copper ion.

5.5. Magnetic measurement studies

The magnetic moments of the complexes were recorded at room temperature and the observed magnetic moment value for the Co(II) complex is 4.98 BM, which is in the range of 4.4 to 5.5 BM observed for the octahedral Co(II) complexes.

The Ni(II) complexes derived from chloride and acetate salts exhibit the magnetic moment values 3.55 and 2.92 BM suggesting tetrahedral environment around metal ion. The value of 1.91 BM for Cu(II) chloride and 1.89 BM for Cu(II) acetate complex suggests the four coordinated tetrahedral complexes, which further supported by their electronic spectral data and CV studies.

5.6. ESR spectral studies

X-band ESR spectra of the polycrystalline Cu(II) complex were recorded at room temperature. The ESR spectra of the mononuclear copper chloride and acetate complexes show a g_{iso} value in the range of 2.066 and 2.092 respectively.

5.7. Antitumor activity of complexes against Ehrlich ascites carcinoma in Swiss Albino mice

5.7.1. Brine shrimp lethality bioassay

The Brine shrimp lethality bioassay has been chosen to assess the in vitro cytotoxic effects of the compounds, as it is an inexpensive, reliable, and quick method for the purpose [24]. All the tested compounds showed considerable cytotoxic activity in the brine shrimp lethality bioassay. LC_{50} concentrations for the compounds are tabulated in Table 2.

5.7.2. Tryphan blue exclusion method (cell viability test)

The compounds were tested using the short-term in vitro cytotoxicity towards EAC cells as a preliminary screening technique of Tryphan blue exclusion method (cell viability test) for their cytotoxic potential [26]. This is one of the methods to assess cytotoxicity of anticancer compounds. This test is based on the principle that living cell membrane has the ability to prevent the entry of dye. Hence, they remain unstained and can be easily distinguished from dead cells, which take the dye. The percentage of viable cells was determined. Results of the short-term in vitro cytotoxicity of the compounds are shown in Table 3. These preliminary experiments

Table 5: Comparative effects of treatments versus cisplatin on reduction of body weights in tumor-induced mice.

Group	Dose (mg/kg) i.p.	% Decrease in weight as compared to respective control (Mean ± SE)	
		Day 12 (Mean ± SE)	Day 15 (Mean ± SE)
Cisplatin	3.5	42.22 ± 11.32	93.10 ± 12.31
$[Cu(L)Cl]\cdot 2H_2O$	50	10.49 ± 9.31	76.19 ± 10.31
$[Cu(L)OAc]\cdot 2H_2O$	50	11.14 ± 6.43	66.79 ± 12.70
Ligand	50	3.56 ± 9.28	59.48 ± 5.68

Table 6: Effect of drugs on the survival time in tumor-induced mice.

Group	Dose (mg/kg)	Median survival time (days)			Mean survival time (days)		
		MST	%T/C	%ILS	(Mean ± SEM)	%T/C	%ILS
Control	—	18.00	—	—	18.33 ± 0.21	—	—
Cisplatin	3.5	34.50	191.67	91.67	34.33 ± 0.33[a]	187.28	87.28
$[Cu(L)Cl]\cdot 2H_2O$	50	26.00	144.44	44.44	26.17 ± 0.31[a]	142.77	42.77
$[Cu(L)OAc]\cdot 2H_2O$	50	25.00	138.88	38.88	24.67 ± 0.21[a]	134.59	34.59
Ligand	50	23.00	127.77	27.77	23.00 ± 0.37[a]	125.48	25.48

[a] $P < .05$ versus control groups, MST = Median Survival Time.

were carried out mainly with five different concentrations of the compounds. All the compounds were found to be cytotoxic and produced 50% cell death at or below a concentration 19.1 μg/ml. At 50 μg/ml concentration, the standard (cisplatin) showed 98% cell death. At 50 μg/ml concentration, the $[Cu(L)OAc]\cdot 2H_2O$, $[Cu(L)Cl]\cdot 2H_2O$ showed more than 80% cell death. All the compounds were found to have considerable cytotoxicity in the cell viability test.

5.7.3. Anticancer studies in Ehrlich Ascites Carcinoma method

Weight variation parameter

The tumor inoculated control animals recorded significant weight gain by day-0. They gained a maximum weight of 19% by day-15. Cisplatin administration (on tenth postinoculation day) significantly ($P < .05$) reduced weight gain as compared to control on day-15. The compounds also significantly ($P < .05$) reduced the weight gain on day-15 as compared to control (Table 4). Comparative effects of treatments versus cisplatin on reduction of body weights in tumor-induced mice are given in Table 5.

Survival time parameter

The effect of compounds on survival of tumor-bearing mice is shown in Table 6. Cisplatin significantly prolonged the median and mean survival times ($P < .05$) with respect to its control. It showed a significant increase in the percentage lifespan of animals (ILS > 50). On the other hand, all the compounds significantly prolonged the mean survival Times. The influence of all the compounds on %ILS was more than 25%. By convention, a 25% increase in lifespan is considered as possible anticancer activity of a test compound [39].

Hematological parameters

The effect of compounds on hematological parameters is shown in Table 7. Tumor induction significantly ($P < .05$) increased the total number of WBC by almost 4 times. Cisplatin administration reversed this effect significantly ($P < .05$). All the compounds significantly ($P < .05$) reversed the tumor-induced rise in total counts of WBC. However, they were not as efficacious as cisplatin in reversing the tumor-induced total counts. On differential counts, tumor-induction caused a significant reduction in lymphocyte and a significant ($P < .05$) increase in neutrophil counts. This was significantly ($P < .05$) reversed towards normal by cisplatin and the test compounds. However, the compounds were less efficacious than cisplatin in their effects. Tumor induction caused significant decrease in RBC and Hb almost to the half of the normal animals [40]. This was significantly ($P < .05$) reversed towards normal by cisplatin and the test compounds.

5.8. Antimicrobial studies

In the light of interesting antimicrobial activities of the coordination complexes, the ligands and their corresponding complexes were screened for antifungal and antibacterial activity against *Aspergillus niger, Candida albicans*, and *Bacillus cirroflagellosus*, respectively, by the cup plate method using Nutrient agar. The radial growth of the colony was recorded on completion of the incubation and the mean diameter for each complex at a single concentration was recorded. The average percentage inhibition of the fungicidal growth medium compared using the Vincent equation [41]: $I = 100(C-T)/C$, where I = percentage inhibition, T = average diameter of the fungal and bacterial growth on the tested plates, and C = average diameter of the growth on the control plates. The screening data of the inhibition of the fungi and bacteria are given in Table 8. From the data, it is clear that the

Table 7: Effect of the compounds on hematological parameters.

Group	Dose (mg/kg)	RBC (Mean ± SE) (Millions/mm^3)	Hb (Mean ± SE) (g%)	WBC (Mean ± SE) (10^3cells/ mm^3)	Differential Leucocyte Count %		
					Lymphocytes	Neutrophils	Monocytes
Normal	—	5.03 ± 0.28	15.72 ± 0.32	8.59 ± 0.16	86.23 ± 0.61	13.03 ± 0.46	1.07 ± 0.33
Control	—	2.14 ± 0.34[a,c]	9.53 ± 0.32[a,c]	32.31 ± 0.67[a,c]	41.80 ± 0.39[a,c]	57.35 ± 0.61[a,c]	1.25 ± 0.43
Cisplatin	3.5	3.26 ± 0.24[a,b]	13.08 ± 0.29[a,b]	10.90 ± 0.19[a,b]	77.97 ± 0.48[a,b]	20.80 ± 0.47[b]	1.22 ± 0.54
$[Cu(L)Cl]\cdot 2H_2O$	50	3.84 ± 0.51[a,b,c]	11.71 ± 0.29[a,b,c]	17.84 ± 0.31[a,b,c]	68.97 ± 0.20[a,b,c]	29.72 ± 0.22[a,b]	1.32 ± 0.31
$[Cu(L)OAc]\cdot 2H_2O$	50	4.49 ± 0.30[a,b,c]	12.79 ± 0.17[a,b,c]	19.27 ± 0.99[a,b,c]	68.10 ± 0.45[a,b,c]	30.55 ± 0.47[a,b]	1.35 ± 0.43
Ligand	50	4.72 ± 0.11[a,b,c]	11.92 ± 0.15[a,b,c]	22.33 ± 0.93[a,b,c]	62.78 ± 0.27[a,b,c]	35.92 ± 0.28[a,b,c]	1.30 ± 0.63

[a] $P < .05$ versus normal.
[b] $P < .05$ versus control mice.
[c] $P < .05$ versus cisplatin.

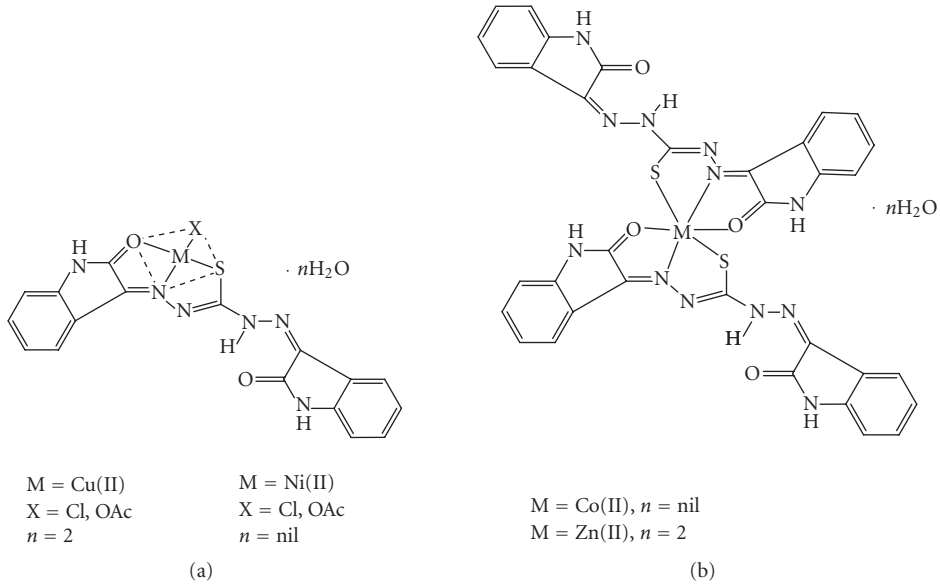

Figure 3: Proposed structures of the complexes.

free ligand N, N′-*bis*(isatin)thiocarbohydrazone is moderately active against *B. cirroflagellosus* where as highly active against fungi *A. niger* and *C. albicans*. On complexation, there is a notable enhancement of both antibacterial as well as antifungal activity. The promising results were observed for the Co(II) complex against both the fungi. The higher fungi toxicity exhibited by the complexes may be ascribed to the fact that the metal complexes are more susceptible to fungal cells than bacterial cells.

6. CONCLUSION

From the elemental analysis, molar conductivity, UV-Visible, magnetic, IR and ^{1}H NMR spectral data it was possible to determine the type of coordination of the ligand in their metal complexes. In all the complexes, only one part of the ligand is coordinated to the metal ion resulting mononuclear complexes. The ligand coordinates essentially through the carbonyl oxygen of the isatin fragment, the nitrogen atom of the azomethine group and sulfur atom after deprotonation to give five membered rings. The ligand acts as a monobasic, tridentate (Figure 3).

The compounds showed considerable cytotoxic activity in the trypan blue exclusion method. In the in vivo cancer model (Ehrlich ascitic carcinoma model), the compounds significantly ($P < .05$) reversed the tumor-induced changes in the parameters monitored viz., percentage increase in body weight, percentage increase in lifespan, tumor-viable count, and hematological parameters (total and DLC of WBC, total RBC, and Hemoglobin count). These effects were almost comparable to cisplatin—the standard drug used in the study. The compounds, however, were found to have good effect in prolonging the lifespan (ILS) as compared to standard drug cisplatin. These findings imply that the compounds might be having some anticancer principles.

Based on the data of the present study, it is very difficult to suggest the possible mechanism of these compounds for anticancer effects. The compounds tested in our present study have shown promising cytotoxic activity when screened using the in vitro method and at the same time were

Table 8: Antimicrobial screening data of ligands and their complexes.

Compound	Representation zone of inhibition		
	Antibacterial	Antifungal	
	B.c	A.n	C.a
ligand	+	++	++
$[Cu(L)Cl]\cdot 2H_2O$	++	++	++
$[Cu(L)OAc]\cdot 2H_2O$	+	++	++
[Ni(L)Cl]	−	+++	++
[Ni(L)OAc]	++	++	++
$[Co(L_2)]$	++	+++	+++
$[Zn(L_2)]\cdot 2H_2O$	+	++	++

Bacillus Cirroflagellosus = B.c.
Aspergillus niger = A.n.
Candida albican = C.a.
10 mm = − (inactive).
10–20 mm = + (weakly active).
21–25 mm = ++ (moderatively active).
26–35 mm = +++ (highly active).
36–40 mm = ++++ (most active).
DMF = 12 mm.
Norfloxacin = 29 P.a and 31 B.c;
Grisofulvin = 20 A.n and 23 C.a.
Index
(1) Concentration of the compound: 1 mg/ml in dimethyl formamide.
(2) Quantity in each cup: 0.1 ml.
(3) Diameter of the cup: 10 mm.
(4) Control of the antibacterial activity: Norfloxaicn.
(5) Control of the antifungal activity: Grisofulvin.
(6) Solvent used: Dimethyl formamide.

shown to have good activity when tested using the Ehrlich ascites carcinoma model. Though it is very difficult to conclude anything at this stage, it can be assumed that after testing against various other cancer models and at different doses these compounds may prove to be safer drugs for tomorrow.

Further, the promising results were observed for the antimicrobial screening especially for the Co(II) complex against both the fungi and what may be attributed to the fact that the metal complexes are potentially active against fungal cells than bacterial cells.

ACKNOWLEDGMENTS

The authors thank the Department of Chemistry and USIC, Karnatak University, Dharwad, for providing research and spectral facilities. For CHNS analysis and recording ESR spectra, STIC, Cochin University and IIT Mumbai are gratefully acknowledged. The authors thank Department of Pharmacology, Manipal College of Pharmaceutical Sciences, MAHE, Manipal, for extending facilities to carry out the antitumor activity. One of the authors, M.P. Sathisha, thanks the Karnatak University, Dharwad, for providing a research fellowship.

REFERENCES

[1] M. A. Ali and S. E. Livingstone, "Metal complexes of sulphur-nitrogen chelating agents," *Coordination Chemistry Reviews*, vol. 13, no. 2-3, pp. 101–132, 1974.

[2] H. Stunzi, "Can chelationbe important in the antiviral activity of isatin β-thiosemicarbazones?" *Australian Journal of Chemistry*, vol. 35, no. 6, pp. 1145–1155,1982.

[3] M. J. M. Campbell, "Transition metal complexes of thiosemicarbazide and thiosemicarbazones," *Coordination Chemistry Reviews*, vol. 15, no. 2-3, pp. 279–319, 1975.

[4] S. B. Padhyé and G. B. Kauffman, "Transition metal complexes of semicarbazones and thiosemicarbazones," *Coordination Chemistry Reviews*, vol. 63, pp. 127–160, 1985.

[5] A. A. A. Emara, S. M. E. Khalil, and K. A. R. Salib, "Di-, tri- and poly-nuclear transition metal complexes of 3,4-diacetyl-2,5-hexanedione," *Journal of Coordination Chemistry*, vol. 36, no. 4, pp. 289–301, 1995.

[6] H. Cheng, D. Chun-Ying, F. Chen-Jie, L. Yong-Jiang, and M. Qing-Jin, "Self-assembled macrocyclic tetranuclear molecular square $[Ni(HL)]_4^{4+}$ and molecular rectangle $[Cu_2Cl_2L]_2$ H_2L = bis[phenyl(2-pyridyl)methanone] thiocarbazone," *Journal of the Chemical Society, Dalton Transactions*, no. 7, pp. 1207–1212, 2000.

[7] B. Rosenberg, "Some biological effects of platinum compounds: new agents for the control of tumours," *Platinum Metals Review*, vol. 15, no. 2, pp. 42–51, 1971.

[8] D. R. Williams, "Metals, ligands, and cancer," *Chemical Reviews*, vol. 72, no. 3, pp. 203–213, 1972.

[9] B. G. Patil, B. R. Havinale, J. M. Shallom, and M. P. Chitnis, "Syntheses and spectroscopic studies of potential antitumor copper(II) complexes with 5-phenylazo-3-methoxy salicylidene thiosemicarbazone and N^4 substituted thiosemicarbazones," *Journal of Inorganic Biochemistry*, vol. 36, no. 2, pp. 107–113, 1989.

[10] D. L. Klayman, J. P. Scovill, J. F. Bartosevich, and J. Bruce, "2-Acetylpyridine thiosemicarbazones. 5. 1-[1-(2-Pyridyl)ethyl]-3-thiosemicarbazides as potential antimalarial agents," *Journal of Medicinal Chemistry*, vol. 26, no. 1, pp. 35–39, 1983.

[11] A. M. Elsome, J. M. T. Hamilton-Miller, W. Brumfitt, and W. C. Noble, "Antimicrobial activities in vitro and in vivo of transition element complexes containing gold(I) and osmium(VI)," *Journal of Antimicrobial Chemotherapy*, vol. 37, no. 5, pp. 911–918, 1996.

[12] A. Scozzafava, L. Menabuoni, F. Mincione, G. Mincione, and C. T. Supuran, "Carbonic anhydrase inhibitors: synthesis of sulfonamides incorporating dtpa tails and of their zinc complexes with powerful topical antiglaucoma properties," *Bioorganic and Medicinal Chemistry Letters*, vol. 11, no. 4, pp. 575–582, 2001.

[13] C. Walsh, "Enabling the chemistry of life," *Nature*, vol. 409, no. 6817, pp. 226–231, 2001.

[14] S. Kirschner, Y.-K. Wei, D. Francis, and J. Bergman, "Anticancer and potential antiviral activity of complex inorganic compounds," *Journal of Medicinal Chemistry*, vol. 9, no. 3, pp. 369–372, 1966.

[15] W. Beerheide, M. M. Sim, Y.-J. Tan, H.-U. Bernard, and A. E. Ting, "Inactivation of the human papillomavirus-16 e6 oncoprotein by organic disulfides," *Bioorganic and Medicinal Chemistry*, vol. 8, no. 11, pp. 2549–2560, 2000.

[16] Z. H. Chohan, A. Scozzafava, and C. T. Supuran, "Unsymmetrical 1,1′-disubstituted ferrocenes: synthesis of Co(ii), Cu(ii), Ni(ii) and Zn(ii) chelates of ferrocenyl -1-thiadiazolo-1′-tetrazole, -1-thiadiazolo-1′-triazole and -1-tetrazolo-1′-triazole with antimicrobial properties," *Journal of Enzyme Inhibition and Medicinal Chemistry*, vol. 17, no. 4, pp. 261–266, 2002.

[17] M. Ul-Hassan, Z. H. Chohan, A. Scozzafava, and C. T. Supuran, "Carbonic anhydrase inhibitors: schiff's bases of aromatic

and heterocyclic sulfonamides and their metal complexes," *Journal of Enzyme Inhibition and Medicinal Chemistry*, vol. 19, no. 3, pp. 263–267, 2004.

[18] M. Ul-Hassan, Z. H. Chohan, and C. T. Supuran, "Antibacterial Zn(II) compounds of Schiff bases derived from some benzothiazoles," *Main Group Metal Chemistry*, vol. 25, no. 5, pp. 291–296, 2002.

[19] Z. H. Chohan, A. Scozzafava, and C. T. Supuran, "Zinc complexes of benzothiazole-derived Schiff bases with antibacterial activity," *Journal of Enzyme Inhibition and Medicinal Chemistry*, vol. 18, no. 3, pp. 259–263, 2003.

[20] F. Maggio, A. Pellerito, L. Pellerito, S. Grimaudo, C. Mansueto, and R. Vitturi, "Organometallic complexes with biological molecules II. Synthesis, solid-state characterization and in vivo cytotoxicity of diorganotin(IV)chloro and triorganotin(IV)chloro derivatives of penicillin G," *Applied Organometallic Chemistry*, vol. 8, no. 1, pp. 71–85, 1994.

[21] V. A. Narayanan, M. Nasr, and K. D. Paull, in *Tin Based Antitumour Drugs*, vol. H 37 of *NATO ASI Series*, Springer, Berlin, Germany, 1990.

[22] Z. H. Chohan, M. Arif, M. A. Akhtar, and C. T. Supuran, "Metal-based antibacterial and antifungal agents: synthesis, characterization, and in vitro biological evaluation of Co(II), Cu(II), Ni(II), and Zn(II) complexes with amino acid-derived compounds," *Bioinorganic Chemistry and Applications*, vol. 2006, Article ID 83131, 13 pages, 2006.

[23] L. F. Audrieth, E. S. Scott, and P. S. Kippur, "Hydrazine derivatives of the carbonic and thiocarbonic acids. I. The preparation and properties of thiocarbohydrazide," *Journal of Organic Chemistry*, vol. 19, no. 5, pp. 733–741, 1954.

[24] B. N. Mayer, N. R. Ferrigni, J. E. Putnam, L. B. Jacobsen, D. E. Nichols, and J. L. McLaughlin, "Brine shrimp: a convenient general bioassay for active plants constituents," *Planta Medica*, vol. 45, pp. 31–34, 1982.

[25] M. N. Ghosh, *Fundamentals of Experimental Pharmacology*, Scientific Book Agency, Calcutta, India, 2nd edition, 1984.

[26] P. U. Devi, F. E. Solomon, and A. C. Sharada, "In vivo tumor inhibitory and radiosensitizing effects of an Indian medicinal plant, Plumbago rosea on experimental mouse tumors," *Indian Journal of Experimental Biology*, vol. 32, no. 8, pp. 523–528, 1994.

[27] P. U. Devi, B. S. S. Rao, and F. E. Solomon, "Effect of plumbagin on the radiation induced cytogenetic and cell cycle changes in mouse Ehrlich ascites carcinoma in vivo," *Indian Journal of Experimental Biology*, vol. 36, no. 9, pp. 891–895, 1998.

[28] A. E. Eckhardt, B. N. Malone, and I. J. Goldstein, "Inhibition of Ehrlich ascites tumor cell growth by *Griffonia simplicifolia I* lectin in vivo," *Cancer Research*, vol. 42, no. 8, pp. 2977–2979, 1982.

[29] F. E. D'Amour, F. R. Blood, and D. A. Belden Jr., *Manual for Laboratory Work in Mammalian Physiology*, The University of Chicago Press, Chicago, Tex, USA, 3rd edition, 1965.

[30] H. W. Seeley and P. J. van Demark, *Microbs in Action: A laboratory Manual of Microbiology*, D. B. Taraporevala Sons & Co. Pvt., Bombay, India, 2nd edition, 1975.

[31] W. J. Geary, "The use of conductivity measurements in organic solvents for the characterisation of coordination compounds," *Coordination Chemistry Reviews*, vol. 7, no. 1, pp. 81–122, 1971.

[32] K. Nakomoto, *Infrared Spectra of Inorganic and Coordination Compounds*, Wiley-Interscience, New York, NY, USA, 2nd edition, 1970.

[33] P. Bindu, M. R. Kurup, and T. R. Satyakeerty, "Epr, cyclic voltammetric and biological activities of copper(II) complexes of salicylaldehyde N(4)-substituted thiosemicarbazone and heterocyclic bases," *Polyhedron*, vol. 18, no. 3-4, pp. 321–331, 1998.

[34] N. W. Alcock, V. M. Tracy, and T. C. Waddington, "Acetates and acetato-complexes—part 2: spectroscopic studies," *Journal of Chemical Society, Dalton Transactions*, no. 21, pp. 2243–2246, 1979.

[35] W. E. Estes, J. R. Wasson, J. W. Hall, and W. E. Hatfield, "Characterization of some mixed-halide copper(II) dimers of the general formula $[Cu_2X_nX'_{6-n}]^{2-}$ ($X = Cl^-$ and $X' = Br^-$): evidence for the preference of chloride bridges in the mixed-halide species," *Inorganic Chemistry*, vol. 17, no. 12, pp. 3657–3664, 1978.

[36] K. Balakrishnan and K. K. Aravindakshan, "Metal complexes of 3,4-dimethoxybenzaldehyde thiosemicarbazone," *Journal of the Indian Chemical Society*, vol. 68, no. 4, pp. 187–190, 1991.

[37] A. B. P. Lever, *Inorganic Electronic Spectroscopy*, Elsevier, Amsterdam, The Netherlands, 1984.

[38] Z. Shirin and R. N. Mukherj, "Synthesis, spectra and electrochemistry of ruthenium(III) complexes with cage-like Schiff-base ligands," *Polyhedron*, vol. 11, no. 20, pp. 2625–2630, 1992.

[39] R. I. Geran, N. H. Greenberg, M. M. MacDonald, A. M. Schumacher, and B. J. Abbott, "Protocols for screening chemical agents and natural products against animal tumors and other biological systems," *Cancer Chemotherapy Reports*, vol. 3, p. 1, 1972.

[40] C. Orberlling and M. Guerin, "The role of virus in the production of cancer," *Advances in Cancer Research*, vol. 2, pp. 353–423, 1954.

[41] J. M. Vincent, "Distortion of fungal hyphae in the presence of certain inhibitors," *Nature*, vol. 159, p. 850, 1947.

Hindawi Publishing Corporation
Metal-Based Drugs
Volume 2008, Article ID 745989, 9 pages
doi:10.1155/2008/745989

Research Article

Kinetic and High-Pressure Mechanistic Investigation of the Aqua Substitution in the *Trans*-Aquaoxotetracyano Complexes of Re(V) and Tc(V): Some Implications for Nuclear Medicine

J. Mattheus Botha[1,2] and Andreas Roodt[1]

[1] *Department of Chemistry, University of the Orange Free State, P.O. Box 339, Bloemfontein 9300, South Africa*
[2] *Sasol Technology R & D, P.O. Box 1, Sasolburg 1947, South Africa*

Correspondence should be addressed to Andreas Roodt, roodta.sci@ufs.ac.za

Received 16 August 2007; Accepted 8 December 2007

Recommended by Jannie Swarts

A kinetic study of the aqua substitution in the $[TcO(OH_2)(CN)_4]^-$ complex by different thiourea ligands (TU = thiourea, NMTU = *N*-methyl thiourea, NNDMTU = *N*,*N*′-dimethylthiourea) yielded second-order formation rate constants (25°C) as follows [NNDMTU, NMTU, TU, respectively]: k_f = 11.5 ± 0.1, 11.38 ± 0.04, and 7.4 ± 0.1 $M^{-1}s^{-1}$, with activation parameters: $\Delta H^{\#}_{k_f}$: 55 ± 2, 42 ± 3, 35 ± 5 kJ mol^{-1}; $\Delta S^{\#}_{k_f}$: −40 ± 8, −84 ± 11, −110 ± 17 J $K^{-1}mol^{-1}$. A subsequent high-pressure investigation of the aqua substitution in the $[ReO(OH_2)(CN)_4]^-$ and $[TcO(OH_2)(CN_4)]^-$ complexes by selected entering ligands yielded $\Delta V^{\#}_{k_f}$ values as follows: Re(V): −1.7 ± 0.3(NCS^-), −22.1 ± 0.9 (TU) and for Tc(V): −3.5 ± 0.3(NCS^-), −14 ± 1 (NNDMTU), and −6.0 ± 0.5 (TU) cm^3mol^{-1}, respectively. These results point to an interchange associative mechanism for the negative NCS^- as entering group but even a pure associative mechanism for the neutral thiourea ligands.

1. INTRODUCTION

Technetium-99m is widely used in over 90% of all current diagnostic nuclear medicinal applications [1–5] due to its favourable nuclear properties ($t_{1/2}$ = 6.02 hours, y = 140 keV 100%) and availability from a generator. It is routinely used for brain, heart, liver, kidney, and bone imaging. Technetium's third-row congener and 5d analog, rhenium, also has applications in nuclear medicine since its two radioactive isotopes, Re-186 and Re-188, have nuclear properties suitable for radiotherapeutic applications [6–8].

The development of technetium myocardial imaging agents commenced with work by Deutsch [9–12], who investigated the $[^{99m}TcCl_2(dmpe)_2]^+$ [dmpe = bis(1,2-dimethylphosphino)ethane] and $[^{99m}TcX_2(diars)_2]^+$ complexes (diars = *o*-phenylenebis(dimethylarsine), X = Cl, Br) [12]. Studies on animal models indicated that the reduction of Tc^{III} is biologically accessible for the cationic $[^{99m}Tc^{III}–Cl_2(dmpe)_2]^+$ complex, yielding neutral $[^{99m}Tc^{II}Cl_2(dmpe)_2]$. The latter then washes from the heart and becomes trapped in the liver. The reduction of Re^{III} to Re^{II} $[^{186}Re^{III}–Cl_2(dmpe)_2]^+$ is 0.2 V more negative compared to the analogous Tc complex and is thus retained in the heart [10]. Kinetic, electrochemical, and structural work on the $[Re/Tc^{II}Cl_2(dmpe)_2]$ complexes has been published and illustrates its importance as initial models [13–18].

Currently, however, other monocationic complexes of technetium-99m are of significant interest because of their extensive use as ^{99m}Tc myocardial imaging agents [19, 20] with examples including *Cardiolite* or $[^{99m}Tc(MIBI)_6]^+$ (MIBI = 2-methoxy-2-methylpropylisocyanide) [21, 22] and *Myoview* $[^{99m}TcO_2(Tetrofosmin)_2]^+$. While the monocationic complexes are traditionally based on the $[O=Tc^{V}=O]^+$, $[Cl–Tc^{III}–Cl]^+$, and Tc^{I} cores, a new class of myocardial imaging agents feature the $[^{99m}Tc^{V}\equiv N]^{2+}$ core, an example being the Tc–N–NOET complex (*bis*(*N*-methoxy-*N*-methyldithiocarbamato)nitridotechnetium(V)).

Two technetium complexes, containing specifically *phosphine* ligands, currently used for myocardial imaging are the above-mentioned *Myoview* and *TechneScan Q12/TechneCard*

($[^{99m}Tc(PR_3)_2(L')]^+$) [23]. In $[^{99m}TcO_2(Tetrofosmin)_2]^+$ the technetium is in a high-oxidation state {Tc(V)} and shows substantial myocardial uptake [24]. It is interesting to note that $[^{99m}TcO_2(dmpe)_2]^+$, which has methyl groups on the phosphine rather than the ether groups as in the tetrofosmin ligand, is not retained in the myocardium [25].

With the ongoing development of new Tc and Re agents, it is essential that their basic coordination chemistry is understood. Nonradioactive rhenium is widely utilized to imitate technetium chemistry on a macroscale and has been extensively pursued for the past two decades or more, describing changes in coordination modes. We reported structural effects induced by different Re-cores while maintaining an equatorial ligand set, utilizing two dmpe ligands, while varying the axial core, to investigate the impact this change induces on the solid-state structure of the coordinated polyhedron and on the bidentate tertiary phosphine ligand, dmpe [26]. Similarly, the effect of different conformers/isomers and energies associated therewith has been described [27]. More recent extensive work by Alberto showed that the *fac*-$[(CO)_3M(H_2O)_3]^+$ {M = Re(I), Tc(I)} core provides excellent access to numbers of model radiopharmaceuticals [28–35].

The "lanthanide contraction" results in similar physical characteristics for analogous Re and Tc complexes (i.e., size or lipophilicity) [1, 6]. Thus, when rhenium is used as the nonradioactive surrogate for the development of Tc chemistry because it is nonradioactive, their similar physical characteristics make it very difficult for biological systems to distinguish between analogous Tc and Re [6] complexes based on properties such as size, shape, and charge. However, firstly, they differ significantly in their redox properties, which can result in different in vivo handling of analogous complexes. Rhenium complexes are more stable in higher-oxidation states and thus are more difficult to reduce (by ca. 200 mV) than their Tc analogs [36]. Thus, Re is more readily reoxidized to perrhenate (ReO_4^-) than Tc is to pertechnetate (TcO_4^-) in vivo, and perrhenate requires the use of stronger reducing agents for the synthesis of Re radiopharmaceuticals.

A second difference is the larger ligand field splitting for Re complexes, which results in slower-ligand substitution onto Re than Tc. We have previously investigated different aspects of the *trans*-dioxo complexes, with the general structure of *trans*-$[MO_2(L_4)]^{n-}$, M = Mo(IV), W(IV), Tc(V), Re(V), Os(VI), and related systems, evaluating structural and reactivity correlations for a range of ligands L. It was shown that a twelve-order of magnitude in reactivity in these systems exists, ranging from the very rapid proton exchange, to the slower hydroxo and aqua substitution and the extremely slow-equatorial ligand substitution [37–41].

Subsequent kinetic studies on the $[ReO(OH_2)(TU)_4]^{3+}$ complex, showed that the *trans*-substitution reactions of the aqua ligand most likely proceed via an interchange dissociative mechanism (I_d) [42]. This outlined a discrepancy in the proposed mechanism for *trans*-substitution reactions on the $[ReO(OH_2)(CN)_4)^-$ complex as concluded earlier in the literature [43, 44]. The substitution rate for the $[ReO(OH_2)(TU)_4]^{3+}$ complex with NCS^- was in the order of ca. 450 000 times faster than for the $[ReO(OH_2)(CN)_4]^-$ complex. Furthermore, the reactions involving $[ReO(OH_2)(TU)_4]^{3+}$ and higher concentrations of the entering ligand showed typical limiting kinetics, while in the $[ReO(OH_2)(CN)_4]^-$ complex, no tendency of limiting kinetics was observed.

We have previously correlated different in vivo reactivities with in vitro behaviour [41] and attempted to link certain sites with biodistribution and bioactivity, but was, and still is, unable to do more detailed comparisons. Thus, since detailed mechanistic studies and data on substitution processes are fairly limited, it prompted us to reinvestigate the type of mechanism obeyed for the $[ReO(OH_2)(CN)_4]^-$ complex when reacted with different entering ligands and extending it to the Tc^V complex, by specifically utilizing advanced high-pressure kinetics. This high-pressure study of the $[MO(OH_2)(CN)_4]^-$ complex (M = Re and Tc), with different entering ligands, is therefore reported here.

2. MATERIAL AND METHODS

All reagents and chemicals were of analytical reagent grade, and double-distilled water was used in all experiments. All pH measurements were done with an Orion 701 pH meter and a combined glass/calomel electrode using standard buffer solutions and standardized hydrochloric acid solutions for calibration. The ionic strength was constant (μ = 1 M) in all the experiments, maintained with $NaNO_3$ as noncoordinating electrolyte. In all calculations, pH = $-\log [H^+]$. $Na_3[ReO_2(CN)_4]$ and $Na_3[TcO_2(CN)_4]$ were prepared as previously described [37]. *Caution:* Technetium-99, although a low-energetic radio-active β-emitter (230 KeV, $t_{1/2} = 2.1 \times 10^5 y$), should always be handled with care and under approved conditions.

Kinetic measurements were done on modified Durrum-Gibson Model D110 and Applied Photophysics SX.18 MV (control experiments; coupled with a J&M Tidas-16 diode array) stopped flow spectrophotometers equipped with constant temperature syringe and cell holder systems (accurate within 0.1°C). These were coupled to a personal computer or Acorn Risc workstation capable of performing least-squares analyses on the absorption values versus time data obtained from the kinetic runs. The SCIENTIST [45] program was used to fit the data to selected functions. High-pressure studies were done on a GBC 916 spectrophotometer in a high-pressure vessel with pill box cells of path length ≈15 mm or in a stopped flow high-pressure vessel [46]. All kinetic runs were performed under pseudo-first-order conditions with the ligand in large excess. The solid lines in the figures represent computer least-squares fits of data, while the experimentally determined values are given as points. The $[MO(L)(CN)_4]^{n+}$ complexes from the reactions between $[MO(OH_2)(CN)_4]^-$ and different entering ligands were characterised as previously described [43, 44].

3. RESULTS AND DISCUSSION

It was previously shown that the complete reaction scheme governing the substitution reactions on the protonated forms of the *trans*-$[MO_2(CN)_4]^{(n+2)^-}$ complexes is limited to the

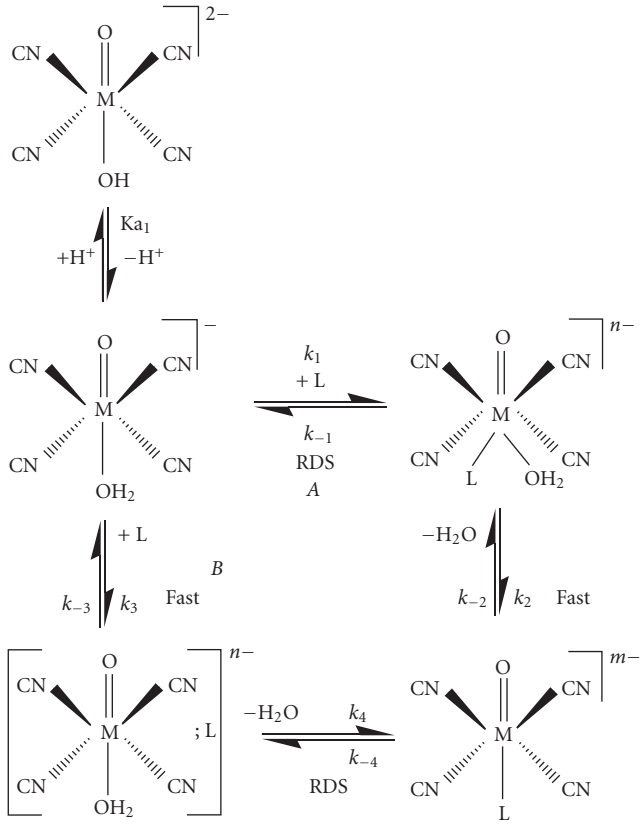

Scheme 1: Illustration of an associative (A; k_1/k_2) or associative interchange (B; k_3/k_4). Activation for the aqua substitution in $[MO(OH_2)(CN)_4]^-$[M = Re(V), Tc(V)]; RDS = rate determining step.

aqua species, *trans*-$[MO(OH_2)(CN)_4]^{n-}$ and with small contributions, under selected conditions from *trans*-$[MO(OH)(CN)_4]^{(n+1)-}$ [37]. Assumptions made and approximations have all been reported previously.

The pK_{a_1} value (of the $[TcO(OH_2)(CN)_4]^-$ complex, Scheme 1) was previously determined from the reaction between $[TcO(OH_2)(CN)_4]^-$ and NCS^- ions as 2.90(5) by Roodt et al. [44]. To further verify this by another ligand system, an independent kinetic pK_a determination was carried out for the reaction between $[TcO(OH_2)(CN)_4]^-$ and NNDMTU and is illustrated in Figure 1. NNDMTU was selected since these reactions showed the largest absorbance changes.

The general expression for the observed pseudo-first-order rate constant {[L] ≫ [M]} shown in (1), as obtained previously, describes the acid-base behaviour of the *trans*-$[MO(OH_2)(CN)_4]^{n-}$ complexes, where k_f and k_r represent the forward and reverse rate constants, that is, the anation/ligation and acid hydrolysis, respectively.

$$k_{\text{obsd}} = \frac{k_f[\text{L}]}{1 + K_{a_1}/[\text{H}^+]} = k_r. \tag{1}$$

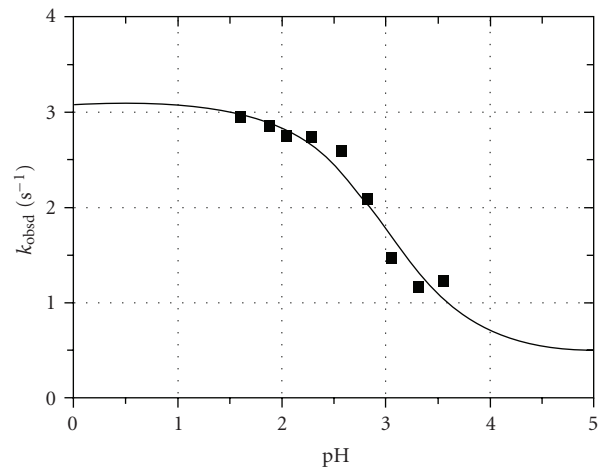

Figure 1: Plot of k_{obsd} *versus* pH for the reaction between $[TcO(OH_2)(CN)_4]^-$ and NNDMTU at 24.8°C, μ = 1.0 M ($NaNO_3$), [NNDMTU] = 0.3 M, and [M] = 5×10^{-5} M, λ = 420 nm.

The data in Figure 1 was fitted to (1), and a pK_{a_1} value as reported in Table 1 was obtained. The acid dissociation constant thus determined from the reaction between $[TcO(OH_2)(CN)_4]^-$ and NNDMTU {2.99 ± 0.19} is in good agreement with the pK_a value reported for the reaction between the metal complex and NCS^- ions (2.90 ± 0.05) [44].

It is therefore evident that if the reaction between $[TcO(OH_2)(CN)_4]^-$ and the different entering ligands (TU, NMTU, NNDMTU) is investigated at a pH value of 0.6 [pK_{a_1} > 2.9, see Table 1], the *trans*-oxo aqua species of the metal complex is more than 99% present in solution. At these high-acidic conditions where $K_{a_1} \ll [H^+]$, (1) simplifies to the well-known simple expression in (2), assuming negligible reverse or concurrent reactions (k_r ca. 0). The k_{obsd} versus [L] data obtained from these runs was fitted to (2), and values for k_f and k_r were consequently obtained (Table 1):

$$k_{\text{obsd}} = k_f[\text{L}] + k_r \approx k_f[\text{L}]. \tag{2}$$

The ligand concentration and temperature dependence study for each of the different thiourea entering ligands (TU, NMTU, and NNDMTU) were therefore completed for the $[TcO(OH_2)(CN)_4]^-$, with the data for NMTU as entering ligand shown in Figure 2.

These k_f versus temperature data sets were used in the Eyring equation [43] to calculate the activation parameters governing the k_f step (Table 1). The intercepts (k_r) in all these runs were zero within standard deviations, thus confirming a large K_f value ($K_f = k_f/k_r$) for each of the different nucleophiles.

The activation entropies (Table 1) for all the reactions studied suggest increased order in the transition state, indicative of association being important.

Following similar arguments used by Grundler et al. [35], and by our group [47], different pathways for the substitution process were therefore considered.

Table 1: Kinetic data for the reaction between $[TcO(OH_2)(CN)_4]^-$ and the different thiourea entering ligands; μ = 1.0 M ($NaNO_3$), pH = 0.6. [(a)]L.S. fits to (2); [(b)]since small-negative intercepts were obtained in some cases, the value was fixed (= 0.00). The standard deviations reported are those from the first fits; [(c)]L.S. fits to (1).

Parameter	T (°C)	NNDMTU	T (°C)	NMTU	T (°C)	TU
k_f ($M^{-1}s^{-1}$)[(a)]	9.3	3.13(6)	5.7	3.26(7)	6.8	2.68(8)
	16.5	6.1(1)	15.9	5.95(6)	15.8	5.0(1)
	25.1	11.5(1)	25.1	11.38(4)	25.5	7.4(1)
k_r (s^{-1})[(a), (b)]	9.3	0.00(1)	5.7	0.00(3)	6.8	0.00(2)
	16.5	0.00(4)	15.9	0.00(5)	15.8	0.00(3)
	25.1	0.00(3)	25.1	0.00(2)	25.5	0.06(2)
pK_{a_1}[(c)]	24.8	2.99(19)	—	—	—	—
$\Delta S^{\#}_{k_f}$ (J K^{-1} mol^{-1})	—	−40(8)	—	−84(11)	—	−110(17)
$\Delta H^{\#}_{k_f}$ (kJ mol^{-1})	—	55(2)	—	42(3)	—	35(5)

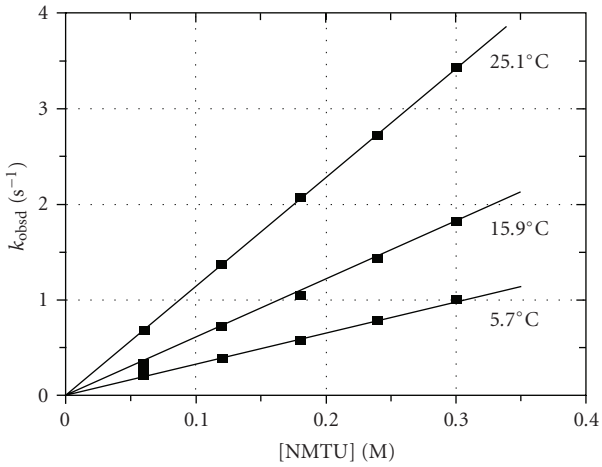

Figure 2: Effect of k_{obsd} versus [NMTU] for the reaction between $[TcO(OH_2)(CN)_4]^-$ and NMTU at different temperatures, μ = 1.0 M ($NaNO_3$), λ = 420 nm, pH = 0.6, and [M] = 5×10^{-5} M.

Firstly, for an *associative* mechanism (Scheme 1, A, k_1 and k_2 pathway), the rate of the reaction is given by

$$\text{Rate} = k_2[MO(OH_2)(L)(CN)_4{}^{n-}] - k_{-2}[MO(L)(CN)_4{}^{m-}]. \quad (3)$$

If it is assumed that the $[MO(OH_2)(L)(CN)_4]^n$ complex is formed under steady-state conditions, its formation and decomposition would be equal yielding

$$[MO(OH_2)(L)(CN)_4{}^{n-}] = \frac{k_1[MO(OH_2)(CN)_4{}^-][L] + k_{-2}[MO(L)(CN)_4{}^{m-}]}{k_{-1} + k_2}. \quad (4)$$

Upon incorporation of the definition of K_{a_1} (= $[MO(OH)(CN)_4{}^{2-}][H^+]/[MO(OH_2)(CN_4{}^-)]$), $[M]_{tot}$ (= $[MO(OH_2)(CN)_4{}^-] + [MO(OH)(CN)_4{}^{2-}]$) and substituting (4) into (3), integration of the rate law {$[L] \gg [M]$}, by assuming a fast k_2 step (Scheme 1), 5 {with $k_2{}' = k_1k_2/(k_{-1} + k_2)$}, and defining the pseudo-first-order rate constant, is obtained:

$$k_{obsd} = \frac{k_2{}'[L]}{1 + K_{a_1}/[H^+]} + k_{-2}. \quad (5)$$

Similar arguments may be used, considering an *interchange* pathway (Scheme 1, k_3 and k_4), incorporating the definition of K_{a_1} (= $[MO(OH)(CN)_4{}^{2-}][H^+]/[MO(OH_2)(CN)_4{}^-]$), $[M]_{tot}$ (= $[MO(OH_2)(CN)_4{}^-] + [MO(OH)(CN)_4{}^{2-}] + [MO(OH_2)(L)(CN)_4{}^{n-}]$), K_3 (= $[MO(OH_2)(L)(CN)_4{}^{n-}]/[MO(OH_2)(CN)_4{}^-][L]$; ($[L] \gg [M]_{tot}$), yielding an expression for the pseudo-first-order rate constant as given in (6), and assuming $K_3[L] \ll 1$,

$$k_{obsd} = \frac{k_4K_3[L]}{K_{a_1}/[H^+] + 1} + k_{-4}. \quad (6)$$

It is clear that (5) and (6) are similar and both adequately describe the experimental results {*associative* mechanism (5): $k_f = k_2{}'$ and $k_r = k_{-2}$; *interchange* mechanism (6): $k_f = k_4K_3$ and $k_r = k_{-4}$ and $K_3 = k_3/k_{-3}$}, and both simplify to (1) and (2), respectively.

The pressure dependence for the substitution process as studied here, at different pressures a and b, is given by [47]

$$\ln(k_a/k_b) = -\Delta V^{\#}_{expt.}(P_a - P_b)/RT. \quad (7)$$

Since the contribution by the reverse step is negligible in all cases in this study as concluded above, this implies that $\Delta V^{\#}_{expt.} \approx \Delta V^{\#}_{k_f}$. The data obtained for the *trans*-$[TcO(OH_2)(CN)_4]^-$ are shown in Figure 3, where (7) was utilized to obtain $\Delta V^{\#}_{expt.}$, and the results are reported in Table 1.

In order to compare the type of mechanism obeyed for *trans*-aqua substitution in the $[ReO(OH_2)(CN)_4]^-$ complex, a high pressure study with NCS^- ions and TU was also performed. Since the reaction between $[ReO(OH_2)(CN)_4]^-$ and L (L = NCS^- and TU) shows equilibrium constants of 87 ± 7 and 7.0 ± 0.4 M^{-1}, respectively [48, 49], similar arguments to the Tc(V) as mentioned above could be used to determine the activation volume, $\Delta V^{\#}_{expt.}$, for which the values are reported in Table 2.

This high pressure kinetic study on the reaction between $[TcO(OH_2)(CN)_4]^-$ and NCS^- ions, NNDMTU and TU

Table 2: Comparative table for the kinetic data and activation parameters for the ligation reactions of $[ReO(OH_2)(CN)_4]^-$ and $[TcO(OH_2)(CN)_4]^-$ at 25°C. [(a)]Refrences [37, 48], [(b)]this work.

Parameter	Metal	NCS^-	NNDMTU	NMTU	TU	HN_3
k_f ($M^{-1}\,s^{-1}$)	Re[(a)]	0.00348(4)	0.059(2)	0.067(2)	0.0399(9)	0.0064(2)
	Tc[(b)]	22.2(3)[(a)]	11.5(4)	11.38(4)	7.4(1)	—
k_fTc/k_fRe	—	6321	195	170	185	—
$\Delta S^{\#}_{k_f}$ ($J\,K^{-1}\,mol^{-1}$)	Re[(a)]	−11(6)	−119(40)	−125(10)	−95(3)	−87(6)
	Tc[(b)]	−9(12)	−40(8)	−84(11)	−110(17)	—
$\Delta H^{\#}_{k_f}$ ($kJ\,mol^{-1}$)	Re[(a)]	17.4(1.9)	45(11)	42(3)	52(1)	60(2)
	Tc[(b)]	62(4)	55(2)	42(3)	35(5)	—
$\Delta V^{\#}_{k_f}$ ($cm^3\,mol^{-1}$)	Re[(b)]	−1.7(3)	—	—	−22.1(9)	—
	Tc[(b)]	−3.5(3)	−14(1)	—	−6.0(5)	—

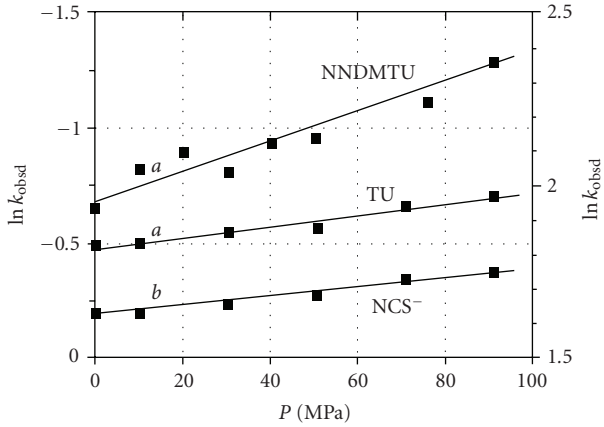

Figure 3: The effect of pressure on the second-order formation rate constant for the reaction between $[TcO(OH_2)(CN)_4]^-$ and NCS^-, NNDMTU, and TU at 25°C, pH = 0.6, [M] = 5×10^{-5} M, λ = 420 nm, *a* refers to left axis, *b* refers to the right axis. [NCS^-] = 0.2 M, [NNDMTU] = [TU] = 0.05 M, μ = 1.0 M ($NaNO_3$).

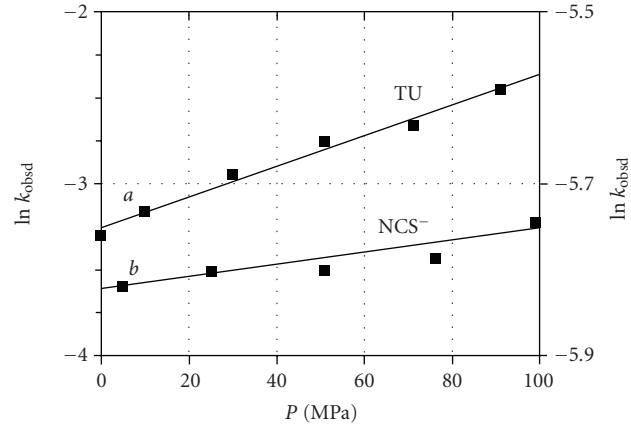

Figure 4: The effect of pressure on the second-order formation rate for the reaction between $[ReO(OH_2)(CN)_4]^-$ and NCS^- ions and TU at 25°C, pH = 0.3, [M] = 1.5×10^{-3} M, *a* refers to left axis, *b* refers to right axis. [NCS^-] =0.6 M, λ_{NCS^-} = 420 nm; [TU] = 1.0 M, λ_{TU} = 350 nm, μ = 1.0 M ($NaNO_3$).

[Figure 3], yields $\Delta V^{\#}_{expt.}$ values of −3.5 ± 0.3, −14 ± 1 and −6.0 ± 0.5 cm^3/mol, respectively. Similarly, the data for the Re(V), as represented in Figure 4 gave $\Delta V^{\#}_{expt.}$ values of −1.7 ± 0.3 and −22.1 ± 0.9 cm^3/mol for NCS^- ions and TU respectively. It is clear that all these indicate small to large negative values, contrary to the experiments on Alberto's Re^I and Tc^I complexes [35].

We previously concluded that with regard to the mechanism, due to the large distortion (metal displaced out of the plane formed by the four *cis* ligands bonded to the metal, away from the *trans*-oxo) observed for the $[MO(L)(CN)_4]^{n-}$ complexes of Mo^{IV}, W^{IV}, Re^V, and Tc^V, a dissociative activation would be favoured during *trans*-aqua substitution reactions [44, 47]. A positive volume of activation (+10.6 ± 0.5 cm^3/mol) was observed for the reaction between the corresponding isostructural $[WO(OH_2)(CN)_4]^{2-}$ complex and N_3^-, forming an important basis of the mechanistic assignment.

However, the current high-pressure study on the $[ReO(OH_2)(CN)_4]^-$ and $[TcO(OH_2)(CN)_4]^-$ complexes clearly indicates a negative volume of activation for all these reactions (Table 2), ranging from slightly negative for the anionic NCS^- as entering ligand, to substantially negative for the neutral thiourea ligands. This yields important evidence, along with the large negative $\Delta S^{\#}$ values, that an associative (A) mechanism or an associative interchange (I_a) mechanism is operative for the activation step during these *trans*-aqua substitution reactions on the M(V) metals. In principle, this is actually quite acceptable, since the $[MO(OH_2)(CN)_4]^{n-}$ complexes of Mo^{IV}, W^{IV}, Re^V and Tc^V are all classic 16 electron species. Clearly, the M(IV) metal centres are softer than the corresponding Re^V and Tc^V, allowing easier dissociation of the aqua ligand in the rate determining step. This is confirmed by the solid state structures of the $[MO(NCS)(CN)^4]^{2-}$ complexes, wherein both of the NCS^- ligands where nitrogen bound. [43, 44].

The formation of the $[MO(L)(CN)_4]^{m-}$ complex in Scheme 1 in an A mechanism yields an activation volume $\Delta V^{\#}_{expt.} = \Delta V^{\#}_{k_f} = \Delta V^{\#}_{k_2}{}'$, which is expected to be large negative, and holds true for the reactions between both $[ReO(OH_2)(CN)_4]^-$ and TU ($\Delta V^{\#}_{k_2}{}'$ = −22.1 (9) $cm^3\,mol^{-1}$) and $[TcO(OH_2)(CN)_4]^-$ and NNDMTU

($\Delta V^{\#}_{k_f} = -14(1)\,\mathrm{cm^3\,mol^{-1}}$) and to a lesser extend for $[TcO(OH_2)(CN)_4]^-$ and TU ($\Delta V^{\#}_{k_f} = -6.0 \pm 0.5\,\mathrm{cm^3\,mol^{-1}}$). It is therefore realistic that the neutral ligands will associate more easily with the $[MO(OH_2)(CN)_4]^-$ species, compared to association between two negative species {$[MO(OH_2)(CN)_4]^-$ and the NCS^- ligand}, supporting the assumption of an associative process. Furthermore, the reaction between $[MO(OH_2)(CN)_4]^-$ and NCS^- yielded activation values of -1.7 ± 0.3 and $-3.5 \pm 0.3\,\mathrm{cm^3\,mol^{-1}}$ for Re^V and Tc^V, respectively. These are considered too small negative values to support a pure associative activation, although electrostriction between the negatively charged complex and entering NCS^- ligand might affect the total value of $\Delta V^{\#}_{\mathrm{expt.}}$.

For an I_a mechanism, the volume of activation can be expressed as the sum of the individual contributions for each step in Scheme 1 (8), where $k_f = k_4K_3$ and ΔV_{K_3} = reaction volume for the equilibrium reaction defined by K_3:

$$\Delta V^{\#}_{\mathrm{expt.}} = \Delta V_{K_3} + \Delta V^{\#}_{k_4}. \tag{8}$$

The k_4 step is associated with a simultaneous bond breaking/formation process, and therefore $\Delta V^{\#}_{k_4}$ is expected to be slightly negative in an interchange associative process. Furthermore, ΔV_{K_3} can be expressed in terms of its individual components (9):

$$\Delta V_{K_3} = \Delta V^{\#}_{k_3} - \Delta V^{\#}_{k_{-3}}. \tag{9}$$

Since $\Delta V^{\#}_{k_{-3}}$ is expected to be positive (associated with bond breaking), and $\Delta V^{\#}_{k_3}$ in turn is slightly negative, ΔV_{K_3} is expected to be either small positive or slightly negative. It is thus clear from (9), that depending on the relative magnitude of the volume change associated with K_3 and k_4, that either an I_d or I_a mechanism is possible. However, since an overall negative tendency for $\Delta V^{\#}_{\mathrm{expt.}}$ was obtained, an associative interchange mechanism is considered more likely for the NCS^- reaction, since there should be significant electrostriction between the NCS^- and $[M]^-$ species. For the neutral thiourea ligands, an even larger-negative activation volume is observed, and a pure associative mode of activation could well be operative.

Upon comparison of the *trans*-substitution reactions on the $[ReO(OH_2)(CN)_4]^-$ and $[TcO(OH_2)(CN)_4]^-$ complexes (Table 2), a few other interesting observations are also made.

Firstly, for the $[ReO(OH_2)(CN)_4]^-$ complex, the order of reactivity for the ligands are: NMTU > NNDMTU > TU > NCS^- > HN_3 and for the $[TcO(OH_2)(CN)_4]^-$ complex: NCS^- > NNDMTU > NMTU > TU. It is clear that the NCS^- ligand shows the fastest reaction with the Tc centre (ca. 6300 times faster), but the slowest reaction with the Re centre [see relative ratio's of k_fTc/k_fRe in Table 2]. A comprehensive explanation of this rate difference is not yet possible. It is, however, known that the Tc^V centre can more readily accept electron density than does the Re^V [50, 51] and to some extend favour, in spite of the negative charge on the NCS^- as entering ligand, association with the Tc^V centre. This is, however, not manifested in the activation volumes. The rate constants of the thiourea ligands are more comparable, showing a great deal of consistency for both metal centres, although a slight dependence on steric bulk/electron density of the TU ligands is apparent, but cannot currently be convincingly explained, see below.

Table 3: Comparison between pK_a values of methyl substituted and unsubstituted compounds [52].

Compound	pK_{a_1}	Compound	pK_{a_1}
Cinnamic acid	4.44	*P*-Methylcinnamic acid	4.56
Malonic acid	2.83	Methylmalonic acid	3.07
Acetic acid	4.75	Trimethylacetic acid	5.03
Pyridine	5.25	2,4-Dimethylpyridine	6.57
Methylamine	10.66	Dimethylamine	10.73

Secondly, since it is known that methyl substituents on a ligand can increase the pK_a value and therefore the electron donating ability thereof (see examples in Table 3 [52]), it is expected in an associative mechanism that the methyl substituted thiourea will react slightly faster than TU, as was concluded from this work on the Re^V system.

Thirdly, the $[MO(OH_2)(CN)_4]^{n-}$ compounds of Tc^V and Re^V react both according to an associative mechanism or partly associative, while the Mo^{IV} and W^{IV} compounds react via a dissociative mechanism. From this, it is clear that the work done on the Mo^{IV} and W^{IV} centres, although all isostructural d^2 species, cannot be applied directly to the Tc^V and Re^V centres, as assumed previously [13]. It also implies that the higher-oxidation state of the Tc^V and Re^V centres favour the more associative activation, while the Mo^{IV} and W^{IV} could favour a dissociative activation mode.

However, even more detailed high-pressure studies, to enable construction of complete volume profiles, are required in future.

These results, along with the fact that the Tc(V) centre is much more reactive than the Re(V), is of particular relevance to nuclear medicine. In the preparation of ^{99m}Tc radiopharmaceuticals or in the labelling of antibodies with ^{99m}Tc, "transfer" ligands are often used to stabilize the required oxidation state, and then the actual labelling is accomplished by simple ligand substitution onto the "transfer complex" [53]. From this work, the best way of optimizing labelling conditions would be to use a S-donor transfer ligand instead of a C- or N-donor transfer ligand so that the exchange process would be dissociative in nature. This would imply that the transfer ligand, rather than the concentration of the antibody or chelating moiety attached to the antibody, would influence the reaction rate and yield a much "cleaner" reaction mixture (concentration of unlabeled antibody in solution would be low). Furthermore, the greater reactivity of Tc compared to Re must be taken into account when developing therapeutic radio-rhenium analogues to known diagnostic ^{99m}Tc radiopharmaceuticals. For example, more drastic conditions are required in the preparation of ^{186}Re diphosphonates (for bone imaging) than in the preparation of ^{99m}Tc diphosphonates [54]. These differences in reactivities between Tc^V and Re^V centres needs to be taken into account before procedures that are

available for certain technetium complexes are applied to the preparation of the rhenium analogues.

ACKNOWLEDGMENTS

Financial assistance from the Research Fund of the Free State University is gratefully acknowledged. Part of this material is based on work supported by the South African National Research Foundation under Grant no. (GUN 2053397). Any opinion, findings, and conclusions or recommendations expressed in this material are those of the authors and do not necessarily reflect the views of the NRF.

REFERENCES

[1] J. R. Dilworth and S. J. Parrott, "The biomedical chemistry of technetium and rhenium," *Chemical Society Reviews*, vol. 27, no. 1, pp. 43–55, 1998.

[2] E. Deutsch, K. Libson, S. Jurisson, and L. F. Lindoy, "Technetium chemistry and technetium radiopharmaceuticals," *Progress in Inorganic Chemistry*, vol. 30, p. 75, 1983.

[3] E. Deutsch and K. Libson, "Recent advances in technetium chemistry: bridging inorganic chemistry and nuclear medicine," *Comments on Inorganic Chemistry*, vol. 3, no. 2-3, pp. 83–103, 1984.

[4] M. J. Clarke and L. Podbielski, "Medical diagnostic imaging with complexes of ^{99m}Tc," *Coordination Chemistry Reviews*, vol. 78, pp. 253–331, 1987.

[5] J. Steigman and W. C. Eckelman, *The Chemistry of Technetium in Medicine*, National Academy Press, Washington, DC, USA, 1992.

[6] E. Deutsch, K. Libson, J.-L. Vanderhyden, A. R. Ketring, and H. R. Maxon, "The chemistry of rhenium and technetium as related to the use of isotopes of these elements in therapeutic and diagnostic nuclear medicine," *Nuclear Medicine and Biology*, vol. 13, no. 4, pp. 465–477, 1986.

[7] W. A. Volkert and T. J. Hoffman, "Therapeutic radiopharmaceuticals," *Chemical Reviews*, vol. 99, no. 9, pp. 2269–2292, 1999.

[8] G. Kemp, A. van Aswegen, A. Roodt, et al., "The use of 186Re-HEDP for pain relief in the palliative treatment of bone cancers," in *Modern Trends in Radiopharmaceuticals for Diagnosis and Therapy*, pp. 627–633, International Atomic Energy Agency, Vienna, Austria, 1998.

[9] M. C. Gerson, E. A. Deutsch, H. Nishiyama, et al., "Myocardial perfusion imaging with ^{99m}Tc -DMPE in man," *European Journal of Nuclear Medicine and Molecular Imaging*, vol. 8, no. 9, pp. 371–374, 1983.

[10] J. L. Vanderheyden, A. R. Ketring, K. Libson, et al., "Synthesis and characterization of cationic technetium complexes of 1,2-bis(dimethylphosphino)ethane (DMPE). Structure determinations of *trans*-$[Tc^{V}(DMPE)_2(OH)(O)](F_3CSO_3)_2$, *trans*-$[Tc^{III}(DMPE)_2CI_2]F_3CSO_3$, and $[Tc^{I}(DMPE)_3]^+$ using x-ray diffraction, EXAFS, and ^{99}Tc NMR," *Inorganic Chemistry*, vol. 23, no. 20, pp. 3184–3191, 1984.

[11] E. Deutsch, A. R. Ketring, K. Libson, J.-L. Vanderheyden, and W. W. Hirth, "The Noah's Ark experiment: species dependent biodistributions of cationic ^{99m}Tc complexes," *International Journal of Radiation Applications and Instrumentation B*, vol. 16, no. 3, pp. 191–217, 1989.

[12] E. Deutsch, K. A. Glavan, V. J. Sodd, H. Nishiyama, D. L. Ferguson, and S. J. Lukes, "Cationic Tc-99m complexes as potential myocardial imaging agents," *Journal of Nuclear Medicine*, vol. 22, no. 10, pp. 897–907, 1981.

[13] A. Roodt, J. C. Sullivan, D. Meisel, and E. Deutsch, "Electron-transfer reactions of technetium and rhenium complexes. 3.[1] Pulse radiolysis studies on *trans*-$[M^{III}X_2(DMPE)_2]^+$ and $[M^{I}(DMPE)_3]^+$ complexes in aqueous and aqueous surfactant media, where M = Tc or Re, X = Cl or Br, and DMPE = 1,2-bis(dimethylphosphino)ethane," *Inorganic Chemistry*, vol. 30, no. 24, pp. 4545–4549, 1991.

[14] K. Libson, M. N. Doyle, R. W. Thomas, et al., "Structural and kinetic investigations of a Tc(III)/Tc(II) redox couple. X-ray crystal structures of *trans*-$[Tc^{II}(DPPE)_2CI_2]$ and *trans*-$[Tc^{III}(DPPE)_2CI_2]NO_3.HNO_3$, where DPPE = 1,2-bis(diphenylphosphino)ethane," *Inorganic Chemistry*, vol. 27, no. 20, pp. 3614–3619, 1988.

[15] J. L. Eglin, L. T. Smith, E. J. Valente, and J. D. Zubkowski, "The synthesis and characterization of *trans*-$ReCI_2(dppe)_2$ and α – $Re_2CI_4(dppe)_2$," *Inorganica Chimica Acta*, vol. 268, no. 1, pp. 151–157, 1998.

[16] D. J. Lewis, R. L. Luck, and J. V. Silverton, "Structure of bis[*cis*-1,2-bis(diphenylphosphino)ethylene]dichlororhenium(II) hexane solvate," *Acta Crystallographica Section C*, vol. 49, part 8, pp. 1424–1426, 1993.

[17] D. Esjornson, M. Bakir, P. E. Fanwick, K. S. Jones, and R. A. Walton, "Metal-mediated reduction of alkanenitriles to imido ligands. Formation of the imido complexes $Re(NCH_2R)X_3$ (dppbe) (R = Me, Et, *i*-Pr; X = Cl, Br) from the reactions of the octahalodirhenate(III) anions with 1,2-bis(diphenylphosphino)benzene in nitrile solvents (RCN)," *Inorganic Chemistry*, vol. 29, no. 11, pp. 2055–2061, 1990.

[18] M. Bakir, P. E. Fanwick, and R. A. Walton, "Mononuclear rhenium(III) and rhenium(II) complexes of 1,2-bis(diphenylphosphino)ethylene: the structure of *trans*-$ReCI_2(dppee)_2$," *Polyhedron*, vol. 6, no. 5, pp. 907–913, 1987.

[19] E. Deutsch, W. Bushong, K. A. Glavan, et al., "Heart imaging with cationic complexes of technetium," *Science*, vol. 214, no. 4516, pp. 85–86, 1981.

[20] S. Jurisson, D. Bering, W. Jia, and D. Ma, "Coordination compounds in nuclear medicine," *Chemical Reviews*, vol. 93, no. 3, pp. 1137–1156, 1993.

[21] B. L. Holman, A. G. Jones, J. Lister-James, et al., "A new Tc-99m-labeled myocardial imaging agent, hexakis(t-butylisonitrile)-yechnetium(I) [Tc-99m TBI]: initial experience in the human," *Journal of Nuclear Medicine*, vol. 25, no. 12, pp. 1350–1355, 1984.

[22] E. Prats, F. Aisa, M. D. Abós, et al., "Mammography and r^{99m}Tc-MIBI scintimammography in suspected breast cancer," *Journal of Nuclear Medicine*, vol. 40, no. 2, pp. 296–301, 1999.

[23] C. J. Smith, K. V. Katti, W. A. Volkert, and L. J. Barbour, "Syntheses and characterization of chemically flexible, water-soluble dithio-bis(phosphine) compounds: $(HOH_2C)_2P$ – $(CH_2)_2S(CH_2)_3S(CH_2)_2P(CH_2OH)_2$, $(HOH_2C)_2PCH_2CH_2$ $S(CH_2)_4SCH_2CH_2P(CH_2OH)_2$, and $(HOH_2C)_2PCH_2CH_2$-$CH_2S(CH_2)_3SCH_2CH_2CH_2P(CH_2OH)_2$. Systematic investigation of the effect of chain length on the coordination chemistry of rhenium(V). X-ray crystal structures of $[ReO_2(HO-H_2C)_2P(CH_2)_2S(CH_2)_3S(CH_2)_2P(CH_2OH)_2]_2(CI)_2$, $[ReO_2$ $(HOH_2C)_2P(CH_2)_2S(CH_2)_4S(CH_2)_2P$–$(CH_2OH)_2]_2(ReO_4^-)_2$, and $[ReO_2(HOH_2C)_2P(CH_2)_3$–$S(CH_2)_3S(CH_2)_3P(CH_2OH)_2]$ (CI)," *Inorganic Chemistry*, vol. 36, no. 18, pp. 3928–3935, 1997.

[24] J. D. Kelly, A. M. Forster, B. Higley, et al., "Technetium-99m-tetrofosmin as a new radiopharmaceutical for myocardial

perfusion imaging," *Journal of Nuclear Medicine*, vol. 34, no. 2, pp. 222–227, 1993.

[25] J. D. Kelly, K. W. Chiu, and I. A. Latham, US Patent 5 045 302, September 1991.

[26] H. P. Engelbrecht, C. S. Cutler, S. S. Jurisson, L. den Drijver, and A. Roodt, "Solid state study on rhenium dimethylphosphinoethane complexes: x-ray crystal structures of *trans*-$[ReO_2(dmpe)_2]PF_6.2H_2O$, *trans*-$[ReO(OH)(dmpe)_2](CF_3SO_3)_2$, *trans*−$[ReN(CI)(dmpe)_2]CF_3SO_3$ and *trans*-$[ReCI_2(dmpe_2)]ReO_4$," *Synthesis and Reactivity in Inorganic and Metal Organic Chemistry*, vol. 35, no. 1, pp. 83–99, 2005.

[27] H. P. Engelbrecht, L. den Drijver, G. Steyl, and A. Roodt, "Solid-state and theoretical structural study on *trans*-$[ReO_2(Eten)_2]CF_3SO_3.LiCF_3SO_3$ (Eten = *N*-ethyl ethylenediamine)," *Comptes Rendus Chimie*, vol. 8, no. 9-10, pp. 1660–1669, 2005.

[28] P. Kurz, B. Spingler, T. Fox, and R. Alberto, "$[Tc^{I}(CN)_3(CO)_3]^{2-}$ and $[Re^{I}(CN)_3(CO)_3]^{2-}$: case studies for the binding properties of CN- and CO," *Inorganic Chemistry*, vol. 43, no. 13, pp. 3789–3791, 2004.

[29] F. Zobi, B. Spingler, T. Fox, and R. Alberto, "Toward novel DNA binding metal complexes: structure and basic kinetic data of $[M(9MeG)_2(CH_3OH)(CO)_3]^+$ (M = ^{99}Tc, Re)," *Inorganic Chemistry*, vol. 42, no. 9, pp. 2818–2820, 2003.

[30] O. Karagiorgou, G. Patsis, M. Pelecanou, et al., "(*S*)-(2-(2′-Pyridyl)ethyl)cysteamine and (*S*)-(2-(2′-Pyridyl)ethyl)$_{-D,L-}$ homocysteine as ligands for the "*fac*-$[M(CO)_3]^+$" (M = Re, ^{99m}Tc) core," *Inorganic Chemistry*, vol. 44, no. 12, pp. 4118–4120, 2005.

[31] Y. Liu, J. K. Pak, P. Schmutz, et al., "Amino acids labeled with $[^{99m}Tc(CO)_3]^+$ and recognized by the L-type amino acid transporter LAT1," *Journal of the American Chemical Society*, vol. 128, no. 50, pp. 15996–15997, 2006.

[32] S. Kunze, F. Zobi, P. Kurz, B. Spingler, and R. Alberto, "Vitamin B12 as a ligand for technetium and rhenium complexes," *Angewandte Chemie International Edition*, vol. 43, no. 38, pp. 5025–5029, 2004.

[33] C. Xavier, J. K. Pak, I. Santos, and R. J. Alberto, "Evaluation of two chelators for labelling a PNA monomer with the *fac*-$[^{99m}Tc(CO)_3]^+$ moiety," *Journal of Organometallic Chemistry*, vol. 692, no. 6, pp. 1332–1339, 2007.

[34] L. Kromer, B. Spingler, and R. Alberto, "Synthesis and reactivity of $[ReBr_2(NCCH_3)_2(CO)_2]^-$: a new precursor for bioorganometallic chemistry," *Journal of Organometallic Chemistry*, vol. 692, no. 6, pp. 1372–1376, 2007.

[35] P. V. Grundler, L. Helm, R. Alberto, and A. E. Merbach, "Relevance of the ligand exchange rate and mechanism of *fac*-$[(CO)_3M(H_2O)_3]^+$ (M = Mn, Tc, Re) complexes for new radiopharmaceuticals," *Inorganic Chemistry*, vol. 45, no. 25, pp. 10378–10390, 2006.

[36] J.-L. Vanderheyden, M. J. Heeg, and E. Deutch, "Comparison of the chemical and biological properties of *trans*-$[Tc(DMPE)_2CI_2]^+$ and *trans*-$[Re(DMPE)_2CI_2]^+$, where DMPE = 1,2-bis(dimethylphosphino)ethane. Single-crystal structural analysis of *trans*-$[Re(DMPE)_2CI_2]PF_6$," *Inorganic Chemistry*, vol. 24, no. 11, pp. 1666–1673, 1985.

[37] A. Roodt, A. Abou-Hamdan, H. P. Engelbrecht, and A. E. Merbach, "Substitution behaviour of oxocyano-complexes of second and third series early transition metals," in *Advances in Inorganic Chemistry*, A. G. Sykes, Ed., vol. 48, pp. 59–126, Pergamon Press, London, UK, 1999.

[38] H. P. Engelbrecht, S. Otto, and A. Roodt, "*trans*-Bis(*N*,*N*-diethylethylenediamine-*N*,N′)dioxorhenium(V) chloride trihydrate," *Acta Crystallographica Section C*, vol. 55, part 10, pp. 1648–1650, 1999.

[39] A. Roodt, J. G. Leipoldt, L. Helm, and A. E. Merbach, "Equilibrium behavior and proton transfer kinetics of the dioxotetracyanometalate complexes of molybdenum(IV), tungsten(IV), technetium(V), and rhenium(V): carbon-13 and oxygen-17 NMR study ," *Inorganic Chemistry*, vol. 33, no. 1, pp. 140–147, 1994.

[40] A. Roodt, J. G. Leipoldt, L. Helm, A. Abou-Hamdan, and A. E. Merbach, "Kinetics and mechanism of oxygen exchange and inversion along the M:O axis in the diprotonated and monoprotonated dioxotetracyanometalate complexes of Re(V), Tc(V), W(IV), and Mo(IV)," *Inorganic Chemistry*, vol. 34, no. 3, pp. 560–568, 1995.

[41] A. Abou-Hamdan, A. Roodt, and A. E. Merbach, "^{13}C and ^{15}N NMR mechanistic study of cyanide exchange on oxotetracyanometalate complexes of Re(V), Tc(V), W(IV), Mo(IV), and Os(VI)," *Inorganic Chemistry*, vol. 37, no. 6, pp. 1278–1288, 1998.

[42] A. Roodt, H. P. Engelbrecht, J. M. Botha, and S. Otto, "Reactivity and mechanism of technetium and rhenium complexes relevant to nuclear medicine," in *Technetium, Rhenium and Other Metals in Chemistry and Nuclear Medicine*, M. Nicolini and U. Mazzi, Eds., vol. 5, pp. 161–166, Plenum Press, New York, NY, USA, 1999.

[43] W. Purcell, A. Roodt, S. S. Basson, and J. G. Leipoldt, "The crystal structure of 4,4′-dipyridinium tetracyanooxothiocyanatorhenate(V)," *Transition Metal Chemistry*, vol. 14, no. 5, pp. 369–370, 1989.

[44] A. Roodt, J. G. Leipoldt, E. A. Deutsch, and J. C. Sullivan, "Kinetic and structural studies on the oxotetracyanotechnetate(V) core: protonation and ligation of dioxotetracyanotechnetate(V) ions and crystal structure of 2,2′-bipyridinium *trans*-oxothiocyanatotetracyanotechnetate(V)," *Inorganic Chemistry*, vol. 31, pp. 1080–1085, 1992.

[45] "MicroMath Scientist Software for windows," Version 4.0, 2000.

[46] R. Van Eldik, D. A. Palmer, R. Schmidt, and H. Kelm, "Volumes of activation for the anation of Pd(II) substituted dien complexes by chloride ion in aqueous solution. A high pressure stopped-flow instrument for studying the kinetics of fast reactions under pressure," *Inorganica Chimica Acta*, vol. 50, pp. 131–135, 1981.

[47] J. G. Leipoldt, S. S. Basson, I. M. Potgieter, and A. Roodt, "Kinetic study of the reaction between *trans*-dioxotetracyanomolybdate(IV) ions and 1,10-phenanthroline," *Inorganic Chemistry*, vol. 26, no. 1, pp. 57–59, 1986.

[48] W. Purcell, A. Roodt, and J. G. Leipoldt, "Kinetic and equilibrium study of substitution reactions of *trans*-tetracyanodioxorhenate(V) ions with monodentate nucleophiles," *Transition Metal Chemistry*, vol. 16, no. 3, pp. 339–343, 1991.

[49] W. Purcell, A. Roodt, S. S. Basson, and J. G. Leipoldt, "Kinetic study of the reaction between *trans*-tetracyanodioxorhenate(V) and thiocyanate ions," *Transition Metal Chemistry*, vol. 14, no. 3, pp. 224–226, 1989.

[50] L. Helm, K. Deutsch, E. A. Deutsch, and A. E. Merbach, "Multinuclear NMR studies of ligand-exchange reactions on analogous technetium(V) and rhenium(V) complexes. Relevance to nuclear medicine," *Helvetica Chimica Acta*, vol. 75, no. 1, pp. 210–217, 1992.

[51] F. Tisato, U. Mazzi, G. Bandoli, et al., "Neutral oxo and nitrido complexes of technetium(V) and rhenium(V) with an unsaturated tetradentate (N_2S_2) ligand. Crystal structure of [*N*,*N*′-ethylenebis(thioacetylacetonylideneiminato](2—)

S,*S*′,*N*,*N*′) nitridotechnetium(V)," *Journal of the Chemical Society Dalton Transactions*, pp. 1301–1307, 1991.

[52] CRC Handbook of Chemistry and Physics, Chemical Rubber Company.

[53] K. Libson, L. Helm, A. Roodt, et al., "Kinetics and mechanism of ligand substitution on analogous technetium(V) and rhenium(V) complexes in technetium and rhenium in chemistry and nuclear medicine 3," in *Technetium and Rhenium in Chemistry and Nuclear Medicine*, M. Nicolini, G. Bandoli, and U. Mazzi, Eds., pp. 31–35, Raven Press, New York, NY, USA, 1990.

[54] E. A. Deutsch, K. Libson, and J. L. Vanderheyden, "The inorganic chemistry of technetium and rhenium as relevant to nuclear medicine," in *Technetium and Rhenium in Chemistry and Nuclear Medicine*, M. Nicolini, G. Bandoli, and U. Mazzi, Eds., vol. 3, pp. 13–22, Raven Press, New York, NY, USA, 1990.